CHARACTERISATION OF THE OPTIC RADIATIONS IN CHILDREN IN HEALTH AND DISEASE

Say Ayala Soriano

A thesis submitted for the degree of Doctor of Philosophy

University College London

January 2016

DECLARATION

I, Say Ayala Soriano, confirm that the work presented in this thesis is my own. Where information has been derived from other sources, I confirm that this has been indicated in the thesis.

ABSTRACT

The normal and abnormal development of the optic radiations through childhood was examined in terms of their anatomical development, using MRI tractography, and their functional development, using visual evoked potentials (VEPs). Neurosurgical applications of these imaging techniques were assessed.

Control cohorts of 74 children and 13 adults were recruited from Great Ormond Street Hospital. The anatomical development of the optic radiations in children from birth was described using tractography. A novel method to improve tractography analysis using VEP data was developed. VEP-enhanced tractography showed a more defined optic radiation in the gathering of the visual cortex, which caused a significant reduction in the mean FA in the adult cohort.

Paediatric patients diagnosed with optic nerve hypoplasia (ONH) were recruited and 23 were compared with a matched control cohort using tractography. ONH patients presented reduced mean FA in the left optic radiation. TBSS analysis of the DTI scans showed that white matter FA was also lower in other areas of the brain outside of the visual system.

Two paediatric seizure patient cohorts were recruited: 21 patients with a single episode of prolonged febrile convulsions and 20 regular users of anti-epileptic medicines. Both cohorts were compared with matched control cohorts using DTI tractography. The anti-epileptic user cohort presented lower mean FA at the front of both optic radiations, but the prolonged febrile convulsions cohort had no statistically-significant differences in mean FA, compared to controls.

Two brain tumour case studies demonstrated that tractography is a valuable surgical tool in complicated paediatric neurosurgical cases where detailed description of white matter tracts can improve the surgical outcome and assist with counselling patients. Two hydrocephalus case studies demonstrated that VEP-enhanced tractography offers a novel method to identify white matter tracts in cases where conventional imaging techniques provide very limited information due to highly-distorted anatomies.

DEDICATION

I dedicate this thesis to my parents, Antonia Soriano Baeza and Pablo Ayala Hernandez, for their unwavering support and encouragement throughout my lifelong long journey of learning.

I also dedicate this work to my partner, Paul Dodds, who has given me constant encouragement and support during my PhD research.

ACKNOWLEDGEMENTS

I was supported by two supervisors, Alki Liasis of Great Ormond Street Hospital and Chris Clark of University College London. Alki supported and encouraged me during the most difficult periods; without him, this thesis would not have been possible. Chris helped to plan the project and his contribution to editing this thesis was invaluable.

I am also very grateful to Dr Dorothy Thompson, a consultant neurophysiologist at Great Ormond Street Hospital, who helped me with patient recruitment and VEP recordings, as did Ruth Lyons and Tessa Mellow.

In the Ophthalmology Department of Great Ormond Street Hospital, Eva Gajdosova and Olga Alvarez Bulnes helped me greatly with patient recruitment for the study, for which I will always be grateful.

Staff from the Radiology Department of Great Ormond Street Hospital, in particular Tina Banks, helped with patient MRI scanning.

Finally, I would like to thank colleagues from the Developmental Imaging and Biophysics Section of the Institute of Child Heath at UCL, who helped with MRI analyses and with whom I shared some patient recruitment. These include Michael Yoong, Jonathan Clayden, Ai Wern Chung and in particular Kiran Seunarine.

CONTENTS

LIST OF FIGURES

LIST OF TABLES

ABBREVIATIONS

ADC	Apparent Diffusion Coefficient
ANCOVA	Analysis of covariance
CBF	Cerebral Blood Flow
CSF	Cerebrospinal Fluid
DESTIR MRI	Double-Echo ShorT Inversion Recovery MRI
DT	Diffusion Tensor
DTI	Diffusion Tensor Imaging
DWI	Diffusion-Weighted Imaging
FA	Fractional Anisotropy
FLASH MRI	Fast Low Angle SHot MRI
HIV	Human Immunodeficiency Virus
fMRI	Functional MRI
FSL	FMRIB (Functional MRI of the Brain) Software Library
GA	General Anaesthetic
GOSH	Great Ormond Street Hospital
LGN	Lateral Geniculate Nucleus
MD	Mean Diffusivity
MRI	Magnetic Resonance Imaging
ONH	Optic Nerve Hypoplasia
ROI	Region of Interest
TBSS	Tract-Based Spatial Analysis
VEP	Visual Evoked Potential
WHO	World Health Organisation

1 INTRODUCTION

There is little information in the literature about the development of the optic radiations in children. The visual system during childhood does not function as a smaller replica of the adult visual system, but is a constantly changing and evolving structure that is characterised by its continuously changing anatomy and function. In this study, the normal and abnormal development of the optic radiations through childhood are examined in terms of their functional and anatomical development.

Abnormal visual system development is related to numerous pathologies. Visual abnormalities such as optic nerve hypoplasia and associated septo-optic dysplasia are related to abnormal visual system development in the intrauterine period, but the origins of these neurodevelopmental disorders are not fully understood. Development of otherwise normal optic radiations can be interrupted by a period of ischemia or other injury or insult. Seizures have the potential to impair the normal development of brain structures and functions by hypoxia. The white matter pathways can be compressed and function impaired by brain pathologies such as tumours and hydrocephalus, which can lead to highly distorted anatomies. Where surgery is required, accurate diagnosis and individualised surgical planning is critically important to achieving successful outcomes by minimising damage to the optic radiations.

This study tests visual function using a multi-channel visual evoked potential procedure. The optic radiation anatomy is imaged using a non-invasive research MRI tractography technique. The aims of this study are to: (i) examine the impact of optic

nerve hypoplasia and seizures on the development of the optic radiations using tractography; (ii) assess the benefits of using VEP measurements to improve MRI tractography; and, (iii) investigate how these techniques could improve the preoperative and postoperative treatment of children with brain pathologies.

1.1 Development of the human visual system

Sight is a vital human sense whose importance has been acknowledged in human culture from the times of ancient Greek philosophy (Jonas, 1954). The visual system is more complex than most other sensory systems of the human body. The development of the visual system through childhood can be characterised in terms of functional development and anatomical development.

1.1.1 Functional development through childhood

All of the sensory systems, including the visual system, have two very important foundations during their development, which are the genetic phase and the posterior environmental-structural phase. The genetic phase of visual development has similar characteristics to other human systems in the early stages of development. Conception is not the only factor in this phase but does determine the genetic load. The environmental-structural phase is determined by gene interactions and also by the stimuli and environment while the sensory system is developing.

Prenatal development sets the basis of the genetic phase and the foundations of the environmental-structural phase, and is considered the first critical period of development.

Visual acuity is defined as the ability of the visual system to discern fine distinctions in the environment. It depends on optical and neural factors, such the health of the retina (including its shape), the ability of the neuronal system to transform the external stimuli into electric activity, and the ability of the brain to interpret it (Walker HK, 1990). Visual acuity increases from birth to maturity at an age of around 4 years. Berardi *et al.* (2000) identify two critical periods of functional development when visual acuity increases greatly, aged up to 1 and between 2.5–4 years old. More generally, Lewis and Maurer (2009) identify multiple sensitive periods in the maturation process in which the development of the visual system is sensitive to

stimuli from the outside world, with the period varying widely across different aspects of vision and ranging from ages of a few months to more than 10 years old.

1.1.2 Anatomical development through childhood

Although anatomical dissections (van Baarsen *et al.*, 2009) and tractographic studies (Govindan *et al.*, 2008) have identified the extent and variations in the size and shape of the optic radiations in adults, there is little information in the literature about the development of the optic radiations in children. This is important because the visual system during childhood does not function as a smaller replica of the adult visual system, but is a constantly changing and evolving structure, which is characterised by the continuously developing anatomy and function. Although animal studies have identified visual system evolution across a range of species (Berardi *et al.*, 2000), these have limited value since the spatial organisation of the human visual cortex is different to other mammalian species (Wandell *et al.*, 2007).

One aim of describing the spatial arrangement in the visual cortex is to identify the different visual areas and their location in relation to tangible anatomical structures that can be easily identified. Once the spatial arrangement is known, it becomes possible to study the interneuronal connections and the links between the different visual centres. The spatial organisation is also important for visual recognition, because the spatial organisation of the visual system enables feature recognition even with visual field deficits.

The optic radiations are composed of distinct yet interconnected sets of cortical and sub-cortical regions. The organisation of the tracts is complex and variable, with their development influenced by genetic predispositions, environmental events and the response of the neurons to stimuli (which changes the connectivity and neurodevelopment and encourages plasticity) (Tau and Peterson, 2010). The period of postnatal development is variously estimated in the literature between 7 years (Berardi *et al.*, 2000) and 10 years (Lewis and Maurer, 2009). Myelination of the tracts is mostly completed by 7 months of age and the sheath thickness increases particularly strongly in the first 2 years, but more slowly thereafter (Magoon and Robb, 1981). This is the same period in which Berardi *et al.* (2000) identify sustained functional development.

Each white matter pathway in the brain develops differently. The optic radiations have two myelination areas (the geniculocortical and the corticogeniculate) that are asynchronous to the anterior pole of the visual pathway (Brody *et al.*, 1987). These areas develop earlier than the posterior pole, which completes the myelination process later (Dubois *et al.*, 2008). Fibres with no temporal-frontal connections develop faster (Lebel *et al.*, 2008).

1.2 Abnormal development of the visual system

Abnormal visual development is multifactorial. Visual abnormalities such as microphthalmia, optic nerve hypoplasia and associated septo-optic dysplasia are related to abnormal visual system development in the intrauterine period (Sowka *et al.*, 2008), but the origins of the diseases are not fully understood and most cases occur sporadically. Anatomical abnormalities found in the visual system of children with optic nerve hypoplasia might not have a functional correlation.

Development of otherwise normal optic radiations can be interrupted by a period of ischemia or other injury or insult, which limits the final function or the achievement of fully-normal anatomical structures. In other cases, lesions have been found to be genetically-driven (McCabe *et al.*, 2011).

Seizures have the potential to impair the normal development of brain structures and functions by hypoxia, particularly for children with long-term epilepsy, because nervous tissue is very sensitive to hypoxia and seizures during infancy impact the neuronal tissue during the time of development. Lack of oxygen for even a very short time can cause harmful lesions (Liu *et al.*, 2012). However, little is known about how seizures affect the white matter pathways of the brain, including the optic radiations, when they are not involved in the epileptic spreading and are not the original focus of the abnormal seizure activity.

White matter pathways can be compressed and their function impaired by brain pathologies such as tumours and hydrocephalus. These pathologies, and epilepsy, can lead to highly distorted anatomies. Where surgery is required, accurate diagnosis and surgical planning is critically important to achieving successful outcomes. Since conventional clinical imaging does not currently identify the white matter pathways to an appropriate resolution to inform surgery, there is a risk of the optic radiations being unintentionally damaged during surgical procedures, leading to a loss of visual

function and impairing future development of the damaged structure. The complications rate of intracranial surgery remains high and developing a clinical imaging tool using tractography to inform surgery could reduce the morbidity rate from such neurosurgical procedures.

1.3 Understanding visual system development

Some of the most important research into the development of the visual system has been carried out on animals, as invasive studies cannot be carried out in humans for ethical reasons. Visual development models for cats and monkeys have highlighted the differences between animal groups. Yet such studies have limited usefulness as humans process visual information in a different way to animals. For example, humans have a large visual cortex, reduced optic disc and reduced optic nerve axons, while monkeys have a small visual cortex, larger optic disc and optic nerve fibres, which means that monkeys have a more detailed visual definition of received stimuli while humans have more detailed analysis and processing of the visual information (Wandell *et al.*, 2007). Moreover, the spatial organisation of the human visual cortex is different to other mammalian species.

The visual cortex was first mapped in humans by studying post-mortems of patients who had developed visual defects after injuries. Using these, and other studies, Poliak (1957) published one of the most accomplished anatomical descriptions of human and animal visual systems. Such descriptions are still valuable because few post-mortem studies of children have been performed for research purposes in recent decades.

While animal studies and dissections contribute to our understanding of the visual system in general, they are less useful for treating patients as even children with normal visual system development can have important variations in their anatomy that are not reflected in atlases (van Baarsen *et al.*, 2009). Functional tests and new anatomical imaging techniques are being developed and used to understand and treat pathologies that affect the visual system on a case-by-case basis.

1.3.1 Functional testing

Amblyopia is described as the visual loss associated with insufficient development of the visual system during the early stages of childhood (Elflein *et al.*, 2015). Children with amblyopia have been studied to identify the impact of reduced visual stimuli on

functional development (Vaegan, 1979), and similar studies for other pathologies could make similar contributions to our knowledge.

Visual function can be tested in patients using visual evoked potentials (VEPs). These are an electrical response from the central nervous system of humans or other animals as a response to visual stimuli, which can be recorded non-invasively from the skin. Standard clinical recording systems, with one to three electrodes, are already commonly used for patient examination at Great Ormond Street Hospital.

1.3.2 Imaging techniques

Magnetic resonance imaging (MRI) techniques are being developed to understand the anatomical development of the visual system. Functional MRI (fMRI) can examine the impact of visual stimuli on brain activity. However, describing individual white matter pathways has not been possible in vivo, with non-invasive techniques, until the development of diffusion tensor imaging (DTI) (Basser, 1995), which identifies abnormalities in white matter fibres, and more recently tractography (Conturo *et al.*, 1999, de Schotten *et al.*, 2011b). The mean fractional anisotropy (FA) of the DTI image is related to the directional coherence of the white matter fibres. Tractography can identify pathways on DTI images using deterministic and probabilistic tracking techniques. These can be used to segment pathways of interest, such as the optic radiations, and determine the mean FA of these pathways. They can also be used to estimate the length of the optic radiations and to identify the locations of pathways in abnormal anatomies, for example in brains with tumours or hydrocephalus. Tractography is principally a research tool at present and is not commonly available in the clinical environment.

1.4 Overview of this study

The development of the visual system through childhood is not well understood (Kier *et al.*, 2004), but efforts to address this knowledge gap are constrained by a lack of suitable non-invasive imaging techniques. For patients with abnormal visual system development or with brain pathologies that can affect the visual system, the development of new clinical imaging techniques could aid both diagnosis and surgical treatment.

Visual evoked potentials are already used clinically to investigate the brain response to visual stimuli. MRI tractography is a non-invasive imaging technique with the potential to provide important information about the visual system anatomy in patients with a variety of pathologies, but has had limited clinical use to date. Tractography requires information about the location of the optic radiations in order to find the tracts, which is more difficult for patients with highly-distorted anatomies. It is possible that VEP information could identify the ends of the optic radiations in the occipital lobe of the brain in order to improve the tractography analysis in such cases.

The aims of this study were to:

1. examine the impact of optic nerve hypoplasia and seizures on the development of the optic radiations in children using tractography;
2. assess the benefits of using VEP measurements to improve MRI tractography; and,
3. investigate how these techniques could improve the preoperative and postoperative treatment of children with brain pathologies.

1.4.1 Objectives

The primary objectives of the study were to:

1. recruit cohorts of control, ONH, seizure, tumour and hydrocephalus patients from Great Ormond Street Hospital clinics for tractography and VEP analysis (Chapter 3);
2. develop and test a robust tractography analysis route (Chapter 3);
3. understand the importance of the optic radiation location, effect of gender and scanning protocol on the tractography results (Chapter 4);
4. assess the potential benefits of using a multi-channel VEP recording system, in place of a standard clinical system, to improve the tractography analysis (Chapter 5);
5. describe the optic radiations in children with ONH using tractography (Chapter 6);
6. examine the impact of seizures, including a single episode of prolonged febrile convulsions and patients requiring anti-epileptic medicines over a long period, on the optic radiations (Chapter 7);

7. assess the benefits of tractography for improving the clinical preoperative and postoperative treatment of children with brain tumours (Chapter 8); and,
8. use VEP measurements to improve tractography of the optic radiations in hydrocephalus patients with highly-distorted anatomies (Chapter 8).

1.4.2 Academic contribution

The development of the optic radiations is characterised with MRI tractography for a larger cohort of controls, with a younger age profile, than previous studies. The number of controls under 5 years old is particularly important as this is the most sensitive period for visual development but is rarely investigated due to the difficulty in recruiting young children. The optic radiation mean FA from tractography is compared with anatomical dissection findings to identify the benefits of MRI for understanding human visual system development with age.

The impact of ONH and of seizures on the optic radiation anatomy is not known. This study uses tractography to examine these impacts on cohorts of ONH and seizure patients for the first time.

A novel technique is developed in this study that uses multi-channel VEP data to improve tractography analysis. The qualitative and quantitative impacts of this technique are examined for a cohort of control children.

Surgeons do not currently have a reliable imaging technique that gives a full description of the optic radiations in children. The clinical benefits of tractography for improving the preoperative and postoperative treatment of tumours and other intracranial lesions are assessed. The benefits of using VEP measurements to improve tractography in children with highly-distorted anatomies, in this case hydrocephalus, are tested for the first time.

1.4.3 Overview of this thesis

An appreciation of the anatomy of the visual system is required to understand some of the theories that are presented in this study. Chapter 2 examines the anatomy and considers insights from previous anatomical dissection studies, including a dissection that was performed in this study. The principles of MRI, tractography and VEPs are also examined in Chapter 2.

Patient recruitment and the MRI and tractography methodologies are discussed in Chapter 3. This chapter also considers whether tractography results from different MRI protocols are comparable.

Two control cohorts are examined using tractography in Chapter 4, in order to understand how the mean FA in the visual system changes with age and to identify possible differences between the left and right optic radiations, and between males and females. This chapter also considers whether the length of the optic radiation can be usefully measured using tractography.

The VEP recording and analysis methodologies used in this study are described in Chapter 5. The benefits of using VEPs to improve tractography analyses are qualitatively and quantitatively examined for a control cohort of adults.

Changes in the optic radiations in children with ONH are examined in Chapter 6 using tractography. A statistical analysis using the TBSS software is also used to identify particular areas of ONH brains with statistically-significant differences in mean FA.

The impacts of seizures on the visual system anatomy are evaluated in Chapter 7 using tractography. Two patient cohorts are examined, the first with patients who have had a single prolonged febrile seizure and the second with patients requiring sustained use of anti-epileptic medicines. Comparing these cohorts gives an indication of the damage caused by a single seizure incident.

The potential benefits of using tractography for preoperative and postoperative treatment in clinical neurosurgery is considered in two case studies in Chapter 8. The first uses tractography to identify optic radiations affected by a tumour and by tuberous sclerosis. The second demonstrates how VEP measurements can underpin tractography in two hydrocephalus patients with highly-distorted anatomies.

The thesis concludes with a general summary in Chapter 9. Potential future studies are also considered in that chapter.

2 UNDERSTANDING AND OBSERVING THE VISUAL SYSTEM

A comprehensive appreciation of the anatomy of the visual system is important for understanding the variations in the optic radiations between patients in preoperative planning. Knowledge of the anatomy is also required to identify the constituent structures of the visual system in the MRI images so tractography can be successfully performed. Knowledge of the distribution and processing of functional information through the visual system is required in order to interpret VEP results. This chapter describes the anatomy of the visual system and includes illustrations from a dissection that was performed as part of this study. It also examines current knowledge of the development of the visual system through childhood.

Magnetic resonance imaging (MRI) has emerged as a key tool for brain imaging. MRI, and in particular diffusion tensor imaging and tractography, are used in this study, and this chapter gives an overview of their principles, previous applications and limitations. Measuring VEPs is the other main diagnostic tool used in this study, and this is similarly examined in this chapter.

2.1 Anatomical description of the visual system

The visual system in humans has evolved from the vertebrates. It is particularly complex in comparison with most other sensory systems of the human body. The visual system has a dedicated area of the cortex, in the occipital lobe, and it is interconnected with many other areas of the nervous system. The areas linked to the visual system are not only of motor nature but have many functions involved in complex tasks such as facial recognition, alertness and language. The visual association areas and the linkage of the visual system and other complex brain connections were not part of this study so are not described here.

The white matter tracts in the brain can be neuro-anatomically divided into: (i) projection fibres, which are descending or ascending pathways arising and terminating in the cortex; (ii) commissural fibres, which connect the hemispheres; and, (iii) association fibres, which connect cortical regions within the same hemisphere (Moore *et al.,* 2011). The optic radiations belong to the projection fibre group that links the cortex with the thalamus, the brainstem and the medulla. Different tractography techniques are optimised for detecting different types of tracts. For example, deterministic tractography has been used to describe the corpus callosum (Catani *et al.*, 2002). In tracts with more variable trajectories, such as the optic radiations, probabilistic tractography might be more appropriate as it estimates the likelihood of each voxel being part of a fibre as a function of the orientation (NIH Blueprint, 2015).

A schematic of the visual system anatomy is shown in Figure 2.1. It is organised into the retina, optic nerve, optic chiasm, optic tract, lateral geniculate nucleus (LGN), optic radiations (Meyer's loop constitutes the most anterior pole of the optic radiations within the temporal lobe) and the striate cortex. Some parts of the anatomy have several different names. In this thesis, these have mostly been simplified to a single term. The following subsections describe each of these components in turn.

McGraw Hill did not grant permission for this diagram to be republished in the online version of this thesis.

Figure 2.1 The optic pathways. The dotted lines represent fibres that carry visual and pupillary afferent impulses from the left half of the visual field. From Riordan-Eva and Cunningham Jr (2011, Figure 14-2).

2.1.1 Retina

The retina is the receptor that transforms external visual information into an electrical signal that is transported by the visual system and interpreted and processed by the visual cortex. It has the shape of three quarters of a sphere and a diameter of 22 mm.

The retina can be divided into 10 layers from the outside to the inside as follows: pigmented layer; layer of rods and cones projecting into the pigment; outer limiting membrane; outer nuclear layer containing the cell bodies of the rods and cones; outer plexiform layer; inner nuclear layer; inner plexiform layer; ganglionic layer; layer of the optic nerve fibres; and, inner limiting membrane.

There are many cells involved in the reception and transformation of light into a signal impulse but the principal ones are the rods and cones. Rods function mainly in dim light and provide black-and-white vision. Cones support daytime vision and the perception of colour. The neurons and nerve fibres that conduct information for cone vision are larger and transmit information two to five times faster than the separate fibres for rod vision.

The retina is organised into the peripheral and the central retina (macula). There are approximately 100 million rods and 3 million cones. An average of 60 rods and 2 cones converge on each ganglion cell and its subsequent optic nerve fibre. The number of cones and rods converging in each ganglion cell are most numerous in the peripheral retina, where rods dominate. This area is more sensitive to weak light because of the high number of rods, which are more sensitive to light than the cones, and because 200 rods converge and are summed at each optic nerve fibre. Towards the central retina, there are only slender cones and no rods, and the number of optic nerve fibres is almost exactly equal to the number of cones. This explains the higher visual acuity in the central retina compared with the periphery. The fovea is located at the centre of the macula and is responsible for sharp central vision.

The retina spatially encodes the image to fit the limited capacity of the optic nerve that carries the information to the visual cortex. Light received from the temporal half of the visual field falls upon the nasal part of the retina and the nasal half of the visual field falls in the temporal part of the retina. From a functional perspective, it separates into the temporal retina and nasal retina within the optic nerve. The axons of the nasal halves of the optic nerve cross to the opposite sides, joining the fibres from the opposite temporal retina before forming the optic tracts described below.

2.1.2 Optic nerve

The optic nerve or the second cranial nerve is formed from all the axons from the ganglion cells of the retina (Doyon *et al.*, 2004, Alberstone, 2009). The optic stalk,

which develops into the optic nerve, is present at the seventh week of intrauterine development. The nerve consists of visual fibres, of which approximately 90% terminate in the lateral geniculate nucleus (LGN). There is disagreement in the literature about the length of the optic nerve (Wichmann and Muller-Forell, 2004) but it is generally considered to be 5–6 cm long. The optic nerve is divided into four segments on the basis of location: intraocular (0.7–1 mm), intraorbital (3 cm), intracanalicular (6–10 mm), and intracranial (10–16 mm) (Peltier *et al.*, 2006).

The myelination process in the optic nerve is complete in the third month of life (Riordan-Eva and Cunningham Jr, 2011). The myelination process of the optic nerve follows a central to periphery approach, starting from the brain. The optic nerve is myelinated up to the lamina cribrosa[1] at birth.

The separation of the temporal and the nasal portion of the fibres begin in the optic nerve as it approaches the optic chiasm (Rasmussen, 1943). The vascularisation of the optic nerve runs at the expense of the ophthalmic artery, which enters the orbit with the optic nerve.

2.1.3 Optic chiasm

The optic chiasm (also known simply as the chiasm) is located in the vicinity of the anterior wall and floor of the third ventricle. The optic chiasm is where the optic nerve fibres from the nasal halves of the retinae cross to join the fibres from the opposite temporal retinae to form the optic tracts. This is accomplished by the fibres originating from the larger nasal halves of both retina crossing and joining the respective uncrossed fibres in the contralateral optic tracts that originate from the smaller temporal retinal halves. Crossed fibres are more numerous in the optic chiasm and optic radiations than uncrossed fibres (Huttenlocher *et al.*, 1982). After passing the optic chiasm, half of the fibres in each optic tract are from one eye and the other half are from the other eye.

The vascularisation of the optic chiasm is supplied by two sources: (i) inferiorly by the superior hypophyseal arteries, which are fed by the internal carotid, posterior

[1] The lamina cribrosa is the mesh-like structure formed of collagen fibres that are connected to the scleral canal wall, where the optic nerve leaves the eye through the spaces left by these fibres.

communicating and posterior cerebral arteries; and, (ii) superiorly from branches of the anterior cerebral arteries. This collateral distribution of the blood supply makes vascular impairment very unlikely (Kidd *et al.*, 2008).

2.1.4 The optic tracts

The optic tracts link the optic chiasms with the LGNs. The optic tracts have cylindrical shapes and are composed of axons from the optic ganglion cells. They are around 5.1 mm long and 3.5 mm high, and lie in the upper anterior, parallel to the posterior cerebral artery.

The axons from the temporal retina remain ipsilateral in the optic chiasm. The axons from the nasal retina cross the chiasm and run towards the opposite optic tract, channelling information from the contralateral eye field in the LGN. Around half the axons cross and the other half remain ipsilateral (Kupfer *et al.*, 1967).

Almost all the fibres from the optic tract gather in the LGN. The axons synapse with the neurons in the LGN. The other small branch of axons (the superium brachium) passes down between the LGN and the medial geniculate nucleus, reaching the superior colliculus and the pretectal area. These axons mediate light reflexes.

Fibres from the central area and the fovea are in the upper part of the optic chiasm. Monocular fibres are in the lower part, and the remaining fibres from the binocular portions of the two nasal retinal halves are arranged in-between.

The non-decussating fibres and the decussating fibres spread all along the initial portion of the tract in an orderly way. It is thought that half of the nasal hemifield decussates at the optic chiasm in humans. This decussation is thought to be the origin of three-dimensional vision and starts 3–4 mm before reaching the chiasm itself (Rasmussen, 1943).

The fibres from the nasal half of the retina dominate the optic chiasm, meaning there is a larger number of contralateral fibres (Poliak, 1957). The anatomy of the axons, including the diameter, affects the amplitude and speed of conduction detected in VEP recordings.

2.1.5 Lateral geniculate nucleus

The LGN (also known as the lateral geniculate body) is part of the dorsolateral aspect of the thalamus. The neurons of the lateral geniculate nucleus send their axons to the optic radiations. The locations of the axons are defined during development (Yanoff *et al.*, 2009).

The LGN has a folded structure with six layers. The outer layers are larger and cover the small layers, which are located in the centre of the LGN. Some of the layers are irregular and non-continuous. All the cells within the same layer belong to the same species. Each layer receives input from only one eye: layers 2, 3 and 5 from the eye of the same side as the LGN, and layers 1, 4 and 6 from the other eye. This means that the information coming from each eye is separated in the LGN.

The three types of cell in the LGN are magnocellular, parvocellular and koniocellular, and are named according to their size from largest to smallest, respectively (Guyton and Hall, 2000). Larger and faster-conducting axons that are superficial gather into the magnocellular layers, which have been related to motion detection and low-spatial-frequency contrast sensitivity. Parvocellular axons mostly run in the centre of the optic tract, with the deepest fibres corresponding to the opposite eye, and have been related in monkeys to colour perception and high-spatial-frequency contrast sensitivity (Sanes *et al.*, 2012). Koniocellular layers modulate information from the other two layers and have two functions: (i) accurately relaying visual information from the optic tract to the visual cortex; and, (ii) serving as a gate for the signals transmitted to the visual cortex. Both signals help the LGN to highlight the visual information that is transmitted to the visual cortex (Bridge *et al.*, 2010).

The vascularisation of the lateral geniculate nucleus is carried out by the posterior choroidal artery, by the anterior choroidal artery or by the anastomosis of both (Kidd *et al.*, 2008)**.**

2.1.6 Optic radiations

Axons leaving the LGN form the optic radiation, also known as the geniculocalcarine tract, to carry information to the visual cortex. The optic radiation starts at the deep face of the LGN and ends on the occipital cortex after passing the temporal and parietal lobes. Most of the fibres gather in the V1 area, although studies of blind people have shown that there might also be projections from the LGN into V2 or V3, as they are

able to perform motor tasks in their blind field which they would not otherwise be able to do (Sherman and Guillery, 2002, Mullen *et al.*, 2010).

The distance from the tip of the anterior Meyer's loop to the tip of the calcarine sulcus is in the range of 95–114 mm (Poliak, 1957, Peltier *et al.*, 2006). The breadth of the optic radiation averages 17 mm at the level of the inferior horn but it increases in thickness along its course from the temporal lobe to the occipital pole, where it measures approximately 23 mm.

The fibres have a curved course around the temporal horn and the lateral ventricles (Izci *et al.*, 2009). The optic radiation splits into three bundles of axons:

- The anterior bundle of the optic radiation passes the temporal horn anteriorly then turns backwards, following a curved course known as Meyer's loop. A thin layer of tapetal fibres separate the lateral ventricle from the optic radiation. The fibres continue their journey to the occipital lobe, passing below the atrium and the occipital horn, until they reach the visual cortex in the region below the calcarine fissure known as the lingual gyrus (Rubino *et al.*, 2005).
- The posterior (or upper) bundle runs posteriorly, passing the atrium and posterior horn and terminating in the striate cortex located above the calcarine fissure, in an area known as the cuneus gyrus (Pujari *et al.*, 2008).
- The central bundle is directed laterally, from the LGN across the roof of the inferior horn.

The shape of the optic radiation changes dramatically from level to level, resembling either an irregular horseshoe (Meyer's loop), a triangle (the portion immediately adjacent to the LGN known as the Wernicke triangle), or a crescent with concavity facing inward (Poliak, 1957).

The optic radiation is so closely related to the other sensory pathways that it is has been described as the: "crossroad of sensory pathways" (Rasmussen, 1943). An anatomically-related sensory pathway is the auditory radiation.

The vascularisation of the optic radiations is carried out by branches of the middle cerebral arteries, which supply the superior optic radiations. The inferior optic radiations are vascularised by branches of the posterior cerebral arteries (Kidd *et al.*, 2008).

Functionally, our understanding of the retinotopic organisation of the optic radiations has remained almost unchanged since that proposed by van Buren and Baldwin (1958) from a study of visual defects following surgery. The anterior portion of fibres in the optic radiation correspond to the part of the visual field immediately adjacent to the vertical meridian. The following fibres going backwards correspond to the inferior quadrant. Ipsilateral and contralateral fibres lie laterally in the most medial and posterior portion. This theory is supported by van Baarsen *et al.* (2009), who found postoperatively that patients presented an inferior quadrant visual defect in temporal resections in cases where the posterior portion of the optic radiation was damaged. They also described how fibres that carry information from the ipsilateral visual field lay anteriorly to the contralateral and that the number of fibres from both visual fields did not extend anteriorly in the temporal lobe to the same extent, as supposed by van Buren and Baldwin (1958).

2.1.7 Primary visual cortex

The primary visual cortex extends in the superior and inferior banks of the calcarine sulcus in the posterior pole of the occipital lobe, extending into the medial wall of the correspondent hemisphere. There is one primary visual cortex in each brain hemisphere. The size varies in the range 1,400–3400 mm^2 and is approximately 2 mm thick. It is approximately equivalent to the anatomically-defined striate cortex. It is sometimes referred to as the V1 area and corresponds to Brodmann area 17. Only one third (1–2 cm) is located within the superficial occipital cortex; the majority is hidden in the depth of the calcarine fissure, and just a small portion is located in the posterolateral face of the occipital pole (Choi *et al.*, 2006). The primary visual cortex is composed of six layers. Information from the LGN that passes through the optic radiations of the ipsilateral hemisphere gathers mainly in the IV layer (Miller *et al.*, 2005).

There are other secondary visual areas located distally to the striate cortex within the occipito-temporal regions. The prestriate cortex is also called the V2, while the extrastriate cortex includes the V3, V4 and V5 areas. These integrate visual sensory information received by the primary visual cortex with other areas of the brain. They are involved in object recognition (occipito-temporal), colour perception within the contralateral hemifield (lingual and fusiform gyri, Brodmann area 4), facial

recognition (mesial occipito-temporal regions), spatial orientation, visual attention (parietal lobe) and with tasks that require the visual information to be combined with sensory modalities. Data about static and moving objects is first processed in the V1 area before being distributed to the rest of the visual areas, and tends to be activated by stimuli-based pattern recognition.

The striate cortex is arranged in columns of ocular dominance. All cells perpendicular to the cortical surface, extending throughout the 6 layers, respond preferentially to the same eye. Adjacent columns show ocular dominance to the other eye. The columns also respond better to stimuli in the same orientation. Each orientation triggers a stronger response in a slightly different column. All 180° are represented in approximately 1 mm of cortex (Newman, 1992).

The upper area in the calcarine sulcus represents the superior retinal information and therefore the inferior visual field. The ipsilateral hemiretina and the contralateral hemifield are represented at each side of the calcarine sulcus (Vanni *et al.*, 2005). For example, the left calcarine cortex corresponds to the left hemiretina of both eyes and the right hemifield of the vision. The central 15° of the visual field is thought to occupy 37% of the striate cortex (Holmes and Lister, 1916). The central 10° of vision, representing the macula, accounts for half of the surface area of the visual cortex (Smith and Richardson, 1966). The fovea is represented in the occipital cortex in the tips of the occipital lobe.

The functional connection between the LGN and the primary visual cortex is still not fully understood. While information from the LGN is known to pass into the V1 area, the proportion of each type of LGN cell that is represented in the V1 area is not known. Central vision in primates is variable among subjects, and it is thought that foveal vision or central vision is augmented in the V1 cortical area in those subjects (Van Essen *et al.*, 1984). This is not a generalised phenomenon, but it could indicate an unequal distribution of the central and peripheral vision in the visual cortex (Lavidor and Walsh, 2004).

The vascularisation of the primary visual cortex is primarily carried out by the posterior cerebral arteries, which are the main blood supply to the calcarine cortex. The occipital poles receive a double blood supply from the posterior and middle cerebral arteries.

2.2 Anatomical dissection of the visual system

Our understanding of the anatomy of the visual system is primarily based on observations from decades-old dissection studies (e.g. Poliak, 1957). A dissection of an adult visual system was performed in this study to better understand and illustrate the anatomy. The tissues were not fixed in formaldehyde[2] so the natural structure of the tissue resembled the living body as far as possible.

One area of interest to this study was the proximity of the lateral ventricles to the optic radiations. Figure 2.2 shows that the separation of the lateral ventricle wall and the optic radiations was 4–5 mm. The wall consistency was very dense.

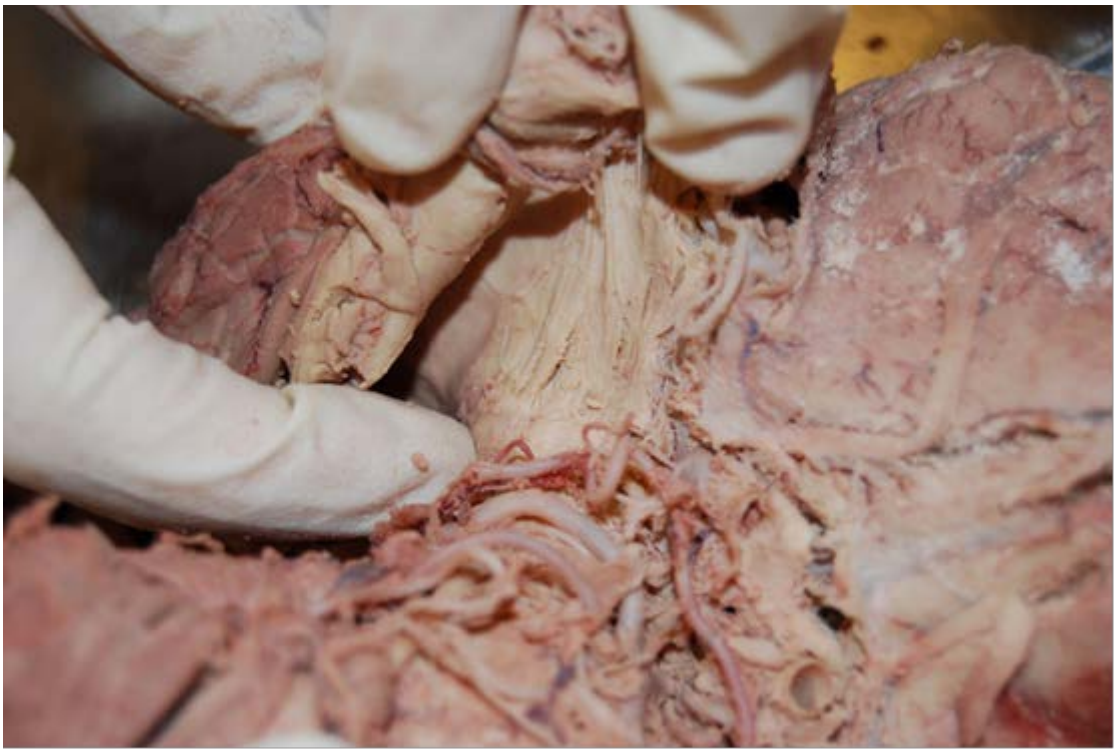

Figure 2.2 Photograph of the fibres that constitute the optic radiation at Meyer's Loop and the surrounding structures. Source: author.

[2] Formaldehyde has been used for a long time to prevent tissues from decomposing. It changes tissue in several ways, including shrinkage, so preserved anatomical structures have smaller measurements than prior to death.

The other main area of interest was the gathering of the optic radiation into the visual cortex and how the fibres were macroscopically organised. Figures 2.3 and 2.4 show the fibres gathering in the striate cortex. Grey matter can be distinguished by its grey-violet colour near the surface of the occipital cortex. White matter is also visible with different directions at the point of gathering. The transitional area is also discernible but is not as well defined as the grey and white matter.

The location of the optic radiations and the temporal lobe and its tip are shown in Figures 2.5 and 2.6. Accurately locating the tip of the optic radiation is important to enable safer epilepsy surgery to be performed.

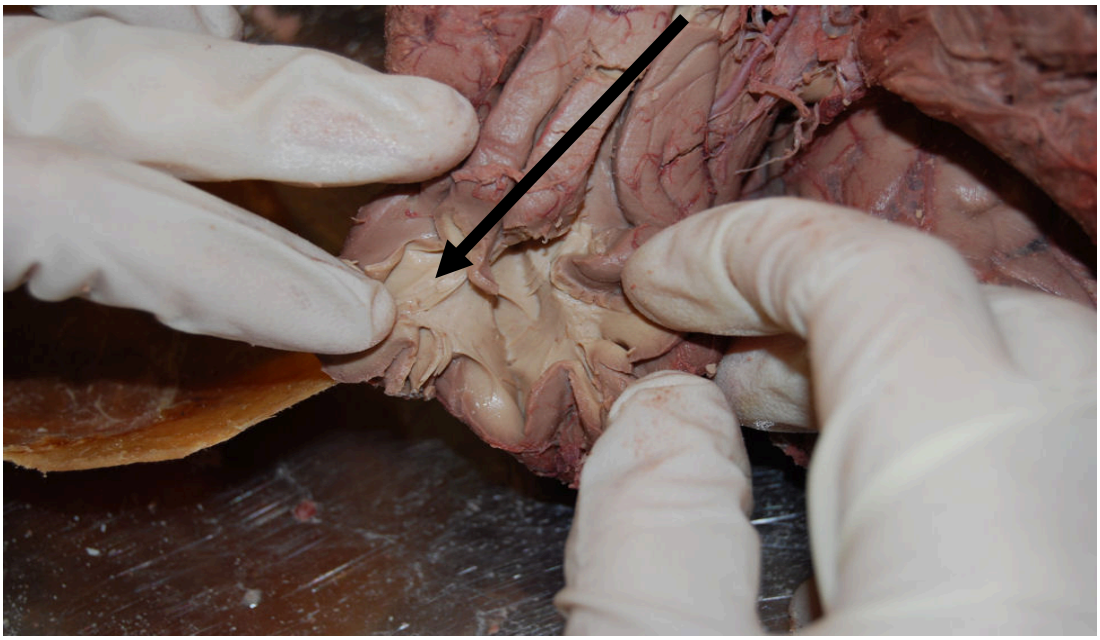

Figure 2.3 Photograph of the occipital lobe, which has been dissected on its medial aspect. The arrow shows where the white matter tracts gather into the striate cortex in different angles and directions. Source: author.

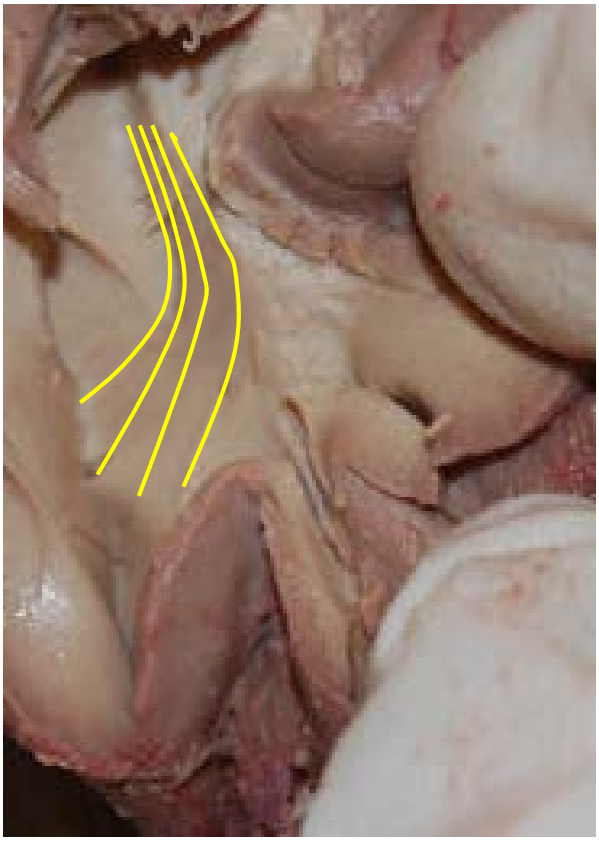

Figure 2.4 Photograph of an optic radiation with the directions highlighted. Source: author.

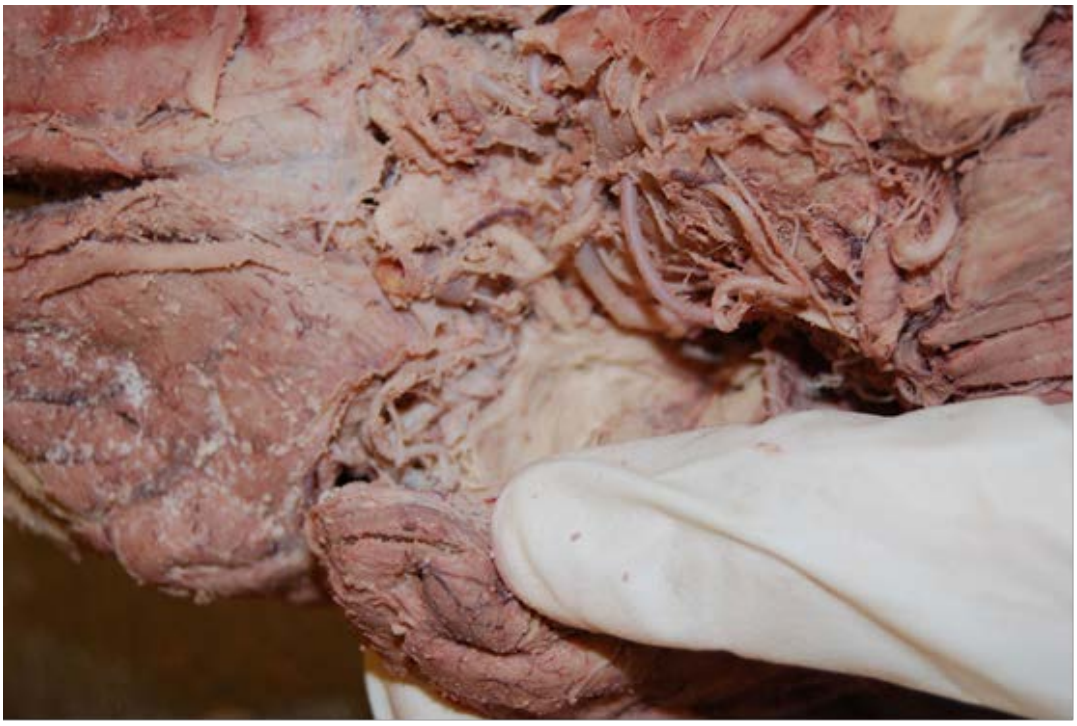

Figure 2.5 Photograph of Meyer's Loop and the tip of the temporal lobe. Source: author.

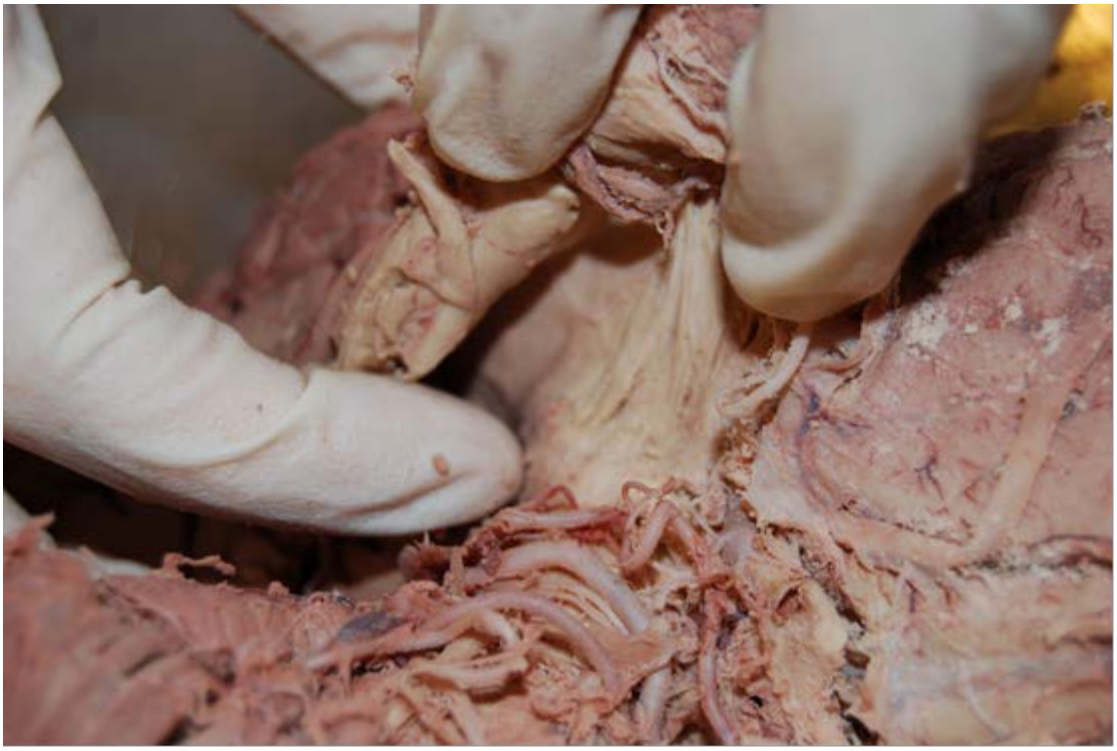

Figure 2.6 Photograph of Meyer's Loop and the lateral ventricle wall, only a few millimetres apart. Source: author.

2.3 Development of and variations in the visual system

This section examines the development of the visual system using insights from the newborn, children and adults. Developmental landmarks are important because functional testing and imaging methodologies must be adapted and the results interpreted in terms of the stage of development. Interpersonal variations are important because they limit the usefulness of atlases for surgery, which makes the development of preoperative and postoperative imaging techniques so important to achieve good surgical outcomes.

2.3.1 Development of the visual system in the newborn

At birth, the brain is approximately 25% of the size of an adult brain, measuring around 16.5 cm in diameter (Boothe *et al.*, 1985). The immaturity of the human brain is apparent not only in motor and verbal systems but in the visual system as well. The visual system lacks many abilities such as detailed vision and restricted size vision, with the newborn unable to appreciate small objects but able to respond to larger structures such as the mother's face (Teller, 1997).

The size of the eye relative to the body is larger in babies than in adults. During the first year, the eye diameter increases and reaches the size of the adult eye when the child is in adolescence. The anterior-posterior length of the eye ball is thought to greatly increase during the first year of life (Larsen, 1971). This change is one of the factors involved in the improvement of the initially-poor visual acuity.

The anterior-posterior change of the diameter of the eye and visual acuity are directly and proportionally related in the first year. The reduced size of the retina implies a reduced size of the perceived image, as well as a less detailed image, in comparison with an adult. It has been estimated that in the newborn detailed vision is approximately one third of normal adult vision (Levin *et al.*, 2011). The reduced size of the eye globe at birth means that a more potent lens is needed to compensate the small anterior-posterior axis. The lens at birth is spherical and has greater refractive power than that of healthy adults. It grows predominantly in the periphery over time, which turns it into a much flatter shape.

The pupillary distance also changes during the first weeks of life, reaching values in the range 48–63 mm. It is thought that the axial length and scleral broadening are regulated by the retina (Levin *et al.*, 2011). The mechanism is still not well understood but the retina has the capability to sense the acuity of the processed image and to then regulate the axial length by scleral broadening.

The corneal diameter increases from around 6.2 mm in the 34th week of gestation to 9.0 mm at birth and 16 mm at adulthood (Tucker *et al.*, 1992). The cornea of the newborn has a larger curvature in the periphery than in the centre, a characteristic which reverses in adulthood. The adult size of the cornea is reached at approximately 2 years of age.

Changes in the human eye after birth do not only take place anatomically, as described above, but also neurophysiologically. The optic radiations in children might be different in its relation with the pole of the temporal lobe compared to adults (van Buren and Baldwin, 1958). In very young children, they may surround the temporal tip, and once the child develops during its first months of life, due to postnatal development of the brain hemispheres, Meyer's loop reaches the anatomical distances and relations observed in adults and older children (Pfeifer, 1920). The number of dendrites and synaptic connections in the striate cortex increases from birth to reach a

peak between 4 months (Klaver *et al.*, 2011) and 2 years (Wong and Sharpe, 1999). This means that the grey and white matter density also increases during the first two 2 years (Huttenlocher and de Courten, 1987).

The accommodation at birth is fixed to a short distance. Normal neonates are hypermetropic by 2–3 dioptres, with a concomitant high prevalence of astigmatism (Wong and Sharpe, 1999). Children with normal development show some target distance accommodation after 3 months (Green *et al.*, 1980), and the accommodation approaches adult norms after 4 months (Haynes *et al.*, 1965). Although pupil reaction appears at 29–31 weeks of gestational age, blinking towards stimuli only appears at 3–4 months after birth.

2.3.2 Development of the visual system through childhood

The adult brain size is reached at 7–8 years of age.

The full length of the optic radiations has not been measured in a single study spanning the period from birth to the teenager years, and the lengths of the optic radiations in the occipital lobe and Meyer's loop are particularly poorly understood. In an MRI study, Taki *et al.* (2011a) found a linear increase in white matter volume between 4 to 20 years of age and a nonlinear decrease in grey matter in the same age period. The cortical grey matter increased until age 20.

The white matter tracts volume showed a lower increase in myelination in females than males in the temporal and occipital lobe tracts. The total increase was 12.4% between ages 4 and 22 (Taki *et al.*, 2011b). The increase in grey matter in males was also higher than in females; the female cohort had an early peak with no decrease in the post-adolescent years, which is different to other tracts such as the parietal and frontal tracts.

2.3.3 Inter-subject anatomical variations in the visual system

Significant variations in the optic radiations have been observed between adult subjects. In healthy subjects, Doyon *et al.* (2004) measured distances between the most anterior part of Meyer's loop and the temporal pole in the range 34–51 mm, with a mean of 44 mm. Meyer's loop did not reach the tip of the temporal horn in all cases.

Early studies of the optic radiations (e.g. Meyer, 1907) were based on gross dissection and concluded that the fibres go anteriorly almost 20 mm, with a few small fibres going even more anteriorly (Huttenlocher *et al.*, 1982). The distance from the tip of Meyer's loop to the tip of the temporal lobe was found to be 22–30 mm in adults (Ramon y Cajal, 1898, Traquair, 1922). The tip of Meyer's loop was located around 5–10 mm lateral to the tip of the temporal horn and amygdala (Probst, 1906: cited in Poliak 1957). The breath of the optic radiation linking the occipital lobe was found to be 17 mm and the average adult length was 105 mm (Ramon y Cajal, 1898).

Over the whole brain, females are thought to present a higher grade of myelination along the white matter tracts than males as a result of earlier development, but no significant differences have been identified within the occipital lobe in adulthood (Watson *et al.*, 2010). One theory for the difference in children is the protective effect of oestrogens, which delays the loss of grey matter in different areas of the brain. Inter-hemispheric differences in the inferior temporal gyrus were found in adults older than 19 years.

Meyer's loop cannot be defined anatomically by micro-dissection techniques alone as it is located in an area of intense and dense white matter tracts. Systems located in the area include fibres from the uncinate fasciculus, occipito-frontal fasciculus, anterior commissure, inferior thalamic peduncle, posterior thalamic peduncle, as well as temporopontine and occipitopontine fibres (Yasargil *et al.*, 2004).

2.4 Principles of MRI and DTI

Magnetic resonance imaging (MRI) is a medical imaging technique that is used to investigate human anatomy non-invasively and without exposing the subject to ionising radiation. This section summarises the basic principles of MRI and particularly diffusion tensor imaging (DTI), which is the principal MRI technique used in this study.

2.4.1 Physical principles of MRI

Almost all human tissues are rich in hydrogen protons, as the human body is largely composed of water, with the concentration changing from tissue to tissue. The hydrogen proton spins exist in one of two possible energy states when placed in the magnetic field: either parallel or antiparallel with the magnetic field. The proton spin

precesses at a frequency which can be described by the Larmor equation. If $\mathbf{B_0}$ is the vector that represents the direction of the main magnetic field, the Larmor equation gives the value of the precessional frequency as $\mathbf{B_0}$ multiplied by the gyromagnetic ratio γ:

$$\boldsymbol{\omega} = \gamma \mathbf{B_0} \qquad (2.1)$$

The difference between the two spin energy states of the protons in the magnetic field is proportional to the strength of $\mathbf{B_0}$. Tissues that are particularly rich in water, such as cerebral spinal fluid (CSF), have particularly high concentrations of hydrogen. When placed in a magnetic field, tissues with high hydrogen concentrations have higher magnetisation. This is referred to as the spin density.

An oscillating electromagnetic field (B_1) is then applied, which is perpendicular to the main magnetic field (B_0). If the radiofrequency (RF) pulse continues in time, some of the lower-energy-state protons absorb energy from the radiofrequency and move into the higher energy state (from parallel to anti-parallel). The total net magnetisation vector **M** changes orientation depending on the duration of the RF pulse. Typically, this duration allows the magnetisation to 'tip' by 90° into the transverse plane. A second, so called 180-degree RF pulse is then applied which reverses the direction of oscillation to form a signal 'echo'. If a receiving coil is placed in the B_0 plane, then the signal is recorded as the rotating magnetisation induces a current into a suitably-positioned coil.

The process by which the excited protons return to their original state is known as relaxation. It can be decomposed into two stages that happen at the same time: recovery of longitudinal magnetisation and loss of transverse magnetisation. The longitudinal magnetisation recovery is the relaxation of the z component of the magnetisation vector **M**, denoted M_z, towards its thermal equilibrium. The relaxation time T1 is the decay constant for this process, so is the time in which the magnetisation recovers 63% of its equilibrium value. The T2 is similarly the decay constant for the loss of transverse magnetisation, the component of **M** perpendicular to $\mathbf{B_0}$, which is denoted M_{xy}. T2 is generally smaller (i.e. shorter) than T1. Transverse magnetisation reflects the non-homogeneous strength of the magnetic field in all tissues, which is caused by the presence of other nuclei than hydrogen and the interactions between them. This results in different Larmor nuclide frequencies and different precession

rates. Since T2 is based on the dephasing of the x–y components of **M**, it is also known as the spin–spin relaxation time.

A series of RF pulses are used to generate an image. Two important parameters for a scan are the echo time (TE) and repetition time (TR). TE is the time between the initial RF pulse and echo sampling. TR is the time between consecutive RF pulses. TE and TR can be changed to manipulate the image contrast. Some common MRI sequences are:

- T1-weighted spin–echo: with a short TR and a short TE.
- T2-weighted spin–echo: with a long TR and a long TE. This sequence is very sensitive to paramagnetic tissues that are rich in blood and is therefore used to locate vascular malformations.
- T2-weighted dual echo: where the first echo is proton density-weighted (a mixture of T1 and T2).
- T1-FLAIR: FLAIR (Fluid Attenuated Inversion Recovery) is used to describe grey and white matter. If performed adequately, it can reveal abnormal migration or other malformations resulting in inadequate white or grey matter relations.
- T2-FLAIR: FLAIR is used to suppress signals from free water, or CSF in the central nervous system, so is used to describe white matter.

2.4.2 Diffusion imaging

Diffusion MRI maps the diffusion process of water in tissues (Le Bihan, 2014). The diffusion coefficient of water is given by the Stokes–Einstein equation:

$$D = \frac{kT}{6\pi r\eta} \qquad (2.2)$$

where k is the Boltzmann constant, T is the absolute temperature, r is the radii of the water particles and η is the water viscosity (Einstein, 1905). Since the rate of diffusion reflects interactions with macromolecules, fibres, membranes and other obstacles, diffusion MRI can identify microscopic details about tissue architecture. It is particularly important to this study because water diffusion in white matter is anisotropic, as it depends on the orientation of the tracts relative to the orientation of the scanner diffusion gradient. This anisotropy can be interpreted as a greater hindrance to water diffusion across axonal structures than along them (Clark *et al.*,

2001). This means that a tract is orientated in the direction of the fastest water diffusion, as a result of the axonal membrane and myelin sheath acting as barriers to the diffusion process.

Diffusion imaging is achieved through the application of strong pulsed magnetic field gradients. Since precession is proportional to the magnetic field strength (Equation 2.1), the protons begin to precess at different rates, which causes phase dispersion. Applying another gradient pulse with the same magnitude but in the opposite direction rephases the spins. Since this refocusing is not perfect for protons that have moved in the intervening period, the MRI signal reduces in magnitude. The signal reduction is related to the magnitude of diffusion and the degree of diffusion sensitivity (provided by the pair of applied gradients) according to the equation (Stejskal and Tanner, 1965):

$$\frac{S(TE)}{S_0} = e^{-\gamma^2 G^2 \delta^2 \left(\Delta - \frac{\delta}{3}\right) D} \quad (2.3)$$

Where *S(TE)* is the signal with the gradient, S_0 is the signal without diffusion weighting, γ is the gyromagnetic ratio, G and δ are the strength and duration of the gradient pulse, Δ is the time between two pulses and D is the diffusion coefficient. Equation 2.2 is normally simplified by gathering all of the gradient terms into a single "b factor", which depends only on the acquisition parameters, and by replacing the diffusion coefficient D with the apparent diffusion coefficient (*ADC*), which indicates that the diffusion process is not free in tissues (Le Bihan and Breton, 1985):

$$\frac{S(TE)}{S_0} = e^{-b \cdot ADC} \quad (2.4)$$

The ADC is affected by changes in the microstructure of the tissue, so can be used to detect changes in the cellular environment. This technique is called diffusion-weighted imaging (DWI), and can be used to diagnose pathologies such as acute strokes in which the ADC is reduced from normal values.

2.4.3 Diffusion tensor imaging

In white matter, the ADC is sensitive to the direction of diffusion measurement. Tissues that have a similar ADC magnitude in all directions are called isotropic. In contrast, anisotropic tissues are tissues that present different values of the ADC with changes in the diffusion gradient direction, which depend on the organised tissue microstructure. The MR image is compartmentalised into many three-dimensional

cubes, called voxels,[3] with the size of each voxel depending on the resolution of the scanner. By measuring values of the ADC according to the gradient direction, it is possible to describe the architecture of the structure enclosed within the voxel, which represents the displacement tendency of water along each axis. The direction with the highest values describes the longitudinal and directional axis of diffusion. The properties of each voxel in a diffusion tensor (DT) image are calculated by tensor mathematics from six or more diffusion-weighted acquisitions, in which each has a different orientation of the diffusion gradients, so the technique is called diffusion tensor imaging (DTI).

DTI extends diffusion MRI by producing a quantitative measure of tissue anisotropy rather than just the diffusion magnitudes. DTI was proposed in the mid-1990s and has emerged as a powerful technique for the measurement of white matter structure and orientation (Basser, 1995, Pierpaoli and Basser, 1996). White matter is particularly anisotropic, which is thought to be caused by myelin in the white matter structure acting as a barrier to water diffusion (Nilsson *et al.*, 2013). While this contributes to anisotropy in white matter, it is not the sole cause, as anisotropy is also present in other areas without myelin (Beaulieu and Allen, 1994). This characteristic explains why the rate of myelination in babies is important for DTI imaging.

Neural axon sizes vary between white matter tracts. In the corpus callosum, the axon density is around 710,000 axons/mm^2, while the optic nerve has around 170,000 axons/mm^2 (Edgar and Griffiths, 2014). The voxel dimension for the scanner used in this study is 2.5 mm, so each voxel has many axons that can have different configurations and trajectories. For this reason, the standard diffusion tensor model assumes a Gaussian distribution of water diffusion that is represented geometrically by an ellipsoid shape for voxels with high anisotropy.

A number of useful parameters are obtained from DTI. The directionally-averaged diffusion in the mean diffusivity (MD) image reflects the degree of myelin and structure in the studied voxel (Beaulieu, 2002). Its value increases when there is

[3] A voxel is a combination of "volume" and "pixel". The magnitude of the parameter on each three-dimensional axis is stored for each voxel. The coordinates of each voxel are not normally stored as the position can be inferred based on its position relative to other voxels.

structural damage in the brain, as occurs in neurodegeneration due to loss of axons. Fractional anisotropy (FA) images quantify how much the magnitude of diffusion changes with direction in space in each voxel on a scale between 0 and 1, where 0 indicates an isotropic tissue and 1 represents maximal anisotropy. CSF and grey matter have very low values of FA. Coherent bundles of white matter such as the optic radiations have FA values of around 0.4–0.5. Tissue damage or degeneration reduces the value of FA towards zero as the architecture of the tissue is altered and diffusion is less restricted and freer across all directions in space. Taken together, MD and FA are complementary measures of brain structural integrity that can be used to quantitatively characterise tissue damage in a wide range of neurological disorders and conditions. For example, demyelination and axonal damage have been assessed using axial diffusivity[4] and FA (Alexander *et al.*, 2007).

2.4.4 Limitations of DTI for describing the architecture of the human brain

The diffusion tensor model assumes that where axon diffusion through a voxel is isotropic, it can be represented by a single dominant orientation. The dominant orientation is the average of the diffusion orientations of the structural components in the voxel. Yet many voxels are likely to have crossing fibres, with different purposes, which are orientated in different directions. A related voxel resolution issue is the presence in some voxels of axons, supportive tissue and aided glial cells. Grey matter or CSF in a voxel reduces the voxel FA. One possible solution is to increase the imaging resolution, but this requires either a stronger magnet than the 1.5 T that is commonly used, or a longer scanning time than might be infeasible for clinical application. An alternative mathematical solution being developed to resolve crossing fibres is to examine diffusion in each voxel from a large number of angles (high-angular-resolution diffusion imaging, known as HARDI).

Another imaging challenge is caused by variations in the diameters of the axons in different parts of the pathways (Pierpaoli *et al.*, 1996). Changes in the angle and

[4] If water diffusion in the voxel is described in three dimensions using an ellipsoid tensor, then the axial diffusivity is the magnitude of the diffusivity along the principal axis of that ellipsoid.

direction of axons within a voxel can cause lower than expected values of mean FA and MD (Dubois *et al.*, 2008).

The configuration, trajectory and density of some white matter fibres can have distorting effects when calculating the DTI, in places where the Gaussian distribution assumption might not be appropriate. Several diffusion tensor models have been developed to compensate for these distortions. Some non-parametric DTI models instead focus on estimating the full distribution of the fibre orientation. Other non-parametric models, such the multi-tensor model, seek to discern the grade of contribution of each white fibre to the total diffusion profile.

2.5 Principles of tractography

Tractography is a further development that exploits the directional information obtained by DTI to visualise neural white matter tracts (Basser *et al.*, 2000). It can be used to assess brain connectivity and to isolate or 'segment' a particular white matter tract of interest (Catani *et al.*, 2002). Aside from invasive post-mortem examinations, tractography is a non-invasive technique available that can describe white matter tracts in a living human brain (Tuch *et al.*, 2003).

Typically, regions of interest in the brain image are defined, and an algorithm is applied that identifies all of the pathways that pass through this "seed" region. Waypoint and excluded areas can also be defined on the brain image in order to focus on the neural tracts of interest. These approaches have been used to reconstruct a wide range of well-known white matter tracts including the cortico-spinal tracts, uncinate fasciculus, fornix, corpus callosum and optic radiations. Tractography has been used to illustrate asymmetry of white matter tracts such as the arcuate fasciculus, for close reproduction of tracts isolated using classical dissection (Lawes *et al.*, 2008) and for a wide variety of clinical applications (e.g. Clark *et al.*, 2003, Powell *et al.*, 2005), to not only explain pathology but also to understand normal development.

The optic radiations have been reconstructed in a number of tractography studies (Yamamoto *et al.*, 2007), primarily for applications that are focused on this structure for neurosurgical planning (Powell *et al.*, 2005, Nilsson *et al.*, 2007). The seed region is generally defined in the vicinity of the lateral geniculate nucleus and fibres are mapped to the visual cortex. Once the tracts have been reconstructed, it is then

possible to report measures of its volume and structural integrity in terms of mean FA, mean MD and the number of streamlines.

The two principal tractography methods in use are deterministic and probabilistic tractography. These are discussed in turn below.

2.5.1 Deterministic tractography

The earliest approach to tractography was the so-called deterministic or streamline tractography method. It utilises the vector field of maximum diffusion vectors (otherwise known as the principal eigenvector for DTI). A set of 'seed' voxels are identified and the algorithm follows the direction of maximum diffusion at that point through the field subject to stopping criteria. These criteria are typically to stop tracking if FA falls below a certain threshold and if the change in angle between subsequent maximum diffusion vectors is greater than a given value. The mathematical interpretation of streamline tractography was originally published by Basser *et al.* (2000).

The main issues with deterministic tractography are: (i) the white matter structures are much more complex than that suggested by the streamlines that are identified at standard voxel resolutions; and, (ii) crossing fibres and other structures within voxels can adversely affect the reconstruction.

2.5.2 Probabilistic tractography

Probabilistic tractography attempts to address some of the issues of deterministic tractography. The aim of probabilistic tractography is to represent the uncertainty in the locations of streamlines by showing the probability of connections between each voxel that has been allocated to the same white matter pathway, throughout the image (Ciccarelli *et al.*, 2006). The principal challenge is to measure the uncertainty when calculating the fibre orientation. This is complicated because there are many fibres and many voxels to consider, and many ways of connecting each pair of adjacent voxels using different orientations. Since it is not feasible to examine all pathways, probabilistic tractography instead samples a large number of pathways to calculate the probability at each voxel.

Probabilistic tractography offers three principal advantages over deterministic tractography.

First, the ends of white matter fibres that are not thick or are angulated as they reach grey matter might be ignored by deterministic tractography if were under the FA threshold or if the pathway angle were too sharp. In probabilistic tractography, this problem is reduced as tracking can continue beyond uncertain regions. For this reason, probabilistic tractography has largely replaced deterministic tractography in the study of white matter tracts that are not thick or that have a very diverse angle of wiring when approaching grey matter, such the optic radiations and the auditory pathway in the temporal lobe.

Second, probabilistic tractography is superior at identifying tracts in areas of noise, for example close to CSF. Deterministic tractography can perform poorly in areas with high noise as crossing tracts that are not of interest to the study can distort the results. In these regions, probabilistic tractography shows a low chance of the pathways following these minor tracts, so their interference can be reduced.

Third, anisotropy in areas of white matter close to grey matter or where many gathering tracts enter the visual cortex can be incorrectly interpreted as the end of a pathway in deterministic tractography. Probabilistic tractography minimises the impact of anisotropy so tends to produce superior tract identification in these areas.

2.5.3 Limitations of DTI tractography for describing the visual system

It is not possible to distinguish between the layers of the retina using MRI tractography with a clinical sequence. This situation might change in the future as higher-resolution scans with more voxels become available. The optic nerve, optic chiasm and optic tracts can be described by tractography (Roebroeck *et al.*, 2008), but identifying crossing fibres in the optic chiasm is difficult. The central chiasm is occupied by fibres coming from the foveal area of the retina. The ventral portion of the central chiasm is linked to fibres from the lateral monocular part of the corresponding visual hemifield. A further level of complexity comes from the fibres that are identified in the optic chiasm by tractography analysis but are not part of the optic nerves. It is unclear, for example, whether the supra-optic commissures are often mistakenly identified as part of the optic chiasm due to lack of resolution. It is difficult to define the number of crossing and non-crossing fibres as the chiasm develops through childhood, using images produced within a reasonable clinical scanning time.

It is possible to map the optic radiations using DTI tractography. However, it is difficult to resolve some of the smaller and more intricate structures, such as Meyer's loop. Another challenge is to resolve the high number of crossing white matter fibres in the vicinity of the optic radiations, many of which are involved in other processes such language and hearing.

The visual cortex cannot currently be easily imaged by DTI tractography using existing clinical MRI scanners because it contains primarily grey matter. It is possible to describe the lamination of the visual cortex using high resolution MRI with long scanning times (Kleinnijenhuis *et al.*, 2012). New high-resolution MRI techniques and improved post-scan analysis might enable the in vivo description of the visual cortical area in children without sedation in the future (Chen *et al.*, 2009). Such studies have only been reported on primates, using several repeated sequences that included DTI.

2.6 Principles of VEPs

Visual evoked potentials are electrical responses from the central nervous system following visual stimuli. They are recorded non-invasively from the skin. VEPs complement MRI by examining visual function rather than anatomy.

VEPs are an important tool for studying visual system development and a useful diagnostic test for many vision pathologies. Abnormal VEP recordings can be used to identify which parts of the visual system are impaired (Brecelj *et al.*, 2008). It is believed that the development of cortical area afferents and changes in the wiring process both cause changes in the VEP wave form. During the development of the central nervous system, the greatest changes measured by the VEP take place in the first 5 years of life (Lenassi *et al.*, 2008).

2.6.1 Physical principles of VEPs

Visual evoked potentials are measured in microvolts per millisecond (mV/ms) and, due to their low amplitude, require amplification and averaging to distinguish them from the background noise created by other electrical activity in the cerebral cortex and neighbouring muscles. The peak amplitude occurs when the child is at preadolescent age. At age 6, the brain has reached 90% of the adult brain volume, but the skin, muscle and scalp are thinner than those of an adult. These tissues thicken

through adolescence and the amplitude, latency and speed of the VEP signal attenuates, while still being strong enough to measure.

A typical VEP wave is shown in Figure 2.7. The P1 is the first positive peak, occurring around 100 ms after the stimuli, and is related to the processing of visual stimuli. It is associated with activation in the posterior fusiform gyrus (Mangun *et al.*, 1997) and in the dorsal occipital areas (Woldorff *et al.*, 1997). It is thought to depend on the stimulus luminance, contrast, orientation and spatial frequency (Creel, 2013). The P1 at age 5 weeks has a peak latency of less than 200 ms, and this reduces to 100 ms at age 4. N1 or N70 is a negative component of the VEP latency recording with a peak latency at 70 ms. The origin of N1 is a postsynaptic cortical element of the pattern VEP and reflects visual processes related to spatial correction (Felice Ghilardi *et al.*, 1991). N2 or N140 is a variable negative component of the VEP latency recording with a peak latency at 140 msec. The amplitudes of the N1 and N2 peaks are related to levels of attention (Haider *et al.*, 1964).

The child population has more ipsilateral–contralateral inequalities in the VEP amplitude than the adult population, which could be caused by the presence of a different number of fibres (Barett *et al.*, 1976). This fibre discrepancy is caused by an anatomical difference in the number of large-diameter fibres, with decreased axon-firing thresholds produced on the contralateral side. The unequal diameter of the axons causes differences in the firing speed, which contributes to the higher amplitude of the VEP (Boon *et al.*, 2007). Once myelination is complete, the conduction velocity becomes much more equal bilaterally and the increased rate of axon firing and connections decreases the speed of conduction, producing a more symmetrical VEP recording. Figure 2.8 shows how these anatomical developments typically affect the VEP wave and particularly the shape of the P1 with age. In adults, once the wiring and myelination process is complete, any inequalities detected in the recording are due to differences in the fibre count (Gregori *et al.*, 2006) or due to inter-individual variations of the normal anatomy that affect recording. The electrodes are placed based on anatomical skull landmarks but the location of the cortex underneath can change from subject to subject (Blume *et al.*, 1974).

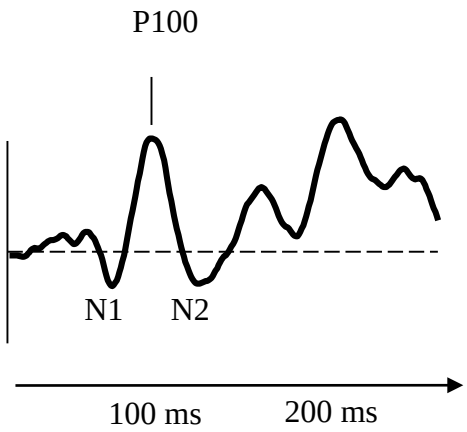

Figure 2.7 Example of a standard pattern reversal VEP. Recorded from a mid-occipital scalp electrode using a checkerboard pattern stimuli.

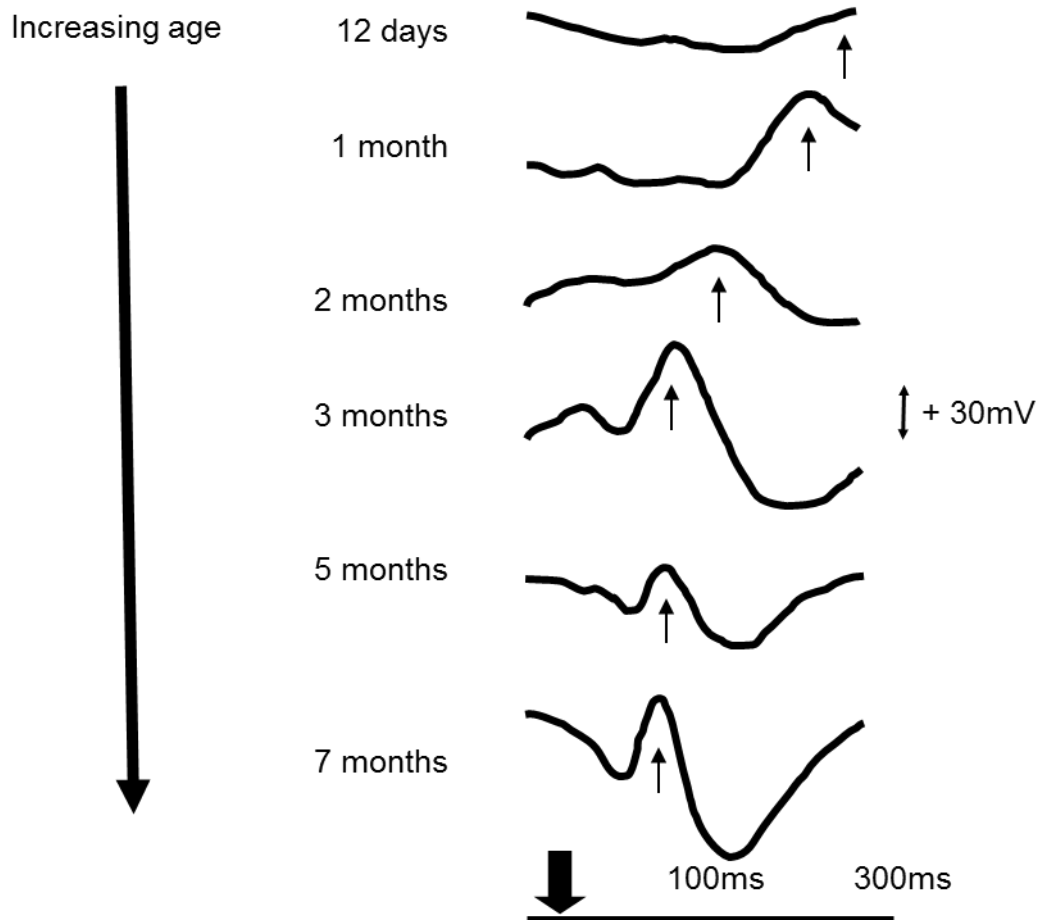

Figure 2.8 Maturation of the VEP wave with age. The P1 is highlighted with an arrow in each case. Created in part using information from Lenassi *et al.* (2008).

The physical size of the brain structures, such the length of the optic radiations, can influence the recorded speed and latency of the VEP. The volume of the brain is related to the length of the optic radiations and is also correlated to head size (Ivanovic *et al.*, 2004). The sizes of the V1, LGN and optic tract have a constant relationship throughout development, and variations between the sizes of these structures in healthy adults can cause differences in processing and receiving visual information (Andrews *et al.*, 1997). The optic disc size differs between males and females and has been linked to the number of optic nerve fibres (Miglior *et al.*, 1994). The axonal length is related to the optic disc size. Smaller optic discs are at greater risk of diseases that damage long axons, as short axons are more prone to be lost during the aging process (Jonas *et al.*, 1992).

As the head size changes, so does the length of the fibres in the optic nerve. The latency variations observed during visual assessment of a subject can be due to the different diameter or length size of the ganglionic and LGN fibres, as well as the length of the rest of the myelinated fibres involved in the visual process (Gregori *et al.*, 2006). Although lower latency is recorded in females than males, this is thought to be related to the relatively small head size of the females, and no influence has been demonstrated from hormones (Guthkelch *et al.*, 1987).

2.6.2 Flash stimuli

The flash stimuli is the test of choice in children with little or no capability of holding fixation on a pattern. It is particularly useful in the diagnosis of children with delayed maturation of the central nervous system, as the flash stimuli VEP remains unchanged, in contrast to the pattern reversal VEP which is highly abnormal, if recorded at all. For cases of cortical blindness, the flash VEP will be also abnormal.

Responses to flash stimuli originate from the cerebral cortex at all ages. They can be measured after week 26 of normal human gestation (Stanley *et al.*, 1991), with the waves becoming increasingly complex over the following 12 weeks. The flash recordings of neonates have positive and negative waves. The mass response of the full field illumination of the flash stimuli causes a quantitative response from the anterior visual pathway (Hood *et al.*, 2003). At 26 weeks, as the VEP develops, a broad negative wave predominates. This attenuates and decreases as the brain matures, with a positive wave appearing at 33 weeks of gestation. The negative wave

is believed to be recorded in the occipital visual cortex after being stimulated by the superior colliculus.

The P1 component of the flash stimuli has its source in the occipital visual cortex, after information from the LGN reaches the visual cortical area. It is believed that the positive wave recorded in the flash stimuli appears when the basilar dendrites on neurones of the visual occipital area wire in the deeper laminae (Stanley *et al.*, 1986). This wiring process is enhanced by post-birth visual stimulation (Tsuneishi, 2002). The P1 in children changes from 260 ms at birth to 100 ms at approximately at 4 months of age, and reduces to adult values when the child is 4–5 years old. This change is due to retinal development, maturation of the cortical and visual areas synaptogenesis, and myelination of the optic radiation. The latency P1 values varies depending on the visual stimuli; with flash stimuli, the peak latency time is around 110 msec. The P1 values remain almost constant until 55 years of age, but tend to be variable between adults aged over 60.

2.6.3 Pattern reversal stimuli

The most common pattern reversal stimuli is a checkerboard pattern (black and white squares), with an interchanging luminance of adjacent squares. The recorded VEP of the visual stimuli from the neural responses to the checkerboard includes the arrival of the stimuli information to the occipital visual area but does not identify any recognition or analysis of the visual information sensed by the visual receptors. The latency of the recorded wave has a peak (P1) that is more reliable and less variable than amplitude when assessing development. The peak latency is also less variable between subjects. It is used to evaluate not only neural development, but also to assess attention, cortical aging, acuity, and binocularity. Peak latency is also a useful tool when assessing vision clinically in children.

The pattern is repeatedly reversed at a given frequency, which can be modified. Other patterns can be used such as spirals, blank or colour boards. The reproducibility of the pattern onset VEPs are very good in the same individual but there can be substantial variations between subjects (Clark *et al.*, 1994).

Historically, there has been uncertainty about the origin of electrical activity from striate and non-striate areas (Clark *et al.*, 1994). Recent developments in functional MRI has enabled the origin to be more localised. The first major component of pattern

onset, C1, with an onset latency between 40–70 ms, has been localised in the primary visual area (Di Russo *et al.*, 2002). The P1 wave has also been studied with combined fMRI and VEPs using pattern onset. The first component of the P1 wave originates in the dorsal extrastriate occipital visual cortex. The second P1 component originates in the ventral extrastriate occipital cortex (Di Russo *et al.*, 2003).

2.7 Studying the optic radiations using tractography and VEPs

The optic radiations are the link between the cells of the retina, which are the visual receptors, and the visual cortex, where the visual information is processed. They are important for several reasons:

- Most visual information gathered in the LGN is transmitted by the optic radiations to the visual cortex.
- The optic radiations are frequently affected by surgical intervention for tumour and epilepsy pathologies.
- There are many crossing white matter fibres in the vicinity of the optic radiations that are involved in other processes such language and hearing.

The optic radiations are of great importance for surgeons and clinicians due to the great diversity of pathologies that can affect them. The thickness and length of the optic radiations makes it possible to resolve them using tractography on DTI images from clinical MRI machines.

Translating research neuroscience methodologies to the operating theatre was an important focus of this study, which meant that using a high-power research MRI scanner would not have been appropriate (even if one had been available), and attempting to improve the scan resolution was also not an option as longer scanning times were considered unviable. This does not affect the novelty of the research – although DTI scans can be displayed on existing surgical neuronavigators, tractography cannot be performed. Moreover, the use of tractography of the optic radiations to improve surgical outcomes in children is novel.

VEPs are used clinically and are non-invasive. They can detect visual abnormalities in children at a very early stage and can be used to describe the maturation of the normally developing visual system (Gonzalez-Frankenberger *et al.*, 2008, Lenassi *et*

al., 2008). Hence VEPs were used in this study, and NeuroScan software was used to combine VEP scans and DTI data.

The most suitable alternative research technique to study the visual cortex is arguably functional MRI (fMRI) (Wiener *et al.*, 1996). fMRI has been combined previously with DTI to identify areas in the visual cortex (Sereno *et al.*, 1995) and to characterise the optic radiations in adults (Toosy *et al.*, 2004). An fMRI study could theoretically have complemented the DTI tractography performed in this study, but it was not possible to perform because it is necessary for patients to remain motionless and cooperative when awake during fMRI scans, or to be under sedation. For very young children and those with epilepsy and visual disturbances, who are generally not cooperative when awake, sedation is the only viable option (Sie *et al.*, 2001, Yu *et al.*, 2011). Ethics committee approval for this study restricted the use of sedation to patients with clinical need. This meant, for example, that the control cohort was scanned either awake (for older children), asleep, or using sedation only if an MRI was required for other pathologies not related to the brain. Moreover, while fMRI has been used for preoperative epilepsy assessment, it is expensive and its use is limited to specialist referral centres. VEPs, in contrast, can be used in all hospitals.

3 MRI, DTI AND TRACTOGRAPHY METHODOLOGIES

Subjects were recruited for this study from across Great Ormond Street Hospital (GOSH), which is a tertiary specialist referral centre for children in the UK. All of the controls and patients underwent an MRI scan to acquire diffusion tensor images (DTI). These scans were processed using bespoke software to identify visual tracts. This chapter describes the recruitment process and these analysis methodologies.

3.1 Patient recruitment

Patient recruitment is one of the most important parts of any study and a recruitment plan and process was developed from the outset. Recruitment commenced once ethics approval had been granted for the study.

Patient consent forms were customised to the age and understanding of the patients and their parents/guardians (hereafter referred to as parents). These are shown in Appendix A. The parents received both the consent form and the entire study protocol. This approach was popular and encouraged some parents to become very involved in the process. The brief information given about the principles of MRI, which included tractography images, helped the parents to understand the techniques. The parents of

all the patients were required to sign a consent form prior to their child participating in the study.

The paediatric population was divided into three groups for recruitment purposes: (i) children younger than 5 years old; (ii) from 5 to 11 years old; and, (iii) older than 11 years. Those under 5 years were given verbal information about the study. Those over 5 years with no comprehension impairments were given a special consent form that was adapted to their age. Teenagers older than 11 years old were given the full information and had the chance to sign the consent form together with their parents, if they wished.

3.1.1 Developing the scanning protocol using adult controls

A control cohort of adults was recruited first to test and improve the MRI and VEP scan protocols. Adults are generally more patient when undergoing such processes than children, which was particularly important for the multi-channel VEP scans as these are time-consuming to set up. The adult cohort was mainly composed of researchers working in GOSH with normal vision. The adults were asked to undergo a visual assessment, VEP functional scan and MRI brain scan. The purpose of the study and the risks and benefits of the tests were explained to all of the subjects. Different MRI protocols were tested on the adult cohort to identify the optimal sequence that produced a good visualisation of the optic radiations in the shortest time.

3.1.2 Scanning procedures for children

Several changes were introduced before scanning commenced in children. The MRI protocols were altered to reduce the scanning time while still attaining high quality images. This is likely to have greatly increased the number of successful scans performed by this study because undergoing tests is stressful for many children and some cannot tolerate even the clinical imaging needed for their own treatment or diagnosis. Much effort was targeted towards reducing the impact of the test, by making the test environment friendlier, interacting with the children and explaining what would happen beforehand. The ‘clinical’ environment of the hospital was minimised by having a parent in the scanner room and by the playing a film or cartoon for older children.

Ethics approval was granted by the ethics committee to scan children of all ages. For patients with ophthalmological diseases, the research scan was similar to the clinical scan. Since children do not generally like being confined to restricted environments such as an MRI machine, where movement and activity is restricted, different approaches were used to scan children of different ages.

Babies younger than one year of age are very tolerant of different environments. MRI scans were performed using the feed and wrap technique. This involves feeding the baby just minutes prior to scanning, after which it tends to fall into a deep sleep. A quiet room next to the scan was adapted for feeding, with mild lighting and soft music on request. After feeding, the baby was wrapped and ear plugs were inserted to protect the baby's ears.

Most children between 1 and 5 years of age required sedation to carry out the imaging. A few, mainly girls, were collaborative without the need for any medication. The children attended an appointment in the clinical MRI slot for sedation and DTI scans were added at the end of the test if there was sufficient time. The children were fasted by protocol up to a maximum of 4 hours before arrival, then a small dose of sedative was given by weight, following the protocol of the Department of Anaesthesia at GOSH. If the child failed to sleep or if they woke up in the middle of the clinical imaging acquisition and moved, the DTI scan was not attempted or abandoned.

Children older than 5 years of age did not require sedation for the study. Some children could not tolerate the scanning time so it was not possible to obtain DTI scans. The most difficult cohort to scan were males aged 4 to 5.5 years. Females tended to adapt better and were more cooperative than males, which is probably due to different behavioural development and better adaptation to unfamiliar environments.

Around 200 subjects were scanned in this study in total, covering a range of ophthalmologic and other diseases. Only a subset of these are examined in this thesis. Around 6 hours was required on average to recruit each patient, gain consent and perform the scans.

3.2 MRI scans

All subjects were scanned on a 1.5 Tesla Siemens Avanto MRI scanner at Great Ormond Street Hospital. Scans were acquired using a head coil for transmission and

an eight-channel phased-array coil for reception. The research imaging protocol consisted of a DTI acquisition followed by a T1-weighted volume scan (3dFLASH[5]) and then a T2-weighted Axial DESTIR scan.[6] This order reflects the importance of each scan for this study.

The scanning order for clinical and research scans was adapted to the requirements of the patient. As a rule, the research scan was carried out after the clinical scan had been completed. However, for patients with tumours and other intracranial lesions, who required a scan with contrast for clinical purposes, a different approach was adopted. The clinical scan without contrast was performed first, followed by the research scan, and the clinical scan with contrast was performed at the end. This order was chosen because it is possible that the gadolinium contrast could alter the diffusion parameters.

A skilled radiographer checked for head movement throughout the scans. The quality of the acquisition was also checked by the author during the scan for movement or other distortions that could impair the tractography analysis.

The protocol scans are compared in Table 3.1 and discussed in the following subsections. The study took place over several years and the MRI scanner received a software update during the scanning campaign. This increased the number of slices and hence the volume of the brain in the DTI 1×60 scan. The scanning time was unchanged and tests showed negligible differences in the tractography results following the upgrade. Most 1×60 scans in this study were performed after the upgrade.

[5] FLASH (Fast Low Angle SHot) MRI is a method of obtaining a rapid yet high-resolution T1 scan.

[6] T2-weighted double-echo short inversion recovery (DESTIR) scans are particularly effective for differentiating between grey and white matter.

	DTI 3×20	DTI 1×60	3dFLASH	Axial DESTIR
Scanning time	16:24	08:21	05:34	05:50
Slices	55	39/60†	176	40
Echo time TE (ms)	89	128	4.94	14 + 115
Repeat time TR (ms)	7600	7800	11	6000
Thickness (mm)	2.5	2.5	1.0	2.0
Gap	None	None	None	None
Matrix	96 × 96	96 × 96	224 × 256	245 × 384
Voxel size (mm)	2.5 × 2.5 × 2.5	2.5 × 2.5 × 2.5	1.0 × 1.0 × 1.0	0.8 × 0.8 × 2.0
FOV	240	240	256	220
Flip	n/a	n/a	15	150
Inversion time	n/a	n/a	0	130
b value (s mm^{-2})	1000	1000	n/a	n/a

Table 3.1 MRI scanning protocol for the study prior to the scanner software upgrade. None of the sequences included a gap. † The number of slices was increased from 39 to 60 for the DTI 1×60 scans following a scanner upgrade in December 2010.

3.2.1 DTI scans

There are no standard parameters for DTI protocols for either clinical or research purposes (Mukherjee *et al.*, 2008). The number of parameters that can be modified is practically limited by the type and availability of the MRI scanner and software. The choice of DTI scan was determined by trading-off the scan resolution and acquisition time. The primary area of interest was the optic radiations but the scanning time needed to delineate small structures such the LGN or the pulvinar nucleus using DTI

would have required a substantially longer scanning time that was considered unacceptable for children. Two DTI acquisitions were used by this study:

- A 20-direction scan repeated three times was used by a previous epilepsy study and some of those scans were used in this study. This scan was a single-shot spin echo planar sequence with diffusion applied in 20 non-collinear directions. An additional acquisition with no diffusion weighting was designated as the B0 image. These 21 scans were taken three times with the aim of improving the signal-to-noise ratio in post-processing. This protocol is referred to as a 3×20 scan in this thesis.
- A new 60-direction protocol was adopted by this study for some patient cohorts after the first 3×20 scans had been processed in order to improve the quality of the images and to reduce the scanning time. This was also a diffusion-weighted echo planar imaging sequence but with 60 unique diffusion-sensitising directions. Full brain coverage was acquired with 2.5 mm isotropic resolution. This protocol is referred to as a 1×60 scan in this thesis.

Increasing the number of sample directions to 60 improved the resolution of the FA and MD maps and reduced the reliance on orientation. As explained in Section 2.1, the optic radiation is a complex structure with many crossing fibres, angulated turns and with sophisticated connectivity regions (principally the LGN and the striate cortex). A greater number of white matter tracts and structures can be described, more accurately, by increasing the number of sample orientations (Landman *et al.*, 2007). While mathematical modelling has shown that at least 20 directions are required to accurately measure anisotropy in these structures, Jones (2004) concludes that 30 or more are preferable in order to accurately calculate tensor vector values and MD. Radiologists at GOSH expressed the opinion that using 60 directions might produce superior images to repeated 30-direction scans (although this has not yet been supported by statistically-significant evidence). Therefore, the decision was taken to use the 1×60 protocol for some cohorts in this study. An important side benefit was a halving of the scanning time compared to the 3×20 protocol, from 16 to 8 minutes.

For a small number of older children, it was possible to perform both 1×60 and 3×20 DTI scans. However, in most cases there was insufficient time and the choice of DTI scan was determined according to the patient cohort. Patients with epilepsy and optic nerve hypoplasia had 3×20 scans as these scans were combined with 3×20 scans from

previous studies. Controls and patients with other ailments not examined previously had 1×60 scans. The impact of using different protocols on the tractography results is examined in Section 3.5.

The b value in the clinical DTI scan should ideally be a number that multiplied by the ADC of the researched tissue achieves a value close to 1 (Mukherjee *et al.*, 2008). The ADC values of the paediatric population, particularly infants and toddlers, are higher than adults due to the longer T2 relaxation time (Neil *et al.*, 1998). The age of the controls and patients included in the study ranged from neonates to adults, but since it was preferable to maintain a homogeneous technique throughout the study, a single b value of 1000 s mm^{-2} was used for all patients. A separate image with a b value of 0 s mm^{-2} was used for the B0 so the ADC could be estimated.

3.2.2 T1 sequence

The T1 sequence was used to check that there were no anatomical abnormalities. Two control scans were rejected from the study following this check. An adult was referred to their GP and to a neurosurgeon following the detection of an invasive tumour. A teenager was diagnosed with a pituitary mass and referred to their GP. These clinical abnormalities were not detected during the pre-scanning questionnaire and examination in either case.

The T1 sequence was also required for localising anatomical landmarks to inform the tractography analyses, and for interpreting the tractography results to inform neurosurgical procedures.

3.3 MRI image processing

The DTI images must be processed before tractography can be performed. Each DTI scan underwent a series of processing steps to produce FA and MD maps of the brain.

Image processing can be split into three broad tasks. First, the DTI sequences are identified and extracted from the scanned data. Second, the images are corrected for eddy currents and the extent of the brain is identified. Third, a diffusion tensor model is fitted at each voxel and used to produce FA maps of the brain that are used for tractography analysis. Table 3.2 describes these steps in more detail.

	Step	Analysis
1	DICOM Sorting	The DICOM image files for each MRI sequence are identified and sorted using either TractoR or in-house Matlab software.
2	Basic image extraction	The basic three-dimensional MRI images are produced from the DICOM files for each MRI sequence.
3	Eddy correction	Uses the eddy correction tool of FSL, with the first B0 image as a reference.
4	Brain extraction	Uses the bet tool of FSL in iterative mode.
5	DTI fitting	Uses the dtifit tool of FSL to produce FA maps.
6	Image conversion	The images are converted to NIfTi or ANALYZE format as required by different parts of the analysis, using the fslchfiletype tool of FSL.

Table 3.2 Image processing methods used by each tractographic route.

Two different image processing routes were available for this study. The first used the TractoR and FSL software suite (Clayden *et al.*, 2011) while the second also used FSL tools but sorted and extracted the images (steps 1 and 2 in Table 3.2) using in-house software written in Matlab. The outputs of the two routes were compared and found to have negligible differences. Having two routes available was useful as some scans that did not follow the typical naming convention or that had other non-standard features could sometimes be processed by one of the two routes but not both.

The outputs of this processing were FA and MD maps for each patient, which were produced using the formulae described by Basser (1995) and Pierpaoli and Basser (1996).

3.4 Tractography analysis

The tracts were identified using the probabilistic Camino Diffusion MRI Toolkit software (Cook *et al.*, 2006). It was necessary to identify the seed point and waypoints for the tracts, as well as 'exclusion' areas with no visual tracts. These were selected separately for both the left and right optic radiations. This part of the analysis in

particular relies on the skill and experience of the scientist to understand the anatomy of the visual tracts, consulting the T1 scan where appropriate, and to identify accurate information for the tractography software in a consistent way for each patient.

Once the tracts had been identified, the optic radiation mean FA was calculated for each patient using a new MATLAB script. The optic radiation lengths were also estimated.

The following subsections explain these steps in more detail.

3.4.1 Placement of the ROI-LGN seed points

The region of interest (ROI) marks the starting point of the streamlines of the white matter tract. This is also known as the seed point of the streamlines. Benjamin *et al.* (2014) compared several approaches to setting seeding points and concluded that the combination of seeding points placed in different anatomical regions might be the most effective way of getting a more accurate tractographic reconstruction of the optic radiations.

Following the approach of Yogarajah *et al.* (2009a), the seed point in this study was chosen in the vicinity of the lateral geniculate nucleus (LGN), which was used as the reference point for setting the ROI. A set of linked and contiguous voxels with the highest FA in the area were selected, as shown in the example in Figure 3.1. The strategy of placing ROIs in the vicinity of the LGN has been used previously in the evaluation of babies who were preterm infants, but using only around 9 seed voxels as the brains are smaller (Bassi *et al.*, 2008). In a study of adults, Yogarajah *et al.* (2009b) used around 16 seeding points in the lateral neighbouring area of the LGN. In this study, the number of seeding points was chosen to reflect the age and the brain anatomy on a case-by-case basis.

3.4.2 Placement of the mid-optic radiation waypoint

The waypoint was identified in the mid-optic radiation and marks the area through which the white matter tract passes. On the FA image, it was identified within high-FA white matter areas of the anatomical optic radiation, as shown in Figure 3.2. The number of voxels selected for the waypoint depended on the subject. The waypoints, like the seed points, were identified in three dimensions.

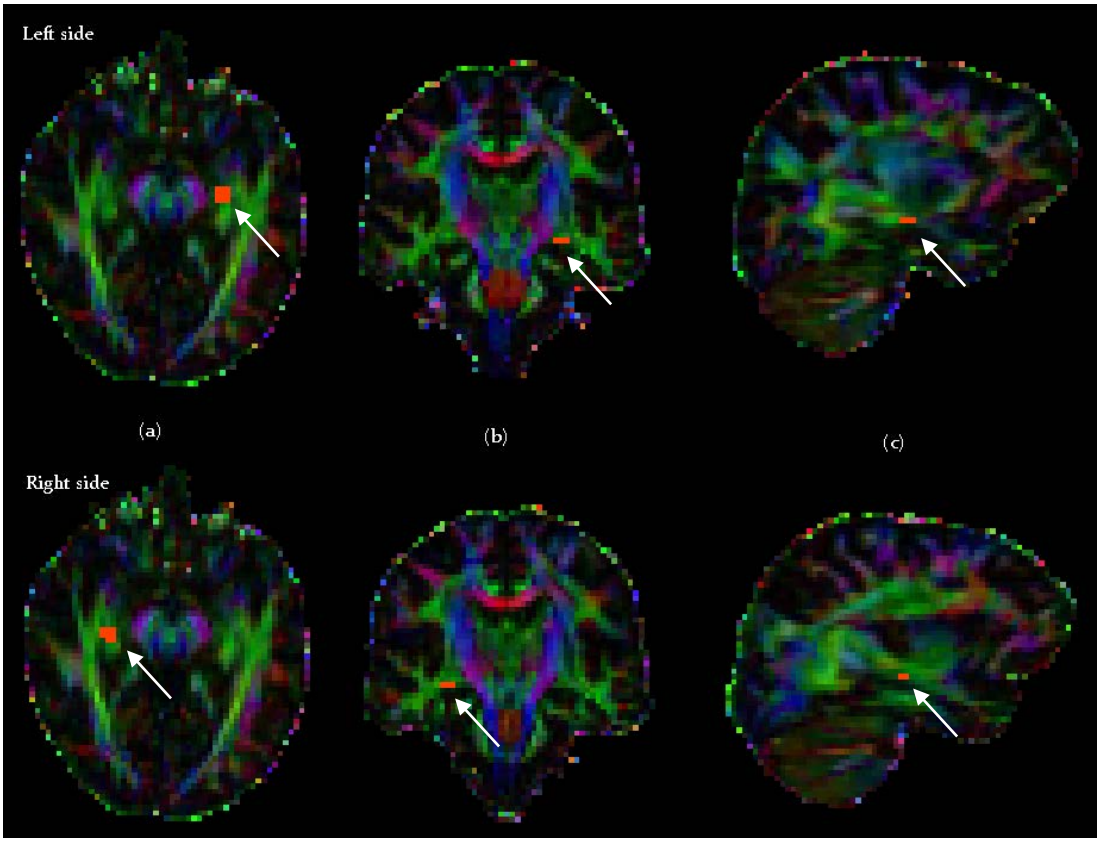

Figure 3.1 Example seed points for a patient on the left and right sides of the brain. The arrows show the locations of the seed points, coloured orange.

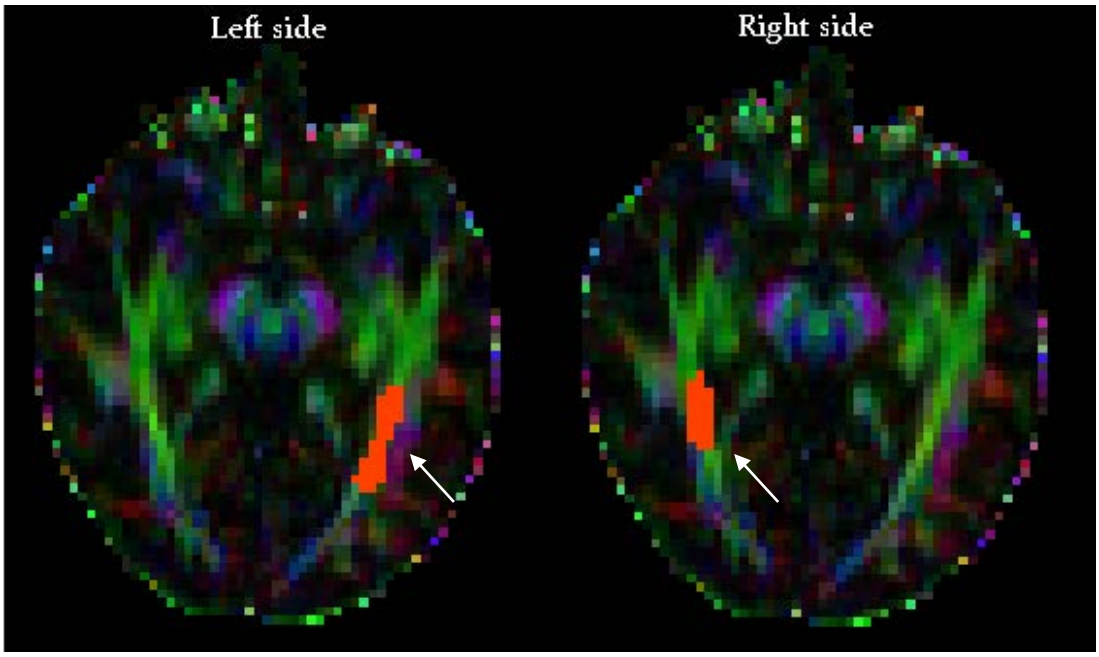

Figure 3.2 Example waypoints for a patient in the right and the left optic radiations. The arrows show the locations of the waypoints, coloured orange.

3.4.3 Exclusion ROI

The exclusion ROIs were placed in key areas of the brain so the neighbouring white matter tracts did not interfere with the reconstruction of the optic radiation itself. Laterally, the most common confounding white matter tracts that interfere with the optic radiations are the acoustic radiations, which gather in the medial geniculate nucleus. The medial geniculate nucleus is of similar size and shape to the lateral geniculate nucleus and is close to Meyer's loop. The method of angular exclusion that was adopted to exclude the acoustic radiations has previously been used by Yamamoto *et al.* (2007) with good results.

Four exclusion areas were chosen for both the left and right optic radiations, as shown in the example in Figure 3.3. These were located in the acoustic radiation, the anterior commissure (forceps major), inferior occipito-frontal fasciculus and uncinate fasciculus, and the forceps posterior, following a similar approach to Yogarajah *et al.* (2009a).

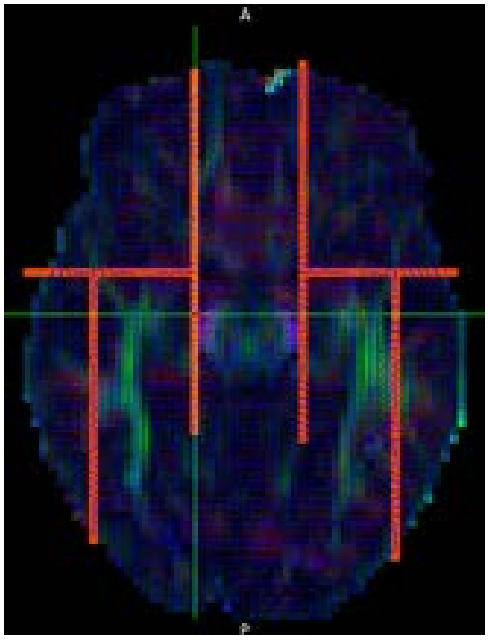

Figure 3.3 Example exclusion areas for a patient in the right and the left optic radiations. The exclusion areas are coloured orange.

3.4.4 Tract probability map

The Camino tracking software uses the seed, waypoint and exclusion information to identify the density of white matter tracts in each voxel (in this study, focusing on the visual tracts). Camino produces tractography maps using the PICo algorithm, which

reconstructs the intended structural area, voxel-by-voxel, using the value of the voxel DT eigenvector and linking it to the neighbouring voxels (Le Bihan and Johansen-Berg, 2012). The PICo algorithm was run with a minimum FA threshold of 0.1 to improve the accuracy of the tractography mapping in the transitional area of grey and white matter within the proximity of the V1 area. No angular threshold was applied, as this would impede the identification of tracts in sensitive-transitional areas such as Meyer's loop and the striate cortex.

The typical probability map is shown in Figure 3.4. These maps were carefully checked for each patient and the procedure was repeated until satisfactory results were achieved.

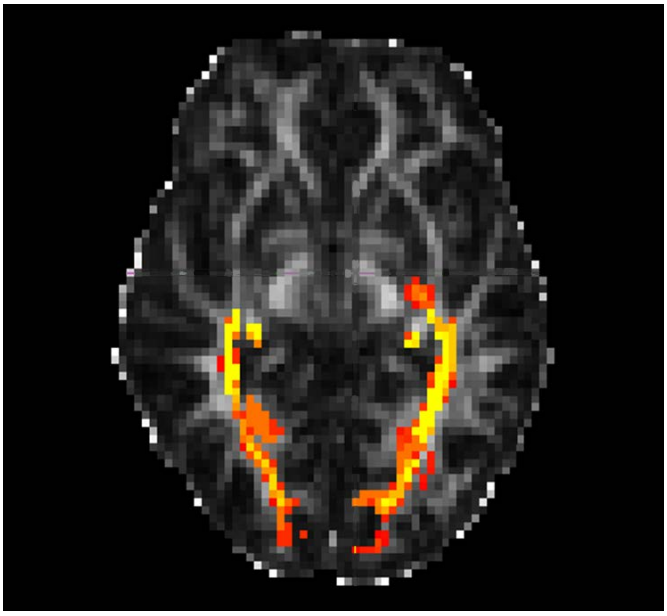

Figure 3.4 Typical tractography probability map.

3.4.5 Tract FA and MD calculation

The final step was to calculate the optic radiation mean FA and MD from the probability maps. A Matlab program was developed to perform this calculation. Following the approach of Winston *et al.* (2011), voxels with a probability lower than 10% were assumed to not contain white matter tracts and were excluded from the calculation. Two methods were tested to calculate the tract mean FA and MD:

1. The FA/MD across all of the tract voxels was averaged using a simple mean. This method was most commonly used within the research group prior to this study and is referred to here as the 'unweighted' method.

2. The FA/MD of each tract voxel was weighted according to the probability of the voxel containing white matter tracts and then averaged. This 'weighted' method was developed in this study as each voxel is likely to contain many white matter tracts.

The problem with the unweighted method was that a small number of patients with unusually wide tracts had lower mean tract FAs than their peers, as a large number of voxels with low probability and low FA (but greater than the 10% threshold) counted equally towards the tract FA as the voxels with high probability and high FA. In the weighted method, these low-probability voxels have less influence on the tract mean FA. The unweighted method is appropriate for determining the mean FA and MD of thicker fibres with almost constant high probability that are studied at the time of full development in adults. The weighted method of determining the mean FA and MD is more appropriate for children with developing brains whose water content and wiring are evolving every few months. In particular, the effect of myelination and crossing fibres is more important in children whose wiring process is still developing.

The optic radiation mean FA from the two methods is compared in Figure 3.5 for the 1×60 control cohort. The differences are mostly small but the weighted method produces a systematically-higher mean FA than the unweighted method. This trend is highlighted in Table 3.3, which shows paired t-test statistics comparing the two methods for each subject in Figure 3.5. There are statistically-significant differences in the mean FA for both the left and right optic radiations, for the full tract and for the front and rear of the tracts.[7] The differences in the mean MD are less clear with only the front having statistically-significant differences between the methods, on both sides.

The weighted method was used throughout this study. The sensitivity of the mean FA to the averaging method demonstrates the difficulty of comparing the tract mean FA results with similar data from other studies that use different tractography analysis

[7] Throughout this thesis, "front" and "rear" are used to refer to the anterior and posterior portions of the optic radiations. The terms "anterior" and "posterior" are used by some authors to describe the temporal and occipital regions of the optic radiations and by others to refer to the two areas of Meyer's loop. The terms "anterior" and "posterior" are purposely not routinely used here unless otherwise specified to avoid confusion.

methods. The type of MRI scanner and the sequence parameters used also affect the tract mean FA.

A further innovation in this study was to compare the tract mean FA for the front and rear of each tract as well as for the full tract. The aim of this division was to detect the changes produced during myelination, as the wiring process develops differently in different parts of the white matter tracts (Dubois *et al.*, 2008). The differences between front and rear were expected to be particularly significant during two periods: (i) the critical first 3 years of development (Barnea-Goraly *et al.*, 2005); and, (ii) posteriorly in the teenage years, when development of most of the other white matter tracts that are influenced by sex hormones ends (Simmonds *et al.*, 2014). The cut-off between the front and rear was located in the proximity of the parieto-occipital sulci, as shown in Figure 3.6. This is the first time that the front and rear optic radiations tracts have been divided and analysed separately for research purposes. This division was used to identify differences between the front and rear of the optic radiations during development and to compare the development in different parts of the tracts in healthy and visually impaired children.

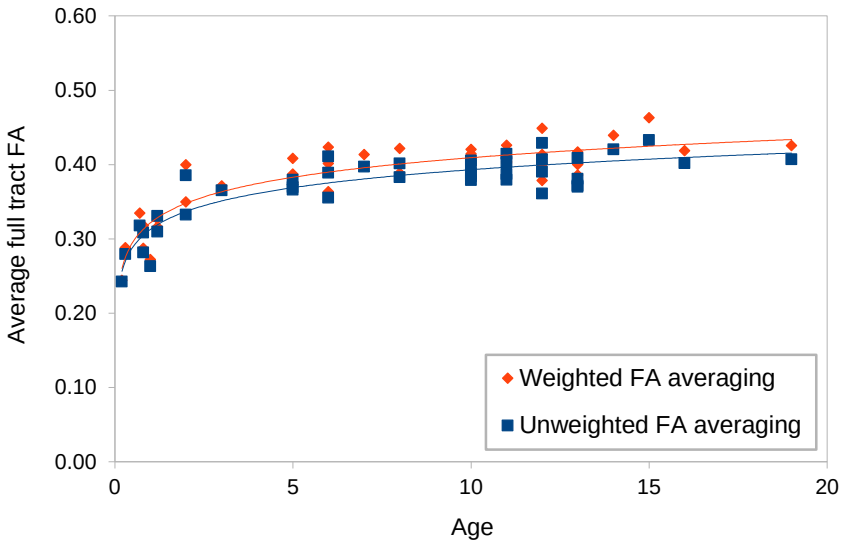

Figure 3.5 Mean FA for the unweighted and weighted averaging methods. Each point is the mean of the left and right full tract for one subject in the 1×60 control cohort of children.

	Mean FA		Mean MD	
	Left	Right	Left	Right
Full tract	<0.0001	<0.0001	<0.05	n/s
Front	<0.0001	<0.001	<0.05	<0.05
Rear	<0.0001	<0.0001	n/s	n/s

Table 3.3 Paired t-test statistics comparing the unweighted and weighted mean FA calculation methods. The comparisons are for the 1×60 control cohort of children.

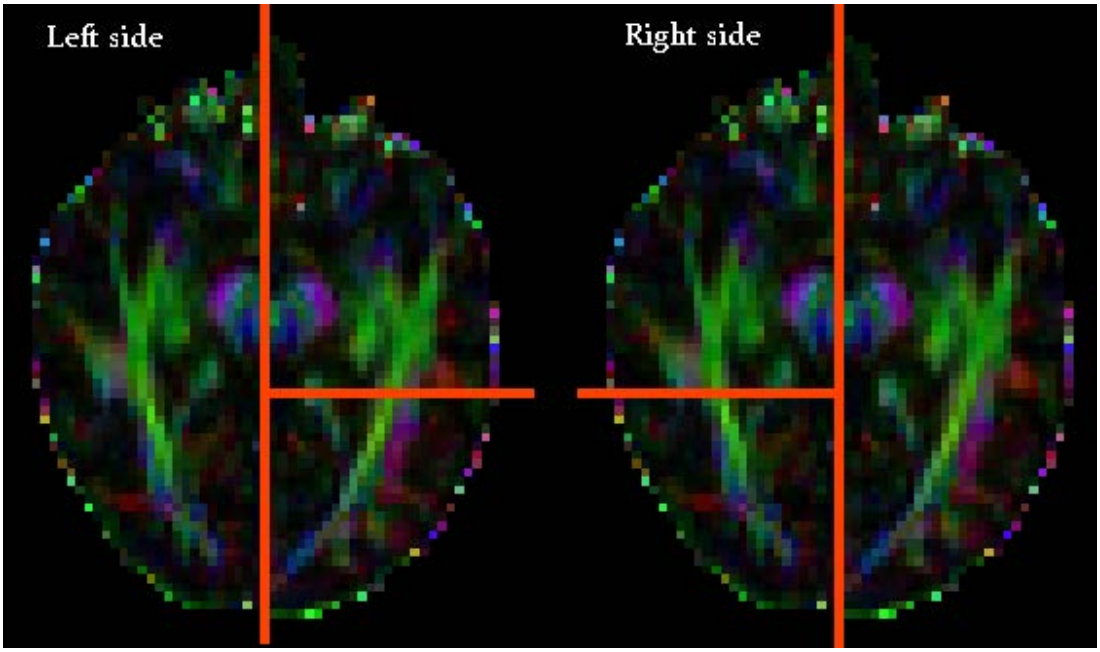

Figure 3.6 Boundaries between the front and back, and between the left and right optic radiations, for a typical brain.

3.4.6 Optic radiation length measurements

The length of the optic paths for each patient were estimated from the FA maps. The most anterior voxel of Meyer's loop was considered the anterior limit of the optic radiation. The posterior limit of the optic radiation was considered to be the last voxel reaching the striate cortex in the vicinity of the calcarine sulcus with an FA greater than 0.1. The three-dimensional coordinates of the start and end points of the tracts were obtained and the straight-line distance between these points was computed as the path length. The process was performed separately in the left and right hemispheres.

3.5 Comparison of 1×60 and 3×20 scans

Since a mixture of 1×60 and 3×20 DTI scans were obtained by this study, it was important to understand whether these could be combined for each patient cohort to increase the size of the sample. The null hypothesis for this evaluation is that the 1×60 and 3×20 scans for the child control cohort produce the same mean FA trend with age.

The cohorts used for this test are described in Section 4.2. A paired t-test cannot be used to identify the differences between the cohorts as each has a different age distribution. An ANCOVA test is instead used in order to remove age as a covariate. ANCOVA tests assume a linear relationship between the dependent variable (i.e. mean FA) and each covariate (age, in this case). Figure 3.5 shows that approximate linear relationships exist for children younger and older than 5 years, but that these relationships are different, meaning that a logarithmic function gives a better overall fit to the data. This is one reason for presenting results for these age cohorts separately in this thesis, in addition to the whole cohort. ANCOVA tests also require the relationship between the covariate and each of the cohorts being tested (e.g. 1×60 and 3×20) to be the same. The ANCOVA results presented in this thesis have undergone a non-homogeneity test for each cohort with age to confirm that this requirement has been met.

Table 3.4 shows the results of the ANCOVA tests for the left and right optic radiations, for the full, front and rear of the tracts, and according to the age the children. There are statistically-significant differences between the 1×60 and the 3×20 scans for half of the tests, particularly but not exclusively for the left optic radiation. The reason is that the 3×20 sequence produces two excitations per phase encoding step and obtains twice as much data as the 1×60 sequence, meaning it has a higher signal-to-noise ratio, which is known to bias FA. So in areas of low FA, such as grey matter, 1×60 scans have higher FA than 3×20 scans.

This means that the null hypothesis is not proven and the 1×60 and 3×20 cohorts should not be combined. In view of this finding, separate 1×60 and 3×20 comparisons were performed in this study.

	Left			Right		
	F	**p**	**Eta**	**F**	**p**	**Eta**
All patients						
Full	6.4	0.013*	0.08	3.4	0.069	0.04
Front	2.8	0.099	0.04	4.2	0.043*	0.06
Rear	8.6	0.005**	0.11	2.4	0.123	0.03
Up to 5 years						
Full	6.9	0.017*	0.27	4.1	0.057	0.18
Front	4.2	0.055	0.18	3.1	0.095	0.14
Rear	6.3	0.021*	0.25	4.6	0.045*	0.20
Over 5 years						
Full	6.0	0.018*	0.11	3.4	0.072	0.06
Front	1.7	0.200	0.03	4.4	0.041*	0.08
Rear	9.9	0.003**	0.16	1.6	0.210	0.03

Table 3.4 Comparison of 1×60 and 3×20 scan results for the control children cohort using ANCOVA tests. Results are presented for the left and right optic radiations, for the full, front and rear of the tracts, and for all children (73), those below 5 (19) and those above 5 years old (51), where the number in brackets is the degrees of freedom. There is homogeneity of regression slopes in all cases. Eta is the Partial Eta Squared, which indicates the fraction of variance in the dependent variable (mean FA) that is explained by the independent variable (cohort). Mean FA is not shown as it is not a meaningful statistic when comparing cohorts with different numbers of patients and different age distributions. * $p<0.05$. ** $p<0.01$.

3.6 Reliability of the tractography results

At present, there is no gold standard assessment method for tractography analyses (Benjamin *et al.*, 2014). The gold standard could be defined as the measurement of the optic radiation in vivo combined with posterior tractographic analysis and dissection. However, it is not possible to confirm the tractography results using dissection when studying controls in clinical research. Most tractography studies have therefore relied on a comparison of the tractography results with the expected anatomy (Nilsson *et al.*, 2007, Yogarajah *et al.*, 2009a).

The classical theory of the arrangement of the optical fibres stipulates that the ipsilateral fibres lie in a lateralised fashion within the temporal lobe (van Buren and Baldwin, 1958). The part of the visual field close to the vertical meridian is represented by the anterior fibres in the optic radiation, while the immediate part that follows carries information about the inferior quadrant of the visual field. The fibres representing the ipsilateral portion of the visual field lie laterally in the temporal lobe and the macular representation of the visual field runs medially in the optic radiation (Levin *et al.*, 2011). However, the arrangement of the peripheral and foveal vision fibres in the optic radiation is not well understood and some overlapping might occur (van Baarsen *et al.*, 2009). The differentiation of the foveal and peripheral fibres is not fully resolved by clinical-time DTI acquisitions but has been obtained in research DTI scans (Yamamoto *et al.*, 2005). Determining the location of the two bundles or loops within the optic radiation would be very useful for two reasons:

1. It is possible that the optic radiation fibres enter the visual primary cortex at particular angles and locations. Connections between the optic radiations and other circuits involved in the visual processing could not studied by means of clinical tractography at the time of this study. As tractography resolution improves, it might become possible to track the two components of the optic radiations using tractography in clinically-timed acquisitions.
2. Pathologies linked to visual defects may not be detected by means of clinical tractography as the technique is not powerful enough to differentiate small areas within the optic radiations.

3.6.1 Identifying anatomical differences caused by pathologies

Children with tumours or lesions within the optic radiations who suffer from severe impairment of the visual function generally have an abnormal anatomy. The anatomical abnormalities can sometimes be observed in the clinical MRI acquisition imaging and compared with the tractography results.

Anatomical abnormalities for many pathologies are more difficult to identify. Following the example of Ciccarelli *et al.* (2003), the DTI maps of the children scanned in this study were analysed in detail before tractography was performed. In cases where the DTI corroborated the MRI findings and the tracked optic radiation pathways followed the expected anatomical routes, any differences within the anatomical white matter tract or in the tract mean FA when compared to the control cohort were assumed to be caused by anatomical abnormalities linked to the pathological process.

3.6.2 Tractography methodology

Besseling *et al.* (2012) concluded that the reproducibility of tractography depends on the tract that is being studied and is user-dependent. Through the course of this study, it became clear that the anatomical knowledge of the researcher is a vital part of performing successful tractography because the evolving anatomical brain structure of a child is more complex than that of an adult brain. Also, there are important anatomical variations in the normal anatomy and much greater variations in patients with abnormalities that have to be identified and accounted for when performing the tractography.

4 DEVELOPMENT OF THE OPTIC RADIATIONS IN HEALTHY CONTROLS

This chapter examines the development of the optic radiations using tractography of DTI images from birth to age 40 in our control cohorts. The large sample size and the greater number of very young subjects than found in previous studies offers the opportunity to better understand the development of the visual tracts in the crucial first 5 years, and also enables a study of the differences between the left and right optic radiations and between males and females. The cohorts of children examined in this chapter are used as the control cohorts in Chapters 6 and 7.

4.1 Introduction

The development of the visual system in the first 5 years is complex and still not fully understood. Section 2.3 has already described the importance of this sensitive and critical period. The success of treatments for ophthalmological conditions depend not only on the pathology but also on the time of instauration of the disease, so it is important to know how the visual system develops throughout this period so that anomalous development can be identified at an early stage.

Myelination of the optic pathways continues during the early childhood and into the teenage years in other white matter pathways (Barnea-Goraly *et al.*, 2005). Mean FA

has been correlated to myelination, and tractography enables the dimensional in vivo anatomical portrayal of the optic radiations and other white matter structures (Le Bihan and Johansen-Berg, 2012). Tractography therefore offers a quantitative tool for understanding how the visual tracts develop with age. This is important because there are few studies of the visual system in children in the literature. Most detailed studies were performed in cadavers with the aim of describing the visual tracts (Poliak, 1957). The aim of most of these studies has been to produce atlases of the optic radiations to facilitate surgery (e.g. Meyer, 1907). While such studies are valuable for understanding the general anatomy of the optic radiations, they are less useful for understanding the development of the optic radiations, and their myelination, because they consider very few young children, so are liable to be biased by variations between controls that occur naturally. Moreover, macroscopic anatomical studies are too imprecise to be able to identify development differences in healthy controls between the left and right optic radiations or between development in males and females.

Some differences in the development of the left and right white matter tracts have been identified. Simmonds *et al.* (2014) identify differences in motor and language pathways. While Jeelani *et al.* (2010) have shown that the left and right optic radiations do not have the same length, based on anatomical scans prior to epilepsy surgery, there is no conclusive evidence that the development of the two optic radiations is different (de Schotten *et al.*, 2011b). Most studies of the optic radiations have similarly aimed to measure the length of the optic radiations. Table 4.1 lists several of these studies; Jeelani *et al.* (2010) is notable as the largest study that examines children. The distance between Meyer's loop and the tip of the temporal lobe is used as an anatomical landmark during surgical resection of the temporal lobe, or adjacent areas, in cases of epilepsy, and all of these studies aim to measure this distance to minimise the risk of visual impairment. Damage to Meyer's loop is associated with visual impairment so the development of a safe resection distance from the tip of the temporal lobe has been a priority for surgeons. Tractography allows individual mapping of the optic radiations in children and adults so could potentially be used to measure the distance between Meyer's loop and the tip of the temporal lobe for each patient, in order to improve surgical outcomes (Yogarajah *et al.*, 2009b). Tractography is likely to be particularly valuable for the many children and young

adults undergoing temporal lobectomies or hippocampal surgery, who have cortical atrophy or other structural abnormalities that distort the anatomical structure.

There is little evidence in the literature about differences in optic radiation development between males and females. White matter development relies on blood and nutrient supply, but most studies examining cerebral blood flow (CBF) have been performed on adults and few that have examined children considered sex differences, although Satterthwaite *et al.* (2014) found divergent CBF evolution between males and females. In adult studies, females presented a higher CBF than males in the visual cortex (Devous *et al.*, 1986). Males had higher magnitudes of white matter in the temporal, occipital and especially parietal areas, but females had higher magnitudes of grey matter.

This chapter examines the development of the optic radiations, from birth to age 40, in two independent cohorts of controls, using tractography. The large sample size and greater number of very young subjects than found in previous studies offers the opportunity to better understand the development of the visual tracts in the crucial first 5 years, and also enables a study of the differences between the left and right optic radiations and between sexes. The lengths of the left and right optic radiations are also measured for this cohort using tractography maps.

Study	Age range	Tissue Type	Measurements in the optic radiations	Subjects
Peltier *et al.* (2006)	Adults	Cadaver	95–114 mm	10
Rubino *et al.* (2005)	Adults	Cadaver	The mean distance to temporal pole is 25 mm (range 22–30 mm)	20
Barton *et al.* (2005)	Adults	Cadaver	Meyer's loop measures approx. 79 mm	29
Ebeling and Reulen (1988)	Adults	Cadaver	98 ± 6.2 mm	25
Jeelani *et al.* (2010)	Children	Live	No statistical relationship between tissue resected and visual defect	109

Table 4.1 Summary of studies examining the length of the optic radiations.

4.2 Description of the cohort

Two independent control cohorts of children were examined with 1×60 and 3×20 DTI scans, respectively. Tables 4.2 and 4.3 describe the 1×60 and 3×20 cohorts, respectively.

Both control cohorts have ages from approximately two months to 18 years. The 3×20 cohort has a similar number of males and females but the 1×60 cohort has around 50% more females than males. The 1×60 cohort has only one male younger than 5 years old. The principal reason for having fewer males is their lack of engagement with the scanning technique; female subjects tend to be more cooperative with clinicians than their male counterparts. Uncooperative children were withdrawn from the study, even when parental consent had been obtained, as the wellbeing of the child was of paramount concern.

The control cohort of adults is described in Table 4.4. 13 adults were included in study and all underwent only the 1×60 DTI protocol. Their ages ranged from 24 to 40 years and there were similar numbers of males and females.

4.3 Development of the optic radiations with age

The mean FA of the optic radiations in the 1×60 control cohorts is shown in Figure 4.1. The distribution is logarithmic, with a rapid increase in the first years of life followed by a steady but small increase that continues into adulthood.

The tract mean FA in the front and rear of the optic radiations is compared for the left and right sides of the 1×60 control cohorts in Figures 4.2 and 4.3, respectively. The front is the area of the optic radiation located within the temporal lobe, while the rear is the area localised within the occipital lobe. Although there are substantial variations in the front and rear tract mean FA of individual controls, these do not correspond to large differences across the whole cohort. This observation can be tested statistically by comparing the front and rear using a paired t-test. Table 4.5 shows that there are no statistically-significant differences between front and rear mean FA for either the 1×60 or 3×20 cohorts of child controls, on either optic radiation, even when the cohorts are disaggregated by sex.

Female		Male	
Code	**Age**	**Code**	**Age**
CO60-45	0.3	CO60-03	0.2
CO60-36	0.7	CO60-11	5
CO60-02	0.8	CO60-22	6
CO60-06	0.8	CO60-28	6
CO60-42	1	CO60-39	6
CO60-09	1.2	CO60-01	10
CO60-19	1.2	CO60-33	10
CO60-14	2	CO60-34	10
CO60-37	2	CO60-10	11
CO60-35	3	CO60-12	11
CO60-21	5	CO60-43	11
CO60-41	5	CO60-04	12
CO60-25	7	CO60-38	12
CO60-24	8	CO60-08	13
CO60-31	8	CO60-18	13
CO60-16	10	CO60-40	16
CO60-32	10		
CO60-23	11		
CO60-07	12		
CO60-13	12		
CO60-17	13		
CO60-44	13		
CO60-30	14		
CO60-27	15		
CO60-20	19		

Table 4.2 Gender and age (years) of the 1×60 control cohort of children.

Female		Male	
Code	**Age**	**Code**	**Age**
CY20-04	0.2	CY20-06	0.2
CY20-10	1.7	CY20-14	0.4
CO60-14	2	CY20-05	0.8
CY20-08	3	CY20-01	2
CY20-16	4	CY20-12	3
CY20-07	5	CY20-15	3
CC20-03	7	CY20-11	7
CC20-12	7	CC20-13	8
CY20-02	7	CY20-09	8
CC20-07	8	CC20-06	9
CC20-02	10	CY20-03	9
CC20-09	10	CC20-10	10
CC20-14	10	CC20-16	10
CC20-04	11	CY20-13	11
CC20-17	11	CC20-11	14
CC20-05	13	CC20-01	15
CC20-08	17	CC20-15	15
		CC20-18	18

Table 4.3 Gender and age (years) of the 3×20 control cohort of children.

Female		Male	
Code	**Age**	**Code**	**Age**
CA60-07	24	CA60-11	26
CA60-10	28	CA60-04	29
CA60-17	28	CA60-06	30
CA60-18	30	CA60-05	31
CA60-21	32	CA60-16	33
CA60-12	38	CA60-02	39
		CA60-01	40

Table 4.4 Gender and age (years) of the 1×60 control cohort of adults.

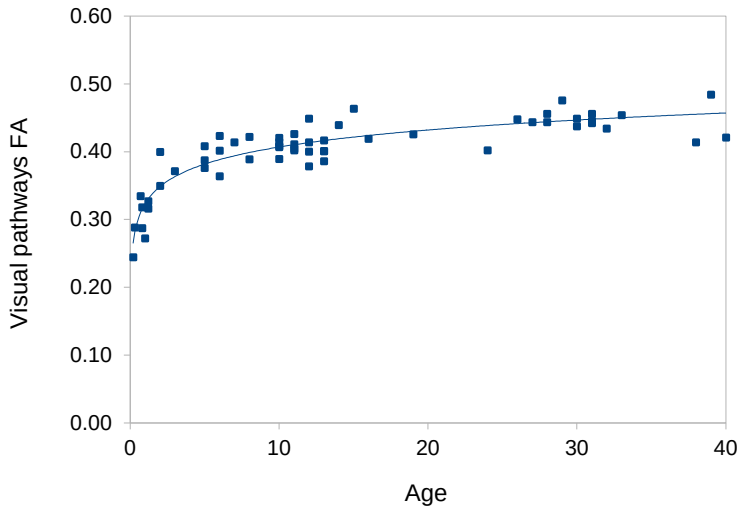

Figure 4.1 Mean FA of the optic radiations in the 1×60 child and adult control cohorts.

The tract mean FA varies between 0.24 and 0.53 and is reasonably constant for controls older than 10 years. These graphs are useful for identifying anomalies and unusual white matter distributions, for example the high rear mean FA of several young children for the left optic radiation, although this pattern appears to be a statistical anomaly in this instance. Most MRI-based studies have not considered children younger than 5 years old and have concluded that there is a linear relationship between mean FA and age, but these results demonstrate that there is much development of the visual tracts in the first 5 years that cannot be well represented using a linear function. Given the high rate of development, this is also likely to be a key period for anatomical abnormalities to develop and become apparent.

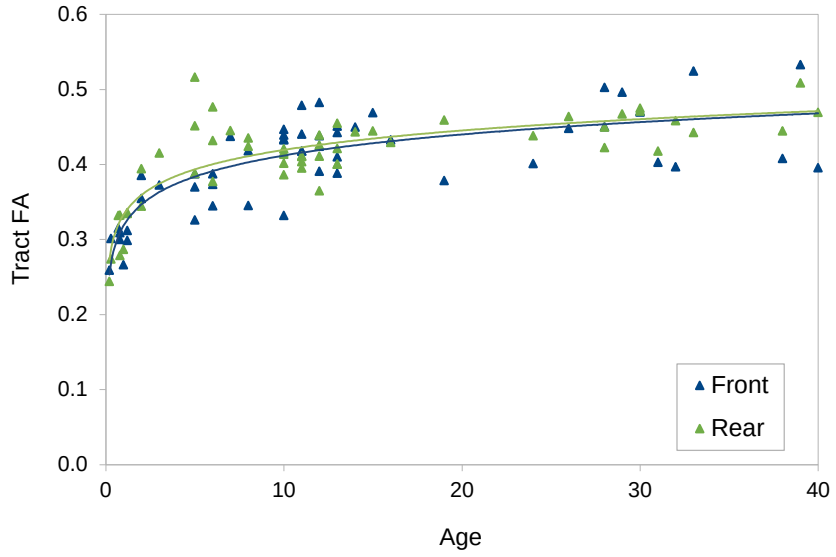

Figure 4.2 Front and rear tract mean FA in the left optic radiation. The 1×60 child and adult control cohorts are combined.

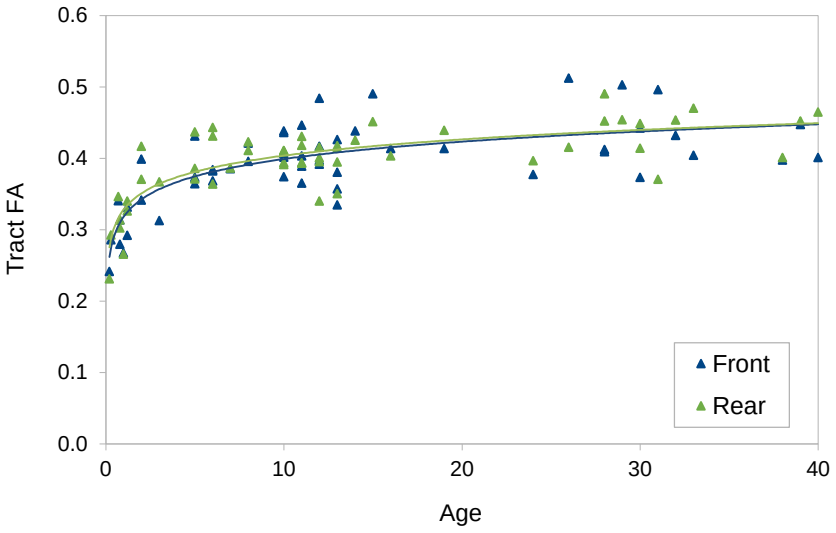

Figure 4.3 Front and rear tract mean FA in the right optic radiation. The 1×60 child and adult control cohorts are combined.

	1×60			3×20		
	Front FA	**Rear FA**	**p**	**Front FA**	**Rear FA**	**p**
All controls, both sides	0.38	0.39	0.13	0.36	0.37	0.44
Left optic radiation	0.39	0.40	0.22	0.37	0.37	0.51
Right optic radiation	0.38	0.38	0.38	0.36	0.37	0.09
Female	0.38	0.38	0.38	0.37	0.37	0.42
Male	0.39	0.41	0.20	0.36	0.36	0.74
Male, left optic radiation	0.38	0.39	0.59	0.37	0.37	0.63
Male, right optic radiation	0.37	0.37	0.18	0.37	0.38	0.36
Female, left optic radiation	0.40	0.41	0.26	0.37	0.36	0.68
Female, right optic radiation	0.38	0.40	0.90	0.35	0.36	0.15

Table 4.5 Paired t-test comparisons of the front and rear tract mean FA for the 1×60 and 3×20 control children cohorts. P values from the T-tests are presented by sex and optic radiation, as well as for the whole cohort. None of the tests show statistically-significant differences.

The tract mean MD in the front and rear of the optic radiations is compared for the left and right sides of the 1×60 control cohorts in Figures 4.4 and 4.5, respectively. The mean MD tends to reduce with age for babies but is relatively constant from age 5, reflecting the reduction in diffusivity as the volume of white matter increases through myelination. Figure 4.5 has one anomalously high value but an investigation showed that the scan had been processed correctly and the anomaly was not reflected in the patient mean FA.

Statistics describing the number of voxels in the tracts are presented in Table 4.6. Tracts are represented by more than 400 voxels on average in each optic radiation, so the tract mean FA is unlikely to be disproportionately influenced by a small number of voxels. The rear has more voxels than the front on average, with 67% and 63% of the total for the left and right optic radiations, respectively. There are, however, substantial variations between controls as reflected by the high standard deviations.

These variations do not cause a bias in the mean FA between the front and the rear because the mean FA is relatively constant throughout the tracts in most of the healthy brains in the control cohort.

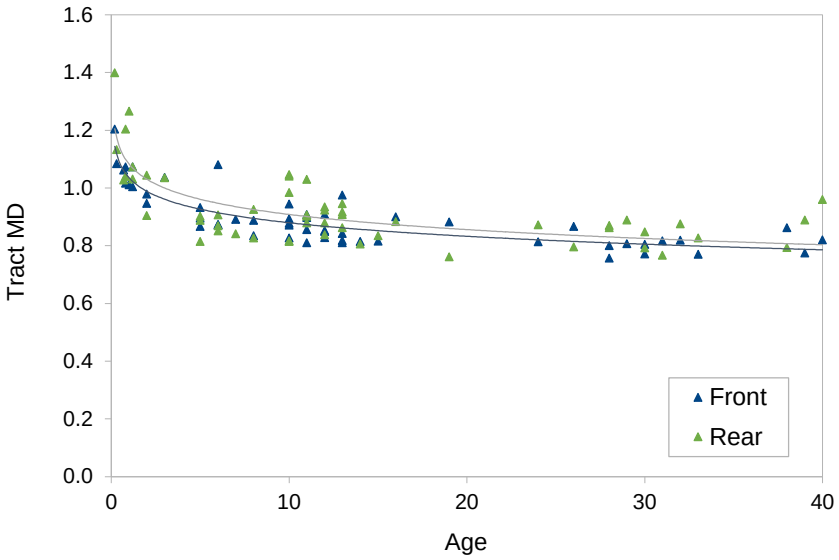

Figure 4.4 Front and rear tract mean MD in the left optic radiation. The 1×60 child and adult control cohorts are combined. All of the mean MD values have been multiplied by 1000.

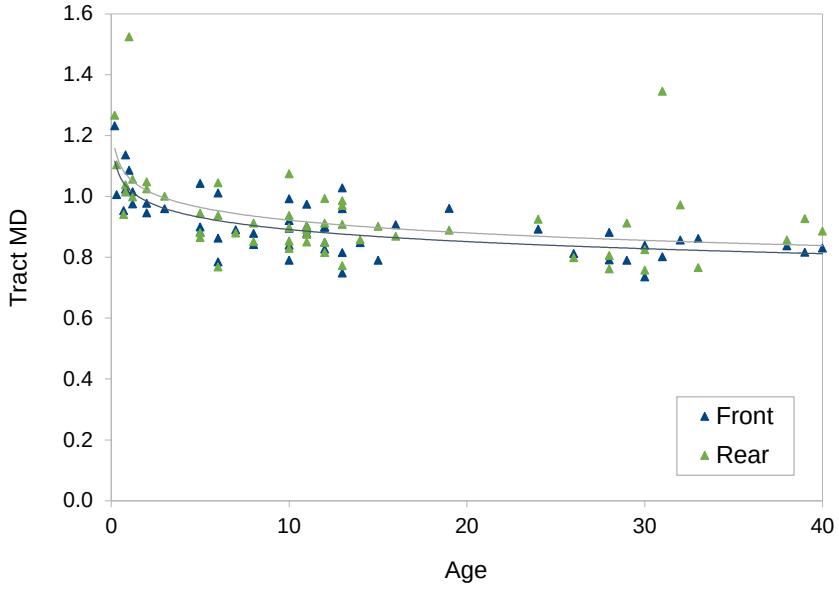

Figure 4.5 Front and rear tract mean MD in the right optic radiation. The 1×60 child and adult control cohorts are combined. All of the mean MD values have been multiplied by 1000.

	Mean ± Standard deviation
Left optic radiation total	455 ± 186
Left optic radiation front	153 ± 87
Left optic radiation rear	303 ± 126
Right optic radiation total	414 ± 209
Right optic radiation front	154 ± 86
Right optic radiation rear	260 ± 160

Table 4.6 Number of voxels representing the left and right optic radiations, for the 1×60 child control cohort.

4.4 Differences between the left and right optic radiations

This section looks for differences between the left and right optic radiations in the 1×60 and 3×20 control cohort. It has been assumed that the development of the left and right optic radiations is indistinguishable (de Schotten *et al.*, 2011a), based on studies of adults. This section complements these studies by examining cohorts including young children, with an age range from 0 to 40.

4.4.1 Control 1×60 cohort

The tract mean FAs of the left and right optic radiations are compared in Figure 4.6 for the 1×60 control cohorts of children and adults. The differences between the left and right sides are shown in Figure 4.7. This graph shows a bias towards the left optic radiation that increases slightly with age. This trend is not influenced by any clearly anomalous data points. The left and right optic radiations are further compared for the front and back of the brain in Figures 4.8 and 4.9, respectively.

The differences between left and right can be compared using a paired t-test with each control contributing one left–right pair. Table 4.7 examines mean FA differences in the 1×60 control cohort of children (i.e. excluding the adult cohort). The left mean FA is higher than the right mean FA in the rear of the optic radiation ($p<0.01$) and across the full tract ($p<0.05$). The difference is principally in the controls over 5 years of age; no statistically-significant differences are apparent for children under 5 years.

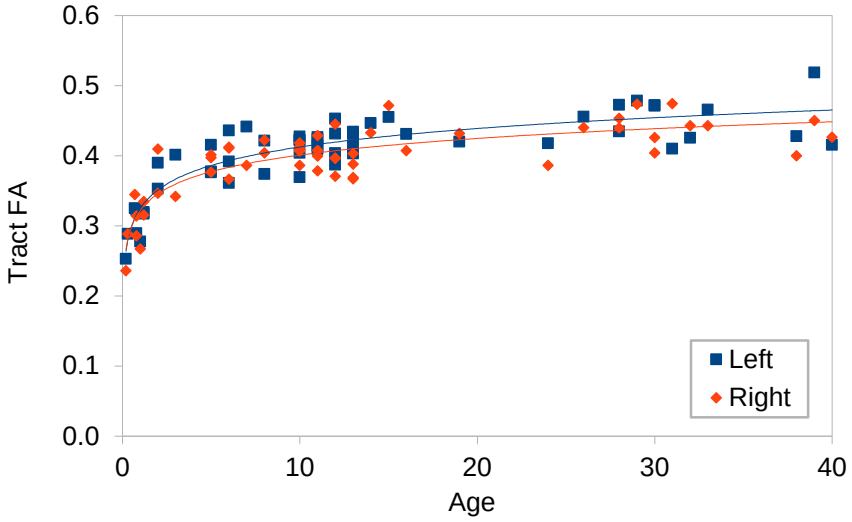

Figure 4.6 Comparison of the full tract mean FA of the left and right optic radiations for the combined 1×60 child and adult control cohorts.

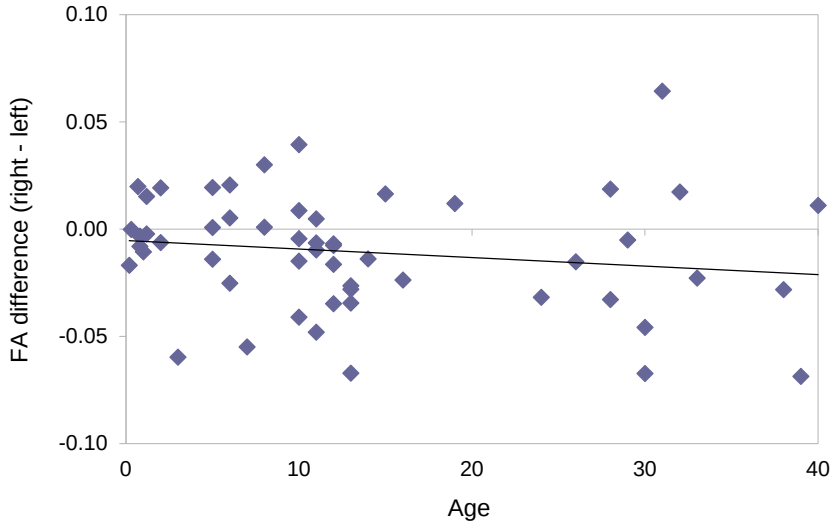

Figure 4.7 Difference in tract mean FA between the left and right optic radiations for the combined 1×60 child and adult control cohorts.

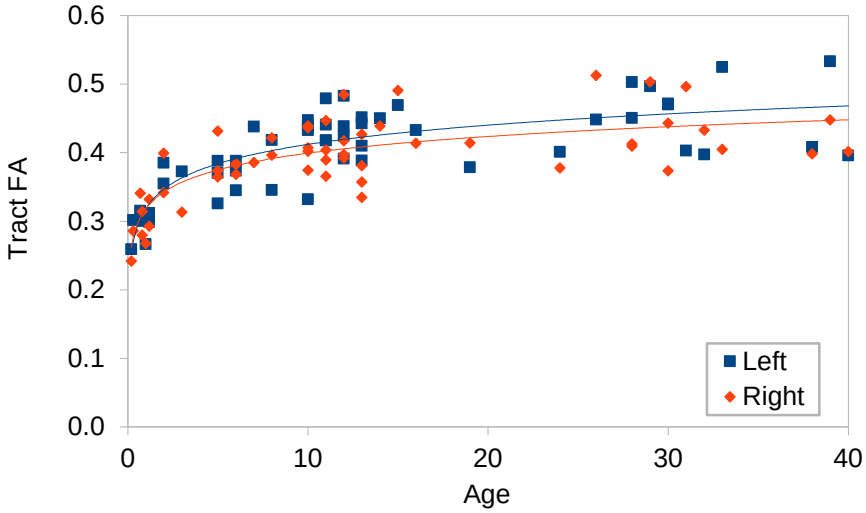

Figure 4.8 Comparison of the front tract mean FA of the left and right optic radiations. The 1×60 child and adult control cohorts are combined.

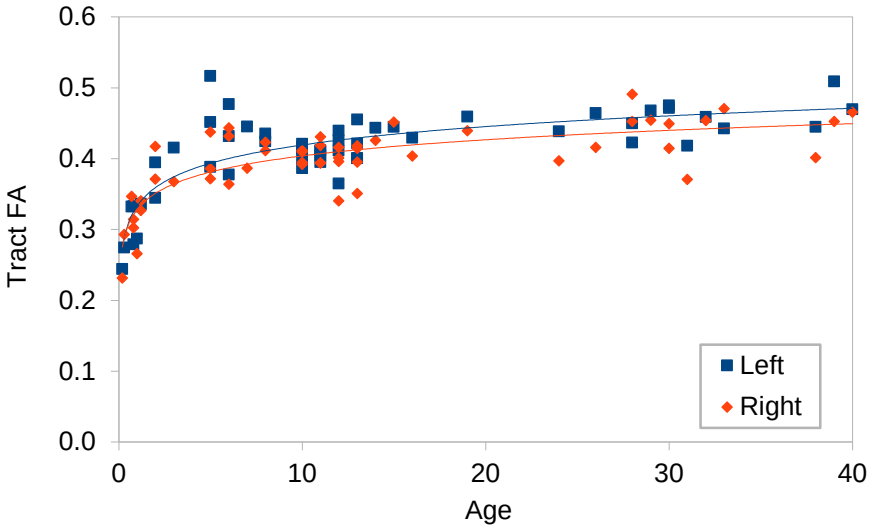

Figure 4.9 Comparison of the rear tract mean FA of the left and right optic radiations. The 1×60 child and adult control cohorts are combined.

	Left FA	Right FA	p
All controls			
Full	0.39	0.38	0.020*
Front	0.39	0.38	0.16
Rear	0.40	0.38	0.005**
Up to 5 years old			
Full	0.34	0.33	0.55
Front	0.33	0.33	0.88
Rear	0.35	0.34	0.31
Over 5 years old			
Full	0.42	0.40	0.021*
Front	0.42	0.41	0.09
Rear	0.42	0.41	0.001**

Table 4.7 Comparison of left and right optic radiation mean FA for the 1×60 control cohort of children. A paired t-test is used in each case. * p<0.05. ** p<0.01.

4.4.2 Control 3×20 cohort

The conclusions from the 1×60 cohort can be tested using the independent cohort of 3×20 controls. Figure 4.10 compares the tract mean FAs of the left and right optic radiations for this cohort. The differences between the two sides are compared using paired t-tests in Table 4.8. The differences are not statistically-significant in either the front or rear of the brain, for either older or younger children. The difference in the front of the brain is close to being statistically-significant for children over 5 years old and a larger sample might provide greater insight. There is no discernible difference between the rear tract mean FAs for the left and right optic radiations, despite the lowest p values being found in this area for the 1×60 cohort.

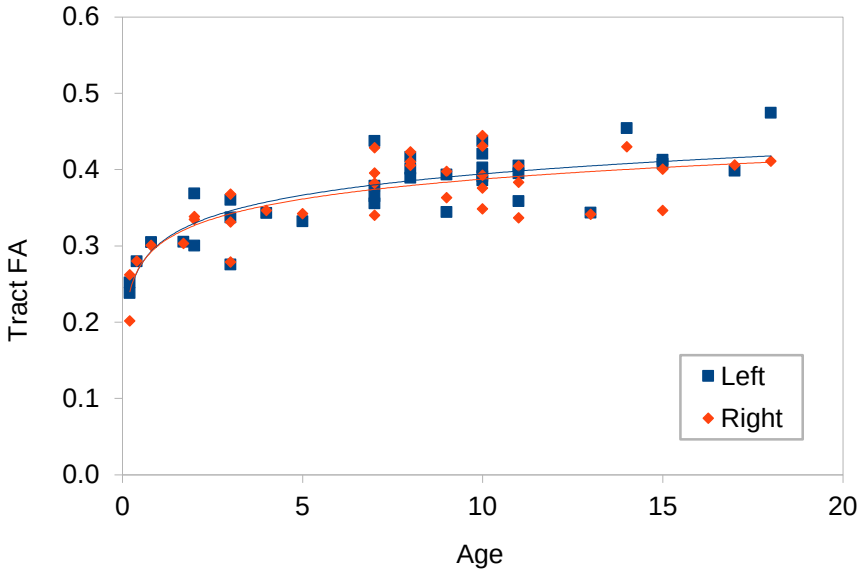

Figure 4.10 Comparison of the full tract mean FA of the left and right optic radiations for the 3×20 control cohorts.

	All controls	Up to 5 years old	Over 5 years old
Full	0.251	0.919	0.190
Front	0.064	0.767	0.056
Rear	0.861	0.701	0.958

Table 4.8 Comparison of left and right optic radiation mean FA for the 3×20 control cohort of children using paired t-tests. * p<0.05. ** p<0.01.

4.5 Differences between males and females

Brain functional development varies between sexes. Differences in language, coordination and motor skills have been intensively studied to better understand behavioural development in males and females from birth (Beltz *et al.*, 2013). It has generally been assumed, however, that visual system development is similar for both sexes with no variations between the left and right optic radiations (de Schotten *et al.*, 2011b). Yet dissection studies have shown that the left optic radiation tends to penetrate deeper into the temporal lobe and is therefore considered to be longer (Jeelani *et al.*, 2010). Moreover, the size and shape of the two hemispheres are not generally constant and equal, and males tend to have a greater amount of CSF (Gur *et al.*, 1991).

All of these insights suggest that visual development could vary between sexes, but this assumption has previously been difficult to test. This section tests the hypothesis that development of the optic radiations differs between sexes, similar to language, coordination and motor skills. The method used was to compare the tract mean FA for both sexes. Separate analyses were again performed for the 1×60 and 3×20 control cohorts.

4.5.1 Control 1×60 cohort

A paired t-test cannot be used to identify differences between males and females as each cohort has a different cohort of patients. ANCOVA is instead used in order to remove age as a covariate variable, following the procedure described in Section 3.5.

There is only one male under 9 years of age in the 1×60 cohort so the statistical comparison is only performed for those children over 5 years of age. Table 4.9 compares male and female tract mean FA using ANCOVA tests for these children. There are no statistically-significant differences between males and females in either optic radiation.

	Left			**Right**		
	F	**p**	**Eta**	**F**	**P**	**Eta**
Over 5 years						
Full	0.320	0.576	0.012	0.070	0.793	0.003
Front	0.139	0.712	0.005	1.898	0.180	0.066
Rear	0.050	0.824	0.002	1.369	0.252	0.048

Table 4.9 Comparison of male and female tract mean FA for the 1×60 control cohort of children using ANCOVA tests. Results are presented for the left and right optic radiations, for the full, front and rear of the tracts. There are 27 degrees of freedom. Eta is the Partial Eta Squared, which indicates the fraction of the variance in the mean FA that is explained by the sex. * p<0.05. ** p<0.01.

4.5.2 Control 3×20 cohort

The 3×20 control cohort has a more symmetrical distribution of young males and females so is more suitable for this comparison. Figure 4.11 compares the full tract mean FA of the two cohorts in the left optic radiation and Figure 4.12 on the right side. There are no clear trends on either side and this is reflected in the ANCOVA statistics in Table 4.10, which show no statistically-significant differences between males and females in either optic radiation.

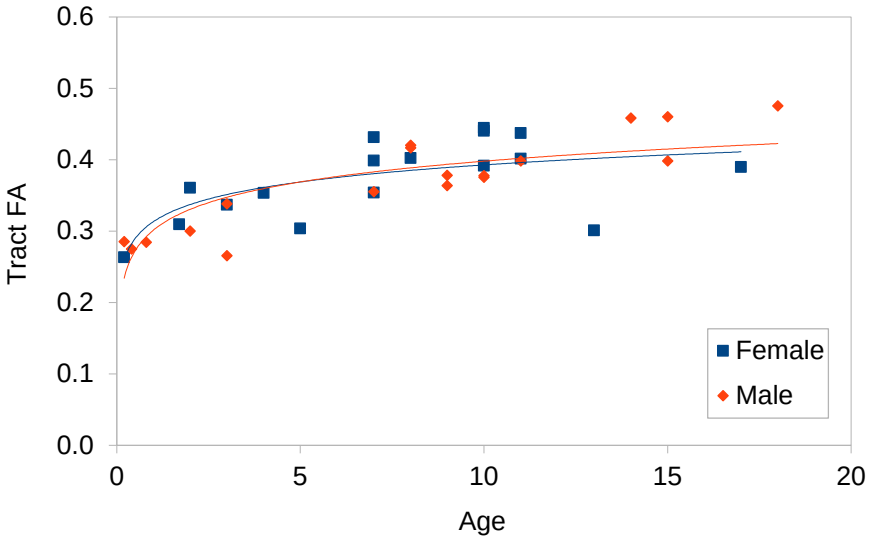

Figure 4.11 Comparison of male and female tract mean FA in the left optic radiation for the 3×20 control cohorts.

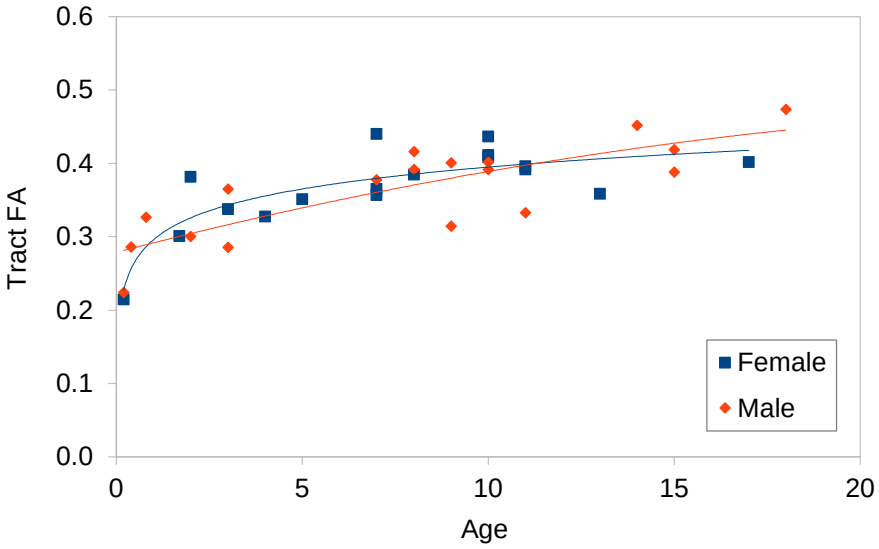

Figure 4.12 Comparison of male and female tract mean FA in the right optic radiation for the 3×20 control cohorts.

	Left			Right		
	F	**p**	**Eta**	**F**	**p**	**Eta**
All patients						
Full	0.584	0.450	0.018	3.024	0.092	0.086
Front	0.383	0.541	0.012	1.993	0.168	0.059
Rear	0.463	0.501	0.014	2.722	0.109	0.078
Up to 5 years						
Full	0.113	0.744	0.012	0.616	0.453	0.064
Front	1.164	0.309	0.115	0.733	0.414	0.075
Rear	0.010	0.922	0.001	0.478	0.507	0.050
Over 5 years						
Full	0.003	0.954	0.000	0.876	0.361	0.042
Front	0.030	0.864	0.001	0.279	0.603	0.014
Rear	0.057	0.813	0.003	0.773	0.390	0.037

Table 4.10 Comparison of male and female tract mean FA for the 3×20 control cohort of children using ANCOVA tests. Results are presented for the left and right optic radiations, for the full, front and rear of the tracts, and for all children (32), those below 5 (9) and those above 5 years old (21), where the number in brackets is the degrees of freedom. * p<0.05. ** p<0.01.

4.6 Analysis of the optic radiation length

Brain volume is used to evaluate the development of healthy children by the World Health Organisation (WHO), as it has been linked and correlated to wellbeing and to the health of the child. The head circumference is a very good indicator of the brain growth (Jaffe *et al.*, 1992) and can be used to detect, if performed correctly, several cranial and systemic pathologies associated with an abnormal deviation, relative to the normal parameters set within the local paediatric population or to the parameters set by the WHO (Courchesne *et al.*, 2003, de Onis and Woynarowska, 2010).

The head circumference has been related to brain volume (Lindley *et al.*, 1999). The circumference is easy to measure and is a not an invasive technique so is included in several hospital protocols, including at Great Ormond Street Hospital (May, 2014). Unfortunately, the brain volume and the defined length of the white matter tracts are not easily measured without employing imaging techniques in the living brain.

Knowing the volume and the length of the white matter tracts is most important in children with known deficits where certain pathologies are expected, particularly if they require surgery. Courchesne *et al.* (2003) have shown that there is an early increase in white matter in children with autism, demonstrating that changes are present at an early stage of development, although they argue that some of the variations might not be have been present at birth. It is possible that white matter tracts might be overdeveloped compared to other tracts for several pathologies, for example in autistic children.

Tractography produces maps that can be used to measure the length of the white matter tracts. These could be used to detect abnormal tract development at an early stage, which could be an early sign of pathology or developmental problems. It is important to characterise the normal development of white matter tracts, from a normalised, representative cohort for the intended population that is large enough to understand the inherent variability, so that changes caused by pathologies can be properly identified and put into context. This section examines the length of the optic radiations in child and adult controls as measured from tractography maps.

4.6.1 Measurements of optic radiation lengths from tractography

The lengths of the left and right optic radiations, as measured from the tractography maps using the procedure described in Section 3.4.6, are compared in Figure 4.13 for the 1×60 control cohorts of children and adults. Optic lengths range from 40 mm for babies to more than 100 mm for some adults. The trend lines suggest no overall difference between the left and right sides over the cohort, although there can be substantial variations for individual patients that generally exceed the mean FA variability in Figure 4.6. This finding is confirmed in Table 4.11, which shows that there are no statistically-significant differences between the left and right optic radiations lengths for any of the control cohorts in comparisons using paired t-tests.

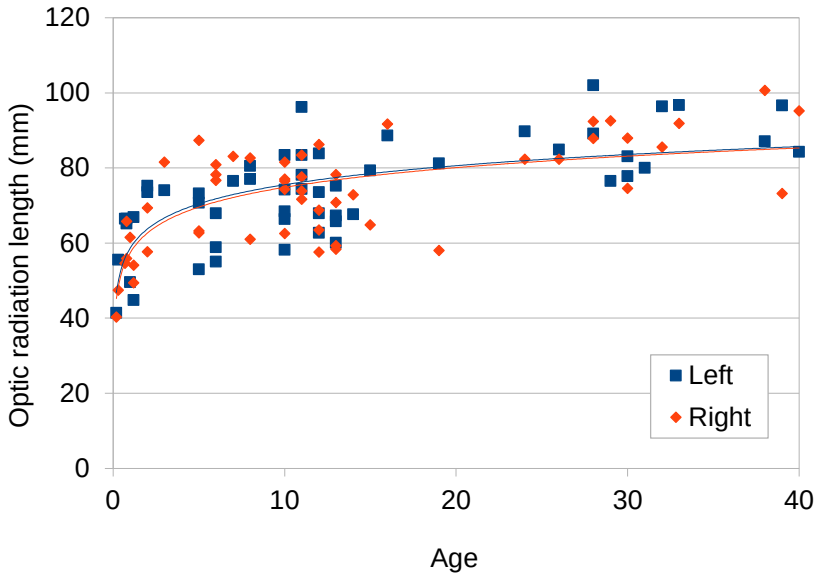

Figure 4.13 Comparison of the lengths of the left and right optic radiations for the 1×60 child and adult control cohorts.

	Adult 1×60		Child 1×60		Child 3×20	
	Left	**Right**	**Left**	**Right**	**Left**	**Right**
Mean	88.0	83.8	69.5	68.8	69.2	70.4
St dev	8.0	14.5	11.5	12.1	10.5	14.0
T-test	0.34		0.73		0.52	

Table 4.11 Left and right optic radiation length statistics for the control cohorts. The means and standard deviations (St dev) have units mm. The lengths are compared using paired t-tests. * $p<0.05$.

The lengths of the left and right optic radiations for child controls with 1×60 and 3×20 scans are compared using ANCOVA tests in Table 4.12. In contrast to the mean FA in Section 3.5, there are no statistically-significant differences between 1×60 and 3×20 scan optic lengths. It is therefore reasonable to combine the 1×60 and 3×20 datasets to create a larger cohort of 89 controls to examine optic lengths, but even this cohort does not have a statistically-significant difference between the left and right optic radiations when using a paired t-test ($p=0.96$). Using an ANCOVA test to remove the age covariate similarly did not identify a statistically-significant difference.

	Left			Right		
	F	**P**	**Eta**	**F**	**p**	**Eta**
Full	0.00	0.986	0.000	0.51	0.476	0.007

Table 4.12 Comparison of 1×60 and 3×20 optic radiation length using ANCOVA tests. Results are presented for the left and right optic radiations. There are 73 degrees of freedom. Eta is the Partial Eta Squared, which indicates the fraction of the variance in the mean FA that is explained by the sex. * p<0.05. ** p<0.01.

4.6.2 Comparison of the optic length with brain volume and mean FA

It is necessary to extract the brain from the diffusion MRI scan in order to perform tractography, which is performed using the FSL *bet* software (Section 3.3). Since the lengths of the optic radiations tend to increase with age, one might expect the optic radiation length to be related to the brain volume. Figure 4.14 shows that there is a weak relationship between the two variables (R^2=0.33) for the 1×60 control cohort, with higher variability for larger brains.

The optic radiation length is compared with the tract mean FA in Figure 4.15 for the left and right sides in the control 1×60 cohort. The correlation is stronger than between the optic radiation length and the brain volume (left R^2=0.47; right R^2=0.39) but there is an offset in the trend line with a mean FA of 0.19 at zero optic radiation length. This graph suggests that increasing brain volume is driven by an increase in the underlying microstructure to a degree.

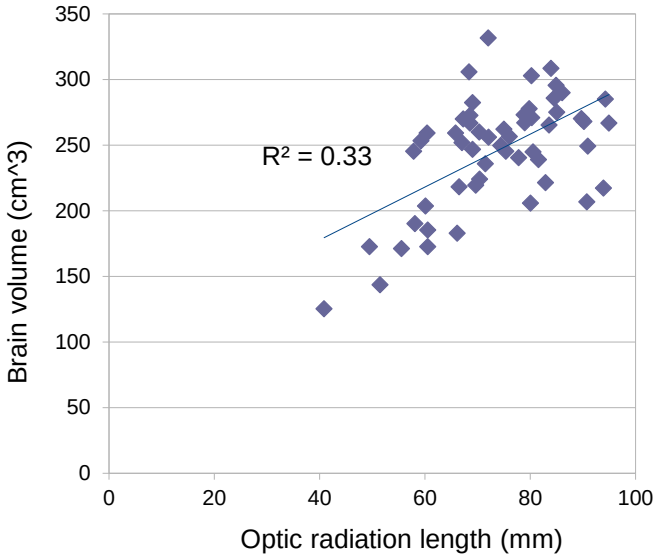

Figure 4.14 Comparison of the average optic radiation length and the brain volume for the control 1×60 cohort. The optic radiation length is the mean length of the left and right optic radiations.

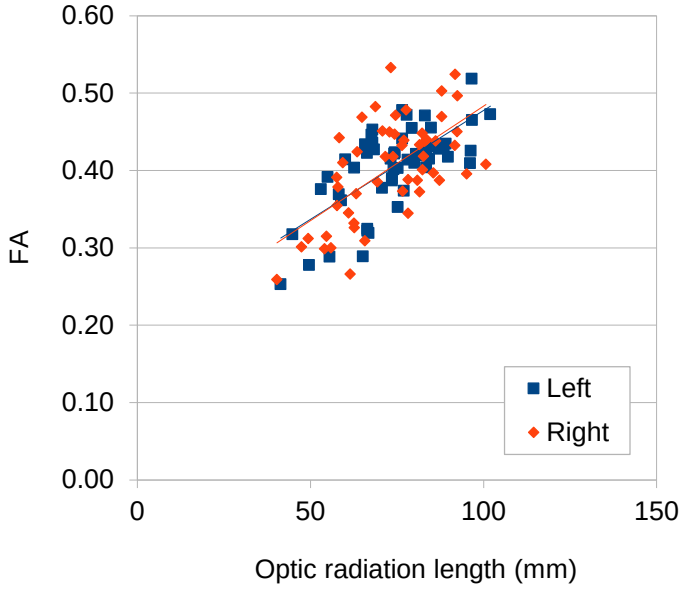

Figure 4.15 Comparison of the optic radiation length and the mean FA for the control 1×60 cohort.

4.7 Discussion

Myelination commences in the LGN in preterm infants after 30–36 weeks of development (Counsell *et al.*, 2002). In the optic tracts and the optic chiasm, myelin is present at adult levels in more than 50% of at-term babies at birth. In contrast, the

optic radiations develop more slowly and the rate of development is not well understood.

The optic radiations have two myelination foci, the geniculocortical and the corticogeniculate, from which myelination extends to other parts of the tracts (Brody *et al.*, 1987). The rate of wiring of the optic radiations is not well understood and is thought to continue into childhood. A microscopic study of the optic radiation proximal and distal and the calcarine cortex and LGN have shown that myelination of the optic radiations is weak at birth (Kinney *et al.*, 1988). Myelination of the optic tracts is mostly completed by 7 months of age (Magoon and Robb, 1981) and at-term babies achieve VEP values similar to adults at around the same time (Bird *et al.*, 1989). The sheath thickness increases particularly strongly in the first few years, through continuous wiring development and plasticity, but more slowly thereafter (Magoon and Robb, 1981). This chapter has shown that the mean FA of the optic radiations has a similar trend, following a logarithmic distribution with age, with a rapid increase in the first four years of life followed by a steady but small increase that continues into adulthood. This is consistent with the mean FA being correlated to myelination. Myelination similarly continues during early childhood and into teenage years in other white matter pathways (Barnea-Goraly *et al.*, 2005).

Examining the wiring process along the optic radiations is beyond the scope of this study as tractography using clinical DTI scanners and protocols does not currently have high enough resolution to describe physiological changes (i.e. microstructural changes that might impair function even in the absence of anatomical changes) at the scale of individual white matter tracts in the optic radiations, as discussed in Section 3.6.

4.7.1 Differences between the right and the left optic radiations

Although Jeelani *et al.* (2010) and Simmonds *et al.* (2014) identify lateral differences in white matter tracts, de Schotten *et al.* (2011b) find no conclusive evidence that the development of the two optic radiations is different. Yet the 1×60 cohort of child controls in this study has a higher mean FA in the left than the right optic radiation. Xie *et al.* (2007) found a similar trend for a small cohort of child controls.

A possible hypothesis is related to the different vascularisation of the left and right hemispheres during development, which could affect the rate of myelination in each

optic radiation. It has long been observed that vascular and nervous tissues tend to follow similar routes and share similar development traits (Larrivee *et al.*, 2009). Vascularisation of the optic radiations commences in the early stages of development from vessels outgrown from the pia and the periventricular vessels (Rowbotham and Little, 1965). The optic radiations are located millimetres from the lateral ventricle walls so Meyer's loop and the parieto-temporal area of the optic radiation have a blood supply from the ventriculofugal arterial vessels, with an origin in the choroidal arteries. The choroidal arteries are branches of the rami striati (Rowbotham and Little, 1965). The other blood supply source for the optic radiation comes from the penetrating arteries with an origin in the pial network (superficial hemisphere) (Pantoni and Garcia, 1997). The penetrating arteries are long and tortuous; the length of each fibre varies from 20 to 50 mm depending on the tortuosity (Moody *et al.*, 1990). The penetrating arterial vessels enter the white matter tract following the path of the myelinated fibres (Van Den Bergh and Van Der Eecken, 1968). This blood supply organisation is common to both hemispheres.

Oxygenated blood from the placenta reaches the aortic arch from the ductus arteriosus (which is supplied by the pulmonary arteries and the right ventricle) and the left ventricle. The right carotid generally originates by the right brachiocephalic artery, which is also the origin of the subclavian artery. The left carotid artery is a direct branch of the aortic arch and is very close to the ductus arteriosus, causing a shunt from the cerebral to the systemic circulation. The presence of the ductus arteriosus in close proximity to the left carotid might cause a greater intra utero supply of oxygenated blood to the left hemisphere in many foetuses. A greater supply of oxygen and nutrients could explain the location of the main centres for more complex tasks such as dexterity and language, as well as increased white matter tracts and myelination in the left hemisphere compared to the right hemisphere. It might be a factor in the right-handedness of most humans.

The left hemisphere is larger than the right in most humans (Purves *et al.*, 2001). There is a tendency towards the left hemisphere presenting perivascular haemorrhages in the preterm population, as well as other vascular events (Guzzetta *et al.*, 1986). The asymmetry of the blood flow is lateralised towards the right hemisphere (Mullaart *et al.*, 1995), especially in premature children with persistent ductus arteriosus. Increased CO_2 and decreased blood supply cause an increase in the cerebral blood

flow and perfusion to cerebral areas (Kurmanavichius *et al.*, 1991, Scherjon *et al.*, 1994). All of these factors support the hypothesis that the systemic shunt effect of the ductus arteriosus causes differences in the flow of the two hemispheres, with an increase in blood flow in the left hemisphere during the foetal and prenatal stage that causes lateralisation seen in early functional and anatomical development of the hemispheres. This hypothesis could be tested in the first instance by looking for in utero vascularisation variations and for patches of myelination of the optic radiations, using non-invasive techniques such as tractography.

Other evidence supports the link between vascularisation and white matter development, by researching links between critical developmental periods and changes in vascularisation. Visual development is particularly sensitive to critical periods such as the three-week period following birth, in which myelination increases rapidly (Counsell *et al.*, 2002). During this time, cerebral blood flow is higher than during the final three weeks of foetal life (Kurmanavichius *et al.*, 1991). The middle cerebral arteries supply up to 80% of the flow during this period to the temporal and parietal areas of the brain.

Devor *et al.* (2003) introduced the term "functional hyperaemia" to describe changes in perfusion and flow occurring in restricted areas of brain tissue that are linked to blood flow, blood volume and oxygenation. In this theory, hemodynamic signals are coupled with neuronal activity and changes in the blood flow, synchronised with changes in calcium concentration, are mediated by astrocytes (Girouard *et al.*, 2010). Astrocyte migration and regulation of the capillary vessels are important factors in the regulation of blood flow (McCaslin *et al.*, 2011). Little is known about the signalling that promotes astrocyte migration (Kowiański *et al.*, 2013). While the importance of astrocytes in the development of the neuroretina has been demonstrated, and some growth factors implicated in the vascularisation of the retina during the prenatal and early postnatal stages have been described, the process is not fully understood (Ma *et al.*, 2012). Recently, Segura *et al.* (2009) have shown how the neuronal and the vascular systems are intimately linked. Vascular sprouts behave in a similar manner to axonal growth during the process of development, sharing some of the signalling

agents and showing similar navigation behaviour until reaching their intended target and stabilising links[8] (De Smet *et al.*, 2009).

4.7.2 Differences between males and females

Differences in CBF, white and grey matter development have been identified by various studies (e.g. Devous *et al.*, 1986, Satterthwaite *et al.*, 2014). Yet the statistical analyses for both the 1×60 and 3×20 control cohorts did not identify any differences in the development of the optic radiations between sexes, so the hypothesis that they are different has not been proven by this study. Statistically-significant differences might be observed in a larger cohort or by using a higher-resolution DTI protocol.

4.7.3 Length of the optic radiations

The length of the optic radiations has been measured for child and adult control cohorts. The mean length for both child cohorts (with 1×60 and 3×20 protocols, respectively) was 69 ± 12 mm. Since the length increases linearly with age, it is meaningless to compare this mean length with cohorts from other studies unless they are age-matched, although few studies have published this measurement for the paediatric population. For the small cohort of 13 adults, the mean length was 86 ± 11 mm, with Figure 4.13 suggesting this to be independent of age. The studies cited in Table 4.1 have measured the length of the optic radiations in adults at approximately 100 mm (Ebeling and Reulen, 1988, Barton *et al.*, 2005, Rubino *et al.*, 2005, Peltier *et al.*, 2006). One reason for a shorter length being found in this study might be that the optic radiations at the rear, which gather into the primary visual cortex, are not being adequately resolved by tractography analysis. Chapter 5 introduces a method for further resolving these tracts using data from VEP recordings.

There were no statistically-significant differences between the lengths of the left and right optic radiations for either cohort. In a dissection study of 109 paediatric patients, Jeelani *et al.* (2010) concluded that the left optic radiation was longer than the right optic radiation, and this study might have reached a similar conclusion with a larger cohort.

[8] Synapsis for nervous tissue or anastomosis for vessels.

For individuals, measuring the length of the optic radiations could assist with preoperative planning. For child cohorts, it should be possible in the future to normalise the data and create tables to describe normal development of the visual system, similar to those published by the WHO. By measuring standard deviations in the normal paediatric population, children with smaller or larger tracts than normal could be identified and the impact of these anatomical anomalies better understood.

4.8 Conclusions

The normal development of the optic radiations has been examined using tractography in terms of mean FA and the optic length. Three cohorts were examined independently: 41 children and 13 adults, each scanned with the 1×60 protocol, and a second cohort of 35 children scanned with the 3×20 protocol. The mean FA of the optic radiations has a logarithmic distribution with age, with a rapid increase in the first four years of life followed by a steady but smaller increase that continues into adulthood. The optic radiation length can be measured from tractography maps and is much more variable with age than the mean FA. This information about normal development is used as a basis for identifying abnormal development in sick children in this study.

Although previous studies have assumed that the left and right optic radiations develop in a similar way, a comparison for the 1×60 cohort in this study concluded that the rear and full mean FA of children over 5 years old was higher for the left tract than for the right tract, which suggests that the tracts develop differently as the visual system matures. However, no statistically-significant difference could be identified for the 3×20 cohort.

Over the whole brain, females are thought to present a higher grade of grey matter than males as a result of earlier development (Gur *et al.*, 1980) but no statistically-significant differences between males and females could be identified in this study, in either optic radiation, for older or younger children scanned using either protocol.

5 IMPROVING TRACTOGRAPHY ANALYSIS USING VISUAL EVOKED POTENTIALS

This chapter examines whether VEP recordings can be used to improve the quality of tractography analysis, by localising the primary visual cortex and using this as a seeding point for the tractography. The results from using this novel methodology are compared with the standard method described in Chapter 4 for healthy subjects.

5.1 Introduction

VEP recordings are widely used in the clinical environment. The theory underlying VEPs is presented in Section 2.5.3. The standard clinical procedure uses one to three electrodes. Multi-channel recording is rarely used in the clinical setting but can provide much more information.

A VEP recording system consists of stimuli that trigger brain activity and a receptor that detects the resulting electrical brain activity. This chapter provides a brief overview of the stimuli and recording systems that are used. The methodology explains the experimental choices that were made for this study. Following an examination of the benefits of VEP recordings for improving tractography, in Section

5.4, the impact of using VEPs on visual tract mean FA is examined for the adult control cohort.

5.1.1 Types of visual stimuli

The two most common stimuli are flashes and checked pattern reversals. The choice of stimuli should depend on the subject cohort and their pathologies. For children, it is imperative that they can focus on the chosen stimuli. If a child cannot see the stimuli or cannot focus his/her attention on it then the recording might be impaired.

The average child born to term with no visual difficulties achieves a 20/20 visual acuity approximately at 6 months of age (National Eye Institute, 2015). Pattern reversal is the most appropriate stimuli for children with no visual difficulties. The check size is an important factor when using pattern reversal: for testing foveal vision, a check size of 10'–20' of arc is appropriate, while a larger check size of 50' of arc is more appropriate for testing para-foveal vision.

For children with very poor vision (20/200 or less) or nystagmus, pattern-onset flash stimuli are likely to produce better results (Creel, 2013). Poor vision and nystagmus limit the ability of the subject to fixate and focus on the stimuli, and the recording obtained with the pattern onset stimuli in these cases shows the activity principally in the central retina.

5.1.2 V1 activation using visual stimuli

In order to identify the primary visual cortex using a VEP recording, it is necessary to choose a pattern linked to brain activity in that area. The pattern reversal stimuli produces VEPs that activate the striate cortex and therefore V1 (Creel, 2013). Although the pattern reversal stimuli stimulates secondarily non-striate areas, its main focus of electrical activity detected is within the striate cortex (Hoffmann *et al.*, 2003). One theory proposes stimulation of non-striate areas prior to the activation of V1, via localised neuronal clusters that were not stimulated during the striate transfer of information (Thompson *et al.*, 2009, Cicmil and Krug, 2015). This theory suggests that stimulated non-striate areas transfer this stimulation to connected primary visual areas that were not stimulated directly. The microscopic and macroscopic relationships between the primary visual cortex and adjacent areas such as V2, V3 and others linked to visual processing are still not fully understood.

Following a mirror model, the area stimulated in the retina of each eye has a processing area within the same location in both primary visual striate cortices. According to this model, any recorded differences are due to anatomical or physiological differences in the conduction between the left and right visual pathways (Graham *et al.*, 2000). For children with anatomical brain abnormalities, this means it should be possible to localise the V1 area and detect the differences, even using pattern onset flash stimuli. In contrast, due to anatomical variability in the location of the visual primary area between subjects, it is very difficult to determine the location of the V2, V3 or the other visual areas with available imaging techniques using a clinical imaging tool in a short enough time for living subjects. Other studies have circumvented this issue by examining pattern onset in anaesthetised children while performing fMRI (Vanni *et al.*, 2004).

5.1.3 Standard clinical VEP recording systems

Standard recording systems use one to three electrodes. Electrodes are placed in the occipital midline, 2–4 cm above the inion. For a single electrode system, the electrode is placed at the central pole of the occipital cortex to test the macular portion of the retina. For a two-electrode system, each electrode is placed 2.5 cm from the midline so that they overlay the occipital cortex of the left and right occipital lobes.

It is necessary for the electrodes to be precisely located, for both reproducibility and measurement accuracy. The intensity and latency of the detected electrical activity vary according to the location and it is necessary that each electrode correspond to the same part of the brain for each subject.

One of the electrodes, called the ground, is placed on the midline of the inter-parietal area or forehead but far away from the recording area. The ground acts as a reference measurement.

5.1.4 Multichannel VEP recording systems

Multichannel VEP systems record several regions of the visual field at the same time. Since more detailed information about the channels of the left and right optic radiations is recorded, dysfunction of small areas can be detected that would not be identified by standard clinical recording systems.

Multichannel recording requires a mathematical model to adapt the electrode receptors to the underlying brain so the recorded electrical activity can be attributed to a specific area of the brain. This attribution of activity to an area of the brain allows not only the detection of abnormalities in the conduction but also the creation of maps using the many recording locations. An example of the software used to analyse the recordings is shown in Figure 5.1.

In full field recording, the right and left visual fields are stimulated and the electrical activity transmitted to the visual cortex is recorded. It can be used to monitor and detect lesions anterior to the optic chiasm. The main response elicited during the recording of the P1 wave using full field recording comes from the central 10°. Hence lesions or deficits in the periphery of the visual system might not be detected during full visual field stimulation recording.

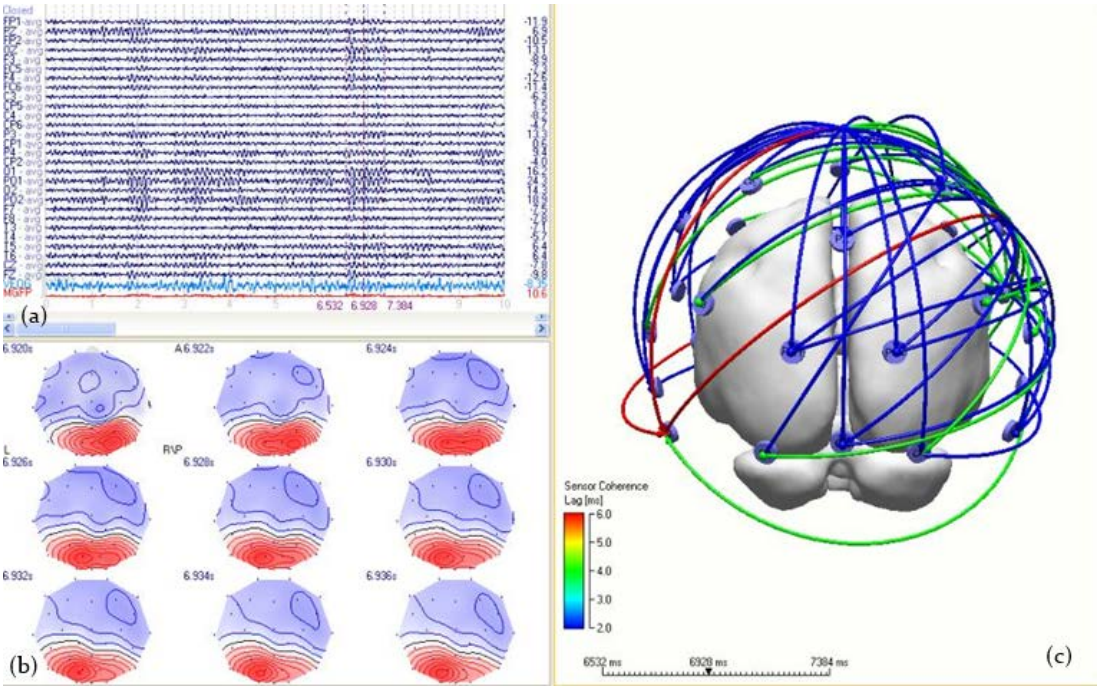

Figure 5.1 NeuroScan functional VEP software. (a) The upper left picture shows the brain activity detected by each electrode. (b) The lower left picture shows the spreading of the brain activation detected with the fitted electrodes. In this case the red region located in the occipital area has been activated. (c) The figure on the right shows a multi-electrode model where the activity detected is represented in a colour code specified in the legend on the left. The colour lines represent the spreading of electrical activity that is detected by each electrode.

Half field recording aims to distinguish the stimulation produced in the nasal hemifield which translates into activation of the temporal retina. The stimulation of the temporal hemifield correlates with activation of the nasal retina (Brecelj, 1992). Monkeys have bilateral visual cortical representation of the fibres in the centre of the retina (Leventhal *et al.*, 1988) and it has been shown that the nasal fovea of the human is also bilaterally represented in the visual cortical areas.

The P1 wave recorded from the occipital midline electrode Oz can be bifid or presented with two positive inflexions. This pattern of bifid wave has been linked to central scotoma and a more detailed analysis of macular vision is needed (Brecelj *et al.*, 1990).

5.2 VEP recording methodology

Multi-channel recording is used in the paediatric epilepsy unit of Great Ormond Street Hospital to identify the focus of the epilepsy. A similar multi-channel system was developed in this study for identifying the locations of the optic radiations.

The scanning technique was developed using an adult population. Two female controls, aged 11 and 13 years, were also tested. The long recording time of around 45 minutes and the requirement for long concentration periods meant that multi-channel recording was difficult to perform on young children.

5.2.1 The recording environment

Subjects were seated in a recording chair with padded arm rest and adjustable height. If the subject was too small to remain seated by themselves, the parent/guardian sat on the chair with the subject on their lap. The distance from the TV screen to the subject's eyes was set to 1 m for all recordings.

The room lighting was turned off during recording, with the room remaining in darkness until the procedure was completed. The fixation of the subject on the screen was monitored using a video camera. The subject's head and eye positions were also monitored by video camera. If the subject was sleeping or not focusing on the screen, then recording was stopped until the problem or lack of attention was resolved. For some non-compliant children, it was necessary to bring the subjects attention towards the stimuli during the recording.

Since a multichannel recording system takes a long time to prepare, the subject was given the choice of watching a DVD on the stimuli television whilst waiting. This was also shown between recordings to allow the subject a rest period so they could maximise their attention during recordings. This procedure is commonly followed in the Department of Ophthalmology at Great Ormond Street Hospital. To minimise errors and other illusionary artefacts at the start of the experiment, recording did not commence until 10 seconds after the stimuli appeared. Each recording was performed for 100 seconds.

5.2.2 Visual stimuli

The chosen stimuli protocol followed the ISCEV standards for clinical VEP recordings (Odom *et al.*, 2010), to be consistent with clinical VEPs performed at Great Ormond Street Hospital.

Since none of the subjects had visual difficulties, pattern reversal stimuli were used. Other studies have used pattern onset in children anaesthetised while performing fMRI (Vanni *et al.*, 2004) but our cohort included subjects that did not require anaesthesia so it was not appropriate to use such methodologies. As discussed in Section 5.1.1, pattern reversal has been shown to be robust, reproducible and with less interpersonal variation than pattern onset flash. Pattern reversal is therefore a reliable tool to record VEPs in healthy children. It directly stimulates the V1 area so the information obtained can be added to the DTI to improve tractography of the optic radiations. Full and half fields were recorded for all subjects.

The stimuli consisted of a high-contrast checkerboard pattern reversal stimuli with a red dot in the centre to attract fixation. White and black squares were used and the colours reversed three times per second. The stimuli were provided and the electrical activity recorded using the STIM package (NeuroScan, USA), which enabled the posterior analysis using Curry software.

5.2.3 Electrode location

The electrodes must be in contact with the scalp, so the skin should be clean to reduce electrical impedance. TEN20 or Quickcell non-allergenic, conductive paste was applied either to the skin or directly to the electrodes to further increase signal

conductivity. The paste is soluble and was removed with warm water after recording had concluded.

The electrodes were built into a non-allergenic and adaptable spandex cap that was fitted to the subject's head, so the same electrode locations were used for each subject. The most appropriate cap was chosen for each subject from a choice of three:

1. a small cap for babies;
2. a standard cap designed for children from age 7 to adults; and,
3. a large cap for children or adults with larger heads – for children, this would generally be caused by a pathology (e.g. hydrocephalus).

Each of the caps had a sling that was fitted under the jaw of the subject, in order to keep the cap tight and to ensure a good connection between the electrodes and the skin. Before fitting the cap, each of the electrodes was filled with conductive paste. After fitting, a blunt needle was used to spread the hair from the recording area of the each of the recording electrodes. The skin of the cheeks, mastoids, tragus and the eyelids where the anatomical and muscle movement detector electrodes were fitted with conductive paste with the help of a sterile mastoid swab.

The blunt needles were sent to the hospital sterilisation service at the end of each recording. The cap was carefully cleaned after each use, with any remaining gel removed with warm water and neutral soap.

The montage of the electrodes is shown in Figure 5.2. All the electrodes followed the 10-20 international placement standard. The VEP was recorded using 40-channel recording.

5.2.4 VEP recording system

The cap was connected to a digitiser and to a 40-channel monopolar digital amplifier (NuAmp).

The digitiser recorded the position of each electrode in three dimensions. It was located at the back of the recording chair in exactly the same position for every subject, with the recording chair and the digitiser no more than 20 cm apart. The topographical location of each electrode and the anatomical reference points were recorded. The anatomical landmarks chosen for the study were the inion, nasion, pre-auricular points and the left and right mastoids. The digitiser transferred the location information to

the NeuroScan Curry software, which created the spherical model to enable the best fit for the coordinates entered with the source location (the electrode position recorded by the system). The topographic mapping of the brain was then produced.

The NuAmp acted as a DC amplifier with a sampling rate of 1000 Hz (NeuroScan, USA). Once the cap had been fitted and the conducting gel applied, the impedance of the electrodes was tested using the NeuroScan software. Additional conductive paste was applied where necessary until all the electrodes had impedances of less than 5 ohms, following the international guidelines of AANP.

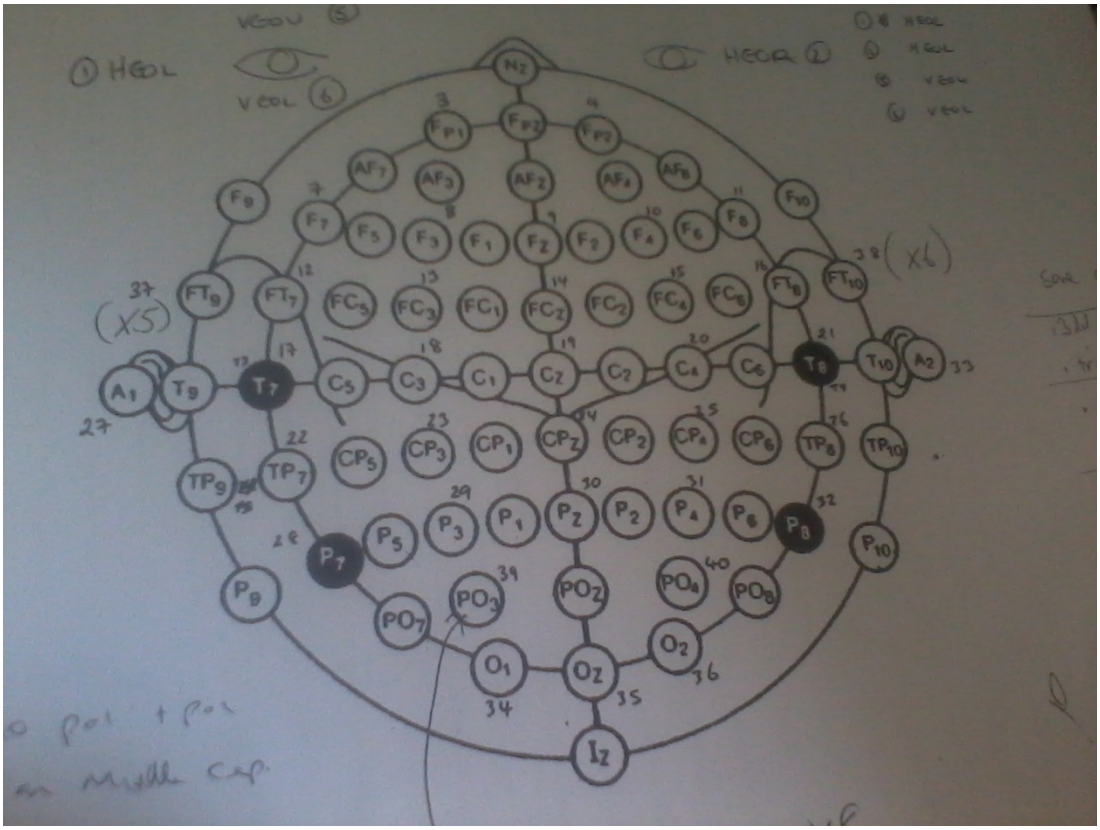

Figure 5.2 Photograph of the montage used for multichannel VEP recording. The position of each of the electrodes fitted into the spherical model used can be seen. The anatomical areas that were digitised and recorded are also shown, such as the nasion. Source: the author.

After fitting the cap and digitising each of the electrodes, the position of each of the electrodes was checked using NeuroScan. Figure 5.3 shows the process of setting up the recording of the VEP data on the software. The orientation of the electrodes is very important during data acquisition and processing with multichannel recording, as using a wrong direction or placing an electrode inaccurately can cause the recorded activity to be misplaced and lead to erroneous results. If this step had not been performed, an error could have led to activity being localised in the wrong area, with incorrect seeding points being identified.

The testing protocol was the same for every patient or control involved in the study:

- Both eyes open (BEO): the VEPs were recorded with both eyes open and with the same stimuli.
- Right eye full field.
- Left eye full field.
- Right eye open left half field.
- Right eye open right half field.
- Left eye open left half field.
- Left eye open right half field.
- BEO flash, for children only.

Each test was performed twice and the one with the least noise and artefacts was used in the study. The amplitude of the response was recorded from peak to peak. The latencies were also recorded but from the peak of the response wave. The EEG recorded from each of the electrodes was digitised using an amplifier with a band pass of 1–250 Hz. The epochs were set in the range of -50 to 300. The averaging was carried out after the epochs and other noise were discarded.

5.2.5 VEP dipole reconstruction and source location

To ensure that the recording had been performed correctly, a three-dimensional reconstruction of the dipole model was visualised using the display mode of the MUSIC algorithm in NeuroScan Curry 6.0 (Mosher *et al.*, 1992) in order to detect any possible errors, as shown in Figure 5.4.

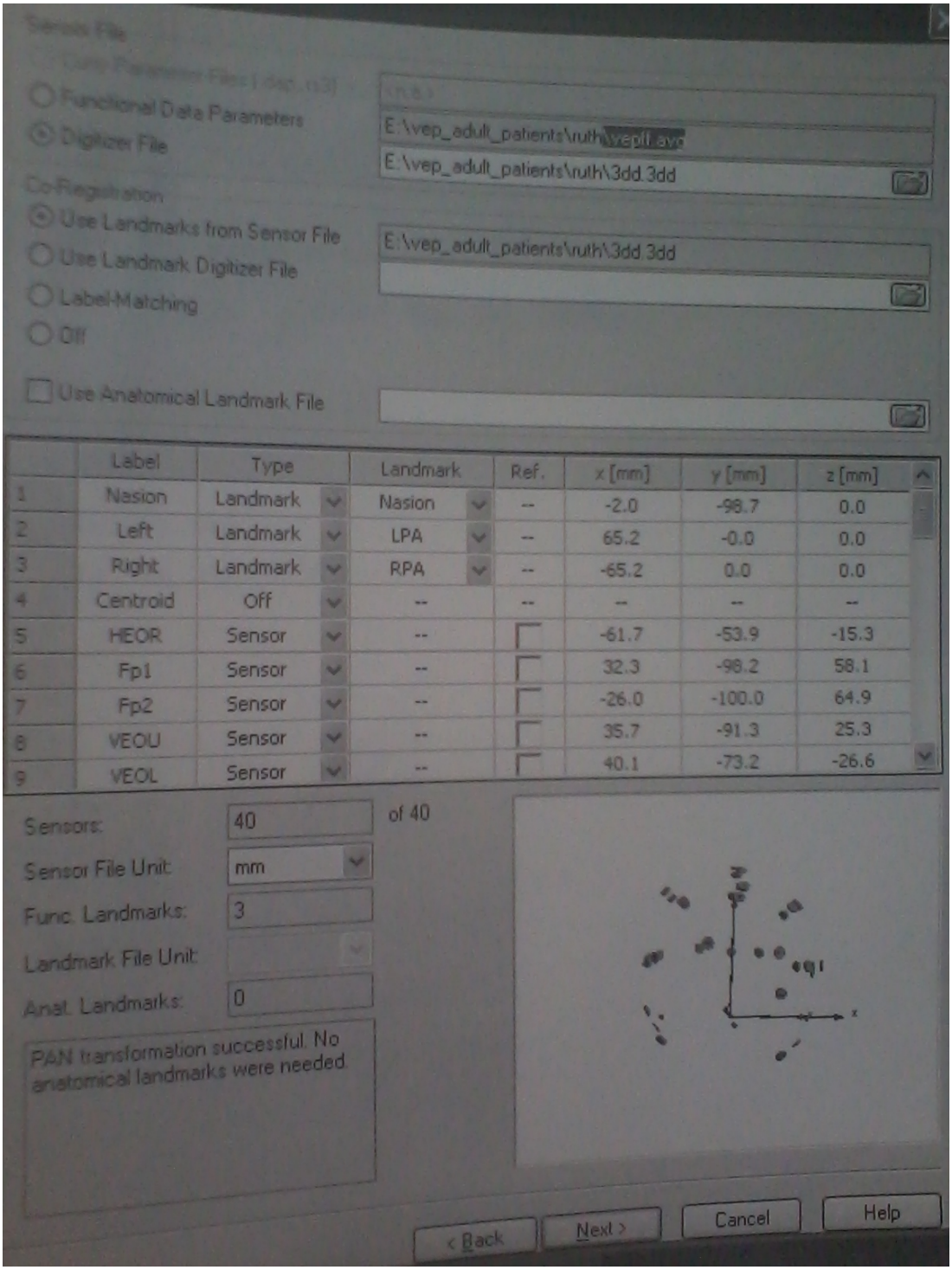

Figure 5.3 Visualisation of the anatomical landmarks and the recording electrodes.

A visual model of the VEP recording and a previously-recorded MRI image was then constructed for each subject using the same MUSIC algorithm (Mosher *et al.*, 1992). This performs a three-dimensional reconstruction of recorded electrical activity. The model used by the software to reconstruct and localise the electrical activity recorded

is an ellipsoid. The ellipsoid shows an estimated confidence interval of the source of the electrical activity recorded, taking account of not only the selected averaged data but also the uncertainty that the noise might have produced in the selected data (Fuchs *et al.*, 2004). The MRI T1 and DTI scans were added to the VEP data and the source location algorithm was performed in Curry. Combining imaging with functional data in this way produces a higher confidence interval of the source location with a better estimation of the electrical cortical activity (Braun *et al.*, 1997).

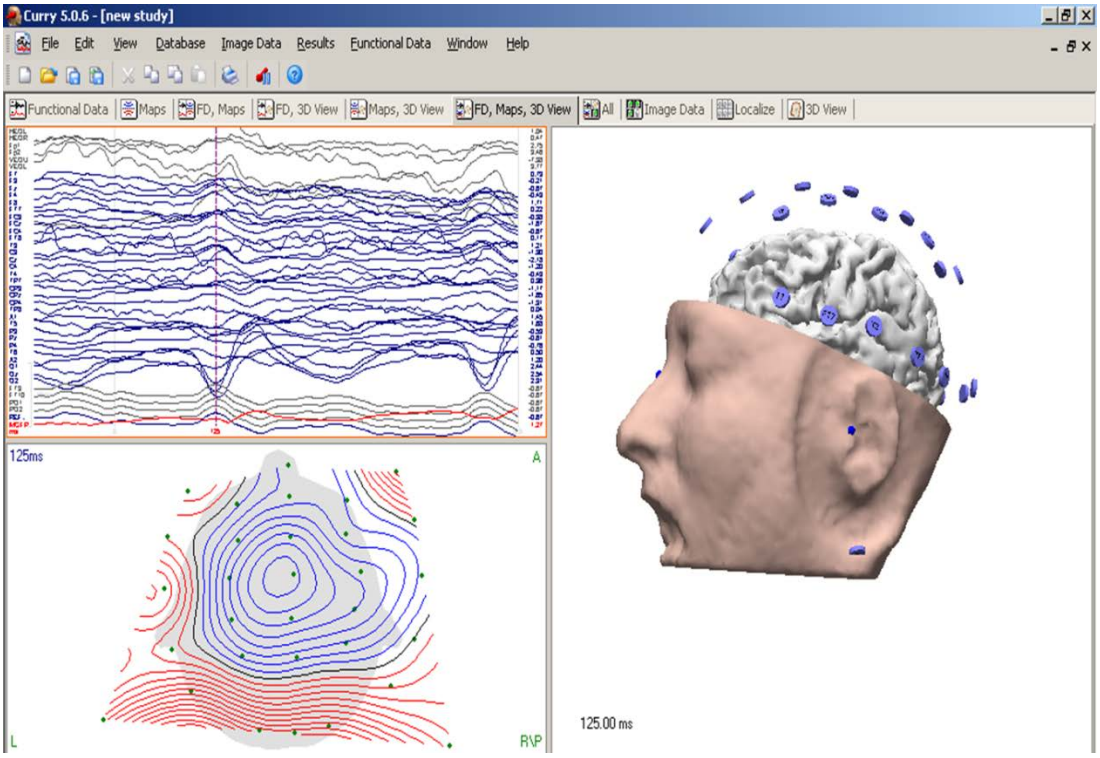

Figure 5.4 Visualisation of the cortical activity and source location prior to adding MRI imaging.

MUSIC uses a triangulation model with more than 22,000 triangles to recreate the cortex. Conductivity is separately calculated for different surfaces (skin, scalp, skull and cortex, as shown in Figure 5.5) (Fuchs *et al.*, 2007). Applying the same calculations to a different segmentation process enables the creation of the model with MRI and DTI imaging (Fuchs *et al.*, 2002).

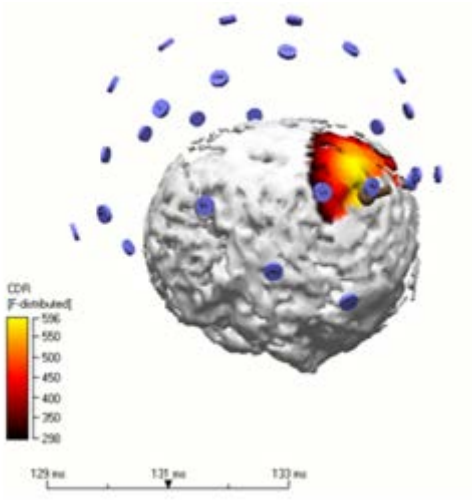

Figure 5.5 Location of the cortical electrical activity recorded with VEP using the ellipsoid model. The electrodes can be visualised as blue dots. The scale on the left shows the probability of the location of the electrical activity in graded colour.

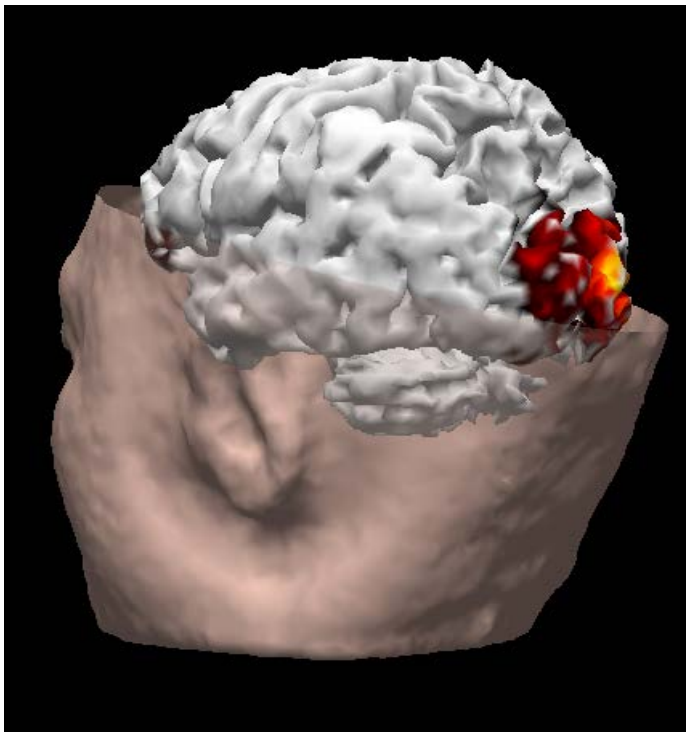

Figure 5.6 Electrical activity recorded with VEPs after being fitted using the ellipsoid model. The skin has been removed to better visualise the location of the simulated cortical activity. The probability of electrical activity within the cortex is shown on a scale from dark red to yellow, where yellow represents the highest probability of activity.

The MUSIC model takes into account the thickness of the skin, scalp, skull and hair for the model reconstruction (Figure 5.6). These parameters can be modified to fit the subject. This is a very important feature of the software; for example, the skin tends to be thinner in young children and babies, while skull thickness increases with age but is lower with certain pathologies, and both of these modify the electrical signal transmission.

5.3 Using VEP recordings to improve tractography

It is of great importance to accurately locate the optic radiation when performing a neurosurgical procedure. Neuronavigation tools offer an imaging source and a good foundation or road map of the area that is being operated. However, it can be difficult to precisely identify the location of structures due to anatomical variations from normality or changes in the pressure inside the cranial cavity once the craniotomy is performed. In delicate procedures such as those required for epilepsy surgery, a minimally-invasive few millimetres might substantially change the patient's outcome by damaging the optic radiations.

T1-weighted scans do not identify the location of the optic radiations and tractography analysis is still being developed for the clinical environment. The primary visual area and the optic radiations cannot be clearly visualised by MRI alone because of inadequate image contrast concerning those structures. The aim of this study was to combine functional activity with DTI images to try to further improve tractography analysis, with the long-term aim of improving clinical outcomes. The functional data from the VEP recordings supplies additional information that can be used to identify the locations of the structures of interest. This section describes how these VEP recordings can be used to improve tractography analysis. The whole procedure was performed independently for each subject.

5.3.1 Segmentation process

The NeuroScan Curry 6.0 software was used for this analysis. The T1-weighted MRI was added to Curry from the original DICOM files. The first step was segmentation in order to visualise the different thresholds for skin, brain, soft tissue and CSF. The parameters for each of these was changed in Curry until the segmentation was performed satisfactorily.

The next step was to add anatomical landmarks to the imaging data. Curry produced a three-dimensional reconstruction of the imaging data with the approximate locations of the nasion, inion, right tragus and left tragus, which were fixed by hand as necessary. The intracranial structures were also identified and registered; their coordinate points are known as the Talairach parameters. Figure 5.7 shows the brain extraction of the different sources and the anatomical layers into which the images can be divided.

The final step in the segmentation process was to create a three-dimensional model by blending the MRI data with the previously-identified anatomical reference structures.

Once segmentation had been completed successfully, a three-dimensional anatomical reconstruction of the brain was created that incorporated the MRI scan and the anatomical structures (Figure 5.8).

5.3.2 Visualising functional recordings

The three-dimensional image is used to show the approximate location of the electrical activity recorded and localised in the cortex by the dipole when the functional data is added and merged with the anatomical data. Fixed sources of electrical activity can be represented in Curry by a dipole or by a colour area. The dipole is created using a source reconstruction model in which the electrode positions are loaded into a virtual coordinate system. Once the model is fitted to the anatomical information that was defined in the segmentation, the fitted dipole is transformed onto the same coordinate system as the anatomical model (Fuchs *et al.*, 2002).

The choice of locations assumes the neural model of orthogonal to cortical flow of electrical neuronal activity. Areas that are the most likely source of electrical activity are identified. Also identified are nearby cortical areas that might be additional sources of neuronal activity, in order to indicate the uncertainty in the location. Figures 5.9 and 5.10 show examples of neuronal activity from transversal and coronal views, respectively.

The combined MRI–VEP images can be exported in ANALYZE format, for use in the clinical environment (e.g. in BrainLab as a navigation tool) or in other neuroscience software.

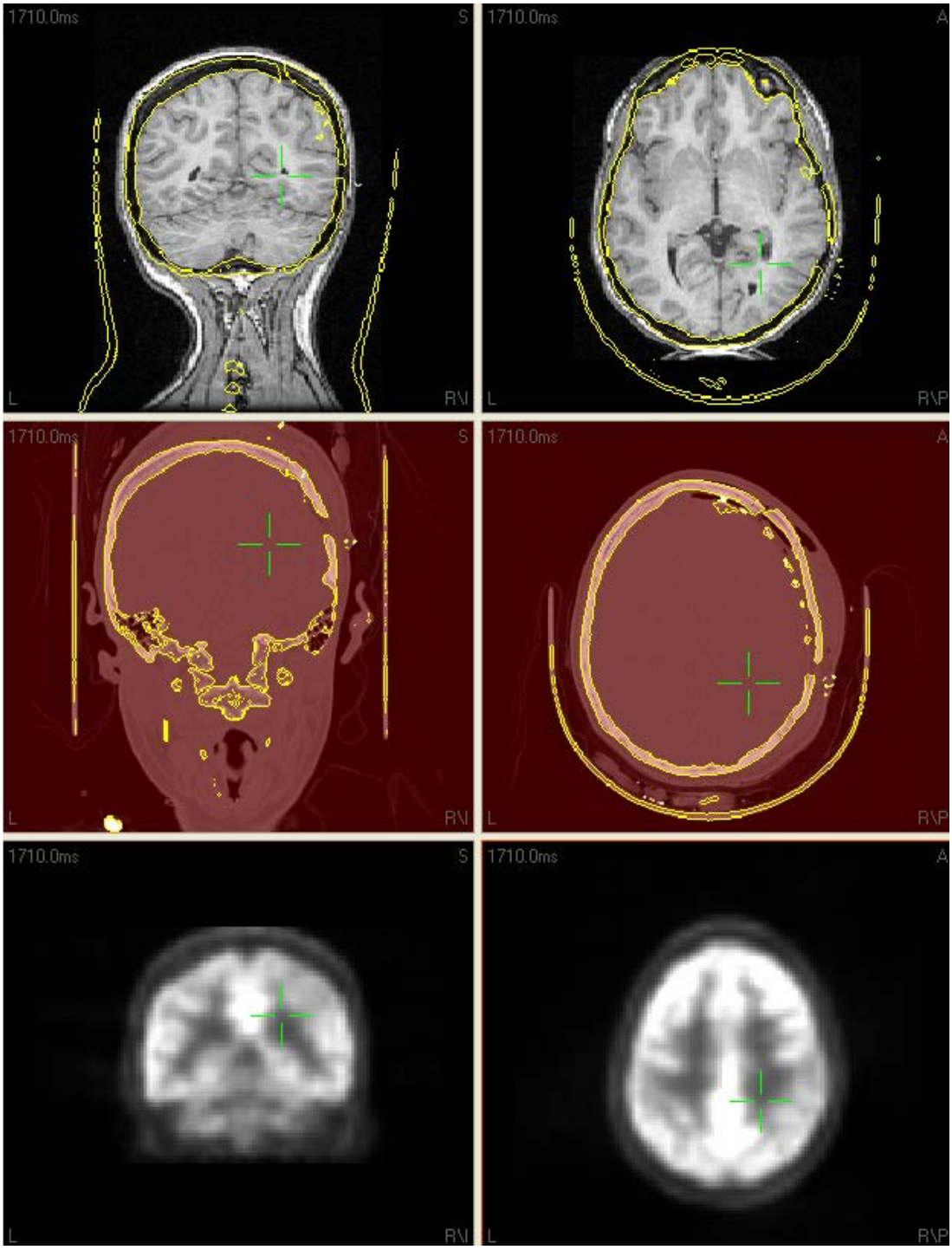

Figure 5.7 Brain extraction in the NeuroScan Curry software. The yellow lines differentiate the skin, skull and brain. The green crosshairs are used to identify the same anatomical areas in different scans in order to achieve high-quality segmentation in three dimensions.

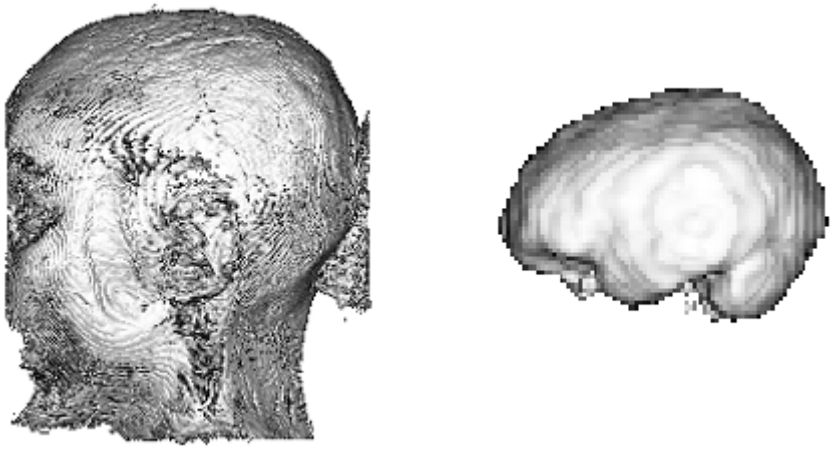

Figure 5.8 Anatomical reconstruction of a subject brain in Curry. The image on the left shows the head shape, including skin, looking towards the left. The image on the right shows a similarly-orientated plain reconstruction of the brain area.

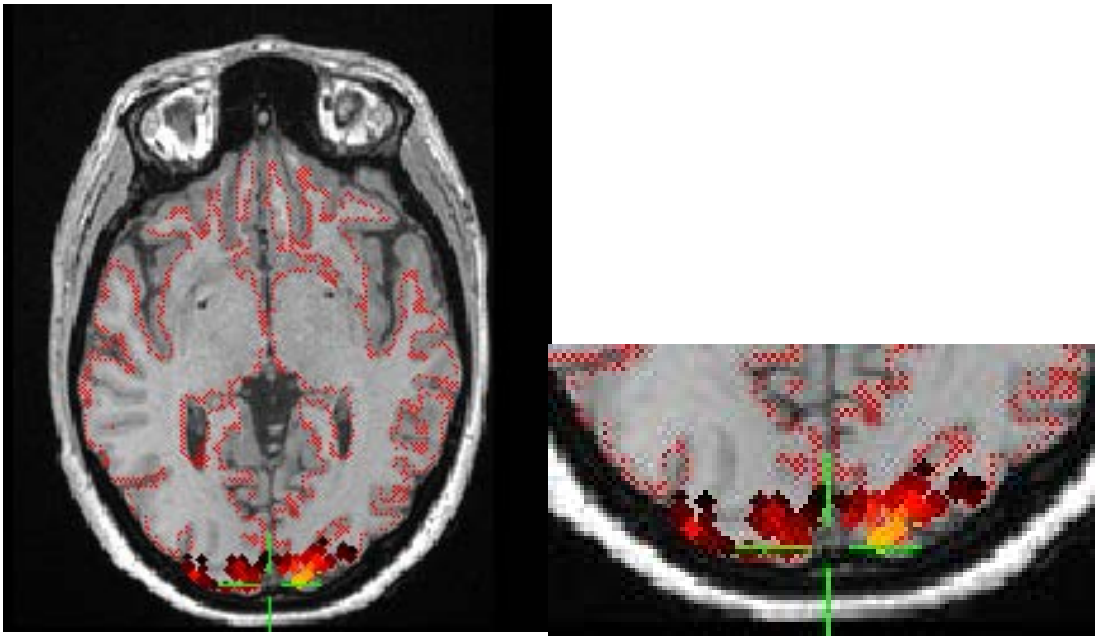

Figure 5.9 Reconstruction of neuronal electrical activity in the occipital lobe from a transversal view. The figure on the right is a magnification of the rear of the brain. The colour code shows the magnitude of the recorded neurophysiological activity, with values ranging from 0.38 µA mm^{-2} (black/dark red) to 0.75 µA mm^{-2} (yellow).

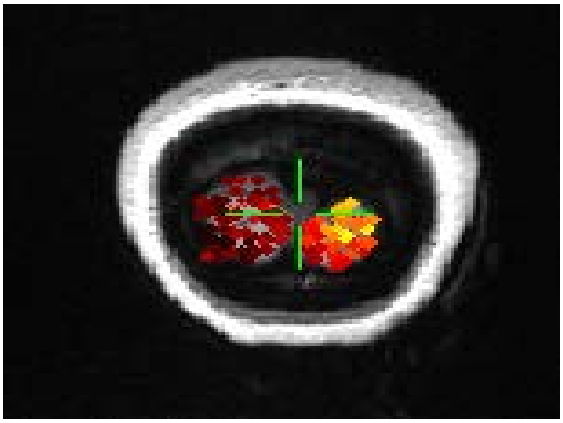

Figure 5.10 Reconstruction of neuronal electrical activity in the occipital lobe from a coronal view. The colour code shows the magnitude of the recorded neurophysiological activity, with values ranging from 0.38 µA mm^{-2} (black/dark red) to 0.75 µA mm^{-2} (yellow).

5.3.3 Combining DTI images and VEP functional recordings

DTI functionality has only recently been added to the NeuroScan Curry software. A similar processing route was followed to that described above for T1-weighted images, except that it was necessary to import the DTI data in NIfTI format. The segmentation was adapted for use with DTI data.

5.3.4 Adding VEP information to the tractography

The VEP recording data, with the dipole source locations, were added to the T1-weighted data using NeuroScan. The source location files were saved in HTM format so they could be exported to an alternative source. The FSL software was then used to co-register the files and to visualise the area corresponding to V1 in each subject. The digitised V1 area was used as a secondary seed ROI in the tractography analysis, in addition to the primary ROI located within the LGN vicinity.

The ROI was limited to areas that the VEP identified as having high probability of being the source of electrical activity (i.e. those coloured yellow in Figures 5.9 and 5.10).

Some patients, such as those with hydrocephalus, have highly distorted anatomies and it is not possible to determine the location of the LGN using clinical imaging alone and hence a seed point for tractography analysis. Tractography is a particularly valuable tool for such patients as the anatomy of the optic radiations is otherwise very

uncertain. For these patients, measuring cortical activity using VEPs and combining this with DTI images enables an alternative seed ROI to be identified so that tractography can be performed. While tractography is normally performed separately for the left and right optic radiations, this approach is not appropriate for subjects with highly distorted anatomies and no exclusion ROIs are defined. This method was used to analyse two hydrocephalus patients and the results are examined in Chapter 8.

5.4 Adult control cohort tractography using VEP

The impact of combining VEP functional data with imaging data was tested using a cohort of adult control subjects, as these were more cooperative in concentrating throughout the VEP recording so were expected to produce functional data with lower noise than children. The same multichannel scanning procedure was performed for all subjects. Tractography was performed both with and without the VEP data and the difference in the mean FA was assessed statistically.

The cohort consisted of 6 males and 6 females aged between 26 and 40, with one further male aged 65. None of the subjects wore glasses at the time of enrolment. They were healthy with no diagnosis of psychiatric or other organic disease that could bias the results. None of subjects had regular anti-epileptic medication or antidepressants at the time of scanning.

5.4.1 Qualitative impact of using functional VEP data on tractography

An example of the impact of including a second ROI seeding region based on VEP data is shown for one subject in Figure 5.11. Each optic radiation was analysed separately but both have been combined in these images. The functional data enables the tractography to identify the visual regions at the rear of the brain that are often omitted by the standard method, and were generally found to improve the tracking of the optic radiations across the cohort.

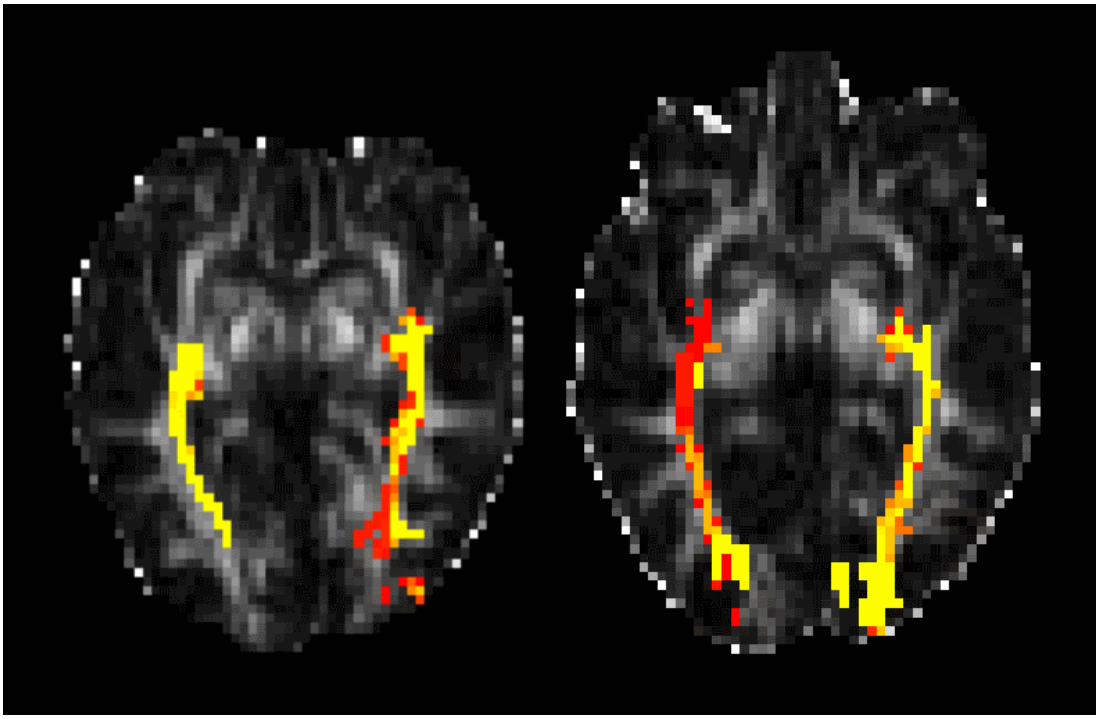

(a) MRI (b) MRI + VEP

Figure 5.11 Impact of including a second ROI seeding region based on VEP functional data. The tractography maps are for the same subject for: (a) defining seed points only in the vicinity of the LGN; and, (b) defining additional seed points in the V1 area based on functional VEP recordings.

5.4.2 Quantitative impact of using functional VEP data on tractography

The numbers of voxels in each optic radiation are summarised in Table 5.1 for the 13 adult controls. Using the functional ROI seed method leads to a much greater number of voxels at the rear on both optic radiations. Although the variability, represented by the standard deviation, is higher for the functional ROI seed method, the relative error[9] is lower than for the standard seed method.

[9] The relative error is the absolute error divided by the mean.

The impact of including a second ROI seeding region, based on VEP data, on the left optic radiation mean FA is shown in Figure 5.12. For the standard method, the mean FA varies between 0.4 and 0.5 across the cohort. A similar trend is observed across the cohort for the new method with a second ROI seeding region, but most of the values are around 0.05 lower. A similar trend is observed for the right optic radiation in Figure 5.13, but with an average difference of around 0.1.

	Left		Right	
	MRI	**MRI + VEP**	**MRI**	**MRI + VEP**
Full	466 ± 185	812 ± 276	336 ± 149	640 ± 246
Front	173 ± 88	173 ± 77	126 ± 68	114 ± 80
Rear	293 ± 116	639 ± 228	209 ± 98	526± 215

Table 5.1 Number of voxels in each optic radiation from the standard and functional ROI seed methods for adult controls. Figures are presented in the form mean ± standard deviation.

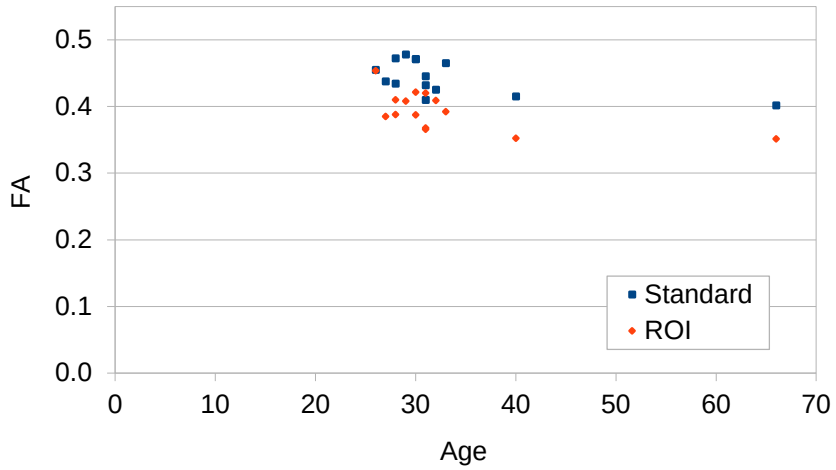

Figure 5.12 Impact of using a functional-derived ROI on the left optic radiation mean FA for adult controls. The mean FA for the standard tractography method is coloured blue and the mean FA for the same subjects with a secondary seed ROI defined using functional VEP data is coloured red.

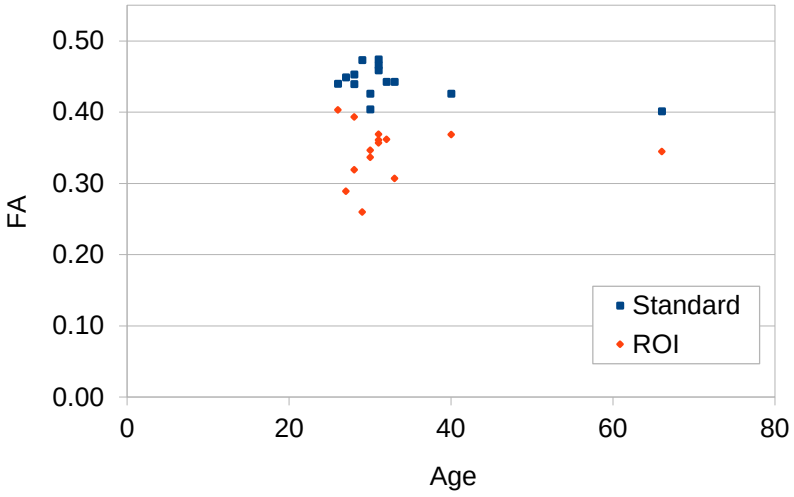

Figure 5.13 Impact of using a functional-derived ROI on the right optic radiation mean FA for adult controls. The mean FA for the standard tractography method is coloured blue and the mean FA for the same subjects with a secondary seed ROI defined using functional VEP data is coloured red.

The cause of the difference in mean FA can be investigated by comparing changes in the front and rear mean FA. The mean FA of the front of the left optic radiation does not show any major differences between the two methods (Figure 5.14). For the rear, however, the mean FA when the extra ROI seeding region is included is lower for all subjects (Figure 5.15). When using an extra seeding region, the optic tracts extend to the rear of the brain and include a greater number of voxels, as illustrated in Figure 5.11. These voxels tend to have lower FA than the other parts of the tract, which causes the mean FA across the tract to reduce. The changes in front of the parieto-occipital sulci tend to be much more minor as the tracts are mainly derived from the primary seed point in the vicinity of the LGN, and this is defined in the same way in both analyses for each patient.

Statistical differences between the two cohorts are examined in Table 5.2. Adding a secondary seeding region causes statistically-significant reductions in the full and rear mean FA on both optic radiations, but has no statistically-significant impact on the front of the optic radiations mean FA.

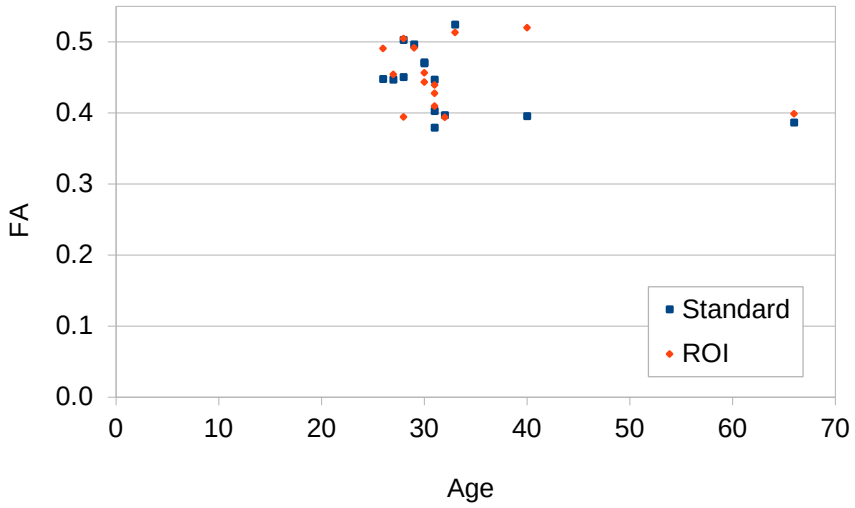

Figure 5.14 Impact of using a functional-derived ROI on the mean FA for the front of the left optic radiation for adult controls. The mean FA for the standard tractography method is coloured blue and the mean FA for the same subjects with a secondary seed ROI defined using functional VEP data is coloured red.

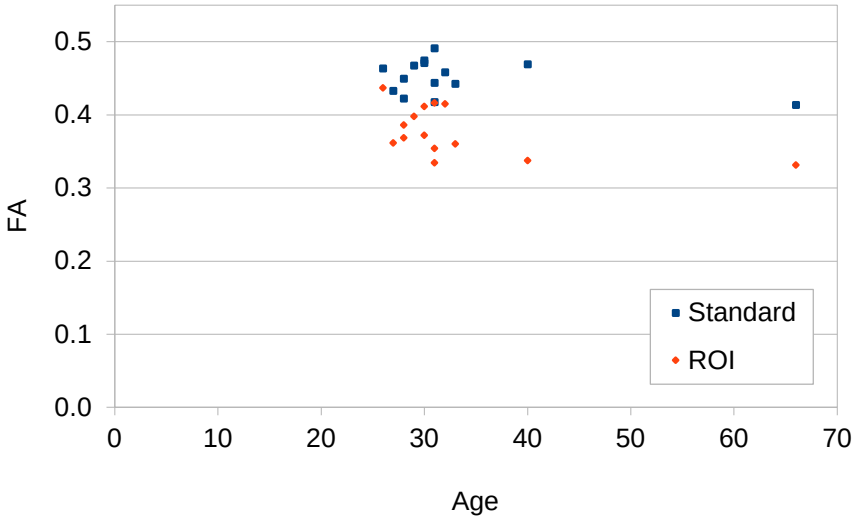

Figure 5.15 Impact of using a functional-derived ROI on the mean FA for the rear of the left optic radiation for adult controls. The mean FA for the standard tractography method is coloured blue and the mean FA for the same subjects with a secondary seed ROI defined using functional VEP data is coloured red.

	Change in mean FA		T-test	
	Left	**Right**	**Left**	**Right**
Full	–0.05	–0.10	<0.00001	<0.00001
Front	+0.01	–0.02	0.463	0.108
Rear	–0.07	–0.12	<0.00001	<0.00001

Table 5.2 Paired t-test comparing the mean FA from the standard and functional ROI seed methods for adult controls.

5.5 Discussion

The tractography is qualitatively improved by including an additional ROI seeding region based on VEP recordings. It is important to consider why this causes a substantial reduction in the mean FA of the rear of the brain.

Mapping white matter tracts using DTI tractography in areas with high amounts of grey matter is difficult. The rear of the optic radiation is at the very end of a transition area between the visual primary cortex and the axonal white matter pathway confined in the optic radiation. It is a very rich area that is characterised by the pruning and division of the terminal ends of the optic radiation, which do not follow a straight line. The tortuous nature of the fibres means that they could spread out in multiple directions, which makes them difficult to follow and acts as a confounding factor for tractography. The photographs of the macroscopic dissection presented in Section 2.2 illustrate the anatomy of these fibres.

In the tractography analysis, the mathematical tracking system excludes voxels in which the FA is lower than the threshold value of 0.1. In contrast with the standard PiCo algorithm (Parker *et al.*, 2003), the tractography algorithm in this study did not include angle limitations, so the rear area, which has many transition voxels between grey and white matter, was not excluded. Yet the probabilistic model has a voxel size of 2.5 mm, which is large in comparison to the size of axonal fibres of the optic radiations (Ebeling and Reulen, 1988). This voxel size is more suitable to examine larger fibres with constant diameters, but it was not possible to produce DTI scans at higher resolutions with the available MRI machine. This resolution is suitable for the

optic radiations in the vicinity of the LGN, where the fibres are more homogenous and larger.

The volumes of the tracked optic radiations are larger when VEP data is used to set ROIs, leading to the inclusion of lower-FA areas at the rear of the optic radiations. A higher-resolution scan might improve the FA estimate in transitional areas with more complex fibres.

5.5.1 Error margins

The dipole sphere fitted model, which aims to locate the V1 area, has an error that is estimated to be in the range 1–1.5 cm (Nuwer *et al.*, 1998, Martínez *et al.*, 2001).

The error margin for the VEP-enhanced DTI tractography in this chapter has not previously been assessed. A similar fMRI study that did not use DTI was estimated to have a marginal positional error of as much as 2–2.5 cm from where the real neuronal activity was localised to the area drawn by the fMRI (Di Russo *et al.*, 2003), despite repeated fMRI tests on the same subject producing positional differences of only up to 1.1 mm (Engel *et al.*, 1997), with further improvement limited by the resolution of the MRI BOLD[10] signal (Dougherty *et al.*, 2003). The area measured with VEPs in this study was used as a locator for the seeding points but not as a measurement of the primary visual cortex. It was beyond the scope of this study to determine the margin of error due to clinical and ethical limitations. It is possible that the error is different for children than for the adults. Since one aim of this study was to identify clinical applications for the procedures, fMRI was not used as it is not easily replicated in clinical paediatric departments with neurophysiology and DTI facilities.

5.5.2 Application to the clinical environment

VEP-enhanced DTI tractography is not currently available as a clinical tool. It was necessary for this study to develop the processing methodology described in this chapter, using the most up-to-date research software, and to make a number of changes to accommodate DTI data in particular. The route will be more suitable for clinical applications when DTI DICOM images can be read by the VEP software. But there

[10] BOLD (Blood-oxygen-level dependent) contrast imaging is used in fMRI to observe active organs.

is still a need to merge output maps with other devices that are used as primary aid tools for surgeons and clinicians, such as neuronavigators. More importantly, although using functional data produces qualitative improvements in the tractography, it is difficult to resolve the optic radiations in the rear of the brain and higher resolution imaging might greatly reduce the error margin in this area.

5.6 Conclusions

A novel technique has been developed and tested in which DTI tractography of the optic radiations is improved using functional data from multi-channel VEP scans. The resulting three-dimensional model describes the location of the primary visual cortex. This data can be used to improve the tractography of the optic radiations by defining the primary visual cortex area as an additional seeding location. This refined method greatly increases the number of tract voxels at the rear of the brain.

The benefits of this technique have been visually examined for 13 adults, and are examined for hydrocephalus patients in Chapter 8. The image processing is difficult and complex but would be suitable for the clinical environment following further development.

Having demonstrated the usefulness of this technique on control and hydrocephalus subjects, a future study could examine other pathologies. For children with optic nerve hypoplasia and other visual pathologies, VEP-enhanced DTI tractography might tell us whether the primary visual area is affected by the pathology or if epilepsy and hearing impairment causes a variation in the located primary visual cortex. The other main area in which to further develop the technique is the resolution of the imaging, which would require a new generation of MRI scanners for improvement.

6 CHANGES IN THE OPTIC RADIATIONS IN CHILDREN WITH OPTIC NERVE HYPOPLASIA

Tractography and VEP analyses are used to examine how optic nerve hypoplasia affects the development of the optic radiations in the paediatric population. Differences in the individual white matter tracts in optic nerve hypoplasia patients are also examined using the TBSS software tool.

6.1 Introduction

Optic nerve hypoplasia (ONH) is described as underdevelopment of the optic nerve (Sowka *et al.*, 2008). Typically, the optic nerve is smaller and the arteries and veins are larger than normal, with Dutton (2004) observing fewer optic nerve fibres at birth compared to controls. It may present as a unilateral or bilateral lesion with variable visual impairment, or can occur in association with other ocular, endocrine and neurological problems (e.g. cerebral palsy, epilepsy, mental retardation) (Kidd *et al.*, 2008). It has been described in association with the absence of the septum pellucidum.

The origin of the disease is not fully understood and most of the cases occur sporadically. Recently, it has been reported that the disease can be linked to

Chromosome 9 abnormalities or to genetic mutations in genes of the SOX family (McCabe *et al.*, 2011). These chromosome abnormalities have been mostly linked to more severe cases of ONH and to septo-optic dysplasia (Cidis *et al.*, 1997). Septo-optic dysplasia is a more severe, variant presentation of ONH that is also known as De Morsier Syndrome. It is characterised as hypoplasia of the optic nerve associated with the absence of the septum pellucidum, as well as other associated midline abnormalities such pituitary hormone deficiencies (Morishima and Aranoff, 1986).

ONH has been found to produce a non-severe, segmental, unilateral visual defect that can be present in either eye at birth in monozygotic twins (Cidis *et al.*, 1997). This supports the theory that ONH could result from genetic predisposition together with environmental events during the development of the visual system.

6.1.1 Epidemiology

ONH cases were rarely reported until De Morsier (1956) described the syndrome. Since then, the reported incidence of the disease in North America and Europe has increased six fold, and is estimated to affect 1 in every 10,000 children (Patel *et al.*, 2006). In the USA, cataracts and ONH were found to be the most common ocular defects in blind children (Dutton, 2004). There is an incidence rate in North West England of 10.9 every 100,000 habitants per year, with particularly high rates in deprived areas with more frequent teenage pregnancies (Patel *et al.*, 2006).

6.1.2 Symptoms and treatment

The cause of optic nerve hypoplasia is not known and no cure is available. No diagnostic protocol has been established besides clinical examination. Children often have some visual improvement in the first 5 years of life. Central hypopituitarism has been observed in 43% of paediatric ONH cases, which is related to cognitive delay (Fink *et al.*, 2012), leading to screening for thyroid hormone deficiency being performed in the UK. The thyroid hormone is implicated not only in peripheral tissue growth but in brain development processes such as neuronal migration, myelination (Shanker *et al.*, 1985) and white matter wiring (Bernal and Nunez, 1995).

ONH symptoms vary from negligible to severe visual impairment. For mild symptoms, parents and clinicians are generally alerted later in development, often not until school age, when deficits such as low stature and visual abnormalities are

observed. More severe cases are generally referred earlier, when the baby fails to fix and follow toys or fails to recognise and interact with familiar faces.

MRI is used clinically to examine the intracranial anatomy of patients with visual defects. DTI tractography is an emerging tool for understanding the intricacies of the pathologies of patients with ONH, and has principally been applied to severe septo-optic dysplasia. A case study from Schoth and Krings (2004) showed reduced mean FA in a patient with septo-optic dysplasia. Using a similar approach but with tractography, Salmela *et al.* (2010) concluded that two patients with septo-optic dysplasia had lower optic radiation mean FA than seven controls. The only study of a cohort of patients using DTI tractography was by Xie *et al.* (2007), who examined 14 patients with amblyopia, but including some with ONH, in a comparison with a paired control cohort, but did not identify a statistically-significant lower mean FA in the ONH optic radiations. Webb *et al.* (2013) examined the links between ONH and behavioural problems in 11 patients with septo-optic dysplasia, using the TBSS software tool, and concluded that the optic radiation and corpus callosum mean FA of these patients is lower than that of a control cohort. Nishi *et al.* (2013) examined the benefits of using DTI to improve evaluations of a patient with unilateral optic nerve hypoplasia and hypoplasia of the contralateral optic pathway in a case study. All of these studies examined severe cases and no studies of the impacts of less severe ONH on the optic radiations have been reported in the literature.

6.1.3 Aim and novelty of this study

The overall aim of this study was to examine how ONH affects, or is affected by, reduced myelination and defects in the optic radiations. A novel methodology was developed that identified overall changes in the optic radiation mean FA using tractography and combined this with a TBSS analysis of mean FA differences across the white matter tracts. As well as looking only at cases of ONH, rather than a mix of ONH and septo-optic dysplasia, it also used a much larger cohort (23 patients) than previous studies. In contrast to all of the previous studies except Xie *et al.* (2007), the ONH patients were paired in all of the analyses with controls of the same age in order to reduce the influence of age-related mean FA differences.

Although clinical MRI protocols (e.g. T1-weighted MRI) are used to examine the optic nerves in patients with severe optical defects, they cannot resolve white matter tracts.

A secondary aim of this study was to examine the potential benefits of DTI tractography as an additional tool in the diagnosis and follow-up of children with suspected ONH.

6.2 Methodology

6.2.1 Testing visual function using VEP recording

Clinical VEP recordings were performed on all of the ONH patients to ascertain the visual impairment of the patients and only those patients solely with ONH were included in the study. Following the Queen Square protocol, three electrodes were placed close to anatomical skull in the mid-occipital, lateral right occipital and lateral left occipital regions. The Oz electrode was placed 2–3 cm above the inion. The lateral electrodes were placed at each side of the occipital cortex at a distance of 2.5 cm from the inion, at the same height as the Oz electrode. The Cz ground electrode was placed in the midline, half-way between the inion and nasion. Furthermore, two electrodes were placed to record blinking, with one below each eye. The ISCEV standards were followed when placing the electrodes (Odom *et al.*, 2010).

The lateral electrodes were placed in the left and right occipital region to record responses from both the left and right visual occipital cortices. The detection of responses from both cortical visual areas enables defects to be detected more accurately and identifies any differences between the two visual fields (Blumenhardt and Halliday, 1979).

The clinical VEP recordings assessed visual function using three tests. The Both Eyes Open (BEO) flash examined the response rate to pattern-onset flash stimuli. The evoked potentials were then examined in the left and then the right eye, in turn. Clinical standard confrontational campimetry measurements could not generally be obtained for these patients due to their poor vision or lack of cooperation.

6.2.2 MRI imaging and tractography

Part of the ONH cohort was only scanned using the 3×20 protocol, so this was used for all patients in this study. Tractography analysis was performed on each patient in the ONH and control cohorts as described in Section 3.4. This was used to calculate the mean FAs of the left and right optic radiations. The mean FA of the front and back

of each optic radiation was also calculated, as a prelude to the more detailed spatial analysis using TBSS. The mean FA values in the two cohorts were compared using ANCOVA statistics to remove the age dependence from each cohort.

6.2.3 TBSS analysis

The TBSS (Tract-Based Spatial Statistics) program, which is part of the FSL toolkit, performs fully-automated, statistical, voxel-based analyses of the whole brain (Smith *et al.*, 2006). It is used to identify particular areas of the brain where there are statistically-significant differences in mean voxel FA between two patient cohorts.

The principal inputs to TBSS are the FA maps of the patients in the two cohorts being compared. The FA maps are aligned into a common space using the FNIRT non-linear registration tool (Andersson *et al.*, 2007). The FA image is created and thinned to create an FA skeleton that represents the centres of all tracts common to the cohort. The aligned FA data of each patient are projected onto this skeleton. Differences are identified across all of the white matter pathways using voxel-wise cross-subject statistics, including visual and other tracts.

In this study, TBSS was used to identify associated anatomical abnormalities related to ONH in areas of the optic radiations that might be distinguished by large localised differences in FA compared to a control cohort average. In contrast to the approach of Webb *et al.* (2013), patients from each cohort were closely paired according to both age and sex so a paired t-test could be performed on the results. The age difference within each pair was less than one year. An FA threshold of 0.2 was used to identify areas of white matter. TBSS does not assume a Gaussian distribution model of voxels, and the voxel-wise two-sample nonparametric permutation tests were performed with 5000 permutations. A reference atlas from Melhem *et al.* (2002) was used as a localisation tool to identify the master skeleton and visualise the statistical results.

The main challenge with using TBSS is aligning the brains in each cohort to a single template, as they have many variations in their shapes and sizes. If the alignment is inaccurate then there is a chance that the voxel containing white matter in subject A does not contain any white matter in subject B. The lack of white matter substance can be caused by anatomical differences or variations, pathology (which is the focus of this study) or just poor alignment. Brains with non-standard anatomies were not considered for this part of the study in order to reduce the influence of anatomical

variations, and the TBSS intermediate outputs and results were carefully checked to ensure that good alignment had been achieved.

6.3 Description of the cohort

The ONH patient cohort was recruited from the Great Ormond Street Hospital ophthalmology and endocrinology departments. The earliest referrals came from the ophthalmology department as visual defects tend to be identified at an early stage of development. Endocrinology referrals tend to be older, at least three years in most cases, as referrals to that department are normally due to delayed growth or a sexual development abnormality.

Children were referred to the study by the lead clinician. Some patients already had ONH diagnosis at the time of referral, while others were referred while still in the process of formal diagnosis, with the MRI as a part of the screening test. Scanned patients with suspected ONH that was not subsequently diagnosed were not used in the study. The parents and patients were informed about the purpose of the research, both verbally and in writing, and patients were enrolled in the study following the receipt of written parental consent. In total, 33 patients were recruited. Another 15 patients were approached but could not take part in the study for a range of reasons, for example the long travel time between their primary residence and the hospital (GOSH is a tertiary referral centre).

Patients with severe septo-optic dysplasia, or with very significant midline abnormalities, were excluded from this study, in order to avoid biasing the results through the inclusion of outliers. Of the 33 recruited patients, 10 were excluded on these grounds, so only 23 were used in this study. These included 12 males and 11 females, with ages ranging from 4 months to 16 years at the time of enrolment. The patient diagnoses are listed in Table 6.1. Two patients presented only right ONH while the rest all presented bilateral ONH. The two cases of septo-optic dysplasia were mild, with no endocrinological or growth retardation; both of these children followed normal schooling for their age.

Sex	Age	Diagnosis	BEO flash	RE & LE symmetry	LE pe 100 ms	RE pe 100 ms
M	716	Bilateral ONH	0	Symmetrical	0	0
F	579	Bilateral ONH	12	Symmetrical	4	0
F	562	Bilateral ONH	0	Symmetrical	0	0
M	468	Bilateral ONH/SOD	28	Symmetrical	47	20
F	475	Bilateral ONH	0	Symmetrical	0	0
F	780	Bilateral ONH	0	Symmetrical	14	10
F	312	Bilateral ONH	0	Symmetrical	0	0
M	260	Bilateral ONH	16	Asymmetry	6	13
M	125	Bilateral ONH	13	Symmetrical	8	0
F	154	Bilateral ONH	0	Symmetrical	0	0
F	493	Bilateral ONH	0	Symmetrical	4	5
M	136	Bilateral ONH	8	Symmetrical	0	16
M	257	Bilateral ONH	0	Asymmetry	9	0
M	55	Bilateral ONH	15	Symmetrical	0	0
M	335	Bilateral ONH	20	Asymmetry	9	12
M	238	Bilateral ONH	0	Symmetrical	0	0
M	367	Bilateral ONH	0	Symmetrical	0	0
M	100	Right ONH	20	Symmetrical	20	0
F	49	Right ONH	0	Symmetrical	0	0
M	780	Bilateral ONH	7	Symmetrical	0	0
F	30	Bilateral ONH	22	Asymmetrical	0	0
F	832	Bilateral ONH	0	Symmetrical	0	0
F	14	Bilateral ONH/SOD	14	Symmetrical	10	12

Table 6.1 Clinical diagnosis of the ONH patients. The sex is listed as Male or Female. The age is displayed in weeks. Two patients were diagnosed with mild septo-optic dysplasia (SOD). For the Both Eyes Open (BEO) flash, results are displayed in milliseconds and 0 indicates a null recorded response with maximal optimal stimuli. "LE pe" and "RE pe" are the potential evoked (pe) in the left eye (LE) and right eye (RE).

The ONH patients were compared against the controls scanned with the 3×20 protocol described in Section 4.4.2 and Table 4.3. Since there were more controls than ONH patients, a subset of 23 controls with a similar age profile to the ONH cohort were chosen for the comparison, as illustrated in Figure 6.1. The Levine test for homogeneity of the two cohorts was used to confirm that age differences would not skew the ANCOVA statistics. There was also a similar split between males and females in each cohort, as shown in Table 6.2. For the TBSS analysis, patients from each cohort were paired according to age and sex, which leads to a smaller sample of patients being analysed from each cohort.

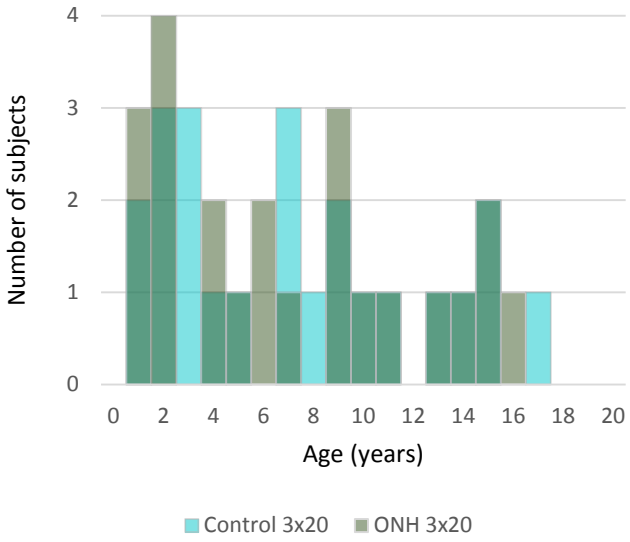

Figure 6.1 Histogram of the ONH and control age profiles. Dark green areas represent one patient from each cohort.

	Controls	ONH
Female	12	11
Male	11	12

Table 6.2 Summary of control and patient cohorts by gender.

6.4 Results

Differences between the control and ONH cohorts were examined in terms of visual tests, optic radiation length, number of tract voxels and FA.

FA differences were assessed using several complementary methods. FA graphs are presented for the left and right optic radiations in Sections 6.4.4 and 6.4.5, respectively, and statistical differences in FA between the cohorts are then examined in Section 6.4.6. The section concludes with an appraisal of within-brain mean FA differences using TBSS.

6.4.1 Visual testing of the ONH patients

The results of the visual tests on the ONH cohort are shown in Table 6.1. There was a wide range of visual impairment from mild visual loss, requiring glasses, to profound blindness, but with most patients suffering moderate to severe visual impairment.

The TBSS program was used to try to identify any correlation, in any part of the optic tracts, between the level of myelination and visual function. FA is correlated to and can be used as a proxy for myelination (Dubois *et al.*, 2008). The ONH cohort was split into two groups according to whether the patients responded to the BEO flash test (as shown in Table 6.1). The TBSS program was used to identify differences in FA between these two groups using a paired t-test. No statistically-significant correlation between the level of myelination, represented by FA, and visual function could be established in any part of the visual tracts.

6.4.2 Optic radiation length differences

The optic radiation lengths for each patient were measured using the method described in Section 3.4.6. The ONH patients appear to have a smaller left optic radiation length than the controls in Figure 6.2, but this is not statistically-significant (ANCOVA test, $p=0.12$). The difference is caused by a small number of patients having an abnormally low length, while no difference is discernible for most patients. Figure 6.3 shows that the discrepancy between cohorts is smaller for the right optic radiation, for which there are fewer ONH patients with abnormally low optic radiation lengths, and there is again no statistically-significant difference (ANCOVA test, $p=0.71$).

6.4.3 Tractography voxel differences

Another method to measure the variation (between ONH patients and controls) of the optic radiations is to count the number of voxels identified by the tractography analysis. The statistics for the two cohorts, including the fraction in the front of the brain, are shown in Table 6.3. The total number of voxels is smaller for the ONH cohort for both optic radiations, while the variance is similar. The ONH cohort has a greater fraction of voxels at the front of the brain than the control cohort for the left optic radiation, suggesting that the reduction principally occurs at the rear of the optic radiations at the gathering of the primary visual cortex. For the right optic radiation, for which the reduction for the ONH cohort is smaller, there are similar fractions of voxels located at the front for both cohorts.

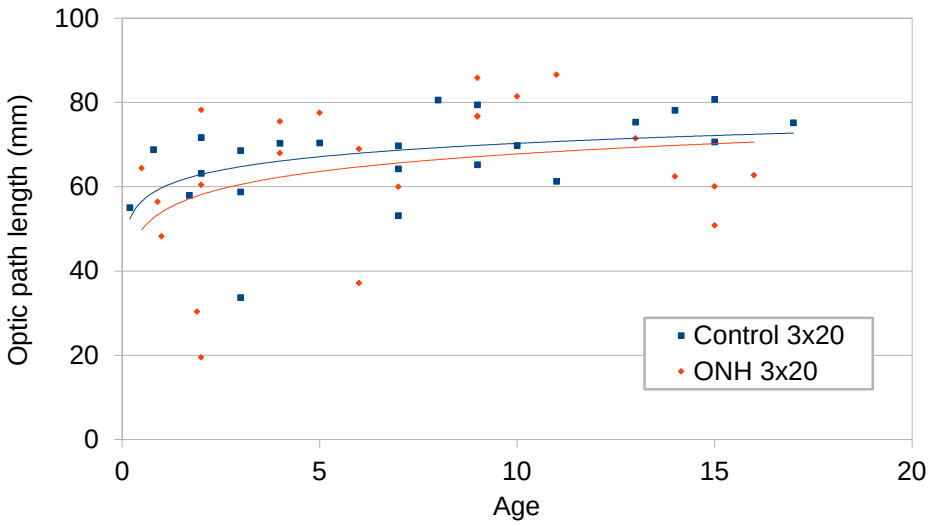

Figure 6.2 Length of the left optic radiation for the ONH and control cohorts. The length was estimated from the tractography maps of the optic radiations.

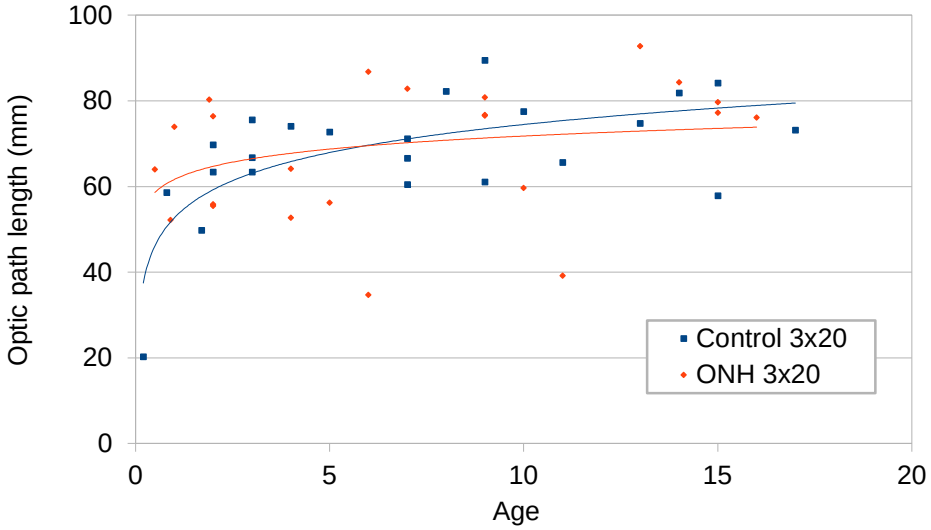

Figure 6.3 Length of the right optic radiation for the ONH and control cohorts. The length was estimated from the tractography maps of the optic radiations.

	Total voxels		Fraction of front voxels	
	Left	**Right**	**Left**	**Right**
Control	422 ± 204	376 ± 191	0.34 ± 0.13	0.43 ± 0.16
ONH	373 ± 191	352 ± 210	0.43 ± 0.15	0.45 ± 0.16

Table 6.3 Number of voxels representing each optic radiation from tractography analysis. The mean fraction of voxels located in the front of the brain is also shown. Figures are presented in the form mean ± standard deviation for each cohort. Each voxel is a cube with sides measuring 2.5 mm.

6.4.4 Mean FA and MD differences: left optic radiation

The mean FA of the left optic radiation is shown for both cohorts in Figure 6.4. The ONH patients have lower values of mean FA on average than the control patients, particularly for the older patients. The mean FA measurements at the front and rear of the left optic radiation are shown in Figures 6.5 and 6.6, respectively. In both graphs, the ONH patients appear to have lower mean FA than the control cohort, with a particularly large difference for older patients in the front of the optic radiations, where the optic radiation is thickest.

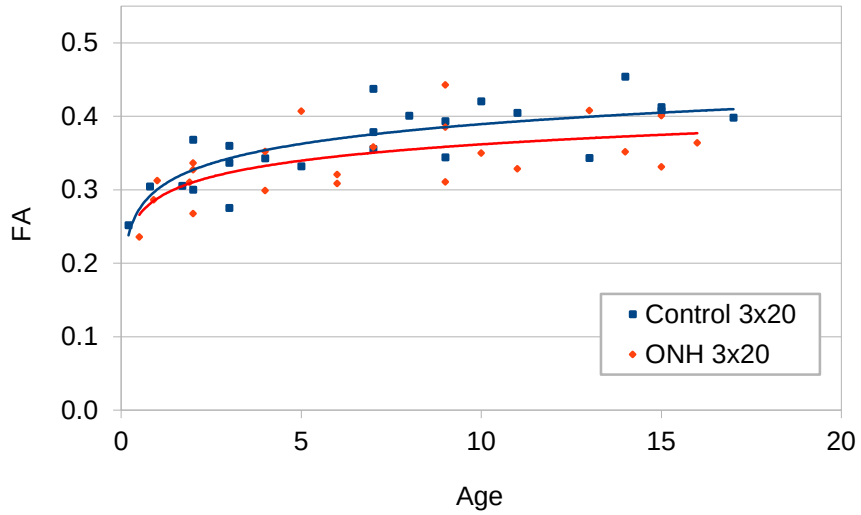

Figure 6.4 Mean FA across the full left optic radiation for the ONH and control cohorts.

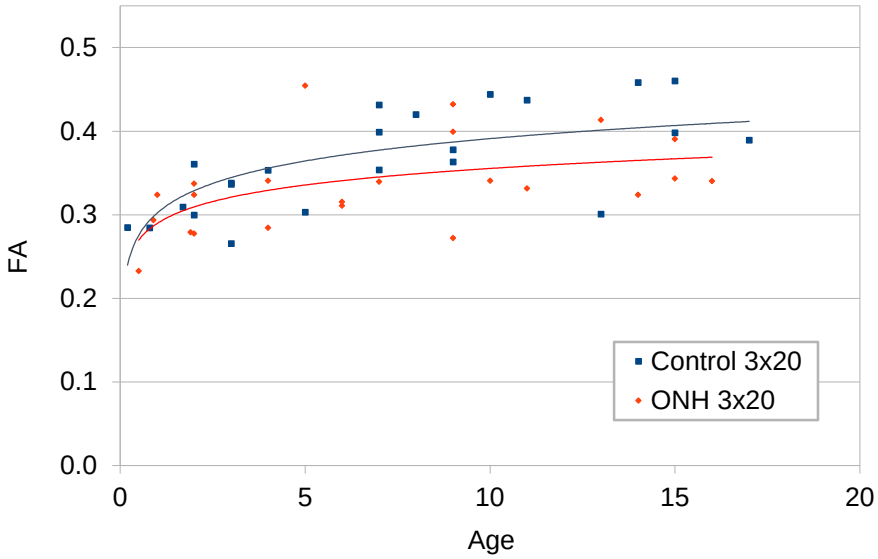

Figure 6.5 Mean FA of the front of the left optic radiation for the ONH and control cohorts.

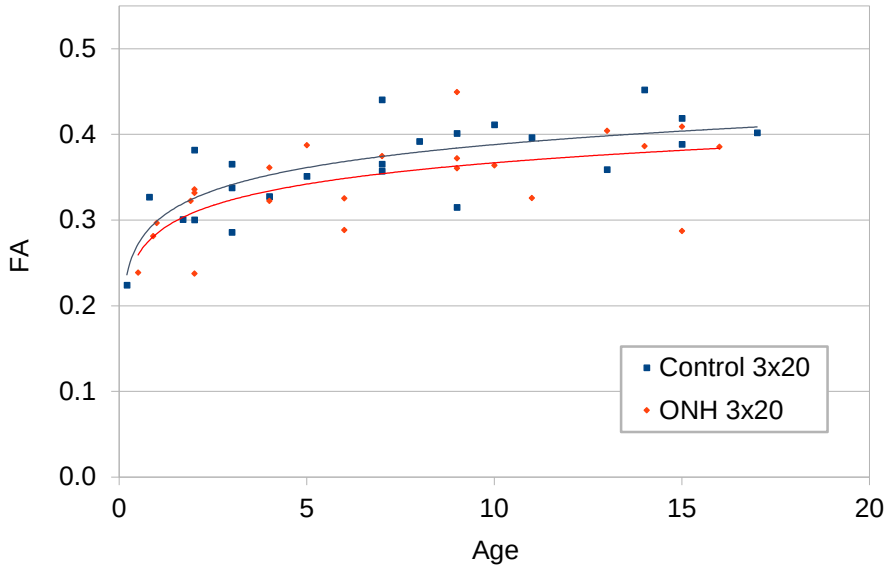

Figure 6.6 Mean FA of the rear of the left optic radiation for the ONH and control cohorts.

The ONH mean FAs are more variable than the control mean FAs due to a subset of ONH cases having unusually low values. This is illustrated in Figure 6.7, which shows the discrepancy of the front and rear optic radiations mean FAs relative to the control cohort regression line for each series (i.e. the left front optic radiation control and ONH mean FAs are plotted relative to the left optic radiation front control regression line, so the front and rear optic radiation control regressions both have the equation y=0). The ONH discrepancies range from –0.14 to +0.10. The ONH discrepancies for the patients in the 13 to 16 age range are particularly negative, which causes the ONH regression equation for those patients aged over 5 years to have a negative rather than a positive gradient with age.

The mean MD measurements for both cohorts for the left optic radiations are shown in Figure 6.8. The mean MD values decrease with age as expected. The trends are similar for both cohorts, with the exception of two ONH outliers. One of these was a 16-year-old male with bilateral ONH. The second was a 6-year-old female with very poor vision and bilateral optic nerve hypoplasia. Neither of these patients had midline abnormalities or developmental disability besides the visual impairment detected at the time of scanning.

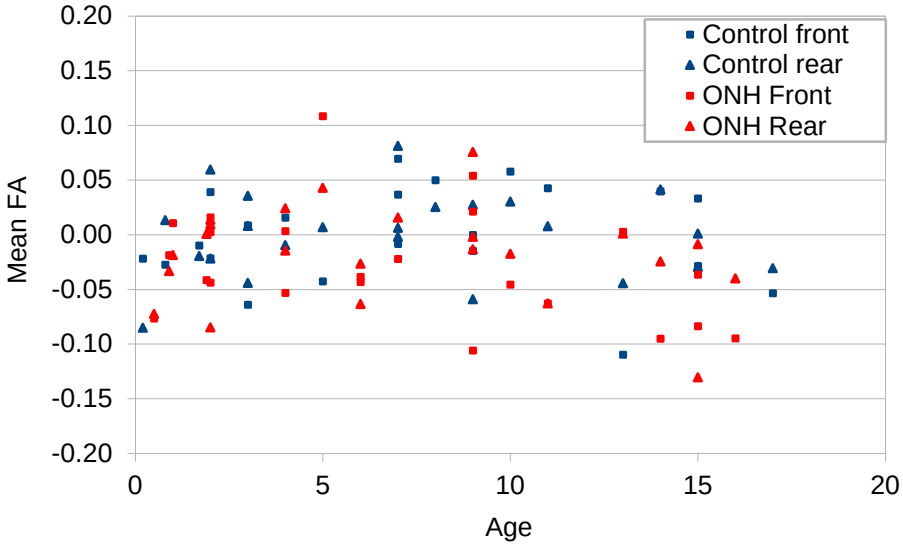

Figure 6.7 ONH and control cohort mean FA discrepancies for the left optic radiation relative to the linear regression of the control cohort. See the main text for details of how the discrepancies are calculated.

6.4.5 Mean FA and MD differences: right optic radiation

The mean FA of the right optic radiation is shown for both cohorts in Figure 6.9. The ONH patients appear to have lower values of mean FA on average than the control patients, but, in contrast to the left optic radiation, the differences are small and do not change with age. The mean FA measurements at the front and rear of the left optic radiation, in Figures 6.10 and 6.11, have different trends. The right front optic radiation trend is similar to the left optic radiation, with the difference between controls and ONH patients increasing with age. In contrast, the difference in FA at the rear does not appear to change with age.

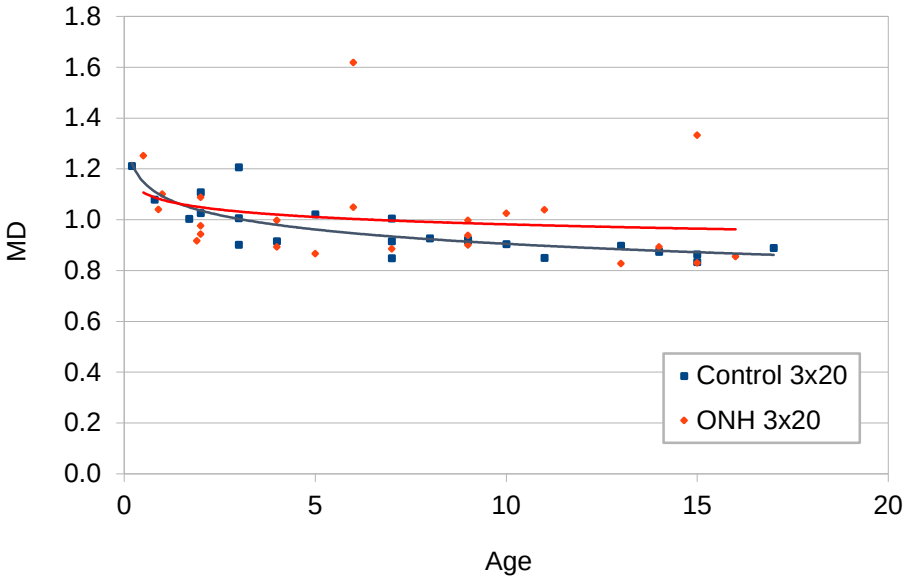

Figure 6.8 Mean MD across the full left optic radiation for the ONH and control cohorts.

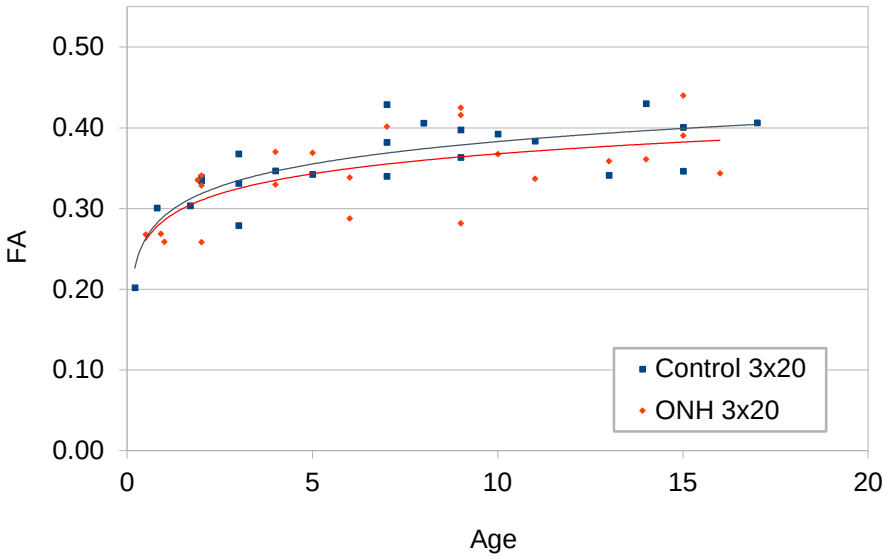

Figure 6.9 Mean FA across the full right optic radiation for the ONH and control cohorts.

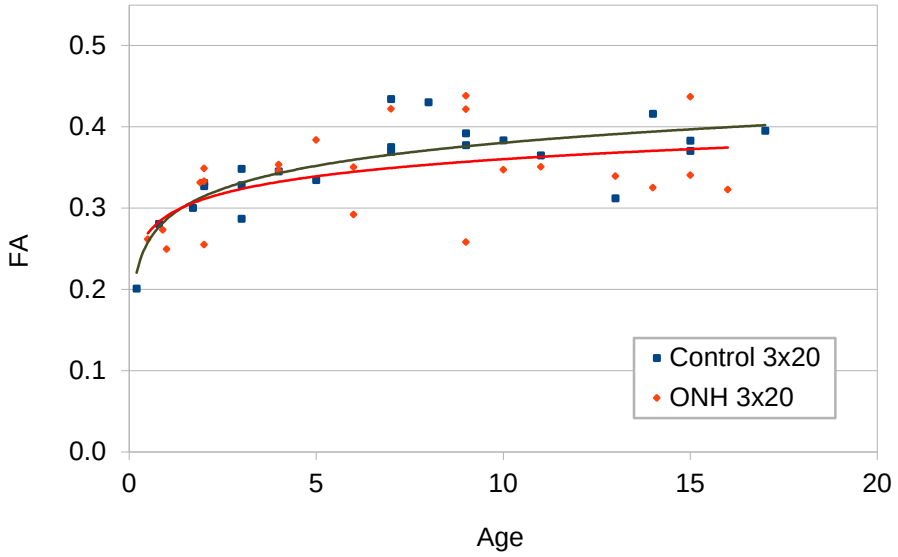

Figure 6.10 Mean FA of the front of the right optic radiation for the ONH and control cohorts.

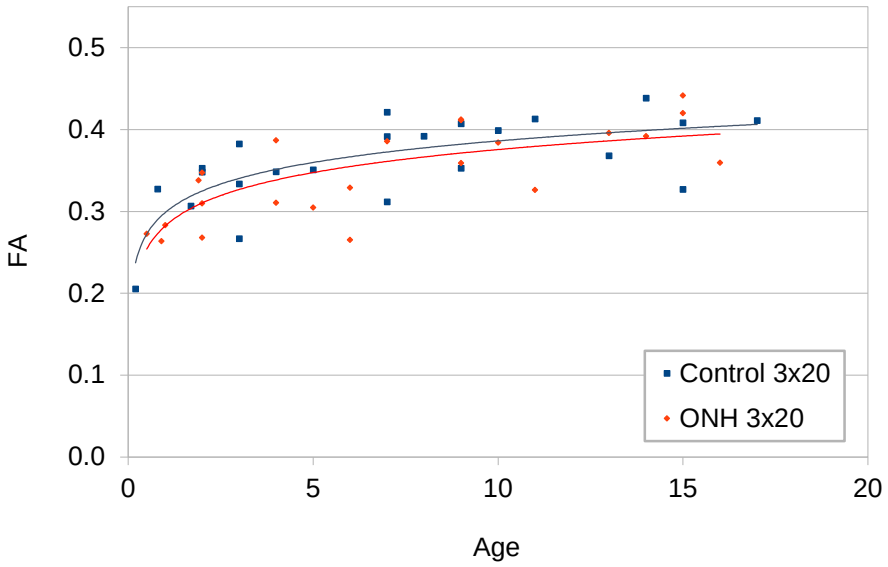

Figure 6.11 Mean FA of the rear of the right optic radiation for the ONH and control cohorts.

The discrepancies in the front and rear optic radiation mean FAs relative to the control cohort regression line for each series are shown in Figure 6.12 for the right optic radiation. In contrast to the left optic radiation, there is little evidence that the control and ONH patient differences are caused by a small number of the cases having unusually low mean FA, with virtually all of the discrepancies lying in a narrower range of –0.10 to +0.10.

The mean MD measurements for both cohorts on the right optic radiation are shown in Figure 6.13. As with the left optic radiation, the mean MD values decrease with age. There are again two outliers; the most significant also has a very high left mean MD, while the other, an 11-year-old female with bilateral ONH and a right convergent squint, is different to the second left-side outlier. With the exception of the outliers, the trends are again similar for both cohorts.

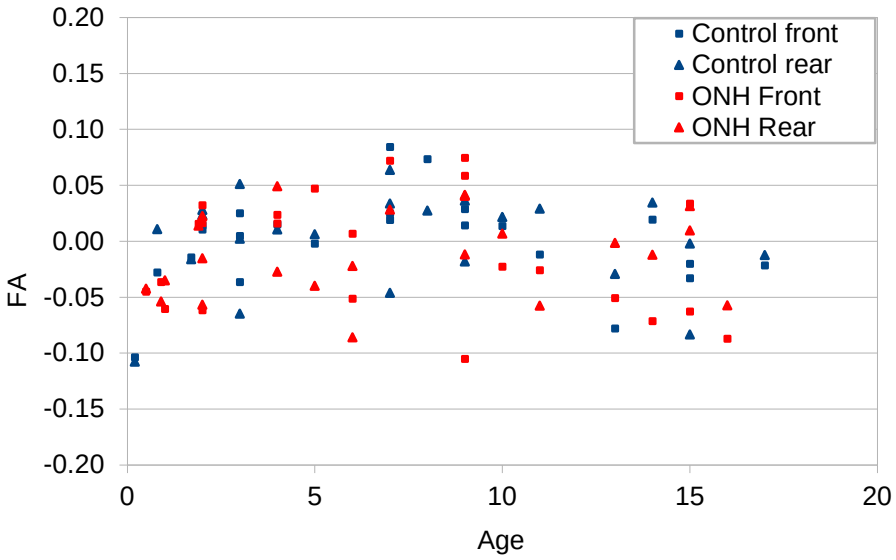

Figure 6.12 ONH and control cohort mean FA discrepancies for the right optic radiation relative to the linear regression of the control cohort. See the main text for details of how the discrepancies are calculated.

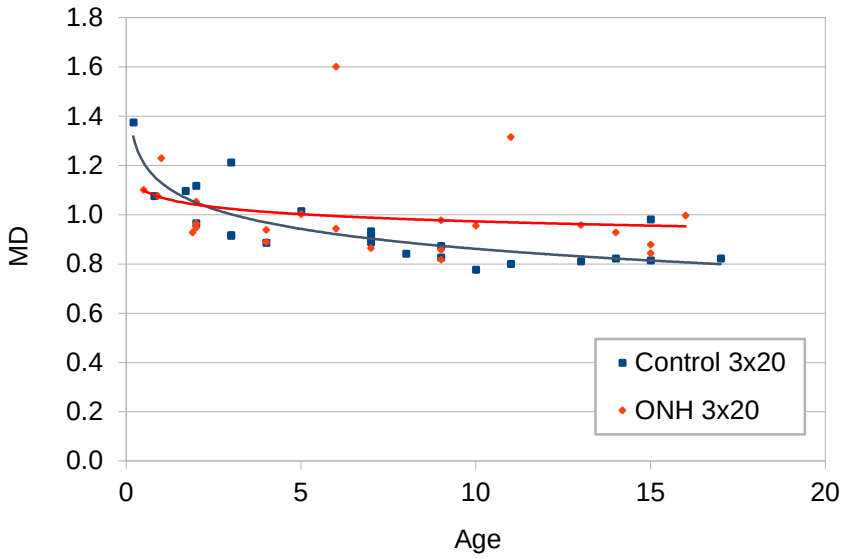

Figure 6.13 Mean MD across the full right optic radiation for the ONH and control cohorts.

6.4.6 Mean FA statistical differences

The differences in mean FA between the control and ONH cohorts was tested using ANCOVA statistics to remove age as a dependent variable. Since the relationship between mean FA and age is not linear in the control cohort (Section 4.3), the tests were performed separately for children up to 5 years and those over 5 years old.

The cohort of children up to 5 years old contained 10 subjects in each cohort, so 17 degrees of freedom. The Levene non-homogeneity test was performed for each ANCOVA test and demonstrated homogeneity of regression slopes with age in all cases. The results are summarised in Table 6.4 for the front, rear and full tracts of the left and right optic radiations. There are no statistically-significant differences between the mean FAs of the two cohorts in any of these areas of the optic radiations.

The cohort of children over 5 years old contained 13 subjects in each cohort. The Levene test again demonstrated homogeneity of regression slopes with age in all cases. For these cohorts, Table 6.5 shows the difference between the ONH and control mean FAs is statistically-significant for the left optic radiation ($p<0.05$), with the differences particularly at the front of the optic radiation ($p<0.01$). The greatest difference for the right optic radiation is similarly at the front but is not statistically-significant.

	Left optic radiation				**Right optic radiation**			
	F	**P**	**Eta**	**Levene**	**F**	**p**	**Eta**	**Levene**
Full	0.014	0.908	0.001	0.855	0.007	0.932	0.000	0.421
Front	0.042	0.841	0.002	0.340	0.423	0.524	0.024	0.618
Rear	0.122	0.732	0.007	0.539	0.404	0.533	0.023	0.683

Table 6.4 Comparison of tract mean FA for the 3×20 control and ONH cohorts aged up to 5 years using ANCOVA tests. Results are presented for the left and right optic radiations, for the full, front and rear of the tracts. * p<0.05. ** p<0.01.

	Left optic radiation				Right optic radiation			
	F	**P**	**Eta**	**Levene**	**F**	**p**	**Eta**	**Levene**
Full	6.673	0.017*	0.225	0.382	1.635	0.214	0.066	0.122
Front	8.237	0.009**	0.264	0.826	2.303	0.143	0.091	0.058
Rear	2.856	0.105	0.110	0.563	0.523	0.477	0.022	0.795

Table 6.5 Comparison of tract mean FA for the 3×20 control and ONH cohorts aged over 5 years using ANCOVA tests. Results are presented for the left and right optic radiations, for the full, front and rear of the tracts. * p<0.05. ** p<0.01.

6.4.7 Within-brain mean FA differences

The differences in white matter FA across the white matter tracts of the ONH and control cohorts were identified using TBSS. Figure 6.14 shows the differences in different slices of the brain. Tracts with statistically-significant differences in mean voxel FA between the cohorts are coloured. The areas where the ONH children present decreased mean FA extend well beyond the optic radiations, with motor and language areas presenting a decreased mean FA. Within the optic radiations, there are differences anteriorly and, to a lesser degree, posteriorly. For both left and right optic radiations, the rear has a smaller number of statistical differences than the Meyer's loop areas at the front, where the differences between the subjects are statistically-significant.

The explanation underlying the decreased mean FA in the Meyer's loop areas, compared with the posterior portions of the optic radiations that gather into the primary visual cortex, might be a lack of visual stimuli reaching the LGN from the retina, as the optic radiations receive most of their information from the LGN. The primary visual cortex receives information from other secondary visual areas as well as accessory areas, which could compensate for the loss of primary visual information. This additional information might underpin myelination, wiring and functional development through the secondary myelination area located in the posterior aspect of the optic radiations. As a result, the rear of the optic radiations would not present much greater impairment than the control cohort.

Some other areas that are close to the temporal lobe, principally language centres, have lower myelination rates in ONH patients. The right hemisphere, where the facial recognition area is located, also has statistically-significant differences.

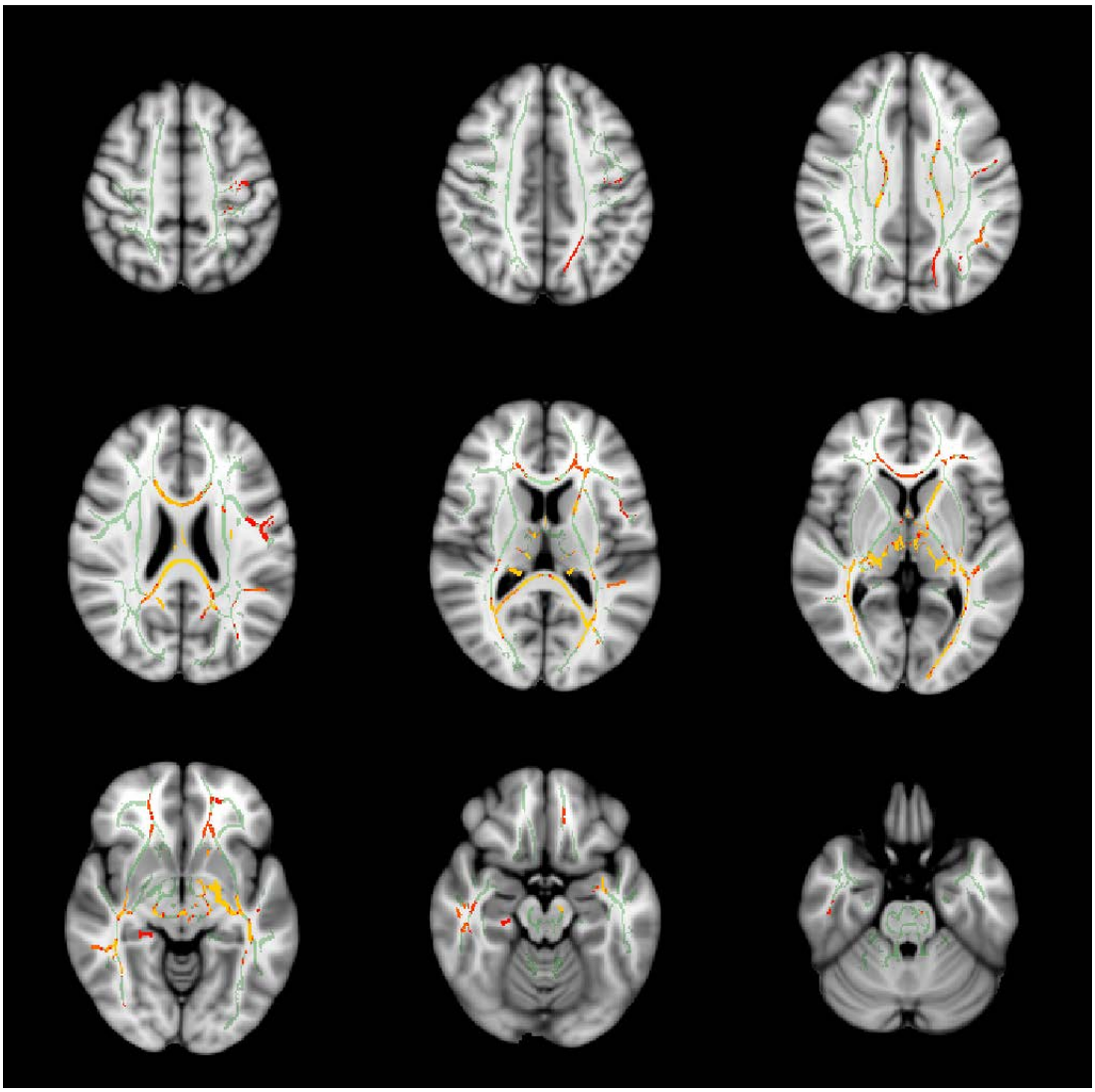

Figure 6.14 Differences in white matter FA between the control and ONH cohorts. Areas of constant FA between the cohorts are shown in green. The red-yellow areas indicate differences between the cohorts, where red represents $p<0.05$ and yellow represents $p<0.01$.

6.5 Discussion

6.5.1 Impact of optic radiation FA changes on visual function

Research is ongoing into functional development and its implications for white matter tracts. TBSS can be used to examine the relationship between myelination and visual function, using FA as a proxy for myelination. However, no statistically-significant differences in FA between groups of patients with and without responses to flash patterns were found in this study, despite the optic nerve being hypoplasic in children with ONH. One possible reason is related to the resolution of the MRI scans. Current DTI clinical imaging has insufficient resolution to be able to identify small wiring defects in the optic radiations, as micrometre-scale axons cannot be represented by 2.5 mm voxels, so the degree of impairment might not have been identified by the scans performed in this project. As imaging techniques improve, higher-resolution scans should enable smaller lesions to be identified (Bridge *et al.*, 2011).

Another possible explanation for the lack of statistically-significant differences is related to information-sharing between the primary visual cortex, V1, where the optic radiations gather, and the secondary visual cortices. It is possible that the secondary visual cortices have a more important role during the development of the visual system than previously thought, particularly in cases of underdevelopment of the visual pathways (Grossberg, 2001). Full visual development includes wiring and intricate connections to visual areas, not just simply the gathering of information from the optic radiations into the primary visual cortex (Grossberg, 1999). The secondary visual centres could conceivably facilitate the development of areas of the visual system in individuals lacking supply of stimuli or visual information from the primary visual cortex, with the effectiveness of these alternative processes depending on the brain plasticity of the individual. The different degrees of brain plasticity and the varying transmission of information from the secondary visual cortices could then explain interpersonal variations in visual function amongst patients with bilateral ONH and similar anatomical handicaps. This would suggest that the primary visual cortex is not only an information filtering system, as suggested by Hubel *et al.* (1977), but a more complex interlinked information-sharing system, as discussed in Grossberg (2003).

6.5.2 Reduction in FA in ONH patients

The tractography analysis shows that the left optic radiation has a statistically-significant lower mean FA in ONH patients older than 5 years than the control cohort, while the right optic radiation has no statistically-significant differences, despite most of the patients having bilateral ONH. Left optic radiation differences occur principally at the anterior portion of the optic radiation, which could be related to a reduced flow of information from the retina to the LGN causing underdevelopment. These results would be consistent with a two-tier myelination process occurring in the optic radiations, in which each tier followed a different development path, affected by different stimuli, causing variations within interlinked white matter tracts (Dubois *et al.*, 2008). Visual impairment through the periods of critical development could cause ever wider differences (Lewald and Getzmann, 2013); the effects of blindness on visual tract development and brain plasticity are not fully understood (Agarwal and Fox, 2013). The results contrast with those of Xie *et al.* (2007), who find no reduction in mean FA for either optic radiation, but for a smaller cohort of amblyopia rather than ONH patients. It is notable that Xie *et al.* (2007) found the left optic radiation to have a higher mean FA than the right optic radiation for both ONH and control cohorts, similar to this study (see Section 4.4).

TBSS is a powerful technique to analyse the impacts of ONH on white matter in patient cohorts, as it identifies specific regions of the white matter tracts that are different in ONH patients than controls and does not require time-consuming tractography. In this study, TBSS corroborates the tractography analysis of the mean FA in the front and rear of the optic radiations. Yet areas located within the temporal lobe of the dominant hemisphere such as the language centre and facial recognition area also had lower mean FA in the ONH cohort than the control cohort. This shows that ONH is not purely related to an abnormal optic nerve, but that these patients have other abnormal white matter tracts. It suggests that ONH should be regarded as a complex syndrome that is not restricted to the visual system. Low mean FA could be related to underdevelopment of accessory information pathways linked to vision that might not achieve optimal development, such as visual association, colour recognition, and tactile and visual memory areas (Ricciardi *et al.*, 2014). The wider effects of ONH might be explained by the interlinked development of white matter tracts along the brain in the early stages of development, when it has high plasticity and reorganisation

capabilities (Iughetti *et al.*, 2011). This enormous plasticity potential can compensate for a high rate of damage, should pathways have abnormal development at an early stage. Even genetic disorders can be counteracted, to certain degree, by appropriate stimuli (Altemeier and Altemeier, 2009). High plasticity is thought to aid recovery from strokes in elderly patients (Lin *et al.*, 2014). However, should damage occur during early development that prevents connections between white matter pathways, then the degree of plasticity is very much reduced (Finger, 2010). The plasticity mechanism is an ongoing area of research that is beyond the scope of this study.

Clinical studies and genetic research have shown that ONH is not a single defect involving vision, but a more generalised disease that might present visual disturbances as a first sign (McCabe *et al.*, 2011, McCabe *et al.*, 2013). The wide range of visual disabilities presented by these children, varying from severe to mild, is not thought to be related to the grade of abnormal size and shape of the optic nerve. Endocrinological, developmental and facial abnormalities might be also associated to ONH, but the importance and phenotypic traits of different genetic malformations have still to be discovered. More generally, further research is required to understand whether the widespread reduction in mean FA is the cause or a consequence of ONH, and whether diagnosed ONH can have different causes in different patients.

6.5.3 Mean MD differences in some patients

Three ONH patients were found to have unusually high mean MD compared to the rest of the cohort and controls, although only one of these had high mean MDs for both optic radiations. None of the three had exceptional symptoms compared to the rest of the cohort; all three had bilateral ONH and none had midline abnormalities or developmental disability besides visual impairment. The VEP tests produced similar pathological results for these patients with the rest of the cohort, and none of the children's siblings had been diagnosed with ONH or other developmental disability. There were no motion artefacts in any of these cases, as all scans were checked carefully and poor-quality scans discarded.

The most unusual case was a 16-year-old male with poor vision that comprised only light perception in each eye. He underwent a stem cell retina implant procedure in China shortly before he was included in this study. The patient in question had already had the treatment performed twice, sponsored by his own parents. While he had light

sensation and perception improvement after the treatment, it was not measureable in the clinical examination. This outcome was consistent with a case study of two patients who underwent stem therapy at the Chinese Institute performing the technique, which did not identify improved vision or show any changes compared to controls, with no apparent clinical changes in the size or shape of the optic nerve or the pupillary constriction (Fink *et al.*, 2013).

There is no obvious explanation of why the mean MD was unusually high for these patients. One possibility is that the mean MD does not fully correlate with the degree of impaired optic radiation myelination that might have been present in these patients; poor correlation has been observed in a study of multiple sclerosis patients (Kolbe *et al.*, 2009).

6.5.4 Using VEPs and DTI tractography for diagnosis and follow-up

The cause of ONH is not known and no cure is available (Garcia-Filion and Borchert, 2013). No diagnostic protocol has been established besides clinical examination using VEPs and, for severe cases, clinical MRI.

Tractography could be used to examine the development and myelination of the optic radiations in patients diagnosed with ONH. It would be necessary to compare development against a control cohort scanned on the same machine with the same protocol, given the differences in mean FA between protocols described in Section 3.5. While this would not facilitate treatment at the moment, it might contribute to a better understanding of ONH and give an indication of the potential suitability for the patient of new treatments that have not yet been developed. Moreover, future improvements in DTI resolution might greatly improve the understanding of the patient's pathology, by enabling individual parts of the optic radiations to be resolved. This would contribute to developing an appropriate follow-up strategy to facilitate the early detection of complications. Early monitoring of children with ONH is recommended by Borchert and Garcia-Filion (2008).

6.6 Conclusions

Children with ONH have visual problems, and in many cases other associated medical pathologies such as hypothyroidism, hypopituitarism and abnormal development of

the midline brain structures. No diagnostic protocol has been established apart from clinical examination. Changes in the optic radiations have not previously been examined in patients with mild ONH using DTI tractography analysis of each individual optic radiation. A novel methodology has been presented in this chapter that identifies overall changes in the optic radiation mean FA using tractography, and combines this with a TBSS analysis of mean FA differences across the white matter tracts. As well as looking at mild rather than severe cases, it has also used a much larger cohort (23 patients) than previous studies, and has paired the ONH patients in all of the analyses with controls of the same age in order to reduce the influence of age-related mean FA differences.

Tractography analyses showed that the left optic radiation had a statistically-significant lower mean FA in ONH patients older than 5 years than the control cohort, while the right optic radiation had no statistically-significant differences. This difference occurred principally at the front of the optic radiations in the region of Meyer's loop. No statistically-significant differences were detected for patients aged up to 5 years. These findings were confirmed in the TBSS analysis, which showed statistically-significant mean FA reductions in both optic radiations but particularly for the left. They indicate that ONH is not purely related to an abnormal optic nerve. Further research is required to understand whether this more widespread reduction is the cause or a consequence of ONH, and whether diagnosed ONH can have different causes in different patients. Higher-resolution DTI would be a valuable tool for such an investigation.

DTI tractography could help to examine the ongoing development and myelination of the optic radiations in patients diagnosed with ONH, particularly if a control cohort were available as a baseline. Higher-resolution DTI would facilitate a better understanding of the patient's pathology, by enabling individual parts of the optic radiations to be resolved.

7 CHANGES IN THE OPTIC RADIATIONS IN CHILDREN WITH SEIZURES

The development of the optic radiations in the paediatric population with seizures is examined using DTI tractography analyses. Two cohorts of patients are examined. The first is composed of children who have suffered a single episode of complex febrile seizures that required medical intervention and hospital admission, but was not yet classified as epilepsy at the time of scanning. The second is composed of children who have been exposed to epilepsy and to anti-epileptic medicines over a period of more than 6 months. Comparing these two cohorts gives an indication of the relative damage to the brain caused by a single seizure and by prolonged episodes of epilepsy.

7.1 Introduction

In 2005, the International League Against Epilepsy defined epilepsy as a brain disease marked by the presence of seizure activity (Fisher *et al.*, 2005). Seizure activity or epileptic seizure was defined as the transient occurrence of signs and symptoms due to abnormal excessive or synchronous neuronal activity in the brain. Epilepsy as a disorder was described as the continuous predisposition to produce epileptic seizures, and by the neurobiological, cognitive, psychological and social consequences. This definition of epilepsy was updated by Fisher *et al.* (2014) as any of: (i) two seizures at

least 24 hours apart; (ii) one unprovoked seizure with a 75% probability of a subsequent seizure; or, (iii) at least two seizures in a setting of reflex epilepsy.

Febrile convulsions are seizures that often occur when the child presents a corporeal temperature higher than 38 °C (NHS, 2014). The incidence of febrile convulsions is thought to be in the range 2–4% for children aged between three months and five years (Trinka *et al.*, 2002). These seizures can be divided into two categories:

1. Simple febrile seizures: single tonic-clonic episodes that do not last longer than 15 minutes. Children with a simple febrile convulsion present a second episode in 33% of the cases (Vestergaard *et al.*, 2008).
2. Complex febrile seizures: seizure that lasts longer than 15 minutes or where the child does not fully recover after one hour of the event. A seizure is classified as complex if the episode repeats within 24 hours or if the child presents focality during the convulsive period. Focality is where the symptoms involve only one part of the body, as opposed to a simple seizure where the movements tend to be symmetrical and involve upper and lower limbs equally.

Convulsive status epilepticus is defined as a seizure, or a series of consecutive seizures, lasting longer than 30 minutes. In some cases, mainly in the paediatric population, convulsive status epilepticus is triggered or related to febrile seizures. Prolonged febrile seizures can be included in the complex febrile seizures cohort and are one of the main causes of status epilepticus in children (Frank *et al.*, 2012).

Mortality related to simple febrile convulsions has not been shown to be higher than that of the healthy population. In contrast, complex febrile seizures present an increased risk of death as well as a higher risk of complications (Vestergaard *et al.*, 2008). Patients who present febrile convulsions within the first year of age, or with temperature lower than 39 °C, have increased risk of complications. These two cohorts, together with the complex febrile convulsions cohort, have a two-fold increased risk of death during the two-year period following the first episode.

7.1.1 Epidemiology of epilepsy

Epidemiology studies carried out at the beginning of the twenty-first century estimate the incidence of epilepsy in developed countries to be 40–70 cases per 100,000 inhabitants per year (Sander, 2003, Ngugi *et al.*, 2010, Ngugi *et al.*, 2011).

In children, the incidence of epilepsy is not well understood, but it is thought to be around 80 cases per 100,000 children per year (Kotsopoulos *et al.*, 2002), which is a prevalence of 1% (Major and Thiele, 2007). Epilepsy is the most common neurological condition in childhood (Terra *et al.*, 2014). The risk of death in cases of early childhood epilepsy is 5–8 times higher than in the non-epileptic population (Grønborg and Uldall, 2014).

7.1.2 Clinical neuroimaging for seizures

Patients are normally referred following their first seizure. There are many pathologies related to epilepsy; for example, the patient cohorts in this study include children with fever-related seizures, tumours, and primary epilepsy linked to abnormal anatomical structures. The International League Against Epilepsy has produced a recommendation and diagnosis framework to clarify and simplify the diagnosis and clinical process of childhood epilepsy in referral and primary care centres (Iliescu and Craiu, 2013).

Neuroimaging is often recommended for children with afebrile seizures, with the presentation of an episode of complex seizure, or with other associated factors (for example, bleeding disorders, VP shunts or HIV). It is used for both surgical planning and follow up. For cases of febrile seizures, the American Academy of Paediatrics recommends appropriate age-managed control of the fever but does not recommend routine neuroimaging (Agarwal and Fox, 2013).

For preoperative surgical planning, neuroimaging is used to:

- Identify the underlying cause of the epilepsy.
- Describe in as much detail as possible the anatomy of the individual patient who will undergo surgery.
- Serve as an intraoperative guide during the surgical procedure.

The most widely-used imaging technique is MRI, with the protocol depending on the hospital and the patient. The protocol normally includes T1 and T2-weighted axial and coronal sections to visualise the patient brain anatomy. These can include:

- T1 and T2-weighted FLAIR. T1 FLAIR is used to visualise grey and white matter. It is useful for identifying the boundaries between the two in order to highlight areas of abnormal migration or growth such as those occurring in

focal cortical dysplasia. T2 FLAIR highlights tissues with a rich concentration of water, which can be linked to abnormalities such as very low-grade tumours or gliosis.

- T1-weighted spoiled gradient echo thin slices (1–2 mm) leaving no gaps. This sequence is used to visualise the impacts of neurovascular diseases by producing an enhanced-contrast image that is sensitive to venous blood. "Spoiled" refers to the use of RF pulses to remove residual transverse magnetisation in order to enhance the image contrast.
- T2-weighted gradient echo. This is very sensitive to blood and hemosiderin and is therefore used to detect cavernomas and vascular malformations.

Hippocampal sequences can be used to measure the hippocampal volume, as hippocampal sclerosis is found in approximately 65% of patients with temporal lobe epilepsy (Yoong *et al.*, 2013).

Functional neuroimaging enables localised brain mapping. This technique requires the cooperation of the patient and cannot be easily performed in young or difficult children. Deterministic rather than probabilistic tractography is available in intraoperative research MRI to describe larger pathways such as the corpus callosum, but is of limited use to describe more intricate pathways such as the optic radiations.

7.1.3 Previous studies of seizure patients using tractography

Little is known about the effect of seizures on the white matter pathways of the brain that are not directly involved in the epileptic focus. The FEBSTAT study identified a link between febrile status epilepticus and mesial temporal sclerosis, and also linked this to temporal lobe epilepsy (Shinnar *et al.*, 2008, Shinnar *et al.*, 2012).

The abnormalities found in children with prolonged febrile seizures extend beyond the hippocampus or the initial epileptic focus. Hemispheric areas such as the temporal lobe or the insula present abnormalities that are detectable with conventional MRI (Shinnar *et al.*, 2012) and with DTI (Yoong *et al.*, 2013). Most febrile convulsions are focal, with 60–99% of them classified as generalised tonic-clonic seizures or secondary generalised seizures. This means that most of the seizures have a triggering area from where the seizure activity spreads (Berg and Shinnar, 1996, Shinnar *et al.*, 2008).

Nervous tissue is very sensitive to ischemia during seizures and a lack of oxygen supply for even a very short time can cause harmful lesions. The lack of oxygen, the time of ischemia and the oxidant metabolites produced during the seizure could have a deleterious effect on both white and grey matter, and should in theory equally affect both hemispheres (Scanlon *et al.*, 2013). Mesial temporal lobe sclerosis has been shown to affect motor tracts as well as limbic tracts in adults with long-term epilepsy, in a study using tractography (Liu *et al.*, 2012). Yet animal studies have suggested that myelin could protect white matter neurons in comparison with grey matter (Lopez *et al.*, 2011). The impact of febrile convulsions and long-term epilepsy on the visual white matter tracts has not been examined previously.

The time required for harmful lesions to develop is thought to be of the order of a few minutes, but lesions in humans resulting from a very short insult, such as a seizure, have not been comprehensively studied, partly because anatomical changes in the white matter areas after a minimal ischemic insult are difficult to image.

7.1.4 Aim and novelty of this study

The impact of epilepsy on the optic radiations has not previously been examined. The aim of this study was to understand for the first time how seizures affect the development of the optic radiations in the paediatric population using DTI tractography. Two cohorts of patients were analysed.

The first cohort was composed of children who had suffered a single episode of complex febrile seizures. This cohort was analysed to understand whether the anatomy of the optic radiations would be affected by a single episode, given that the time for harmful lesions to develop was thought to be in the order of minutes.

The second cohort was composed of children who had been exposed to epilepsy and to anti-epileptic medicines on a regular basis. This cohort was analysed to understand how long-term sustained epilepsy affects the optic radiations, relative to the damage caused by a single seizure.

More generally, a further aim was to develop a preoperative tractography MRI with a more accurate surgical protocol that could be added to the standard epilepsy protocol, with no increased risk to the patient, with the aim of avoiding surgical damage to the optic radiations. This would improve the anatomical description of the white matter

connection areas prior to surgery, taking account of anatomical variations between patients that are not apparent from atlases and other imaging sources. Improved imaging was also expected to provide an additional visual aid for the clinician and parents to help them better understand the underlying causes and impacts of epilepsy.

7.2 Methodology

The prolonged febrile convulsions cohort was scanned using the 3×20 DTI protocol as many of the patients were shared with another study that commenced prior to this one. Tractography analysis was performed on each patient as described in Section 3.4, and this was used to calculate the mean FAs for the left and right optic radiations. The mean FAs of the front and rear of each optic radiation were also calculated. These mean FA values were compared with age-paired controls from the 3×20 control cohort. ANCOVA statistics were used to remove the age dependence from each cohort.

The epilepsy cohort was recruited entirely by this study from Great Ormond Street Hospital and included children with structural or anatomical abnormities that were the source of the epilepsy. They were all scanned using the 1×60 DTI protocol. The tractography and mean FA analysis was performed using the same process as for the prolonged febrile convulsions cohort.

7.3 Description of the cohort

Seizures and epilepsy have many causes and the source of the epileptic activity in some cases cannot be identified. Since the purpose of this study was to examine the impacts of seizures on the optic radiations, it was important that these were not the focus of the epileptic activity. Children with visual seizures or visual triggering of the epileptic activity were therefore not included in the patient cohorts.

A total of 115 patients were recruited for the study. Many patients could not be used due to their unsuitability following the initial assessment, uncooperative behaviour during scanning, or a lack of matched controls (controls and patients were recruited concurrently over a long period and were not chosen by age, in order to maximise the size of the cohorts). Table 7.1 lists the inclusion criteria for the two patient cohorts.

The final prolonged febrile convulsions cohort contained 21 patients who had had an episode of prolonged febrile convulsions persisting for more than 30 minutes. The

MRI was carried out within one month of the epileptic episode and none of the patients had previous or ongoing use of anti-epileptic medicines at the time of scanning.

The anti-epileptic user cohort contained 20 patients. These patients had epilepsy over a period of at least two years, used anti-epileptic medicines and had often shown resistance to treatment, causing them to be referred to Great Ormond Street Hospital. The patients had a diverse range of seizures as only the patients with visually-related seizures were excluded.

Inclusion/exclusion criteria	**Prolonged febrile convulsions cohort**	**Anti-epileptic user cohort**
Age	0 to 18	5 to 18
Number of epileptic activity episodes	One	Many
Type of epileptic activity	Prolonged febrile convulsions	All except visually-related seizures
Length of epileptic activity	At least 30 mins	Episodes for at least two years
Use of anti-epileptic medicine	No	Yes
Scanning time from *last* epileptic activity to MRI scan	Less than 1 month	Less than 1 month

Table 7.1 Inclusion/exclusion criteria for patients in the epilepsy cohorts.

7.3.1 Prolonged febrile convulsions cohort

The prolonged febrile convulsions cohort was partly recruited from the general neurology clinic as a part of a study into convulsive status epilepticus at Great Ormond Street Hospital, which was looking for changes in the hippocampus and motor areas of the brain, and correlating those changes with cognitive development. The remainder of the cohort was recruited by this study.

All the children were scanned within one month of the prolonged febrile seizure episode. A visual assessment was carried out by the main clinician on the day of scanning, before any sedation or other non-regular medication was given, using a

standard interview and clinical visual assessment. The DTI sequence was added at the end of the clinical protocol.

Gender was almost equally distributed in the cohort, with 11 males and 10 females, as shown in Table 7.2. Many of the patients were aged under 5 years, which is unsurprising given that initial seizures often occur in the early years. Figure 7.1 shows the age pairings between the patients and the controls.

7.3.2 Anti-epileptic user cohort

The anti-epileptic user cohort was selected from the epilepsy programme at Great Ormond Street following referral by the leading care clinician. Some of the children had tumours or structural lesions that merited surgery. There were children with several years of treatment for intractable seizures and with mixed anti-epileptic medicines that did not control the seizures. None of the children suffered a convulsion during scanning.

The sex and age of each epilepsy patient are listed in Table 7.3. The sex was equally distributed in the cohort. In contrast with the prolonged febrile convulsions cohort, the age distribution is weighted more towards older children, reflecting the long-term nature of the epilepsy in many patients.

Patient	Sex	Age
EY20-27	Female	0.2
EP60-32	Male	0.3
EY20-51	Female	0.4
EY20-06	Female	0.8
EP60-21	Female	1.7
EY20-02	Female	2
EP60-05	Male	2
EP60-06	Male	3
EY20-16	Male	3
EY20-31	Female	3
EP60-17	Male	4
EY20-22	Male	5
EY20-35	Male	6
EY20-48	Male	6
EP60-13	Male	7
EP20-17	Female	8
EY20-05	Female	9
EY20-12	Male	11
EY20-57	Male	11
EY20-07	Female	12
EY20-46	Female	15

Table 7.2 Description of the prolonged febrile convulsions cohort. All patients were referred with suspected complex febrile convulsions following a first seizure lasting more than 30 minutes, which had occurred in the month prior to the MRI scan. Only 3×20 DTI scans were used in this study; some patients were scanned using both 3×20 and 1×60 protocols and are coded as EP60-.**

Patient	Sex	Age	Type of seizures
EP60-18	Female	5	Tonic-clonic
EP60-01	Male	5	Tonic-clonic
EP60-29	Male	5	Partial motor
EP60-02	Male	6	Absence
EP60-07	Male	6	Partial motor
EP60-30	Female	7	Absence
EP60-42	Female	7	Absence
EP60-20	Female	8	Tonic-clonic
EP60-12	Male	10	Tonic-clonic
EP60-23	Male	10	Absence
EP60-46	Female	11	Tonic-clonic
EP60-31	Female	12	Tonic-clonic
EP60-15	Female	13	Partial motor
EP60-44	Male	13	Partial motor
EP60-41	Female	14	Tonic-clonic
EP60-04	Male	14	Tonic-clonic
EP60-28	Male	14	Absence
EP60-35	Female	15	Absence
EP60-25	Female	16	Tonic-clonic
EP60-14	Male	16	Grand mal

Table 7.3 Description of the anti-epileptic user cohort. All patients had had epilepsy over a period of at least two years and were regular users of anti-epileptic medicines. Only patients with visually-related seizures were excluded from the cohort.

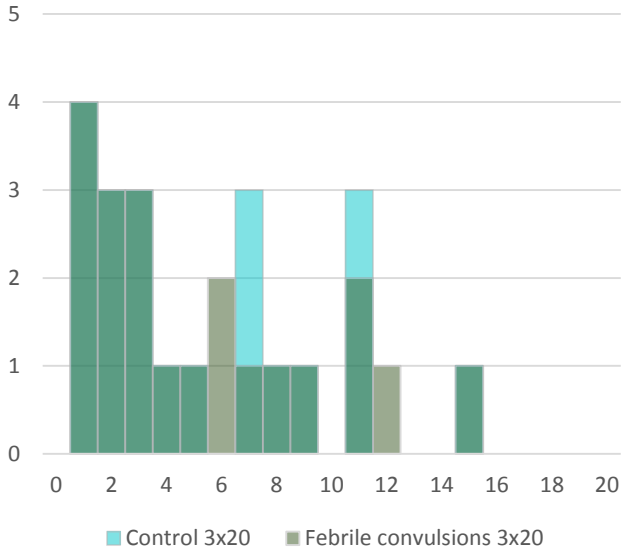

Figure 7.1 Histogram of the febrile convulsions and control cohort age profiles. Dark green areas represent one patient from each cohort.

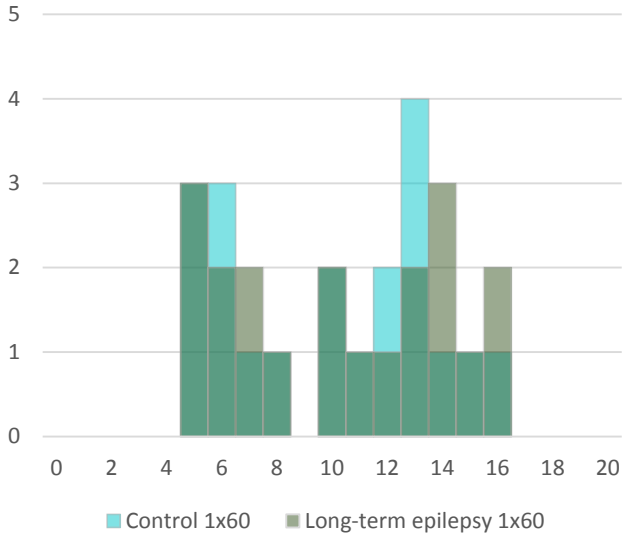

Figure 7.2 Histogram of the anti-epileptic user and control cohort age profiles. Dark green areas represent one patient from each cohort.

7.4 Results

Results are presented separately for the prolonged febrile convulsions cohort and the anti-epileptic user cohort.

7.4.1 Prolonged febrile convulsions cohort

The mean FA of the left optic radiation is shown for the prolonged febrile convulsions cohort and the associated control cohort in Figure 7.3. The overall differences between the two cohorts are very small. The mean FA measurements at the front and rear of the left optic radiation are shown in Figures 7.4 and 7.5, respectively, and similarly have only small differences between the two cohorts. The right optic radiation has similar trends to the left optic radiation, as shown in Figure 7.6 for the whole tract.

The lack of clear variations between the prolonged febrile convulsions and control distributions is reflected in Figures 7.7 and 7.8 for the left and right optic radiations. These graphs show the discrepancy of the optic radiation front and rear mean FAs relative to the control cohort regression line for each series (i.e. the left front control and prolonged febrile convulsions mean FAs are plotted relative to the left front control regression line, so the front and rear control regressions both have the equation y=0). The variability of each cohort appears similar.

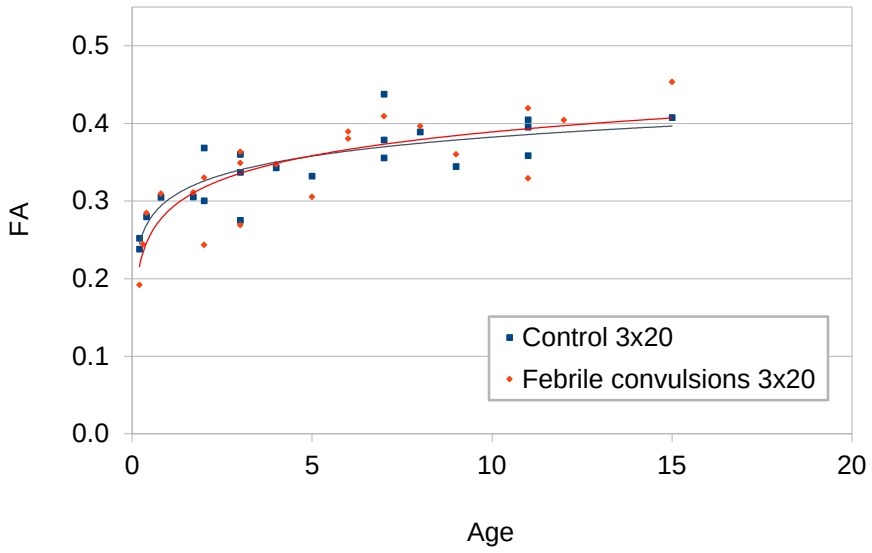

Figure 7.3 Mean FA across the full left optic radiation for the febrile convulsions and control cohorts.

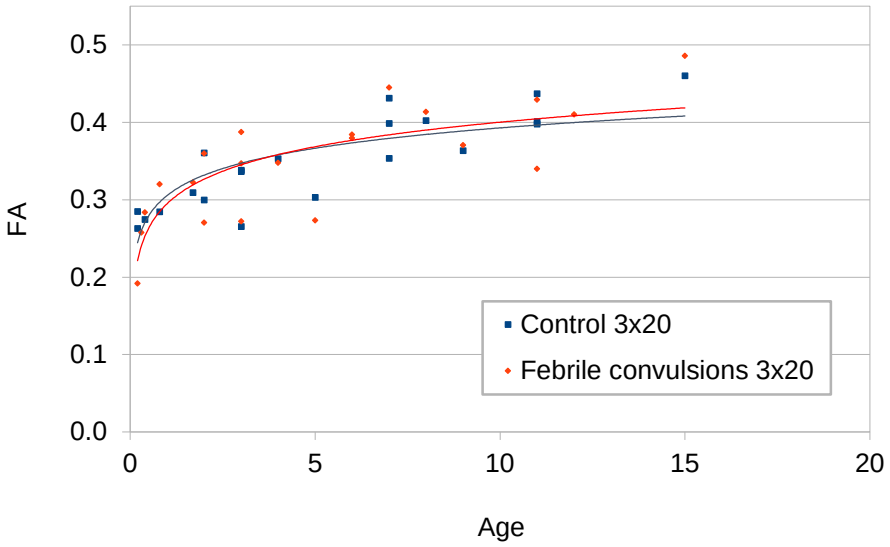

Figure 7.4 Mean FA of the front of the left optic radiation for the febrile convulsions and control cohorts.

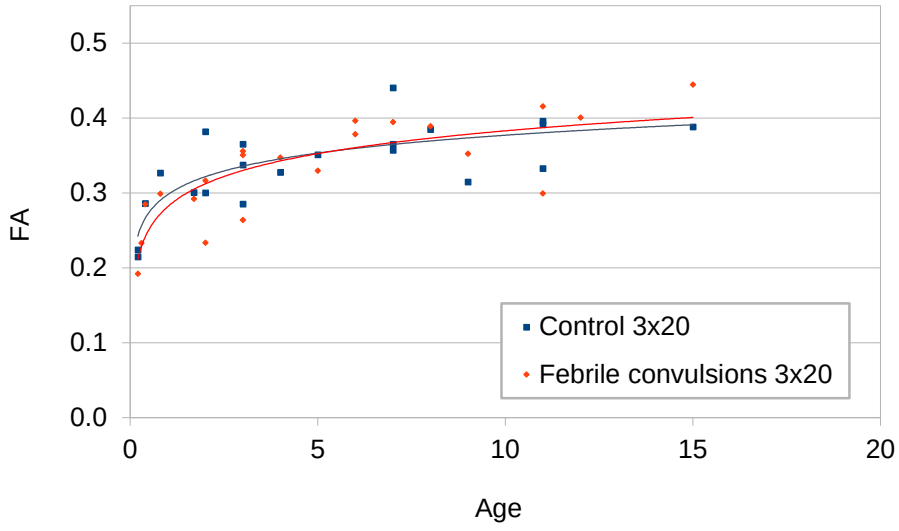

Figure 7.5 Mean FA of the rear of the left optic radiation for the febrile convulsions and control cohorts.

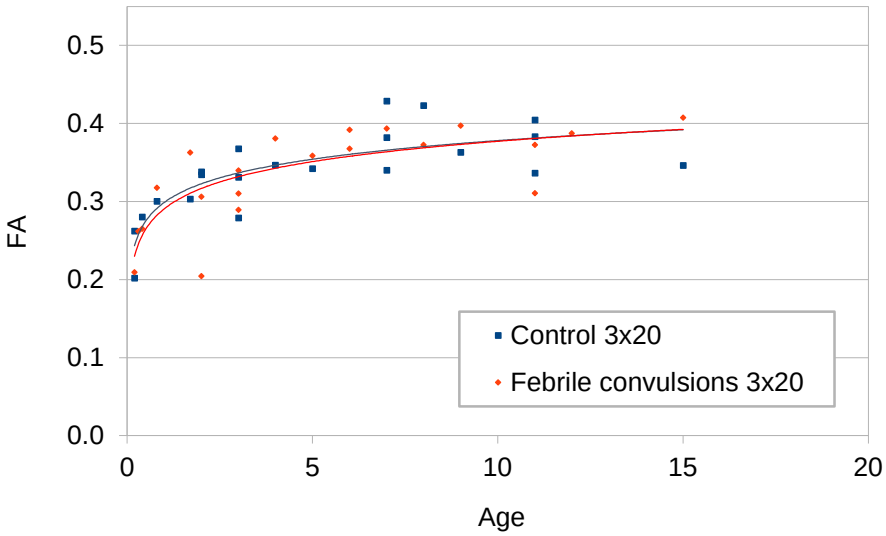

Figure 7.6 Mean FA across the full right optic radiation for the febrile convulsions and control cohorts.

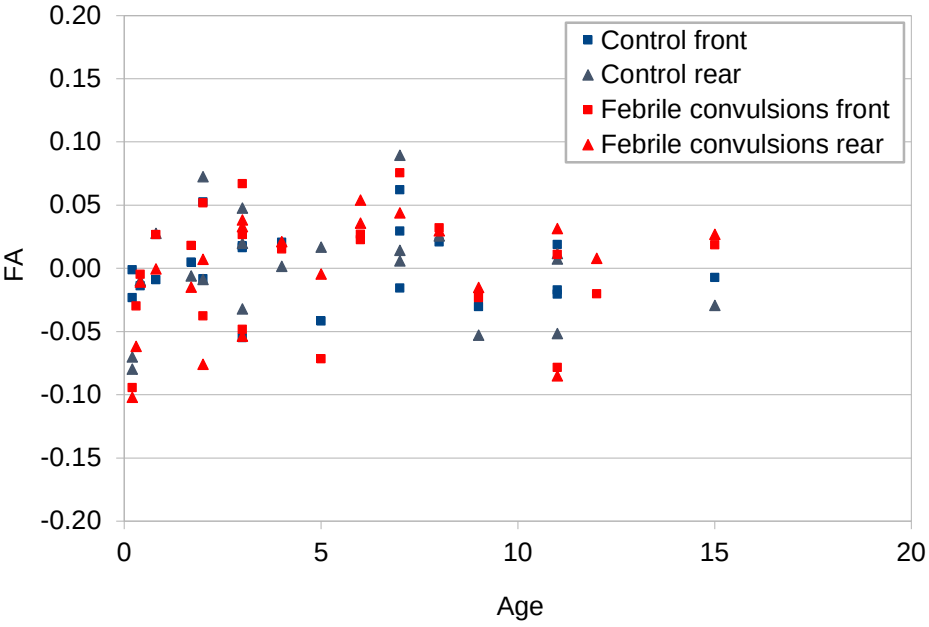

Figure 7.7 Prolonged febrile convulsions and control cohort mean FA discrepancies on the left optic radiation relative to the linear regression of the control cohort. See the main text for details of the discrepancy calculation.

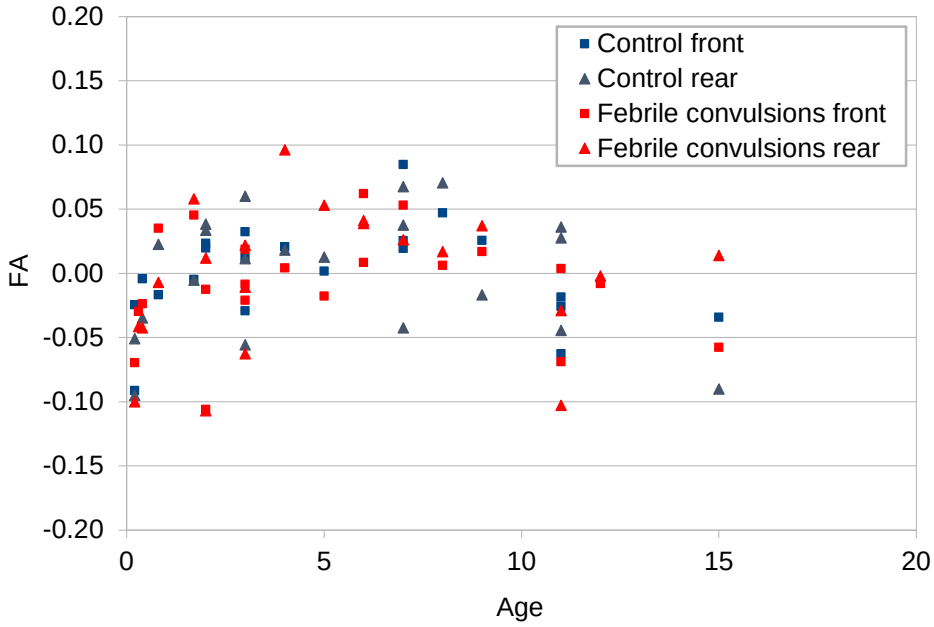

Figure 7.8 Prolonged febrile convulsions and control cohort mean FA discrepancies on the right optic radiation relative to the linear regression of the control cohort. See the main text for details of the discrepancy calculation.

ANCOVA tests were used to identify differences in mean FA between the prolonged febrile convulsions and control cohorts. There were 39 degrees of freedom and a Levene test demonstrated homogeneity of all regression slopes for both cohorts with age. Table 7.4 shows the ANCOVA results. As suggested by the mean FA graphs, there are no statistically-significant differences in mean FA between the control and prolonged febrile convulsions cohorts.

	Left			Right		
	F	**P**	**Eta**	**F**	**p**	**Eta**
Full	0.072	0.789	0.002	0.083	0.774	0.002
Front	0.004	0.948	0.000	0.408	0.527	0.010
Rear	0.105	0.747	0.003	0.068	0.796	0.002

Table 7.4 Comparison of optic radiation mean FA for the 3×20 control and prolonged febrile convulsions cohorts using ANCOVA tests. Results are presented for the left and right optic radiations, for the full, front and rear of the optic radiations.

Another method of comparing the prolonged febrile convulsions and control cohorts is to count the number of voxels in the optic radiations. Table 7.5 shows that the prolonged febrile convulsions cohort has fewer voxels on both sides than the control cohort, with the difference statistically-significant on the left side ($p<0.05$) when using an ANCOVA test. Since the fraction of front voxels is similar for both cohorts, the lower number of voxels in the prolonged febrile convulsions cohort must occur across the optic radiations.

	Total voxels		**Fraction of front voxels**	
	Left	Right	Left	Right
Control	412±172	347±205	36%	45%
Prolonged febrile convulsions	294±122	267±111	37%	45%
F	6.70	2.45		
P	0.013*	0.126		
Eta	0.147	0.059		

Table 7.5 Optic radiation tractography voxels in each brain hemisphere for the prolonged febrile convulsions and control cohorts. The mean fraction of voxels located in the front of the brain is also shown. Figures are presented in the form mean ± standard deviation for each cohort. Each voxel is a cube with sides measuring 2.5 mm. F, P and Eta are the ANCOVA statistics of differences between the two cohorts on the left and right side. * $p<0.05$.

7.4.2 Anti-epileptic user cohort

The mean FA of the left optic radiation is shown for the anti-epileptic user cohort and the associated control cohort in Figure 7.9. The control cohort mean FAs are higher at all ages, with the difference more pronounced than for the prolonged febrile convulsions cohort in Figure 7.3.

For the front of the left optic radiation, the control cohort mean FA is higher than the anti-epileptic user cohort mean FA, particularly for the teenage cohort (Figure 7.10). Most of the younger patients had had less exposure to anti-epileptic medicines and to

the epilepsy itself than the older children, who had had a longer disease period. Yet the opposite trend occurs at the rear of the optic radiation, with the younger cohort presenting the greatest reduction in mean FA (Figure 7.11).

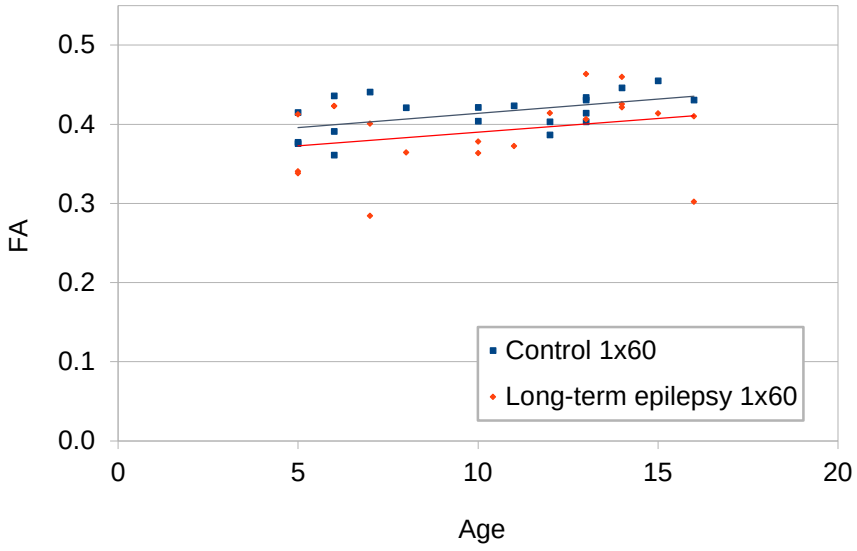

Figure 7.9 Mean FA across the full left optic radiation for the anti-epileptic user and control cohorts.

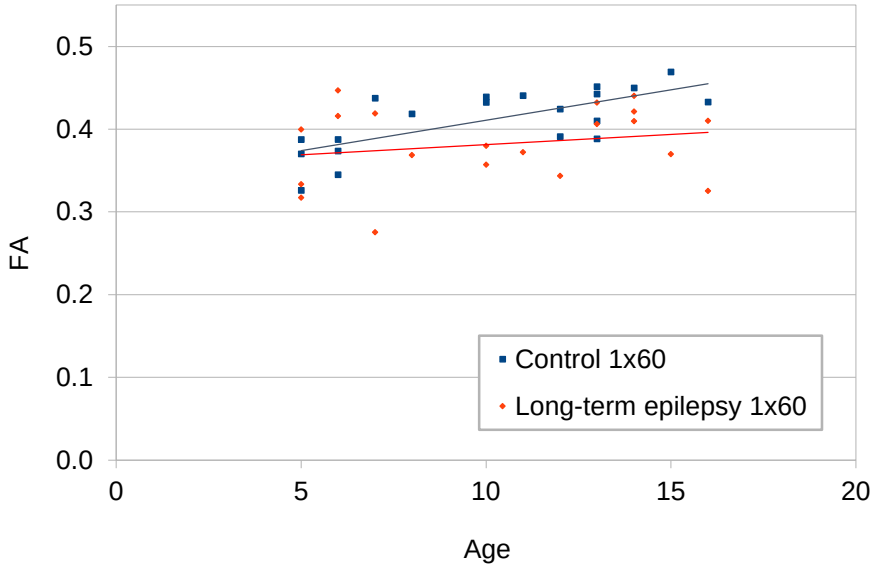

Figure 7.10 Mean FA of the front of the left optic radiation for the anti-epileptic user and control cohorts.

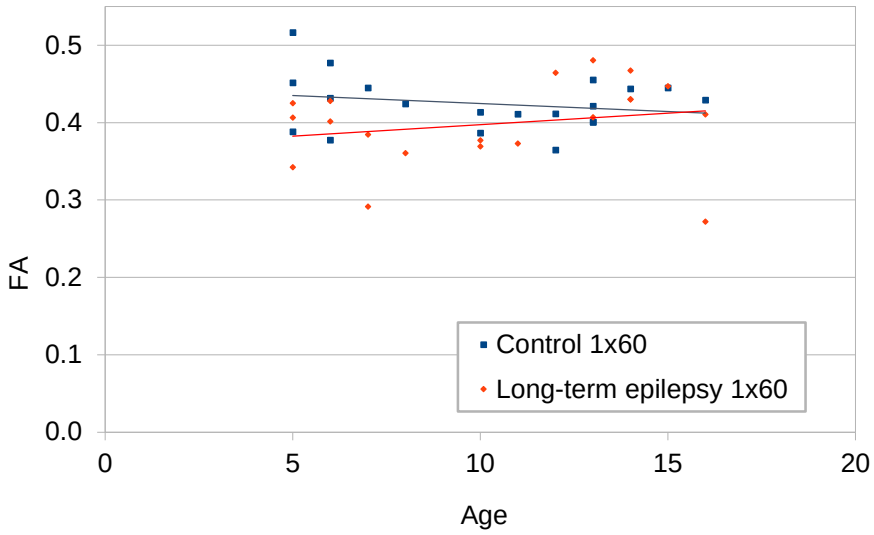

Figure 7.11 Mean FA of the rear of the left optic radiation for the anti-epileptic user and control cohorts.

The right optic radiation has similar trends to the left optic radiation, as shown in Figure 7.12 for the full optic radiation and in Figures 7.13 and 7.14 for the front and rear of the optic radiations, respectively.

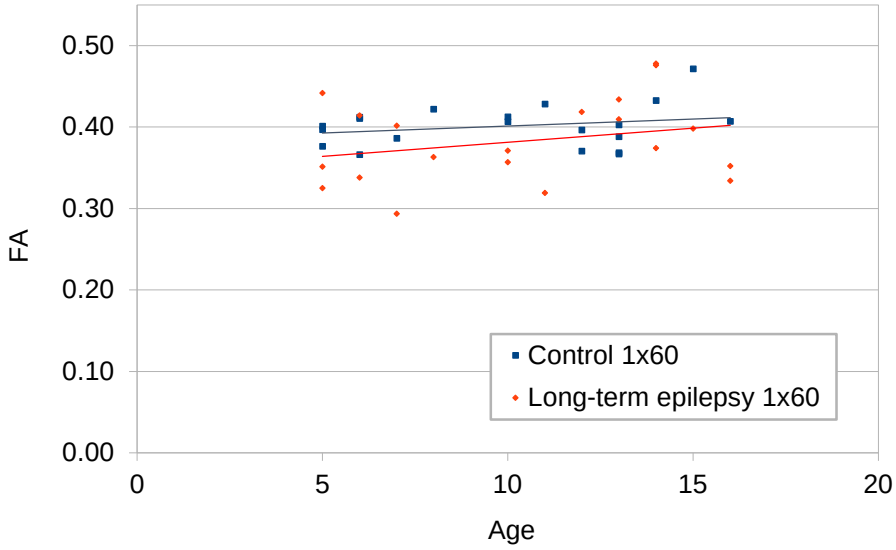

Figure 7.12 Mean FA across the full right optic radiation for the anti-epileptic user and control cohorts.

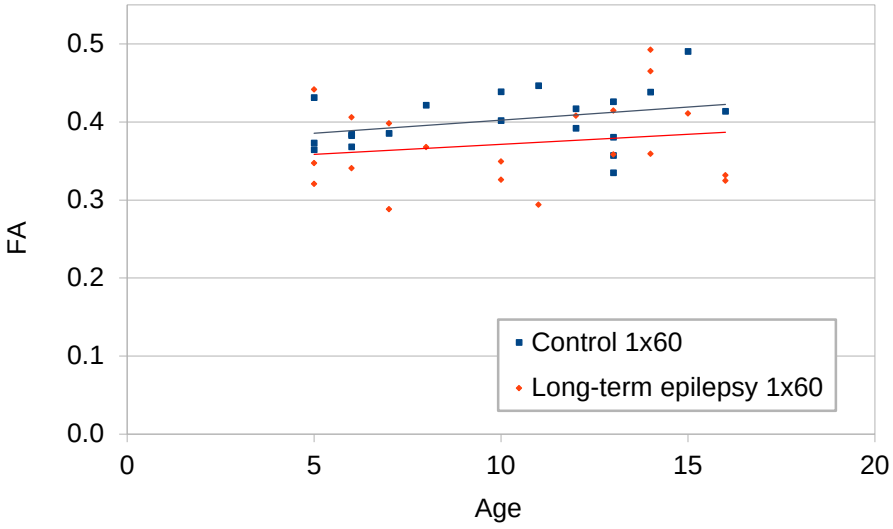

Figure 7.13 Mean FA of the front of the right optic radiation for the anti-epileptic user and control cohorts.

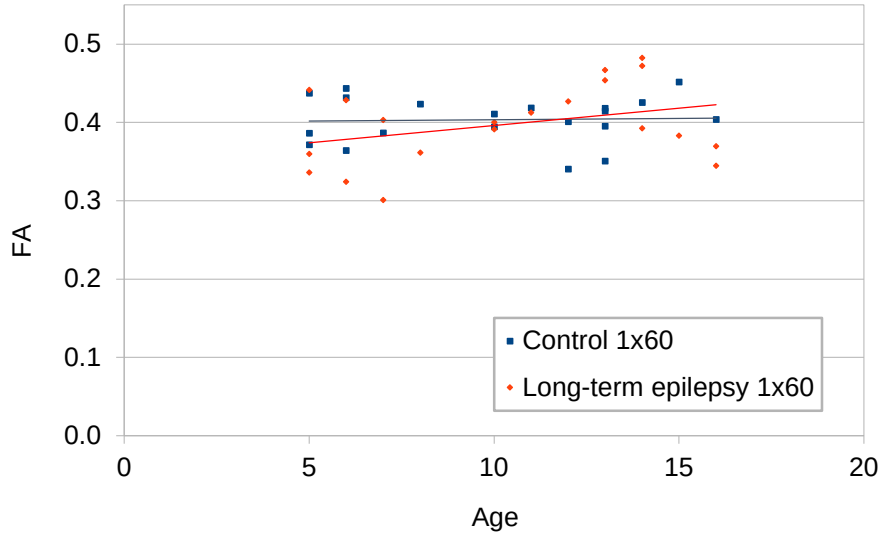

Figure 7.14 Mean FA of the rear of the right optic radiation for the anti-epileptic user and control cohorts.

The mean FAs of the optic radiations for the anti-epileptic user cohort are more variable than the control mean FAs, as a result of some cases having unusually low mean FA. This is illustrated in Figures 7.15 and 7.16 for the left and right optic radiations, respectively, which show the discrepancy relative to the control cohort regression line for each series.

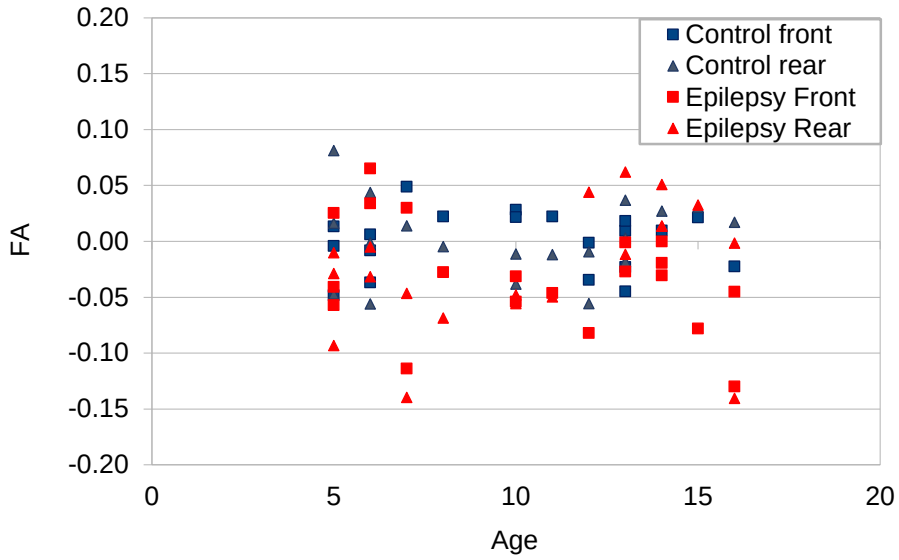

Figure 7.15 Anti-epileptic user and control cohort mean FA discrepancies for the left optic radiation relative to the linear regression of the control cohort. See the main text for details of how the discrepancies are calculated.

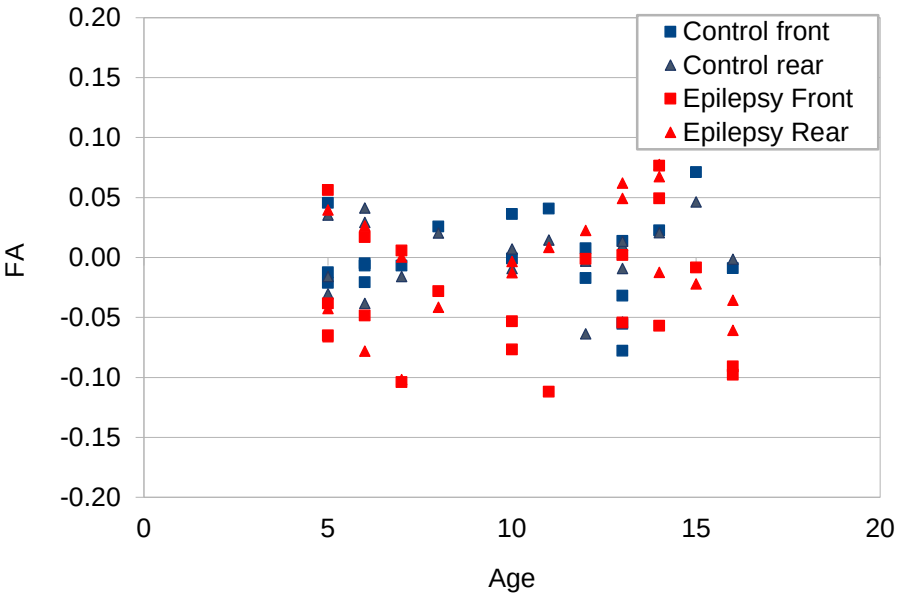

Figure 7.16 Anti-epileptic user and control cohort mean FA discrepancies for the right optic radiation relative to the linear regression of the control cohort. See the main text for details of how the discrepancies are calculated.

ANCOVA tests were used to identify differences in mean FA between the anti-epileptic user and control cohorts. There were 45 degrees of freedom. Levene tests demonstrated homogeneity of regression slopes with age for the left but not the right optic radiations. Table 7.6 shows that the differences in mean FA are statistically-significant at the front but not at the rear, for both optic radiations ($p<0.05$).

The anti-epileptic user and control cohorts can also be compared by counting the number of voxels in the optic radiations, which are shown in Table 7.7. The mean and standard deviation for the control patients is similar to the 3×20 cohort used for the prolonged febrile convulsions results in Table 7.5. The anti-epileptic user cohort has significantly more voxels on both the left ($p<0.01$) and the right ($p<0.05$) optic radiation than the control cohort, in contrast to the prolonged febrile convulsions cohort that had fewer voxels than the controls. The anti-epileptic user patients tend to have a smaller fraction of voxels at the front than the control patients for the left optic radiation but a greater fraction at the front for the right optic radiation.

	Left			**Right**		
	F	**P**	**Eta**	**F**	**p**	**Eta**
Full	4.36	0.044*	0.105	2.41	0.129	0.061
Front	6.17	0.018*	0.143	4.49	0.041*	0.108
Rear	3.22	0.081	0.080	0.27	0.608	0.007

Table 7.6 Comparison of optic radiation mean FA for the 3×20 control and anti-epileptic user cohorts using ANCOVA tests. Results are presented for the left and right optic radiations, for the full, front and rear of the optic radiations. * $p<0.05$.

7.5 Discussion

The anti-epileptic user cohort has a lower mean FA in the optic radiations than the control cohort, despite the patients not having any visual epileptic activity or visual impairment. This finding could reflect neuronal malfunction or programmed cell death, which can result from ischemia linked to traumatic brain injury and epilepsy (Liou *et al.*, 2003).

	Total voxels		Fraction of front voxels	
	Left	**Right**	**Left**	**Right**
Control	391 ± 164	350 ± 167	38%	41%
Anti-epileptic user	589 ± 229	518 ± 233	37%	47%
F	9.48	6.77		
P	0.004**	0.013*		
Eta	0.204	0.155		

Table 7.7 Optic radiation tractography voxels on each brain hemisphere for the anti-epileptic user and control cohorts. The mean fraction of voxels located in the front of the optic radiation is also shown. Figures are presented in the form mean ± standard deviation for each cohort. Each voxel is a cube with sides measuring 2.5 mm. F, P and Eta are the ANCOVA statistics of differences between the two cohorts on the left and right optic radiations. * p<0.05. ** p<0.01.

Epileptic seizures are characterised by overstimulation, both in certain neuronal circuits and in glial cells. The extent of damage in different areas of the brain depends on the relative amounts of white and grey matter they contain. The affected areas are thought to be those immediately in communication with the triggering or neighbouring network of neurons that are overexcited by the seizure, rather than global brain hypoxia (Fukuda *et al.*, 2010). Yet the results of this study show that the optic radiations could be affected by epileptic activity, despite them not being involved by the overexcitability of the epileptic seizure.

Section 7.4.2 shows that epilepsy patients requiring anti-epileptic medicines have lower mean FA at the front of each optic radiation. This is consistent with the high likelihood of periventricular white matter lesions in patients with severe ischemia, who later develop periventricular white matter injury, which could result from oxygenation and blood supply factors (Kinney *et al.*, 1988). The development of the blood brain barrier and the rest of the capillary network development comes from the anterior and posterior intracranial circulation, and white matter and grey matter follow different paths during vascular system development (Marin-Padilla and Knopman, 2011).

Developing brains could be susceptible to more significant and earlier instauration of widespread epileptic activity than adult brains. This might explain why the rate of occurrence of febrile epileptic convulsions decreases with age, as the brain develops and matures. The extent and magnitude of the damage found in patients with epilepsy has been observed to depend on the subject's age at the time of epileptic seizure onset (Hossain, 2005). Brain development during the critical period might be impaired in children with early onset of epileptic activity (Anderson *et al.*, 2011).

7.5.1 Hypotheses of the impact of epilepsy on the optic radiations

Several hypotheses have been developed that might explain these results, and which could form the basis of further research.

The first hypothesis is the existence of an area in the brain, most likely the thalamus, which prevents the spread of overexcitability of a given network to the rest of the neuronal mess during a seizure. The importance of the thalamus as a "gather and distribution centre" of the central nervous system is increasingly recognised (Neubauer *et al.*, 2014). Poor functioning of such a damage prevention system could enable epileptic activity to spread widely across the brain, causing status epilepticus. Even in cases of partial motor seizures, which commonly occur in children with structural brain abnormalities, activity can spread widely with low intensity to cause hypoxic episodes in remote brain networks that are connected to the thalamus (Gigout *et al.*, 2013).

The second hypothesis is related to neurotransmitter behaviour. In this theory, inhibitory neurotransmitters reduce neuronal network overstimulation during seizures by acting when neuronal stimulation reaches a threshold intensity. If there were a low concentration of inhibitory neurotransmitters in a neuronal area, overstimulation would not be controlled and could expand to the thalamus and then to the many neural networks that are linked to it, including the optic radiations, where neurons would be subjected to overstimulation and therefore to ischemia if the white matter inhibitory neurotransmitters were ineffective.

The third hypothesis combines the first two hypotheses. Glial cells have an important role in maintaining a healthy environment for neurons and their axons (Nijboer *et al.*, 2008, Nijboer *et al.*, 2013). New inhibitory neurotransmitters are regularly identified

in the literature and they have been postulated as potential targets for new anti-epileptic medicines to treat epilepsy. Neurotransmitters that are linked to the inhibitory action of the thalamus, where they also might interact, could maintain and limit the spread of unwanted brain activity. An imbalance in neurotransmitter actions might cause poor functioning of the thalamus and fail to prevent the spread of epileptic activity.

Epilepsy could be a secondary manifestation of a more generalised disease, rather than a primary disease. This would explain why the white matter and the grey matter are affected differently. The rate of development (as measured by the presence of oligodendrocytes and their precursors) could have an important role in the susceptibility of a tissue to resist ischemia (Riddle *et al.*, 2006). Some of the neurotransmitters produced by these cells could promote apoptosis and therefore increase the tissue damage of the area exposed to ischemia (Kinney and Back, 1998).

There is another possible explanation for the lower mean FA in epilepsy patients. Repeated epileptic activity can affect brain tissue, the accompanying glial cells (Marin-Padilla, 1996) and apoptosis (Ghazizadeh and Naziroglu, 2014), particularly in the hypothalamus. This might lead to some children developing structural abnormalities, which could require surgery and other interventions that aim to decrease the area of abnormal tissue that is identified as the main triggering focus of their epileptic activity. The cortex, thalamus and putamen are more likely to be damaged by severe ischemia than white matter (Johnston *et al.*, 2001), so this might explain why the mean FA might not be severely decreased in children with prolonged febrile seizures. Changes might occur in grey matter and the cortices before the effect of ischemia and oxygen deprivation are detectable in white matter tracts. This hypothesis could be tested by examining the thalamus and the limbic system using tractography.

This study did not examine measurements of the hippocampus and linked areas. Future research could combine DTI tractography and measurements of the hippocampus in a longitudinal study of children with epilepsy, to identify any correlation between decreased mean FA and increased anatomical abnormalities in the hippocampal area and linked grey and white matter areas.

Another method to test these theories would be to examine the cerebellum in epilepsy patients using DTI tractography. Although it is connected with the thalamus, it is not thought to be affected by spreading epileptogenic seizure activity, and there are virtually no reports of epileptic activity linked to tumours or other structural abnormalities present in the cerebellum. A study could compare the mean FA in the cerebellar pathways with controls. If the hypotheses above are correct, the myelination process in pathways linked to the limbic system would also be affected, in addition to many other pathways not linked with the network mess of activated neurons.

7.5.2 Impact of a single prolonged seizure

Another aim of this study was to understand whether damage from epileptic activity can be detected after the first seizure or is a more gradual instauration process. The prolonged febrile convulsions cohort were all scanned following a single seizure episode. There were no statistically-significant differences in mean FA between the prolonged febrile convulsions cohort and the paired control cohort, suggesting that a single seizure episode does not cause widespread damage to the optic radiations. It is possible that small-scale damage occurs to the optic radiations that cannot be detected using current clinical tractography protocols, but which might become apparent through improved MRI resolution in the future. This finding also does not rule out the impairment of other white matter pathways that are closer to the epileptic focus, such as motor or cognitive pathways.

The time required for the brain to reorganise and recover from a limited-length insult has not been fully established in the paediatric population. It is possible that some of the damage following the first seizure was mitigated in the period prior to scanning. It would be necessary to perform DTI scans within minutes or hours of the onset of the convulsive period to understand the impact of the repair mechanisms of the brain.

7.5.3 Impact of anti-epileptic medicines

The children in the anti-epileptic user cohort had been taking anti-epileptic medicines for at least 6 months at the time of scanning. It was not possible to identify the specific influence of anti-epileptic medicines in these children because their treatment had already commenced prior to their MRI scan, so it was not possible to compare the

optic radiations before and after the anti-epileptic treatment was started. Since we did not have a cohort of healthy controls taking anti-epileptics, it was not possible to attribute the differences between the cohorts to epilepsy. The use of anti-epileptic medicines in this cohort could therefore have acted as a confounding factor. A longitudinal tractography study of epilepsy patients, recruiting prolonged febrile convulsion patients and following those that are diagnosed with epilepsy, would provide more information about the impact of anti-epileptics on the optic radiations.

7.5.4 Preoperative tractography protocol for epilepsy

Neuroimaging for preoperative epilepsy surgery planning has the objectives of: (i) finding the underlying abnormal anatomical structure linked to the epileptic activity; (ii) describing in detail the anatomy of the individual patient who will undergo surgery; and, (iii) serving as an intraoperative guide during the neurosurgical procedure.

The number of tests is chosen according to the patient, the lesion location(s) and the availability of imaging. The most widely-used technique is MRI, with the choice of protocols depending of the hospital and the patient. At Great Ormond Street Hospital, a range of sequences, including various T1 and T2-weighted protocols, are chosen according to the needs of the patient. Adding a DTI protocol and performing tractography could assist with patient care in two important ways:

1. Identifying critical white matter tracts so surgical procedures can be altered to minimise the risk of tract damage.
2. Providing an additional visual aid for the clinician and parents to help them better understand the underlying causes and impacts of epilepsy.

Each patient has a different anatomy, so it is not practical to use anatomical atlases for surgical planning. Identifying tracts is particularly important for patients with distorted anatomies. The value of DTI tractography in supporting surgical procedures in this way is demonstrated in Section 8.3 for brain tumour patients.

Based on testing of a range of DTI protocols, the new 60-direction protocol that was adopted by this study was the most suitable for paediatric preoperative planning, as it produced higher-quality images in a shorter scanning time compared to other protocols. This protocol is fully described in Table 3.1 and Section 3.2.

7.6 Conclusions

Epilepsy is the most common neurological condition in childhood, with a prevalence of 1%, while 2–4% of children under 5 years old suffer an episode of febrile convulsions. Little is known about how seizures affect the white matter pathways of the brain that are not involved in the epileptic focus. This chapter has examined the impact of seizures on the optic radiations in the paediatric population using DTI tractography.

A cohort of 20 children with long-term epileptic activity have been compared with age-matched controls. The epilepsy cohort presented a decreased mean FA for the front of both optic radiations compared with the control cohort, despite the patients having neither visual epileptic activity nor visual impairment. Several hypotheses are proposed that could explain this conclusion, including the poor functioning of the thalamus or neurotransmitters, or structural damage caused by repeated seizure episodes.

A cohort of 21 children who had suffered a single episode of prolonged febrile convulsions were also compared with age-matched controls. This cohort did not present lower mean FA in either optic radiation, suggesting that a single seizure episode might not be sufficient to cause widespread damage to the optic radiations. It is possible that small-scale damage was not detected using the clinical tractography protocol, or that the patients recovered to some extent between the seizure and the MRI scan. Other motor or cognitive white matter pathways near the epileptic focus could have been more affected by the seizure.

The new 60-direction DTI tractography protocol adopted by this study was identified as the most suitable for improving paediatric preoperative planning, as it produced higher-quality images in a shorter scanning time than other protocols that were tested.

8 TRACTOGRAPHY APPLICATIONS IN NEUROSURGERY

Understanding the relationship between brain structure, and three-dimensional mapping of the brain, are foundations of successful neurosurgery. The living brain is not susceptible to dissections and manipulations without causing extreme damage. The aim of this chapter is to examine how tractography imaging can help neurosurgeons to perform safer and better informed surgical procedures, by providing safe and non-invasive descriptions of individual white matter tracts that account for variations between patients and the impacts of pathologies.

The potential benefits of tractography are examined in two case studies. The first case study demonstrates the benefits of DTI tractography for patients with a brain tumour and with tuberous sclerosis. The second case study examines hydrocephalus patients, and demonstrates the value of VEP-enhanced tractography, which was introduced in Chapter 5.

8.1 Introduction

Neurosurgery is constantly evolving as new technologies and techniques become available and increasingly complex cases are operated on. Technology has been and continues to be an important tool for diagnosis and treatment of several brain

pathologies, and improvements have contributed to improving outcomes and reducing complications by minimising unintended damage.

Tractography is a new imaging technique that describes individual white matter tracts and it is starting to be included in several hospital protocols for preoperative imaging, for example at Great Ormond Street Hospital where this study took place. For many pathologies, for example hydrocephalus, few or no case reports have been published using tractography, and there are no standard DTI or tractography analysis protocols for this purpose (Liasis *et al.*, 2009).

8.2 Methodology

Children were recruited following referrals from the lead clinician. All four cases were inpatients at the Neurosurgery department at GOSH. The standard recruitment protocol and consent described in Section 3.1 was used in all cases. The patient and family were approached by the author and written and verbal information about the study was provided. The patient was included in the study when consent was granted.

DTI was added to the clinical scan MRI protocol and analysed as described in Section 3.4. DTI and tractography maps of the white matter were produced in all cases. The tractography analysis method from Section 3.4 was used for both brain tumour cases.

For the hydrocephalus patients, visual function was tested using VEPs and analysed using the NeuroScan software, as described in Section 5.3. The aim of using a three-dimensional display of visual electric activity was to produce maps that could be co-registered with the DTI maps so ROIs could be located and used as an aid to produce tractography maps of the optic radiations. Since the brain anatomy was so distorted in both cases, it was difficult to identify anatomical structures related to the primary visual cortex so it was not possible to use the tractography method developed in Section 3.4. Instead, the hydrocephalus ROI seeding points were identified using functional information from the VEPs. The tractography maps were produced for the optic radiations and given to the clinician as an aid to the surgery. In one case, a third ventriculostomy was performed, while a VP shunt was the chosen procedure in the other.

The original aim was to repeat the MRI and functional VEP procedure following surgery. However, this was not possible in either case, because one patient had

complications during the surgery and the second woke up during the MRI scan and could not be reassessed before discharge. The comparison of preoperative and postoperative scans for hydrocephalus patients is a future research ambition.

8.3 Case study 1: Use of tractography in brain tumours

In industrialised countries, tumours are among the highest cancer diagnoses; for example, they account for 22% of all cancers in Canada (Rosychuk *et al.*, 2012). Tumours are the highest oncological cause of death in children (Baldwin and Preston-Martin, 2004). The idiosyncrasy and the nature of many tumours is still poorly understood and most paediatric brain tumours are thought to have genetic or radiation exposure as their main causes (Baldwin and Preston-Martin, 2004).

Accurate diagnosis and surgical planning is critically important to achieve successful outcomes in neurosurgery. Novel imaging techniques such as tractography are particularly useful for contributing to surgical planning when treating complex tumours, for example those that touch or compress neighbouring motor or sensory pathways.

In the two cases presented here, tractography was used as a preoperative decision-making tool.

8.3.1 Brain Tumour

This patient was an otherwise healthy 6 year old girl, weighing 23 kg. She presented a delayed history of 6 weeks of weakness in the left lower extremity. She was first scanned on her first A&E attendance; symptoms included being unable to walk without dragging her leg having difficulty getting out of bed unaided and “emotional behaviour”. She was emergency referred to the Neurosurgery Department of Great Ormond Street Hospital and an MRI was performed the same day. The parents were informed about the likelihood of a malignant tumour.

The patient was enrolled in the study after referral by the lead consultant. The consultant requested the tractography of the involved white matter pathways neighbouring the tumour. The surgery was scheduled for the following day as it was necessary to remove the tumour promptly. The standard tractography algorithm was used on this occasion. The tractography was produced and sent to the lead clinician.

The tractography images were on display in theatre on a laptop and the corresponding conventional MRI images were displayed on the Neuronavigator (BrainLab).

Figures 8.1 and 8.2 show the T1-weighted and DTI scans of the tumour, respectively. The tumour had a rounded shape with a cystic component of around 3 cm in diameter. It was causing some oedema of the surrounding tissues and in particular the superior longitudinal fasciculus, whose damage had decreased the ability of the patient to repeat words and had caused unilateral neglect, and the thalamic radiations, which are projection fibres that communicate the thalamic nuclei with the cerebral cortex and the internal capsule, transmitting motor information. The mass had a double component: solid and liquid characterised by two different densities. There were no satellite lesions in other locations and the mass was not attached to the underlying bone. The nature of the tumour was described as malignant before the surgery with the likely diagnosis of glial in origin.

The preoperative MRI suggested that the motor pathway had been invaded by the tumour. In fact, the white matter tractography, shown in Figure 8.3, indicated that the superior longitudinal fasciculus had in fact been displaced by the tumour together with the inferior fronto-occipital fasciculus. The tractography was used preoperatively to plan the surgery and intraoperatively to perform the procedure. After the visualisation of the tractographic reconstruction of the motor white matter pathways and the tumour was made available, the excision of the mass was modified and the tract was left intact. The tumour mass was entirely removed during the procedure. The patient did not have any motor deficits afterwards and the symptoms improved dramatically once the mass had been removed.

The histological analysis of the mass showed it to be an Oligodendroglyoma type II, following the WHO classification, which is a slow growth primary tumour. Postoperative MRI was planned but the DTI sequence could not be carried out as a result of patient refusal, due to finding the scanning room distressing.

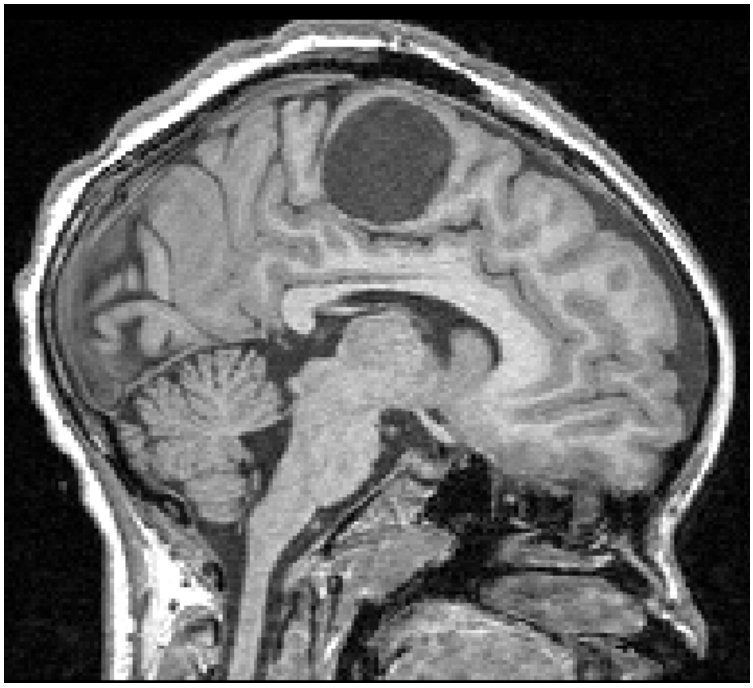

Figure 8.1 Sagittal T1-weighted view of the first brain tumour patient. The tumour is the dark grey rounded shape located within the parietal area.

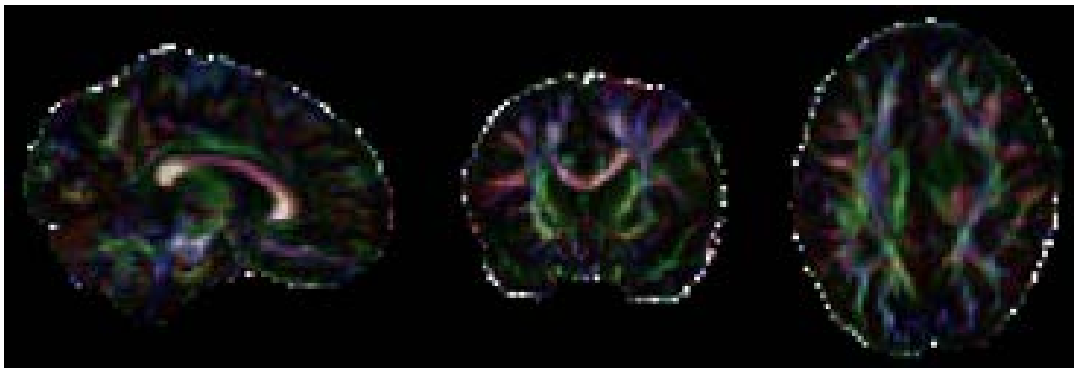

Figure 8.2 DTI showing the intracranial tumour on the three sections.

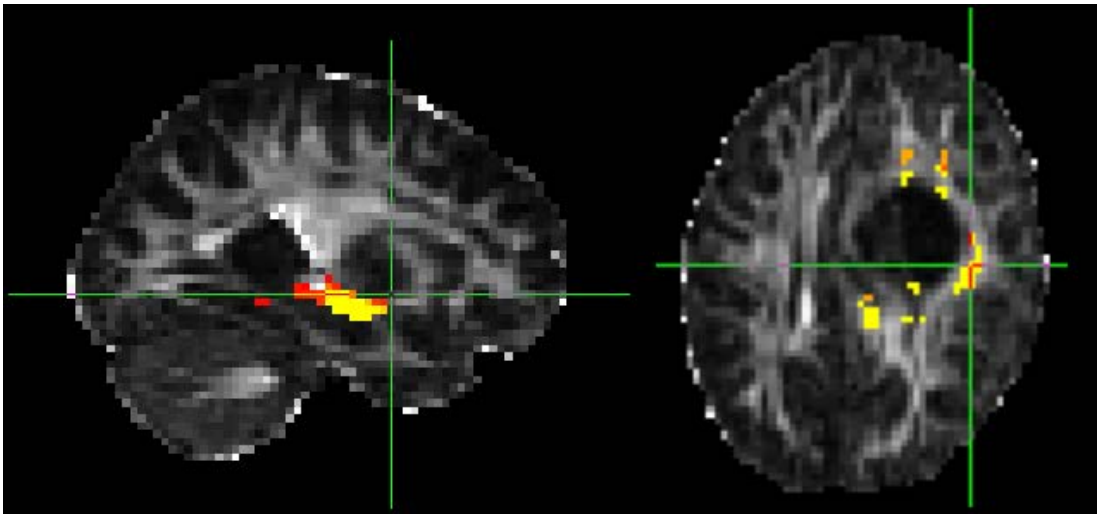

Figure 8.3 Tractography of the left white matter pathways surrounding the mass. White matter motor tracts are shown in yellow and red (inferior longitudinal fasciculus and the inferior fronto-occipital fasiculus). There were no pathways within the tumoral mass.

8.3.2 Tuberous Sclerosis

Tuberous sclerosis is a mostly autosomal dominant disease but there are sporadic cases described that are associated with chromosome 16p13.3 translocation (European Chromosome 16 Tuberous Sclerosis Consortium, 1993). It is considered to be a multi-organ disease. The estimated incidence is 1 per 5800 live births in the UK (O'Callaghan *et al.*, 1998). Tuberous sclerosis are considered benign slow growth masses that are present in many organs including the brain, eyes, kidneys and liver. The syndrome is associated with epilepsy and symptoms include learning difficulties (Krueger and Northrup, 2013). The lesions are formed of hamartomas (Jones *et al.*, 1999) and are thought to have an origin in the mutation of the tumour suppressors TSC1 (situated in chromosome 9) and TSC2 (situated in chromosome 16). The lesions found in the brain can be described as cortical tubers and sub-ependymal nodules (most of the time multiple), arising from the walls of the lateral ventricles. These subependymal lesions are histologically defined as abnormal conglomerates and are thought to be glial cells. The characteristic glial cells found in the subependymal lesions are frequently multinucleated with enlarged cytoplasm. In older children and in adults, most of the lesions include calcifications. Some of the nodules develop MRI enhancement, leading to a transformation into an aggressive lesion such as an astrocytoma.

The 2012 International Tuberous Sclerosis Complex Consensus Conference recommended MRI as the optimum imaging technique for diagnosing tuberous lesions (Northrup and Krueger, 2013). The average tuberous lesion presents as a hyperintense region on a T2-weighted image with heterotopic changes in the surrounding grey matter. The radial pattern of presentation of tuberous lesions could be caused by abnormal neuronal migration.

The patient was a 16-year-old female with long-term epilepsy associated with tuberous sclerosis. She had been treated conservatively with regular follow-up since diagnosis, which occurred after she presented her first focal motor epileptic seizure as a baby. The seizures had improved with medication but she still had very sporadic epileptic activity characterised by absence seizures. Her parents were concerned about blurred vision, which accompanied the aura of the seizures. Visual testing did not find any changes within the visual system and no functional reason was found for the sporadic blurred vision. The parents consulted the neurosurgeon that had been treating her since the initial diagnosis regarding surgical intervention and removal of the tuberous lesions located within the temporal lobe, which they believed might be compressing the optic radiation. Consent was given by the parents and the patient for inclusion in this study.

Figure 8.4 shows the tractography analysis for this patient. The figures show the left and right optic radiations added to the T1-weighted image slices of the brain. Slice (a) shows a tuberous lesion located within the right temporal lobe. The same lesion can be visualised in slice (b). Slices (c) and (d) clearly show the left and right optic radiations without any compression or disruption.

The patient was shown the images presented by the neurosurgeon in charge of her case. Introductory information was given about the brain anatomy so she could understand where the temporal lobes and the occipital lobes were located in her own brain and how the optic radiations were located in relation to them. The parents were very pleased with the analysis as it was the first time that someone had demonstrated how the optic radiations might interact with the lesions in their child. Although they had seen previous MRI scans, the locations of the white matter tracts relative to the lesions had not been apparent. They agreed that given the lack of physiological or structural explanation for the blurred vision, there was not a strong case for a major surgical intervention as this could have caused visual impairment among other

complications. The parents agreed to continue with the patient's routine follow-up and visual testing.

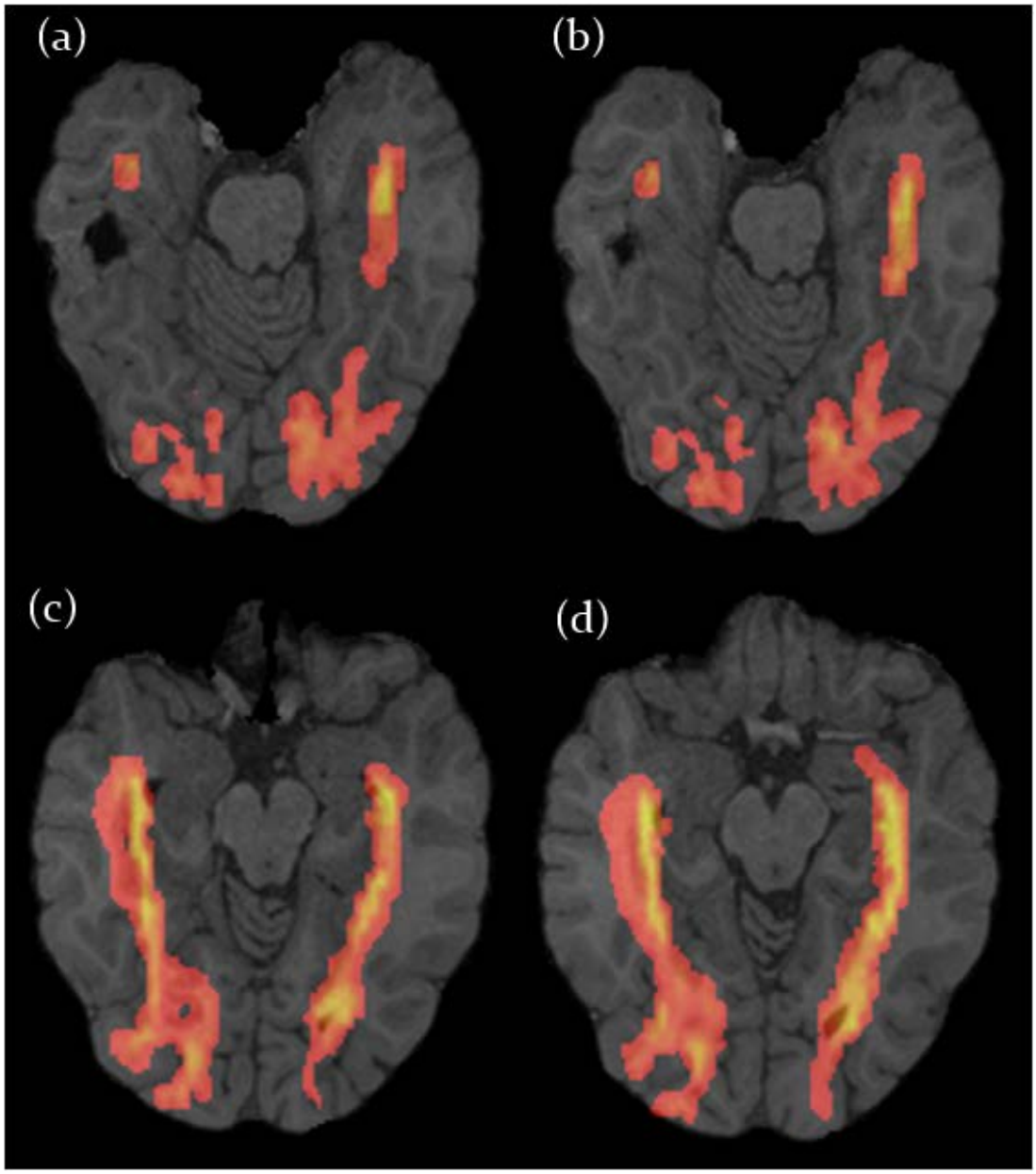

Figure 8.4 Tuberculos sclerosis lesions in the second brain tumour patient. The lesions in black can be seen near to the optic radiations, which are coloured red and yellow. The tractography results were co-integrated with the MRI T1-weighted scan in this image. See the main text for details of each image.

8.3.3 Discussion

For the first patient, the tractography process from scanning to the operating room took around 4 hours. The MRI scan was carried out in the afternoon and the analysis in the evening, with the results being ready for review by the clinical team in the early morning. The tractography analysis greatly increased the clinical understanding of the tumoral mass and the white matter tracts surrounding it, and led to modifications in the original surgical plan. It is possible that tractography will influence more general changes in surgical approaches as more patients are analysed. This case demonstrates the benefits of training doctors to use novel imaging techniques in order to increase the information available during surgery and improve outcomes.

The tractography produced in this study was displayed on a laptop in the operating theatre (with all the software installed for visualising the imaging and ready for additional analysis if required). At the time of this case intervention, the neuronavigator (BrainLab) did not have the capability of adding DTI or tractography images to the software so the pictures could not be displayed in real time during surgery. The neuronavigator enables localisation of lesions and intraoperative targets while operating using a three-dimensional system of localisers that are set before the intervention. It allows the targeting of surgical lesions or structures using the preoperative imaging. Brainlab has now been modified to enable DTI and tractography images to be shown, so the information can now be used in real time and can serve as a locator and extra aid for the surgeon.

The tuberous sclerosis case, to our knowledge, is the first time that tractography has been used to counsel patients in surgical and anatomical matters. Having visual maps of lesions and understanding their relationship to nearby white matter tracts was very important to the patient. In chronic conditions or when planning surgical interventions in children, parents often lack the knowledge and the understanding of what is intended. The stress suffered when their child has poor health can urge them to press the clinician to intervene. In this case, the parents reacted very positively to receiving a clear explanation underpinned by visual maps. The benefits of tractography extend beyond improving surgical outcomes to informing decisions about interventions and to explaining conditions to patients and parents. As such, it can be a very useful tool for several aspects of complex cases such tumours and epilepsy.

8.4 Case study 2: Use of tractography for hydrocephalus

Hydrocephalus is described as an abnormal accumulation of cerebrospinal fluid within the intracranial cavity. This increase in the volume of intracranial fluid can cause increased intracranial pressure. The anatomy of the underlying brain tissue might be severely distorted in serious cases and visual symptoms might be present even in minor cases due to compression of the optic radiations (Corns and Martin, 2012). Although still frequent in the paediatric population, hydrocephalus has decreased in incidence, probably as a result of a lower number of children having spina bifida (due to wider use of folic acid during pregnancy) and intra-ventricular haemorrhage. In the United States, hydrocephalus accounts for more than 0.5% of all paediatric admissions (Sivaganesan *et al.*, 2012). In the UK, spina bifida affects 0.001% of new born babies and most have associated hydrocephalus. This can cause learning disabilities, visual and speech impairments, and other developmental issues (NHS, 2013).

In children, presentation might differ according to the onset of hydrocephalus (acute or chronic) and the state of the cranial sutures (closed or opened). If the cranial sutures remain open, an increase in head circumference might be the first sign. May (2014) states that measurement of the head circumference should be performed and recorded by a health care professional in the child's medical records and further hydrocephalus investigations should be carried out if appropriate. Children with missed early hydrocephalus often have increased head circumference. In older children with closed cranial sutures, the clinical presentation might vary. Symptoms of raised intracranial pressure such as headache, nausea, vomiting or papilledema are common. The cause of hydrocephalus in older children with closed sutures and within normal limit head circumference is different to early-developed hydrocephalus and is commonly related to intracranial masses such tumours, vascular malformations or infections (Mori *et al.*, 1995).

To understand the pathology of hydrocephalus, it is important to clarify the flow of the cerebral-spinal-fluid (CSF). The CSF flows in a single direction from the lateral brain ventricles through the foramina of Monro, then reaches the third ventricle and the aqueduct of Sylvius into the fourth ventricle. From there, the CSF travels through the foramina of Luschka and Magendie into the subarachnoid space, where the CSF is absorbed passively into the venous sinuses by the arachnoid villi (Orešković and Klarica, 2011). Hydrocephalus appears if the fluid flow is obstructed (non-

communicating) or if there is an imbalance between CSF production and absorption (communicating). This classification is based on the presence or absence of a blockage of the CSF flow along the normal pathway.

Imaging is used to inform decisions on when and how to treat hydrocephalus. In cases with early stage presentation and clear symptoms, imaging has proven a helpful preoperative tool. The different surgical modalities of treatment require a good knowledge and description of the anatomy. Hydrocephalus can be related to other intracranial abnormalities and sometimes the individual anatomy differs very much from normal, especially in new-born babies where hydrocephalus is associated with other malformations. In cases of ventriculomegalia in otherwise asymptomatic children, imaging can be crucial as a follow-up tool.

Once hydrocephalus is diagnosed and classified then the treatment or intervention needs to be decided. CT scan is currently the most common imaging tool due to its speed and availability in hospitals. But this exposes the patient to an increased level of radiation compared to otherwise healthy children during their lifetime (Fazel *et al.*, 2009, Smith-Bindman *et al.*, 2009). MRI is an alternative and safer imaging method for in-utero diagnosis of hydrocephalus (D'Ercole *et al.*, 1993). The increasing availability and shorter acquisition time for newer scanners means that MRI could become the favoured imaging technology for the paediatric population in the future (O'Neill *et al.*, 2013). For cases in which a third ventriculostomy or foraminotomy are the preferred interventional techniques, MRI can describe the exact location of the third ventricle, the related pathways (visual) and the basilar artery (DeFlorio and Shah, 2014).

This case study examined two babies that had recently been diagnosed with hydrocephalus, one intra-utero and the other shortly after birth. Conventional MRI and DTI scans were acquired for both children prior to planned surgical interventions.

8.4.1 Hydrocephalus patient A

The first patient was a female aged 34 weeks at the time of presentation. The baby was born at full term with no known complications during pregnancy. The child was not born from a consanguineal union and the parents did not have common relatives. There was an attempt to alleviate the hydrocephalus using an intrauterine third ventriculostomy, which failed. The large head size led to a birth by Caesarean section.

A VP shunt was placed in situ shortly after birth (Figure 8.5). A third ventricle cyst of 2 cm diameter can be seen in the coronal slice (Figure 8.6). Other views of the hydrocephalus region are shown in Figures 8.7 and 8.8. The baby underwent the VP shunt insertion with no complications.

The VEPs of the child were performed using the quick cap technique with a recording of 64 channels. The anatomical position of each electrode was recorded. The VEP recording was not only useful for preoperative planning but as a complete assessment of the visual status of the baby prior to the procedure. Standard textbook anatomical landmarks cannot be used for patients such as this one as seeding points would not produce any reliable results because the normal anatomical landmarks cannot be easily identified. Even in detailed MRI clinical sequences, the LGN and the V1 area cannot be easily identified.

Figure 8.9 shows the MRI and the activity localised in three of the recordings. The picture was taken from the original recording book of the author. The dotted circle shows the channels with VEP activity. The figure on the right shows in dark grey the activity localised on the recording map. The VEP information was used to set the seeding points for the tractography and the results are shown in Figure 8.10. The right and left optic radiations are adjacent to the wall of the lateral ventricles. Both optic radiations run towards the occipital cortex, which is also in an unusual position. The occipital cortex is not fully overlaid by the occipital bone, but anteriorly displaced and in close proximity to the parietal bone, which partially overlays it. The visual cortex would normally be situated in the paramedian areas, in close proximity to the inion, but in this case is grossly displaced laterally. The information gathered through the combination of VEPs and posterior tractography analysis gave the surgeon more accurate information than would have been available from standard clinical imaging.

The baby had an uneventful postoperative period and a follow-up scan was planned. The feed and wrap technique allowed conventional MRI acquisition but the baby awoke before the end of the procedure so a DTI acquisition could not be obtained.

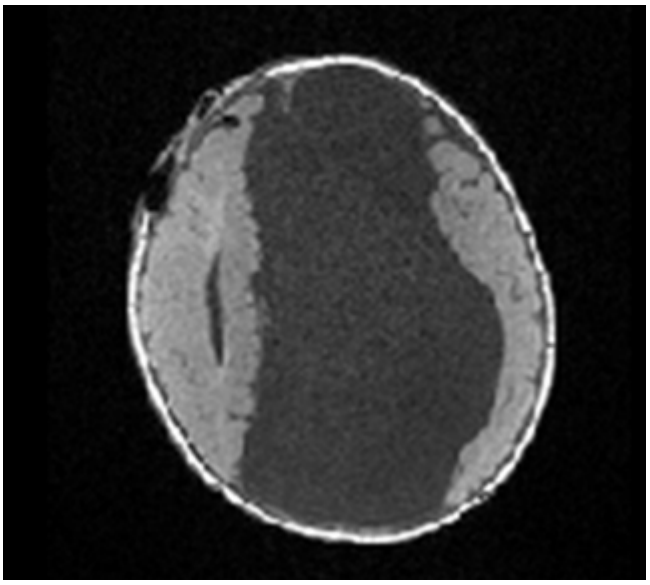

Figure 8.5 VP shunt on the right of the frontal lobe of hydrocephalus patient A. A disruption of the bone (in white) shows the insertion point of the valve. The severe grade of hydrocephalus is clear from the dark grey region that fills the intracranial cavity. The remaining brain tissue (grey and white matter) are represented in the left and right regions of the intracranial cavity.

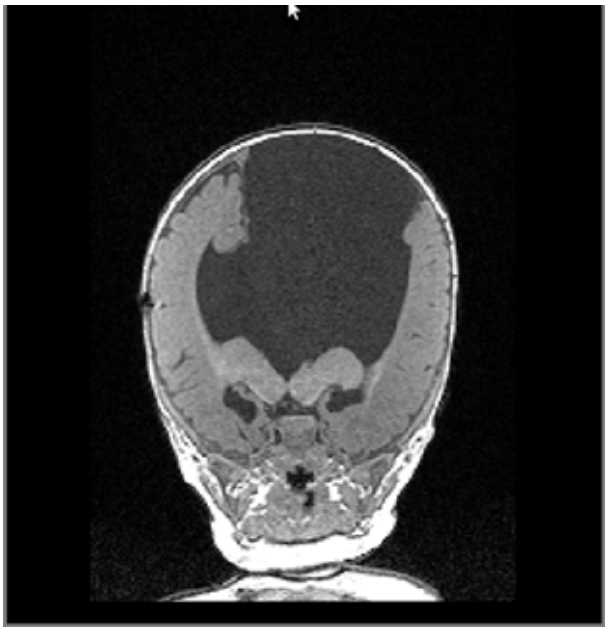

Figure 8.6 Coronal view of the 33 weeks female hydrocephalus patient showing the severe grade of hydrocephalia.

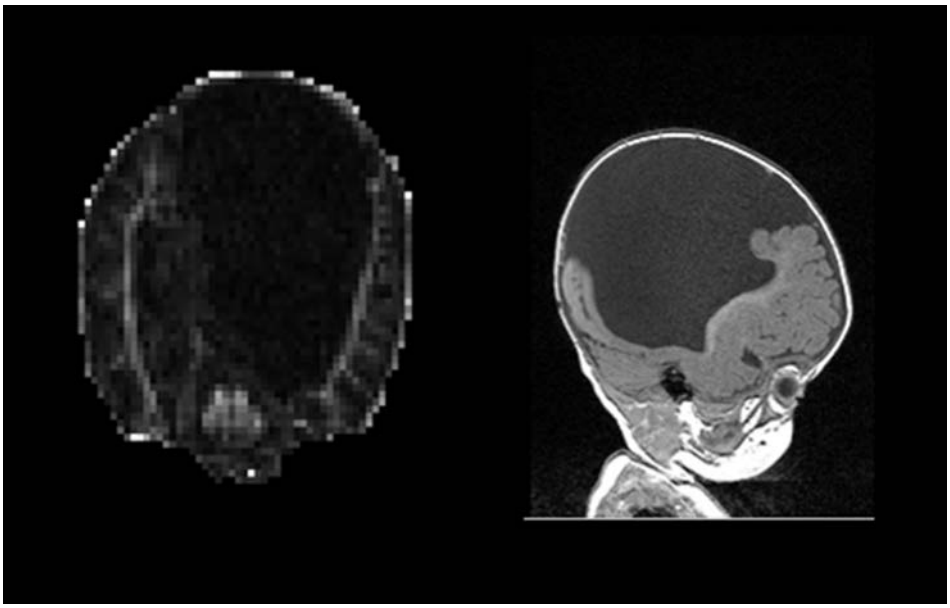

Figure 8.7 Coronal and sagittal and MRI images of the hydrocephalus patient A brain. The picture of the left shows the FA map derived from the DTI acquisition.

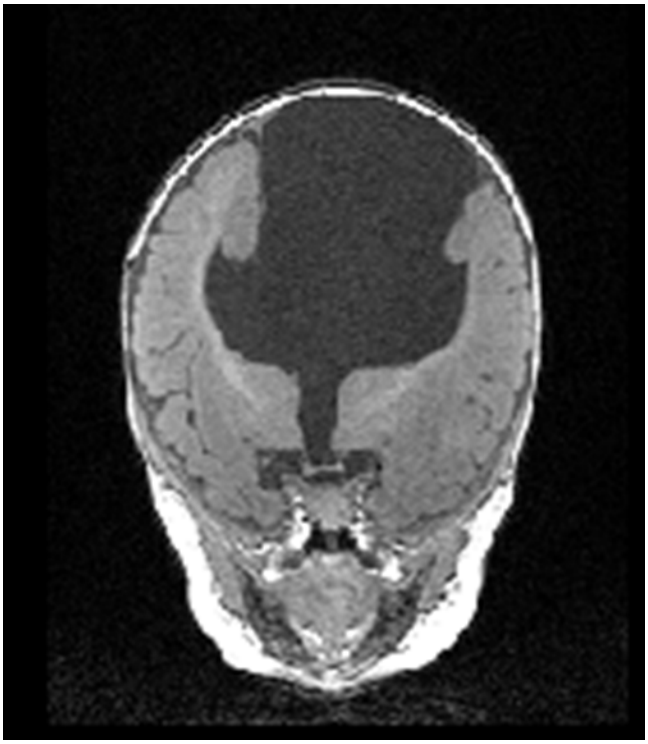

Figure 8.8 Coronal view of the brain of hydrocephalus patient A. Both hemispheres can be visualised. The CSF is filling the intracranial cavity and it can be clearly visualised in the midline in dark grey.

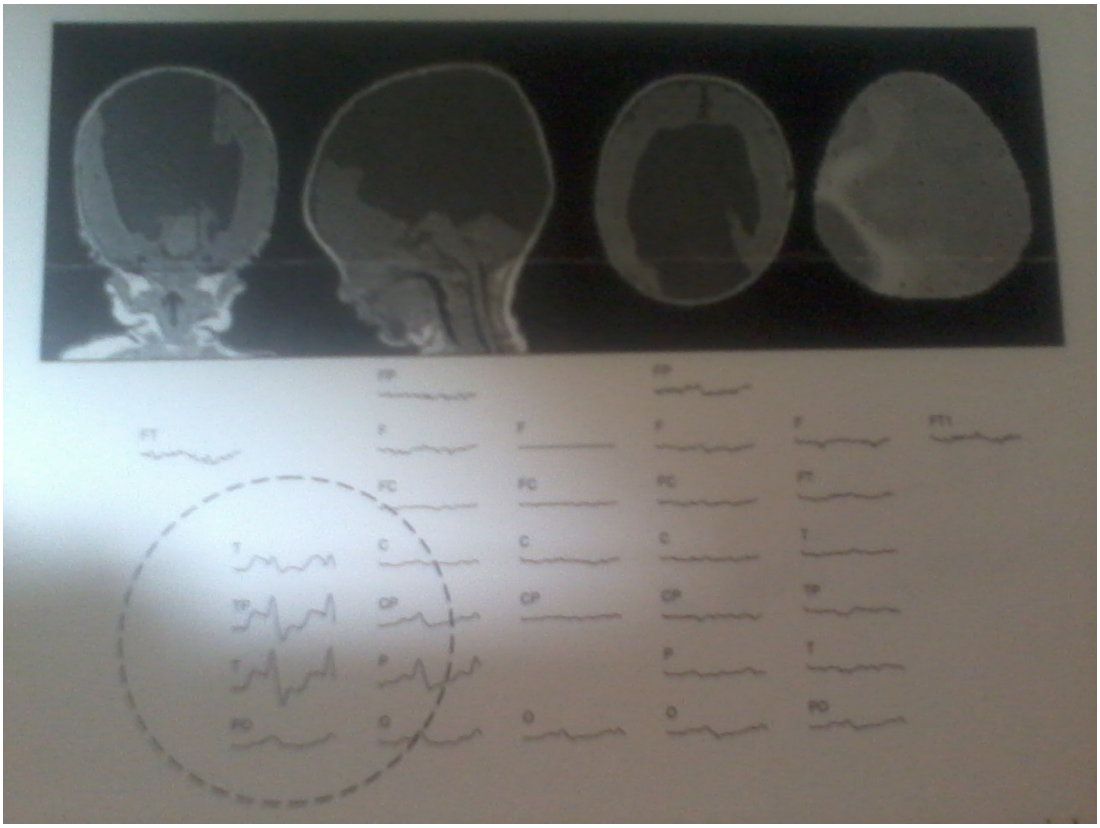

Figure 8.9 Clinical notes for the VEP of hydrocephalus patient A. These were given to the clinician after the multichannel recording was completed.

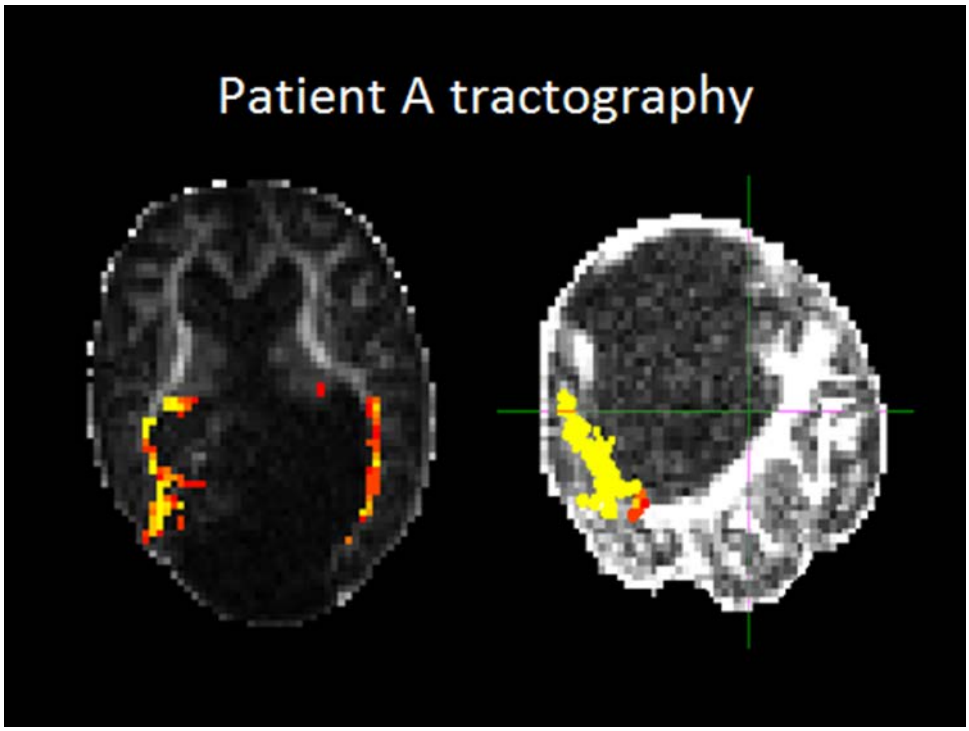

Figure 8.10 Tractography of the optic radiations in hydrocephalus patient A. The VEP functional recordings were used to set tractography seeding points.

8.4.2 Hydrocephalus patient B

The second hydrocephalus patient was a 62-week-old female who presented as an emergency referral to the Neurosurgery Department at Great Ormond Street Hospital. She was born by vaginal delivery with no complications. The pregnancy concluded without any incidences or known maternal infections. She was observed crying while eating from 6 months of age and her parents noticed that she was unable to follow toys. The patient was referred by her GP due to increased head circumference size.

A clinical MRI, including DTI, and a VEP scan were performed preoperatively. The MRI (Figure 8.11) was performed using the "feed and wrap" technique and it did not require sedation or additional medication. The VEP scan was performed with a 64-channel quick-cap, using reverse pattern visual stimuli described in Section 5.2.2. The VEP was used to add additional seeding points for the posterior tractography analysis of the optic radiation.

Figure 8.12 shows a coronal view of the patient brain. The lateral ventricles appear disproportionally enlarged compared to a healthy control of the same age and size. The left figure shows the tractography colour maps of the optic radiations overlaid onto FA maps. Tractography enabled the visualisation of the optic radiations, which otherwise would have been very difficult to identify with conventional MRI due to the distorted anatomy.

Surgical intervention was required and a successful third ventriculostomy was performed. For the postoperative MRI, a feed and wrap technique was tried but was unsuccessful, and a CT head scan was performed instead.

8.4.3 Discussion

Case reports have been published with DTI added to high-contrast, pattern-reversal VEPs (Liasis *et al.*, 2009). That study was able to find the source of the P1 and N1 component and to match them to the cortical surface area of interest. The analysis in this study has not only identified the cortical source location of the P1 component of the VEP wave, but has also identified the optic radiations using tractography informed by VEP recordings. This case study has shown how VEP-enhanced tractography can describe the optic radiations in individuals with distorted anatomies, without any need for sedation or invasive procedures. In both cases, the imaging results contributed to the surgical planning and aided the treatment and posterior follow up. The parents of

both children had a very positive attitude to MRI as it did not employ ionising radiation.

It is important for a clinician to know the location of the primary visual cortex and the associated optic radiations, because there are few approaches for VP shunt insertion and finding an optimum location for the draining catheter in the lateral ventricles has been related to a lower rate of complications (Yamada *et al.*, 2013). Experience has shown that the different techniques available to inform the approach to achieving the optimum location do not always guarantee a successful operation that is free of complications (Khan *et al.*, 2013).

There are many potential visual complications and other issues with paediatric hydrocephalus. Locating the white matter tracts was found to be very valuable in this study; by having not only information about the neuronal electrical activity of the V1 area, given by the VEP recordings, but also anatomical information about the location of the optic radiations, the clinicians were able to better plan the VP shunt insertion.

A larger cohort would be required to draw conclusions about statistical improvements to the surgical technique from VEP-enhanced tractography. Yet the two case studies in this chapter have provided qualitative evidence of the value of the technique that can provide a base for a broader study and randomised trial that compares the conventional technique with the one used here.

Children with hydrocephalus often have visual impairment. One cause is compression of the optic radiations due to the lateral ventricles having increased volumes. From the second month of extrauterine life, development of the cortical occipital visual areas starts interacting with the subcortical areas and taking control of different functions. The visual impairment in these severe hydrocephalic children could be due to the compression of the visual cortex, which is known to be able to function even with a thickness of less than 1 cm (Woods *et al.*, 1987), or could be due to the compression of the optic radiations (Dyet *et al.*, 2006, Atkinson *et al.*, 2008). It would be interesting to understand whether visual impairment affects myelination within the optic radiations.

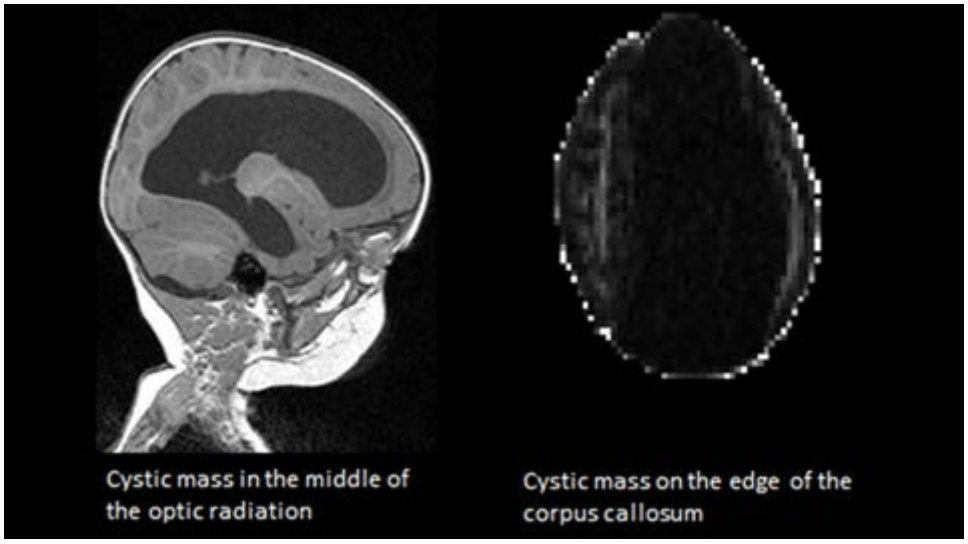

Figure 8.11 Sagittal and transversal view of hydrocephalus patient B.

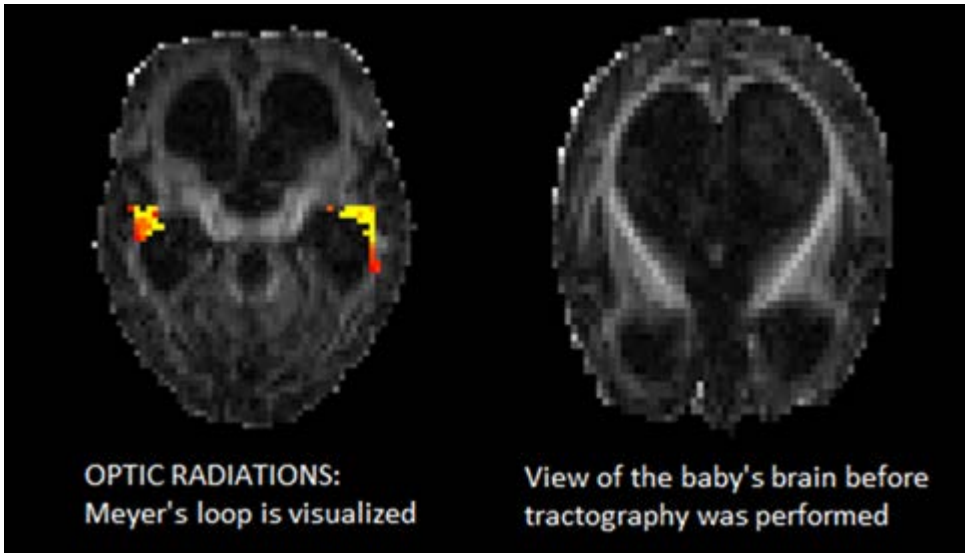

Figure 8.12 DTI tractography of the optic radiations of hydrocephalus patient B.

8.5 Conclusions

This chapter has described four case studies that examined the benefits of the tractography and VEP methodologies developed by this study for neurosurgical applications. Tractography can be a valuable surgical tool in complicated paediatric neurosurgical cases where knowledge of white matter tracts can improve the surgical outcome. Moreover, VEPs can facilitate DTI tractography in patients with complex anatomies such as hydrocephalus, offering a novel method to identify white matter tracts in cases where conventional imaging techniques provide very limited information.

Tractography can also help to inform patients and parents about tumours or other pathologies. The tuberous sclerosis case, to our knowledge, is the first in which tractography has been used to counsel patients in surgical and anatomical matters. The counselling benefits of tractography are particularly valuable when treating the paediatric population, as the visual nature can have a great impact in helping patients and parents to better understand pathologies.

9 OVERALL CONCLUSIONS AND FUTURE RESEARCH

This chapter summarises the conclusions of the thesis in Sections 9.1 to 9.5 and identifies further work for the future in Section 9.6. The thesis concludes with a short summary of the principal findings in Section 9.7.

9.1 Development of the visual system

Sight is a vital human sense and the visual system is particularly complex in comparison with most other sensory systems of the human body. The visual system is organised into the retina, optic nerve, optic chiasm, optic tract, lateral geniculate nucleus (LGN), optic radiations (Meyer's loop constitutes the most anterior pole of the optic radiations within the temporal lobe) and the striate cortex (Section 2.1).

The anatomy of the visual system in adults is understood from anatomical dissections (van Baarsen *et al.*, 2009) and more recently a tractography study (Govindan *et al.*, 2008). Although animal studies have identified evolving visual system evolution across a range of species, these have limited value since the spatial organisation of the human visual cortex is different to other mammalian species (Wandell *et al.*, 2007). Significant variations in the optic radiations have been observed between adult subjects (Section 2.3). For example, the distance between the most anterior part of Meyer's loop and the temporal pole has been measured in the range 34–51 mm (Doyon

et al., 2004). This means that a tractography-based atlas of the optic radiations is of little use for preoperative surgical planning, even for patients with a normal anatomy.

9.1.1 Anatomical dissection of the visual system

This study has concentrated on the development of the optic radiations in children, for which there is little information in the literature. As a first step to better understand and illustrate the anatomy of the optic radiations, a dissection was performed in an adult cadaver for this study, as described in Section 2.2. This was used to identify the principal anatomical structures and inform the subsequent tractography analysis.

9.1.2 Visual system development through childhood

The development of the visual system through childhood can be characterised in terms of functional development and anatomical development.

Visual acuity increases from birth to maturity at an age of around 4 years (Berardi *et al.*, 2000). The two important foundations for visual system development are the genetic phase, which is largely influenced at conception, and the posterior environmental-structural phase. The environmental-structural phase is determined by gene interactions but also by the stimuli and environment while the sensory system is developing. There are thought to be multiple sensitive periods in the maturation process in which the development of the visual system is sensitive to stimuli from the outside world, with the period varying widely across different aspects of vision and ranging from ages of a few months to more than 10 years old (Lewis and Maurer, 2009).

This thesis has focused primarily on the anatomical development of the optic radiations. Each white matter tract in the brain develops at a different rate. The organisation of the tracts is complex and variable, with their development influenced by genetic predispositions, environmental events and the response of the neurons to stimuli. The period of development is variously estimated in the literature between 7 years and 10 years (Berardi *et al.*, 2000, Lewis and Maurer, 2009). Myelination of the optic radiations is thought to be mostly completed by 7 months of age and the sheath thickness increases particularly strongly in the first 2 years, but more slowly thereafter (Magoon and Robb, 1981). Overall, the development of the optic radiations in humans through childhood is not well understood.

9.2 Characterising normal development of the optic radiations

Magnetic resonance imaging (MRI) is often used to investigate anatomical malformations in the brain, but conventional scans cannot describe individual white matter pathways in vivo. The development of diffusion tensor imaging (DTI) and more recently tractography has led to the first non-invasive techniques that are able to identify the optic radiations (Sections 2.4 and 2.5). DTI tractography is the principal method used in this thesis. The fractional anisotropy (FA) of the DTI scan depends on the rate of myelination, which means that the magnitude of the mean FA in the visual tracts can be used as a proxy for the development of white matter pathways.

Visual function can be tested in patients using visual evoked potentials (VEPs). These are an electrical signal from the central nervous system as a response to visual stimuli, which can be recorded non-invasively from the skin (Section 2.6). In this thesis, a novel methodology is tested in which VEPs are used to improve the quality of the tractography analysis, particularly for patients with distorted anatomies.

9.2.1 Observing development using tractography

Around 200 subjects were scanned in this study in total, covering a range of ophthalmologic and other diseases. Two DTI protocols were used, depending on the patient cohort. A 20-direction protocol, repeated 3 times and denoted 3×20, was used in previous and ongoing studies and continued to be used in this study for shared patients. A new 60-direction protocol, denoted 1×60, was introduced in this study, and was found to produce better-quality images in a shorter scanning time. Tractography was performed for all scans following the clear, comprehensive methodology described in Section 3.4. A comparison of 1×60 and 3×20 control cohorts showed statistically-significant differences in mean FA in both left and right optic radiations, for younger and older children, so it was not possible to combine tractography analyses from the two scan types in any of the analyses (Section 3.5). The reason is that the 3×20 sequence produces two excitations per phase encoding step and obtains twice as much data as the 1×60 sequence, meaning it has a higher signal-to-noise ratio, which is known to bias FA. This means that in areas of low FA, such as grey matter, 1×60 scans have higher FA than 3×20 scans. If the signal-to-noise ratios were exactly matched then FA maps could be compared between scanners more

easily. However, this is difficult to achieve in practice, and the sensitivity of the mean FA magnitude to both the scanner and the choice of protocol means that absolute mean FA results from different studies cannot generally be directly compared.

The mean FA was calculated for each optic radiation of each patient, including front, rear and full tract FAs. The cut-off between the front and the rear was located in the proximity of the parieto-occipital sulci. There were no statistically-significant differences between the front and rear mean FA for the control patients (Section 4.3).

The normal development of the optic radiations was examined using tractography for a cohort of 41 children and 13 adults, each scanned with the 1×60 protocol, and independently with a second cohort of 35 children scanned with the 3×20 protocol. These cohorts included 26 children aged 5 years or under, enabling the development of the optic radiations to be characterised in the crucial first few years. The mean FA was found to have a logarithmic distribution with age, with a rapid increase in the first four years of life followed by a steady but small increase that continues into adulthood (Section 4.3). This finding is significant because many studies assume a linear relationship between mean FA and age, yet this study shows this to be a poor assumption for young children.

Previous studies have assumed that the left and right optic radiations develop in a similar way (e.g. de Schotten *et al.*, 2011a). Yet a dissection study has shown that the left optic radiation tends to penetrate deeper into the temporal lobe and is therefore considered to be longer than the right (Jeelani *et al.*, 2010). A comparison for the 1×60 cohort in this study concluded that the rear ($p<0.05$) and full ($p<0.01$) optic radiation mean FA of children over 5 years old was higher for the left optic radiation than for the right optic radiation, which suggests that the optic radiations develop differently as the visual system matures and hence challenges the assumption made by previous studies (Section 4.4). However, no statistically-significant differences could be identified for the 3×20 cohort.

Previous studies have similarly assumed that the optic radiations develop similarly in males and females (de Schotten *et al.*, 2011b). Over the whole brain, it has been suggested that females have a higher proportion of white-to-grey matter than males as a result of earlier development, but no significant differences have been identified within the occipital lobe in adulthood (Watson *et al.*, 2010). Male and female mean

FAs were compared for each protocol in Section 4.5. There were no statistically-significant differences between males and females in either optic radiation, for older or younger children scanned using either protocol.

Knowing the volume and the length of the optic radiations is important for children with known deficits where certain pathologies are expected, particularly if they require surgery. Unfortunately, the brain volume and the length of the optic radiations are not easily measured in the living brain without employing imaging techniques. Tractography produces maps that can be used to measure the length of the optic radiations. Lengths were estimated from the tractography maps for the 1×60 cohort in Section 4.6. An increasing trend with age was observed, although the variability was higher than for the tract mean FA. There were no statistically-significant differences between the left and right optic radiations.

9.2.2 Improving tractography analysis using VEPs

VEP recordings are widely used in the clinical environment. An aim of this study was to consider whether optic radiation tractography could be improved by using information from VEP recordings, as mapping white matter tracts in areas with high amounts of grey matter, such as in the vicinity of the visual primary cortex, is difficult. The experiment was performed on a cohort of 12 adults, as they were more co-operative and therefore more suitable to undergo the VEP recording than children. A 40-channel recording was performed on each subject using a spandex cap with an array of electrodes attached to their head (Section 5.2). The DTI scan was combined with the VEP data in the NeuroScan software to identify the V1 area, and this was then used to define a secondary seed ROI for the tractography analysis. Tractography was performed both with and without the VEP information for each patient and the difference in mean FA was assessed statistically.

Adding the functional VEP data enabled the tractography analysis to identify the primary visual cortex that is often omitted by the standard method, and were generally found to improve the tracking of the optic radiations across the cohort (Section 5.4). The change principally occurred through the inclusion of additional voxels at the rear of the optic radiations. Since these tended to have lower mean FA than the rest of the tract, the rear and total mean FA was lower for both optic radiations for VEP-enhanced tractography ($p<0.00001$).

For patients with highly-distorted anatomies such as those with hydrocephalus, it is difficult to identify the optic radiations using standard tractography because the primary ROI in the vicinity of the LGN cannot be identified. VEP-enhanced tractography offers an alternative ROI to identify the optic radiations, and the potential benefits of this method are examined in Section 8.4.

9.3 Changes in the optic radiations in children with optic nerve hypoplasia

ONH is described as underdevelopment of the optic nerve (Sowka *et al.*, 2008). Visual abnormalities such as ONH and associated septo-optic dysplasia are related to abnormal visual system development in the intrauterine period, but the origins of the diseases are not fully understood. It may present as a unilateral or bilateral lesion with variable visual impairment, or can occur in association with other ocular, endocrinal and neurological problems (Kidd *et al.*, 2008). Anatomical abnormalities found in the visual system of children with ONH might not have a functional correlation.

MRI is used clinically to examine the intracranial anatomy of patients with visual defects. DTI tractography is an emerging tool for understanding the intricacies of the pathologies of patients with ONH, and has been applied to severe septo-optic dysplasia in a case study (Schoth and Krings, 2004). Another study used the TBSS software to perform a statistical, voxel-based analysis of the whole brain and concluded that the optic radiation mean FA in ONH patients was lower than for a control cohort (Webb *et al.*, 2013). The principal aim of this study was to examine how mild ONH affects, or is affected by, reduced myelination and defects in the optic radiations. A novel methodology was developed that identified overall changes in the optic radiation mean FA using tractography and combined this with a TBSS analysis of FA differences across the white matter tracts. It also used a much larger cohort (23 patients) than any previous studies.

No statistically-significant differences in mean FA were found between the ONH patients aged up to 5 years and the matched controls (Section 6.4.6). However, ONH patients aged over 5 years had lower mean FA for the left optic radiation than the matched controls ($p<0.01$), with the difference predominantly at the front of the optic radiation ($p<0.01$). There were no statistically-significant differences for this cohort for the right optic radiation. This result contrasts with those of Xie *et al.* (2007), who

found no reduction in mean FA for either optic radiation for a smaller cohort of amblyopia patients, although it is possible that that study did not consider sufficient patients to detect possible differences. The TBSS analysis corroborates the tractography results and the analysis of the full, rear and front mean FA in the optic radiation. It shows that ONH is not purely related to an abnormal optic nerve, but that these patients have other abnormal anatomical structures, such as lower myelination rates in the language centres, so ONH should be regarded as being more complex than a visual system syndrome.

A secondary aim of this study was to examine the potential benefits of DTI tractography as a tool in the diagnosis and follow-up of children with suspected ONH. At present, tractography could be used to better understand the development and myelination of the optic radiations in patients diagnosed with ONH. While this would not facilitate treatment at the moment, it might contribute to understanding the cause of the ONH and give an indication of the potential suitability for the patient of new treatments that have not yet been developed.

9.4 Changes in the optic radiations in children with seizures

Epilepsy is the most common neurological condition in childhood, with a prevalence of 1%, while 2–4% of children under 5 years old suffer an episode of febrile convulsions. Little is known about how seizures affect the white matter pathways of the brain that are not directly involved in the epileptic focus. The abnormalities found in children with prolonged febrile seizures extend beyond the hippocampus or the initial epileptic focus. Hemispheric areas such as temporal lobe or insula present abnormalities are detectable with conventional MRI (Shinnar *et al.*, 2012) and with DTI (Yoong *et al.*, 2013). This study aimed to understand the impact of seizures on the optic radiations in the paediatric population using DTI tractography. A secondary aim was to identify a suitable tractography protocol for preoperative planning.

A cohort of 21 children who had suffered a single episode of prolonged febrile convulsions were compared with age-matched controls. This cohort did not present lower mean FA in either optic radiation, suggesting that a single seizure episode might not cause widespread damage to the optic radiations. It is possible that small-scale

damage cannot be detected using current clinical tractography protocols, or that the patients recovered to some extent between the seizure and the MRI scan.

A cohort of 20 children with long-term epileptic activity were also compared with age-matched controls. The epilepsy cohort presented a decreased mean FA in the left optic radiation compared with the control cohort, despite the patients having neither visual epileptic activity nor visual impairment. This insight could be explained by a number of hypotheses and further research is required to better understand the results.

The new 60-direction DTI tractography protocol adopted by this study was identified as the most suitable for improving paediatric preoperative planning, as it produced higher-quality images in a shorter scanning time than the other protocols that were tested.

Clinical MRI is becoming more widely-available. In the near future, it will be possible for children who present with a very first epileptic seizure to be scanned with a short MRI protocol including DTI, as performed in this study. If the child continues to have seizures and requires anti-epileptic medicines, then the DTI protocol can be repeated and tractography performed in a longitudinal study, which would enable changes due to repeated episodes and medication to be detected. A large cohort of healthy children would be needed to establish standard values of mean FA along all the tracts for comparison.

The impact of subclinical epileptic activity on white matter tracts is another area for future research. Routine DTI studies and EEG recordings could be combined to better understand the relative impacts of anti-epileptic medication and recurring subclinical epileptic activity.

Recently, biomarkers of hypoxia and vascular damage related to seizures have been described. A future research avenue would be to compare the elevation of any of these biomarkers with mean FA and white matter changes (Parfenova *et al.*, 2010).

9.5 Use of tractography in neurosurgery

Neurosurgery is constantly evolving as new technologies and techniques become available and increasingly complex cases are operated. Technology has been and continues to be an important tool for diagnosis and treatment of several brain pathologies, and improvements have contributed to improving outcomes and reducing

complications by minimising unintended damage. The aim of this study was to consider how DTI tractography, including VEP-enhanced tractography, could contribute to preoperative planning and hence improve surgical outcomes in a series of case studies.

Tumours are the highest oncological cause of death in children (Baldwin and Preston-Martin, 2004). Accurate diagnosis and surgical planning is critically important to achieve successful outcomes in neurosurgery. Novel imaging techniques such as tractography are particularly useful for contributing to surgical planning when treating complex tumours, for example those that touch or compress neighbouring motor or sensory pathways. The first case study patient had a tumour with a rounded shape, with a cystic component of around 3 cm in diameter, which was thought from the preoperative MRI to be invading the inferior fronto-occipital pathway (Section 8.3.1). In fact, tractography analysis indicated that the inferior fronto-occipital pathway and the superior longitudinal fasciculus had in fact been displaced by the tumour. The tractography was used preoperatively to plan the surgery and intraoperatively to perform the procedure. The tumour mass was entirely removed during the procedure and the patient did not have any motor deficits afterwards.

The second case study patient had long-term epilepsy associated with tuberous sclerosis (Section 8.3.2). She had been treated conservatively with regular follow-ups since diagnosis, which occurred after she presented her first focal motor epileptic seizure as a baby. Her parents were concerned about blurred vision which accompanied the aura of the seizures. The parents consulted the neurosurgeon regarding surgical intervention and removal of the tuberous lesions located within the temporal lobe, which they believed might be compressing the optic radiations. The DTI 1×60 protocol was performed and tractography analysis showed that the optic radiations were not being compressed or disrupted by tuberous lesions. It was agreed that there was not a strong case for a major surgical intervention, in view of the potential side effects. This is the first time, to our knowledge, that tractography has been used to counsel patients in surgical and anatomical matters.

The final two case studies examined patients with hydrocephalus, which is an abnormal accumulation of cerebrospinal fluid within the intracranial cavity (Section 8.4). The anatomy of the underlying brain tissue might be severely distorted in serious cases and visual symptoms might be present even in minor cases due to compression

of the optic radiations (Corns and Martin, 2012). It is important for a clinician to know the location of the primary visual cortex and the associated optic radiations, because there are few approaches for VP shunt insertion and finding an optimum location for the draining catheter in the lateral ventricles has been related to a lower rate of complications (Yamada *et al.*, 2013). Imaging is used to inform decisions on when and how to treat hydrocephalus. In both case studies, the distorted anatomies made it difficult to identify the LGN as part of the standard tractography procedure. Instead, VEP recordings were used to identify an alternative seed ROI and the VEP-enhanced tractography methodology developed in Chapter 5 was used to identify the optic radiations, without any need for sedation or invasive procedures. The imaging results contributed to the surgical planning and aided the treatment and posterior follow-up in both cases. These case studies provide qualitative evidence of the value of VEP-enhanced tractography, which can provide a base for a broader study and randomised trial in the future.

Tractography is not yet available as a standard clinical tool. Brainlab, and other neurosurgical navigation devices, are starting to include DTI capability in their software and processing algorithms. In the future, these software packages should be able to import and overlay tractography images onto conventional MRI scans in order to inform tumour or epileptic focus resection. The improved understanding from tractography should enable more accurate and localised resection of the affected area with less risk of damaging the optic radiations. A novel VEP-enhanced tractography methodology has been introduced in this study. The additional complication of performing the VEP recording and using several software packages means that it is likely to remain primarily a research tool for the time being. It is possible that higher-resolution imaging might better resolve the optic pathways that coalesce at the primary visual cortex, and also contribute to improved tractography in this region in the future.

9.6 Future research

As with many imaging studies, an improvement in the image resolution would enable a better understanding of the anatomy in both normal and abnormal brains. The data acquired on the 1.5 T scanner used in this thesis has a voxel size of 2.5 mm, which is suitable for examining larger fibres with constant diameters but is large in comparison to the size of axonal fibres of the optic radiations (Ebeling and Reulen, 1988). A

higher-resolution scan might improve the mean FA estimate in transitional areas with more complex fibres. For example, the optic radiation fibres spread out in multiple directions at the rear of the optic radiation near the visual primary cortex, which makes them difficult to follow with tractography analyses. While the VEP-enhanced method was introduced to circumvent this issue, an improvement in the image resolution might render it redundant for normal anatomies. The resolution is a function of the scanner magnetic field strength, which tends to be 1.5 T for most clinical scanners. It can be also improved through increasing the number of slices, but at the cost of increasing the scan time, which can affect the compliance of children and also reduces the number of patients that can be scanned.

The TBSS analysis showed that ONH is not purely related to an abnormal optic nerve, as these patients have other abnormal anatomical structures. Further research is required to understand whether this widespread reduction in FA is the cause or a consequence of ONH. The wide range of visual disabilities presented by these children, varying from severe to mild, is not thought to be related to the grade of abnormal size and shape of the optic nerve, which suggests that there could be a range of causes. One issue is that current DTI imaging has an insufficient resolution to be able to identify small lesions in the optic nerve, and this might change with improved resolution. The techniques developed in this study could also be applied to patients with other visual abnormalities such as amblyopia or microphthalmia.

Several hypotheses were proposed to explain the reduction in optic radiation mean FA in patients using anti-epileptic medicines, which could form the basis of future research. Moreover, DTI tractography and measurements of the hippocampus could be combined in a longitudinal study of children with epilepsy, to identify any correlation between decreased mean FA and increased anatomical abnormalities in the hippocampal area. DTI tractography could also be used to examine the cerebellum in epilepsy patients as it is not thought to be affected by spreading epileptogenic seizure activity, despite being connected with the thalamus.

This study has demonstrated the value of both standard and VEP-enhanced DTI tractography for preoperative and intraoperative planning. Tractography produced in this study was displayed on a laptop in the operating theatre. Clinical MRI scanners with DTI capability are becoming more common and the next step is to develop a robust clinical tractography route that can be integrated with neuronavigators such as

BrainLab, to which DTI capabilities have recently been added. Tractography can be applied to other pathways as well as the optic radiations, for example the auditory and motor pathways. For the impact of diseases on the pathways of individual patients to be fully understood, it would be necessary to standardise the mean FA values for children of all ages. Since the mean FA is sensitive to the scanner and chosen protocol, it would most likely be necessary to choose a benchmark protocol for each scanner in order to minimise the number of scans of controls that would be required.

The two hydrocephalus case studies have provided qualitative evidence of the value of VEP-enhanced tractography. It was not possible to obtain postoperative scans in either case and performing a comparison of preoperative and postoperative scans for hydrocephalus patients is a future research ambition. A larger cohort would be required to draw conclusions about statistical improvements to surgical outcomes due to VEP-enhanced tractography, and to understand the limitations of tractography for these patients. It would be interesting to understand whether visual impairment affects myelination within the optic radiations, and whether this could then provide insights into the correlation found between myelination and ONH in Chapter 6. Another research avenue would be to apply VEP-enhanced tractography to ONH and other pathologies, which might indicate whether the primary visual area is affected by the pathology or if epilepsy and hearing impairment cause a variation in the located primary visual cortex.

9.7 Final summary of principal findings

1. A brain dissection has been performed in an adult cadaver to identify the principal anatomical structures of the visual system and inform the tractography analysis.

2. A new MRI DTI protocol has been introduced and a tractography analysis route from previous studies has been improved and standardised through the addition of several novel features. The normal anatomical development of the optic radiations has been characterised from birth in terms of the mean FA from DTI, in two cohorts comprising 76 control subjects in total. The mean FA was found to have a logarithmic distribution with age, with a rapid increase in the first four years of life followed by a steady but small increase that continues into adulthood, in contrast to many studies that assume a linear relationship between mean FA and age. The mean FA of the left optic radiation was higher than for the right tract in

one cohort, but no statistically-significant differences could be found between males and females. A method has been demonstrated to measure the length of the optic radiation from tractography analyses; the variability of this length was much greater than the mean FA variability for the same cohort.

3. A novel VEP-enhanced tractography route has been developed and tested. A 40-channel recording was performed on each subject and combined with the DTI scan to identify the V1 area, which was then used to define a secondary seed ROI for the tractography analysis. A comparison of the two methodologies on 11 adult controls concluded that the VEP-enhanced method generally improved the tracking of the optic radiations across the cohort by better representing the tracts at the rear of the optic radiation.

4. DTI tractography has been used to investigate how mild optic nerve hypoplasia (ONH) affects, or is affected by, reduced myelination and defects in the optic radiations. A cohort of 23 ONH patients was compared with matched-age controls. ONH patients aged over 5 years had lower mean FA for the left optic radiation than the matched controls, but no statistically-significant differences in mean FA were found for ONH patients aged up to 5 years. There were no statistically-significant differences for the right optic radiation. A statistical voxel-based analysis of white matter differences across the whole brain was performed on the ONH and control cohorts using the FSL TBSS software. This corroborated the tractography results and showed that ONH is not purely related to an abnormal optic nerve, but that these patients have other abnormal anatomical structures. This suggests that ONH should be regarded as being more complex than a visual system syndrome.

5. Little is known about how seizures affect the white matter pathways of the brain that are not involved in the epileptic focus. The impact of seizures on the optic radiations in the paediatric population has been examined using DTI tractography for a cohort of 21 children who had suffered a single episode of prolonged febrile convulsions and a separate cohort of 20 children using anti-epileptic medicines. The prolonged febrile convulsions cohort did not present lower mean FA in either optic radiation than the matched controls, suggesting that a single seizure episode might not cause widespread damage to the optic radiations. In contrast, the anti-epileptic user cohort presented a decreased mean FA at the front of both optic

radiations compared with the control cohort, despite the patients having neither visual epileptic activity nor visual impairment. The 60-direction DTI tractography protocol adopted by this study was identified as the most suitable for improving paediatric preoperative planning.

6. The value of DTI tractography for preoperative planning has been investigated for brain tumour and tuberous sclerosis patients. Although the preoperative MRI suggested that the tumour was invading the motor pathway, tractography analysis indicated that the inferior fronto-occipital fascicle had in fact been displaced by the tumour. The tractography was used preoperatively to plan the surgery and intraoperatively to perform the procedure. The tumour mass was entirely removed during the procedure and the patient did not have any motor deficits afterwards. For the tuberous sclerosis patient, there was concern that tuberous lesions located within the temporal lobe might be compressing the optic radiations and causing blurred vision. Tractography analysis showed that the optic radiations were not being compressed or disrupted, so it was agreed that there was not a strong case for a major surgical intervention. This is the first time, to our knowledge, that tractography has been used to counsel patients in surgical and anatomical matters.

7. Hydrocephalus can severely distort the brain anatomy and can compress the optic radiations. It is important for a clinician to know the location of the primary visual cortex and the associated optic radiations, because there are few approaches for VP shunt insertion and finding an optimum location for the draining catheter in the lateral ventricles has been related to a lower rate of complications. The standard tractography analysis route often cannot be used because the primary seed ROI, the LGN, cannot be identified. As an alternative, the new VEP-enhanced tractography route developed in this study was tested for two hydrocephalus patients, with the VEP recordings used to identify an alternative seed ROI. This was successful in both cases, contributing to surgical planning and aiding the treatment and posterior follow-up. The next step is to develop a robust clinical route to enable this technique to be applied more widely.

REFERENCES

Agarwal, M. & Fox, S.M., 2013. Pediatric Seizures. *Emergency Medicine Clinics of North America,* 31**,** 733-754.

Alberstone, C.D., 2009. *Anatomic basis of neurologic diagnosis* New York, NY, USA: Thieme.

Alexander, A.L., Lee, J.E., Lazar, M. & Field, A.S., 2007. Diffusion tensor imaging of the brain. *Neurotherapeutics,* 4**,** 316-29.

Altemeier, W.A. & Altemeier, L.E., 2009. How can early, intensive training help a genetic disorder? *Pediatr Ann,* 38**,** 167-70, 172.

Anderson, V., Spencer-Smith, M. & Wood, A., 2011. Do children really recover better? Neurobehavioural plasticity after early brain insult. *Brain,* 134**,** 2197-221.

Andersson, J.L.R., Jenkinson, M. & Smith, S., 2007. *Non-linear optimisation.* Available at: www.fmrib.ox.ac.uk/analysis/techrep.

Andrews, T.J., Halpern, S.D. & Purves, D., 1997. Correlated size variations in human visual cortex, lateral geniculate nucleus, and optic tract. *J Neurosci,* 17**,** 2859-68.

Atkinson, J., Braddick, O., Anker, S., Nardini, M., Birtles, D., Rutherford, M.A., Mercuri, E., Dyet, L.E., Edwards, A.D. & Cowan, F.M., 2008. Cortical vision, MRI

and developmental outcome in preterm infants. *Arch Dis Child Fetal Neonatal Ed,* 93**,** F292-7.

Baldwin, R.T. & Preston-Martin, S., 2004. Epidemiology of brain tumors in childhood—a review. *Toxicology and Applied Pharmacology,* 199**,** 118-131.

Barett, G., Blumhardt, L., Halliday, A.M., Halliday, E. & Kriss, A., 1976. A paradox in the lateralisation of the visual evoked response. *Nature,* 261**,** 253-5.

Barnea-Goraly, N., Menon, V., Eckert, M., Tamm, L., Bammer, R., Karchemskiy, A., Dant, C.C. & Reiss, A.L., 2005. White matter development during childhood and adolescence: A cross-sectional diffusion tensor imaging study. *Cerebral Cortex,* 15**,** 1848-1854.

Barton, J.J.S., Hefter, R., Chang, B., Schomer, D. & Drislane, F., 2005. The field defects of anterior temporal lobectomy: a quantitative reassessment of Meyer's loop. *Brain,* 128**,** 2123-2133.

Basser, P.J., 1995. Inferring microstructural features and the physiological state of tissues from diffusion-weighted images. *NMR Biomed,* 8**,** 333-44.

Basser, P.J., Pajevic, S., Pierpaoli, C., Duda, J. & Aldroubi, A., 2000. In vivo fiber tractography using DT-MRI data. *Magn Reson Med,* 44**,** 625-32.

Bassi, L., Ricci, D., Volzone, A., Allsop, J.M., Srinivasan, L., Pai, A., Ribes, C., Ramenghi, L.A., Mercuri, E., Mosca, F., Edwards, A.D., Cowan, F.M., Rutherford, M.A. & Counsell, S.J., 2008. Probabilistic diffusion tractography of the optic radiations and visual function in preterm infants at term equivalent age. *Brain,* 131**,** 573-82.

Beaulieu, C., 2002. The basis of anisotropic water diffusion in the nervous system – a technical review. *NMR in Biomedicine,* 15**,** 435-455.

Beaulieu, C. & Allen, P.S., 1994. Water diffusion in the giant axon of the squid: implications for diffusion-weighted MRI of the nervous system. *Magn Reson Med,* 32**,** 579-83.

Beltz, A.M., Blakemore, J.E.O. & Berenbaum, S.A., 2013. Chapter 26 - Sex Differences in Brain and Behavioral Development. *In* J.L.R. Rubenstein & P. Rakic (eds.) *Neural Circuit Development and Function in the Brain.* Oxford: Academic Press, 467-499.

Benjamin, C.F.A., Singh, J.M., Prabhu, S.P. & Warfield, S.K., 2014. Optimization of tractography of the optic radiations. *Human Brain Mapping,* 35**,** 683-697.

Berardi, N., Pizzorusso, T. & Maffei, L., 2000. Critical periods during sensory development. *Current Opinion in Neurobiology,* 10**,** 138-145.

Berg, A.T. & Shinnar, S., 1996. Complex febrile seizures. *Epilepsia,* 37**,** 126-33.

Bernal, J. & Nunez, J., 1995. Thyroid hormones and brain development. *Eur J Endocrinol,* 133**,** 390-8.

Besseling, R.M., Jansen, J.F., Overvliet, G.M., Vaessen, M.J., Braakman, H.M., Hofman, P.A., Aldenkamp, A.P. & Backes, W.H., 2012. Tract specific reproducibility of tractography based morphology and diffusion metrics. *PLoS One,* 7**,** e34125.

Bird, C.R., Hedberg, M., Drayer, B.P., Keller, P.J., Flom, R.A. & Hodak, J.A., 1989. MR assessment of myelination in infants and children: usefulness of marker sites. *AJNR Am J Neuroradiol,* 10**,** 731-40.

Blume, W.T., Buza, R.C. & Okazaki, H., 1974. Anatomic correlates of the ten-twenty electrode placement system in infants. *Electroencephalogr Clin Neurophysiol,* 36**,** 303-7.

Blumenhardt, L.D. & Halliday, A.M., 1979. Hemisphere contributions to the composition of the pattern-evoked potential waveform. *Exp Brain Res,* 36**,** 53-69.

Boon, M.Y., Suttle, C.M. & Dain, S.J., 2007. Transient VEP and psychophysical chromatic contrast thresholds in children and adults. *Vision Research,* 47**,** 2124-2133.

Boothe, R.G., Dobson, V. & Teller, D.Y., 1985. Postnatal development of vision in human and nonhuman primates. *Annu Rev Neurosci,* 8**,** 495-545.

Borchert, M. & Garcia-Filion, P., 2008. The syndrome of optic nerve hypoplasia. *Curr Neurol Neurosci Rep,* 8**,** 395-403.

Braun, C., Kaiser, S., Kincses, W.-E. & Elbert, T., 1997. Confidence Interval of Single Dipole Locations Based on EEG Data. *Brain Topography,* 10**,** 31-39.

Brecelj, J., 1992. A VEP study of the visual pathway function in compressive lesions of the optic chiasm. Full-field versus half-field stimulation. *Electroencephalography and Clinical Neurophysiology/Evoked Potentials Section,* 84**,** 209-218.

Brecelj, J., Stirn-Kranjc, B., Pečarič-Meglič, N., Škrbec, M. & Sustar, M., 2008. P188 Detecting normal and abnormal crossing of the optic nerve fibres: VEP asymmetries versus chiasm. *Clinical Neurophysiology,* 119, Supplement 1**,** S118-S119.

Brecelj, J., Štrucl, M. & Hawlina, M., 1990. Central fiber contribution to W-shaped visual evoked potentials in patients with optic neuritis. *Documenta Ophthalmologica,* 75**,** 155-163.

Bridge, H., Hicks, S.L., Xie, J., Okell, T.W., Mannan, S., Alexander, I., Cowey, A. & Kennard, C., 2010. Visual activation of extra-striate cortex in the absence of V1 activation. *Neuropsychologia,* 48**,** 4148-54.

Bridge, H., Jindahra, P., Barbur, J. & Plant, G.T., 2011. Imaging reveals optic tract degeneration in hemianopia. *Invest Ophthalmol Vis Sci,* 52**,** 382-8.

Brody, B.A., Kinney, H.C., Kloman, A.S. & Gilles, F.H., 1987. Sequence of central nervous system myelination in human infancy. I. An autopsy study of myelination. *J Neuropathol Exp Neurol,* 46**,** 283-301.

Catani, M., Howard, R.J., Pajevic, S. & Jones, D.K., 2002. Virtual in Vivo Interactive Dissection of White Matter Fasciculi in the Human Brain. *NeuroImage,* 17**,** 77-94.

Chen, C.-C., Huang, F., Shao, H.-X., Jin, J.-H., Li, Z.-P. & Zhang, C.-S., 2009. Sectional Anatomy of the Optic Pathways on the Coronal Plane. *Journal of the Chinese Medical Association,* 72**,** 515-520.

Choi, C., Rubino, P.A., Fernandez-Miranda, J.C., Abe, H. & Rhoton, A.L., Jr., 2006. Meyer's loop and the optic radiations in the transsylvian approach to the mediobasal temporal lobe. *Neurosurgery,* 59**,** 228-236.

Ciccarelli, O., Behrens, T.E., Altmann, D.R., Orrell, R.W., Howard, R.S., Johansen-Berg, H., Miller, D.H., Matthews, P.M. & Thompson, A.J., 2006. *Probabilistic diffusion tractography: a potential tool to assess the rate of disease progression in amyotrophic lateral sclerosis*.

Ciccarelli, O., Parker, G.J., Toosy, A.T., Wheeler-Kingshott, C.A., Barker, G.J., Boulby, P.A., Miller, D.H. & Thompson, A.J., 2003. From diffusion tractography to quantitative white matter tract measures: a reproducibility study. *Neuroimage,* 18**,** 348-59.

Cicmil, N. & Krug, K., 2015. Playing the electric light orchestra-how electrical stimulation of visual cortex elucidates the neural basis of perception. *Philos Trans R Soc Lond B Biol Sci,* 370.

Cidis, M.B., Warshowsky, J.H., Goldrich, S.G. & Meltzer, C.C., 1997. Mirror-image optic nerve dysplasia with associated anisometropia in identical twins. *J Am Optom Assoc,* 68**,** 325-9.

Clark, C.A., Barrick, T.R., Murphy, M.M. & Bell, B.A., 2003. White matter fiber tracking in patients with space-occupying lesions of the brain: a new technique for neurosurgical planning? *Neuroimage,* 20**,** 1601-8.

Clark, C.A., Hedehus, M. & Moseley, M.E., 2001. Diffusion time dependence of the apparent diffusion tensor in healthy human brain and white matter disease. *Magn Reson Med,* 45**,** 1126-9.

Clark, V.P., Fan, S. & Hillyard, S.A., 1994. Identification of early visual evoked potential generators by retinotopic and topographic analyses. *Human Brain Mapping,* 2**,** 170-187.

Clayden, J.D., King, M.D., Maniega, S.M., Bastin, M.E., Storkey, A.J. & Clark, C.A., 2011. TractoR: Magnetic resonance imaging and tractography with R. *Journal of Statistical Software,* 44**,** 1-18.

Conturo, T.E., Lori, N.F., Cull, T.S., Akbudak, E., Snyder, A.Z., Shimony, J.S., McKinstry, R.C., Burton, H. & Raichle, M.E., 1999. Tracking neuronal fiber pathways in the living human brain. *Proc Natl Acad Sci U S A,* 96**,** 10422-7.

Cook, P.A., Bai, Y., Nedjati-Gilani, S., Seunarine, K.K., Hall, M.G., Parker, G.J. & Alexander, D.C., 2006. Camino: Open-Source Diffusion-MRI Reconstruction and Processing *14th Scientific Meeting of the International Society for Magnetic Resonance in Medicine*, Seattle, WA, USA, 2759.

Corns, R. & Martin, A., 2012. Hydrocephalus. *Surgery (Oxford),* 30**,** 142-148.

Counsell, S.J., Maalouf, E.F., Fletcher, A.M., Duggan, P., Battin, M., Lewis, H.J., Herlihy, A.H., Edwards, A.D., Bydder, G.M. & Rutherford, M.A., 2002. MR Imaging Assessment of Myelination in the Very Preterm Brain. *American Journal of Neuroradiology,* 23**,** 872-881.

Courchesne, E., Carper, R. & Akshoomoff, N., 2003. Evidence of brain overgrowth in the first year of life in autism. *Jama,* 290**,** 337-44.

Creel, D.J., 2013. Visually Evoked Potentials. *In* H. Kolb, R. Nelson, E. Fernandez & B. Jones (eds.) *The Organization of the Retina and Visual System.* Salt Lake City, Utah: Webvision. Available at: http://webvision.med.utah.edu/book/electrophysiology/visually-evoked-potentials.

D'Ercole, C., Girard, N., Boubli, L., Potier, A., Chagnon, C., Raybaud, C. & Blanc, B., 1993. Prenatal diagnosis of fetal cerebral abnormalities by ultrasonography and magnetic resonance imaging. *European Journal of Obstetrics & Gynecology and Reproductive Biology,* 50**,** 177-184.

De Morsier, G., 1956. Studies on malformation of cranio-encephalic sutures. III. Agenesis of the septum lucidum with malformation of the optic tract (translated). *Schweiz Arch Neurol Psychiatr,* 77**,** 267-92.

de Onis, M. & Woynarowska, B., 2010. WHO child growth standards for children 0-5 years and the possibility of their implementation in Poland (translated). *Med Wieku Rozwoj,* 14**,** 87-94.

de Schotten, M.T., Dell'Acqua, F., Forkel, S.J., Simmons, A., Vergani, F., Murphy, D.G.M. & Catani, M., 2011a. A lateralized brain network for visuospatial attention. *Nat Neurosci,* advance online publication.

de Schotten, M.T., Ffytche, D.H., Bizzi, A., Dell'Acqua, F., Allin, M., Walshe, M., Murray, R., Williams, S.C., Murphy, D.G.M. & Catani, M., 2011b. Atlasing location, asymmetry and inter-subject variability of white matter tracts in the human brain with MR diffusion tractography. *NeuroImage,* 54**,** 49-59.

De Smet, F., Segura, I., De Bock, K., Hohensinner, P.J. & Carmeliet, P., 2009. Mechanisms of vessel branching: filopodia on endothelial tip cells lead the way. *Arterioscler Thromb Vasc Biol,* 29**,** 639-49.

DeFlorio, R.M. & Shah, C.C., 2014. Techniques That Decrease or Eliminate Ionizing Radiation for Evaluation of Ventricular Shunts in Children With Hydrocephalus. *Seminars in Ultrasound, CT and MRI,* 35**,** 365-373.

Devor, A., Dunn, A.K., Andermann, M.L., Ulbert, I., Boas, D.A. & Dale, A.M., 2003. Coupling of total hemoglobin concentration, oxygenation, and neural activity in rat somatosensory cortex. *Neuron,* 39**,** 353-9.

Devous, M.D., Sr., Stokely, E.M., Chehabi, H.H. & Bonte, F.J., 1986. Normal distribution of regional cerebral blood flow measured by dynamic single-photon emission tomography. *J Cereb Blood Flow Metab,* 6**,** 95-104.

Di Russo, F., Martínez, A. & Hillyard, S.A., 2003. Source Analysis of Event-related Cortical Activity during Visuo-spatial Attention. *Cerebral Cortex,* 13**,** 486-499.

Di Russo, F., Martinez, A., Sereno, M.I., Pitzalis, S. & Hillyard, S.A., 2002. Cortical sources of the early components of the visual evoked potential. *Hum Brain Mapp,* 15**,** 95-111.

Dougherty, R.F., Koch, V.M., Brewer, A.A., Fischer, B., Modersitzki, J. & Wandell, B.A., 2003. Visual field representations and locations of visual areas V1/2/3 in human visual cortex. *J Vis,* 3**,** 586-98.

Doyon, D., Marsot-Dupuch, K. & Francke, J.P., 2004. *The cranial nerves* Teterboro, NJ, USA: Icon Learning Systems.

Dubois, J., Dehaene-Lambertz, G., Soares, C., Cointepas, Y., Le Bihan, D. & Hertz-Pannier, L., 2008. Microstructural correlates of infant functional development: example of the visual pathways. *J Neurosci,* 28**,** 1943-8.

Dutton, G.N., 2004. Congenital disorders of the optic nerve: excavations and hypoplasia. *Eye (Lond),* 18**,** 1038-48.

Dyet, L.E., Kennea, N., Counsell, S.J., Maalouf, E.F., Ajayi-Obe, M., Duggan, P.J., Harrison, M., Allsop, J.M., Hajnal, J., Herlihy, A.H., Edwards, B., Laroche, S., Cowan, F.M., Rutherford, M.A. & Edwards, A.D., 2006. Natural history of brain lesions in extremely preterm infants studied with serial magnetic resonance imaging from birth and neurodevelopmental assessment. *Pediatrics,* 118**,** 536-48.

Ebeling, U. & Reulen, H.J., 1988. Neurosurgical topography of the optic radiation in the temporal lobe. *Acta Neurochirurgica,* 92**,** 29-36.

Edgar, J.M. & Griffiths, I.R., 2014. Chapter 7 - White Matter Structure: A Microscopist's View. *In* H. Johansen-Berg & T.E.J. Behrens (eds.) *Diffusion MRI (Second Edition).* San Diego: Academic Press, 127-153.

Einstein, A., 1905. Über die von der molekularkinetischen Theorie der Wärme geforderte Bewegung von in ruhenden Flüssigkeiten suspendierten Teilchen. *Annalen der Physik,* 17**,** 549-560.

Elflein, H.M., Fresenius, S., Lamparter, J., Pitz, S., Pfeiffer, N., Binder, H., Wild, P. & Mirshahi, A., 2015. The prevalence of amblyopia in Germany: data from the prospective, population-based Gutenberg Health Study. *Dtsch Arztebl Int,* 112**,** 338-44.

Engel, S.A., Glover, G.H. & Wandell, B.A., 1997. Retinotopic organization in human visual cortex and the spatial precision of functional MRI. *Cereb Cortex,* 7**,** 181-92.

European Chromosome 16 Tuberous Sclerosis Consortium, 1993. Identification and characterization of the tuberous sclerosis gene on chromosome 16. *Cell,* 75**,** 1305-1315.

Fazel, R., Krumholz, H.M., Wang, Y., Ross, J.S., Chen, J., Ting, H.H., Shah, N.D., Nasir, K., Einstein, A.J. & Nallamothu, B.K., 2009. Exposure to Low-Dose Ionizing Radiation from Medical Imaging Procedures. *New England Journal of Medicine,* 361**,** 849-857.

Felice Ghilardi, M., Sartucci, F., Brannan, J.R., Onofrj, M.C., Bodis-Wollner, I., Mylin, L. & Stroch, R., 1991. N70 and P100 can be independently affected in multiple sclerosis. *Electroencephalography and Clinical Neurophysiology/Evoked Potentials Section,* 80**,** 1-7.

Finger, S., 2010. Chapter 51: recovery of function: redundancy and vicariation theories. *Handb Clin Neurol,* 95**,** 833-41.

Fink, C., Garcia-Filion, P. & Borchert, M., 2013. Failure of stem cell therapy to improve visual acuity in children with optic nerve hypoplasia. *Journal of American Association for Pediatric Ophthalmology and Strabismus,* 17**,** 490-493.

Fink, C., Vedin, A.M., Garcia-Filion, P., Ma, N.S., Geffner, M.E. & Borchert, M., 2012. Newborn thyroid-stimulating hormone in children with optic nerve hypoplasia: Associations with hypothyroidism and vision. *Journal of American Association for Pediatric Ophthalmology and Strabismus,* 16**,** 418-423.

Fisher, R.S., Acevedo, C., Arzimanoglou, A., Bogacz, A., Cross, J.H., Elger, C.E., Engel, J., Forsgren, L., French, J.A., Glynn, M., Hesdorffer, D.C., Lee, B.I., Mathern, G.W., Moshé, S.L., Perucca, E., Scheffer, I.E., Tomson, T., Watanabe, M. & Wiebe, S., 2014. ILAE Official Report: A practical clinical definition of epilepsy. *Epilepsia,* 55**,** 475-482.

Fisher, R.S., van Emde Boas, W., Blume, W., Elger, C., Genton, P., Lee, P. & Engel, J., Jr., 2005. Epileptic seizures and epilepsy: definitions proposed by the International League Against Epilepsy (ILAE) and the International Bureau for Epilepsy (IBE). *Epilepsia,* 46**,** 470-2.

Frank, L.M., Shinnar, S., Hesdorffer, D.C., Shinnar, R.C., Pellock, J.M., Gallentine, W., Nordli Jr, D.R., Epstein, L.G., Moshé, S.L., Lewis, D.V. & Sun, S., 2012. Cerebrospinal Fluid Findings in Children with Fever-Associated Status Epilepticus: Results of the Consequences of Prolonged Febrile Seizures (FEBSTAT) Study. *The Journal of Pediatrics,* 161**,** 1169-1171.e1.

Fuchs, M., Kastner, J., Wagner, M., Hawes, S. & Ebersole, J.S., 2002. A standardized boundary element method volume conductor model. *Clin Neurophysiol,* 113**,** 702-12.

Fuchs, M., Wagner, M. & Kastner, J., 2004. Confidence limits of dipole source reconstruction results. *Clin Neurophysiol,* 115**,** 1442-51.

Fuchs, M., Wagner, M. & Kastner, J., 2007. Development of volume conductor and source models to localize epileptic foci. *J Clin Neurophysiol,* 24**,** 101-19.

Fukuda, S., Yokoi, K., Kitajima, K., Tsunoda, Y., Hayashi, N., Shimizu, S., Yoshida, T., Hamajima, N., Watanabe, I. & Goto, H., 2010. Influence of premature rupture of membrane on the cerebral blood flow in low-birth-weight infant after the delivery. *Brain and Development,* 32**,** 631-635.

Garcia-Filion, P. & Borchert, M., 2013. Prenatal determinants of optic nerve hypoplasia: review of suggested correlates and future focus. *Surv Ophthalmol,* 58**,** 610-9.

Ghazizadeh, V. & Naziroglu, M., 2014. Electromagnetic radiation (Wi-Fi) and epilepsy induce calcium entry and apoptosis through activation of TRPV1 channel in hippocampus and dorsal root ganglion of rats. *Metab Brain Dis*.

Gigout, S., Louvel, J., Rinaldi, D., Martin, B. & Pumain, R., 2013. Thalamocortical relationships and network synchronization in a new genetic model "in mirror" for absence epilepsy. *Brain Res,* 1525**,** 39-52.

Girouard, H., Bonev, A.D., Hannah, R.M., Meredith, A., Aldrich, R.W. & Nelson, M.T., 2010. Astrocytic endfoot Ca2+ and BK channels determine both arteriolar dilation and constriction. *Proc Natl Acad Sci U S A,* 107**,** 3811-6.

Gonzalez-Frankenberger, B., Harmony, T., Ricardo-Garcell, J., Porras-Kattz, E., Fernandez-Bouzas, A., Santiago, E. & Avecilla-Ramirez, G., 2008. Habituation of visual evoked potentials in healthy infants and in infants with periventricular leukomalacia. *Clin Neurophysiol,* 119**,** 2879-86.

Govindan, R.M., Chugani, H.T., Makki, M.I., Behen, M.E., Dornbush, J. & Sood, S., 2008. Diffusion Tensor Imaging of Brain Plasticity After Occipital Lobectomy. *Pediatric Neurology,* 38**,** 27-33.

Graham, S.L., Klistorner, A.I., Grigg, J.R. & Billson, F.A., 2000. Objective VEP perimetry in glaucoma: asymmetry analysis to identify early deficits. *J Glaucoma,* 9**,** 10-9.

Green, D.G., Powers, M.K. & Banks, M.S., 1980. Depth of focus, eye size and visual acuity. *Vision Res,* 20**,** 827-35.

Gregori, B., Pro, S., Bombelli, F., Riccia, M.L. & Accornero, N., 2006. Vep latency: Sex and head size. *Clinical Neurophysiology,* 117**,** 1154-1157.

Grønborg, S. & Uldall, P., 2014. Mortality and causes of death in children referred to a tertiary epilepsy center. *European Journal of Paediatric Neurology,* 18**,** 66-71.

Grossberg, S., 1999. How does the cerebral cortex work? Learning, attention, and grouping by the laminar circuits of visual cortex. *Spatial vision,* 12**,** 163-85.

Grossberg, S., 2001. Linking the laminar circuits of visual cortex to visual perception: Development, grouping, and attention. *Neuroscience & Biobehavioral Reviews,* 25**,** 513-526.

Grossberg, S., 2003. How does the cerebral cortex work? Development, learning, attention, and 3-D vision by laminar circuits of visual cortex. *Behavioral and cognitive neuroscience reviews,* 2**,** 47-76.

Gur, R.C., Mozley, P.D., Resnick, S.M., Gottlieb, G.L., Kohn, M., Zimmerman, R., Herman, G., Atlas, S., Grossman, R., Berretta, D. & et al., 1991. Gender differences in age effect on brain atrophy measured by magnetic resonance imaging. *Proc Natl Acad Sci U S A,* 88**,** 2845-9.

Gur, R.C., Packer, I.K., Hungerbuhler, J.P., Reivich, M., Obrist, W.D., Amarnek, W.S. & Sackeim, H.A., 1980. Differences in the distribution of gray and white matter in human cerebral hemispheres. *Science,* 207**,** 1226-8.

Guthkelch, A.N., Bursick, D. & Sclabassi, R.J., 1987. The relationship of the latency of the visual P100 wave to gender and head size. *Electroencephalogr Clin Neurophysiol,* 68**,** 219-22.

Guyton, A.C. & Hall, J.E., 2000. *Textbook of medical physiology,* 10th Edition ed. Philadelphia, Pa.; London: W. B. Saunders.

Guzzetta, F., Shackelford, G.D., Volpe, S., Perlman, J.M. & Volpe, J.J., 1986. Periventricular intraparenchymal echodensities in the premature newborn: critical determinant of neurologic outcome. *Pediatrics,* 78**,** 995-1006.

Haider, M., Spong, P. & Lindsley, D.B., 1964. Attention, vigilance, and cortical evoked-potentials in humans. *Science,* 145**,** 180-2.

Haynes, H., White, B.L. & Held, R., 1965. Visual accommodation in human infants. *Science,* 148**,** 528-30.

Hoffmann, M.B., Straube, S. & Bach, M., 2003. Pattern-onset stimulation boosts central multifocal VEP responses. *J Vis,* 3**,** 432-9.

Holmes, G. & Lister, W.T., 1916. Disturbances of vision from cerebral lesions, with special reference to the cortical representation of the macula. *Brain,* 39**,** 34-73.

Hood, D.C., Odel, J.G. & Winn, B.J., 2003. The Multifocal Visual Evoked Potential. *Journal of Neuro-Ophthalmology,* 23**,** 279-289.

Hossain, M.A., 2005. Molecular mediators of hypoxic–ischemic injury and implications for epilepsy in the developing brain. *Epilepsy & Behavior,* 7**,** 204-213.

Hubel, D.H., Wiesel, T.N. & LeVay, S., 1977. Plasticity of ocular dominance columns in monkey striate cortex. *Philos Trans R Soc Lond B Biol Sci,* 278**,** 377-409.

Huttenlocher, P.R. & de Courten, C., 1987. The development of synapses in striate cortex of man. *Hum Neurobiol,* 6**,** 1-9.

Huttenlocher, P.R., de Courten, C., Garey, L.J. & Van der Loos, H., 1982. Synaptogenesis in human visual cortex — evidence for synapse elimination during normal development. *Neuroscience Letters,* 33**,** 247-252.

Iliescu, C. & Craiu, D., 2013. Diagnostic approach of epilepsy in childhood and adolescence. *Maedica (Buchar),* 8**,** 195-9.

Iughetti, L., Casarosa, E., Predieri, B., Patianna, V. & Luisi, S., 2011. Plasma brain-derived neurotrophic factor concentrations in children and adolescents. *Neuropeptides,* 45**,** 205-11.

Ivanovic, D.M., Leiva, B.P., Perez, H.T., Olivares, M.G., Diaz, N.S., Urrutia, M.S., Almagia, A.F., Toro, T.D., Miller, P.T., Bosch, E.O. & Larrain, C.G., 2004. Head size and intelligence, learning, nutritional status and brain development. Head, IQ, learning, nutrition and brain. *Neuropsychologia,* 42**,** 1118-31.

Izci, Y., Seçkin, H., Ates, Ö. & Baskaya, M.K., 2009. Supracerebellar transtentorial transcollateral sulcus approach to the atrium of the lateral ventricle: microsurgical anatomy and surgical technique in cadaveric dissections. *Surgical neurology,* 72**,** 509-514.

Jaffe, M., Tal, Y., Hadad, B., Tirosh, E. & Tamir, A., 1992. Variability in head circumference growth rate during the first 2 years of life. *Pediatrics,* 90**,** 190-2.

Jeelani, N.U.O., Jindahra, P., Tamber, M., Poon, T., Kabasele, P., James Galton, M., Stevens, J., Duncan, J., McEvoy, A., Harkness, W. & Plant, G., 2010. 'Hemispherical asymmetry in the Meyer's Loop': a prospective study of visual-field deficits in 105 cases undergoing anterior temporal lobe resection for epilepsy. *Journal of neurology, neurosurgery and psychiatry,* 81**,** 985-991.

Johnston, M.V., Trescher, W.H., Ishida, A. & Nakajima, W., 2001. Neurobiology of hypoxic-ischemic injury in the developing brain. *Pediatr Res,* 49**,** 735-41.

Jonas, H., 1954. The Nobility of Sight. *Philosophy and Phenomenological Research,* 14**,** 507-519.

Jonas, J.B., Schmidt, A.M., Muller-Bergh, J.A., Schlotzer-Schrehardt, U.M. & Naumann, G.O., 1992. Human optic nerve fiber count and optic disc size. *Invest Ophthalmol Vis Sci,* 33**,** 2012-8.

Jones, A.C., Shyamsundar, M.M., Thomas, M.W., Maynard, J., Idziaszczyk, S., Tomkins, S., Sampson, J.R. & Cheadle, J.P., 1999. Comprehensive Mutation Analysis of TSC1 and TSC2—and Phenotypic Correlations in 150 Families with Tuberous Sclerosis. *The American Journal of Human Genetics*, 64**,** 1305-1315.

Jones, D.K., 2004. The effect of gradient sampling schemes on measures derived from diffusion tensor MRI: a Monte Carlo study. *Magn Reson Med,* 51**,** 807-15.

Khan, F., Shamim, M.S., Rehman, A. & Bari, M.E., 2013. Analysis of factors affecting ventriculoperitoneal shunt survival in pediatric patients. *Childs Nerv Syst,* 29**,** 791-802.

Kidd, D.P., Newman, N.J. & Biousse, V. (eds.) (2008) *Neuro-ophthalmology*, Philadelphia, USA: Elsevier.

Kier, E.L., Staib, L.H., Davis, L.M. & Bronen, R.A., 2004. MR imaging of the temporal stem: anatomic dissection tractography of the uncinate fasciculus, inferior occipitofrontal fasciculus, and Meyer's loop of the optic radiation. *AJNR Am J Neuroradiol,* 25**,** 677-91.

Kinney, H.C. & Back, S.A., 1998. Human oligodendroglial development: relationship to periventricular leukomalacia. *Semin Pediatr Neurol,* 5**,** 180-9.

Kinney, H.C., Brody, B.A., Kloman, A.S. & Gilles, F.H., 1988. Sequence of central nervous system myelination in human infancy. II. Patterns of myelination in autopsied infants. *J Neuropathol Exp Neurol,* 47**,** 217-34.

Klaver, P., Marcar, V. & Martin, E., 2011. Neurodevelopment of the visual system in typically developing children. *Prog Brain Res*, 189**,** 113-36.

Kleinnijenhuis, M., Zerbi, V., Kusters, B., Slump, C.H., Barth, M. & van Cappellen van Walsum, A.M., 2012. Layer-specific diffusion weighted imaging in human primary visual cortex in vitro. *Cortex*.

Kolbe, S., Chapman, C., Nguyen, T., Bajraszewski, C., Johnston, L., Kean, M., Mitchell, P., Paine, M., Butzkueven, H., Kilpatrick, T. & Egan, G., 2009. Optic nerve diffusion changes and atrophy jointly predict visual dysfunction after optic neuritis. *NeuroImage,* 45**,** 679-686.

Kotsopoulos, I.A., van Merode, T., Kessels, F.G., de Krom, M.C. & Knottnerus, J.A., 2002. Systematic review and meta-analysis of incidence studies of epilepsy and unprovoked seizures. *Epilepsia,* 43**,** 1402-9.

Kowiański, P., Lietzau, G., Steliga, A., Waśkow, M. & Moryś, J., 2013. The astrocytic contribution to neurovascular coupling – Still more questions than answers? *Neuroscience Research,* 75**,** 171-183.

Krueger, D.A. & Northrup, H., 2013. Tuberous Sclerosis Complex Surveillance and Management: Recommendations of the 2012 International Tuberous Sclerosis Complex Consensus Conference. *Pediatric Neurology,* 49**,** 255-265.

Kupfer, C., Chumbley, L. & Downer, J.C., 1967. Quantitative histology of optic nerve, optic tract and lateral geniculate nucleus of man. *Journal of Anatomy,* 101**,** 393-401.

Kurmanavichius, J., Karrer, G., Hebisch, G., Huch, R. & Huch, A., 1991. Fetal and preterm newborn cerebral blood flow velocity. *Early Hum Dev,* 26**,** 113-20.

Landman, B.A., Farrell, J.A., Jones, C.K., Smith, S.A., Prince, J.L. & Mori, S., 2007. Effects of diffusion weighting schemes on the reproducibility of DTI-derived fractional anisotropy, mean diffusivity, and principal eigenvector measurements at 1.5T. *Neuroimage,* 36**,** 1123-38.

Larrivee, B., Freitas, C., Suchting, S., Brunet, I. & Eichmann, A., 2009. Guidance of vascular development: lessons from the nervous system. *Circ Res,* 104**,** 428-41.

Larsen, J.S., 1971. The sagittal growth of the eye. IV. Ultrasonic measurement of the axial length of the eye from birth to puberty. *Acta Ophthalmol (Copenh),* 49**,** 873-86.

Lavidor, M. & Walsh, V., 2004. The nature of foveal representation. *Nat Rev Neurosci,* 5**,** 729-35.

Lawes, I.N., Barrick, T.R., Murugam, V., Spierings, N., Evans, D.R., Song, M. & Clark, C.A., 2008. Atlas-based segmentation of white matter tracts of the human brain using diffusion tensor tractography and comparison with classical dissection. *Neuroimage,* 39**,** 62-79.

Le Bihan, D., 2014. Diffusion MRI: what water tells us about the brain. *EMBO Molecular Medicine,* 6**,** 569-573.

Le Bihan, D. & Breton, E., 1985. Imagerie de diffusion in vivo par résonance magnétique nucléaire. *C R Acad Sci Paris,* T.301, Série II**,** 1109–1112.

Le Bihan, D. & Johansen-Berg, H., 2012. Diffusion MRI at 25: Exploring brain tissue structure and function. *NeuroImage,* 61**,** 324-341.

Lebel, C., Walker, L., Leemans, A., Phillips, L. & Beaulieu, C., 2008. Microstructural maturation of the human brain from childhood to adulthood. *Neuroimage,* 40**,** 1044-55.

Lenassi, E., Likar, K., Stirn-Kranjc, B. & Brecelj, J., 2008. VEP maturation and visual acuity in infants and preschool children. *Doc Ophthalmol,* 117**,** 111-20.

Leventhal, A.G., Ault, S.J. & Vitek, D.J., 1988. The nasotemporal division in primate retina: the neural bases of macular sparing and splitting. *Science,* 240**,** 66-7.

Levin, L.A., Nilsson, S.F.E., Ver Hoeve, J., Wu, S.M., Kaufman, P.L. & Alm, A., 2011. *Adler's Physiology of the Eye*: Elsevier.

Lewald, J. & Getzmann, S., 2013. Ventral and dorsal visual pathways support auditory motion processing in the blind: evidence from electrical neuroimaging. *Eur J Neurosci,* 38**,** 3201-9.

Lewis, T.L. & Maurer, D., 2009. Effects of early pattern deprivation on visual development. *Optom Vis Sci,* 86**,** 640-6.

Liasis, A., Hildebrand, D., Clark, C., Katz, X., Gunny, R., Stieltjes, B. & Taylor, D., 2009. Sensory function in severe semilobar holoprosencephaly. *Neurocase,* 15**,** 110-8.

Lin, Y., Daducci, A., Meskaldji, D.E., Thiran, J., Michel, P., Meuli, R., Krueger, G., Menegaz, G. & Granziera, C., 2014. Quantitative Analysis of Myelin and Axonal Remodeling in the Uninjured Motor Network After Stroke. *Brain Connect*.

Lindley, A.A., Benson, J.E., Grimes, C., Cole, T.M., 3rd & Herman, A.A., 1999. The relationship in neonates between clinically measured head circumference and brain volume estimated from head CT-scans. *Early Hum Dev,* 56**,** 17-29.

Liou, A.K.F., Clark, R.S., Henshall, D.C., Yin, X.-M. & Chen, J., 2003. To die or not to die for neurons in ischemia, traumatic brain injury and epilepsy: a review on the stress-activated signaling pathways and apoptotic pathways. *Progress in Neurobiology,* 69**,** 103-142.

Liu, M., Concha, L., Lebel, C., Beaulieu, C. & Gross, D.W., 2012. Mesial temporal sclerosis is linked with more widespread white matter changes in temporal lobe epilepsy. *NeuroImage: Clinical,* 1**,** 99-105.

Lopez, P.H., Ahmad, A.S., Mehta, N.R., Toner, M., Rowland, E.A., Zhang, J., Dore, S. & Schnaar, R.L., 2011. Myelin-associated glycoprotein protects neurons from excitotoxicity. *J Neurochem,* 116**,** 900-8.

Ma, S., Kwon, H.J. & Huang, Z., 2012. A functional requirement for astroglia in promoting blood vessel development in the early postnatal brain. *PLoS One,* 7**,** e48001.

Magoon, E.H. & Robb, R.M., 1981. Development of myelin in human optic nerve and tract. A light and electron microscopic study. *Arch Ophthalmol,* 99**,** 655-9.

Major, P. & Thiele, E.A., 2007. Seizures in children: determining the variation. *Pediatr Rev,* 28**,** 363-71.

Mangun, G.R., Hopfinger, J.B., Kussmaul, C.L., Fletcher, E.M. & Heinze, H.J., 1997. Covariations in ERP and PET measures of spatial selective attention in human extrastriate visual cortex. *Hum Brain Mapp,* 5**,** 273-9.

Marin-Padilla, M., 1996. Developmental neuropathology and impact of perinatal brain damage. I: Hemorrhagic lesions of neocortex. *J Neuropathol Exp Neurol,* 55**,** 758-73.

Marin-Padilla, M. & Knopman, D.S., 2011. Developmental aspects of the intracerebral microvasculature and perivascular spaces: insights into brain response to late-life diseases. *J Neuropathol Exp Neurol,* 70**,** 1060-9.

Martínez, A.g., DiRusso, F., Anllo-Vento, L., Sereno, M.I., Buxton, R.B. & Hillyard, S.A., 2001. Putting spatial attention on the map: timing and localization of stimulus selection processes in striate and extrastriate visual areas. *Vision Research,* 41**,** 1437-1457.

May, L., 2014. Head circumference: measuring a child. *GOSH Clinical Guidelines.* London, UK: Great Ormond Street Hospital. Available at: http://www.gosh.nhs.uk/health-professionals/clinical-guidelines/head-circumference-measuring-a-child.

McCabe, M.J., Alatzoglou, K.S. & Dattani, M.T., 2011. Septo-optic dysplasia and other midline defects: The role of transcription factors: HESX1 and beyond. *Best Practice & Research Clinical Endocrinology & Metabolism,* 25**,** 115-124.

McCabe, M.J., Gaston-Massuet, C., Gregory, L.C., Alatzoglou, K.S., Tziaferi, V., Sbai, O., Rondard, P., Masumoto, K.H., Nagano, M., Shigeyoshi, Y., Pfeifer, M., Hulse, T., Buchanan, C.R., Pitteloud, N., Martinez-Barbera, J.P. & Dattani, M.T., 2013. Variations in PROKR2, but not PROK2, are associated with hypopituitarism and septo-optic dysplasia. *J Clin Endocrinol Metab,* 98**,** E547-57.

McCaslin, A.F., Chen, B.R., Radosevich, A.J., Cauli, B. & Hillman, E.M., 2011. In vivo 3D morphology of astrocyte-vasculature interactions in the somatosensory cortex: implications for neurovascular coupling. *J Cereb Blood Flow Metab,* 31**,** 795-806.

Melhem, E.R., Mori, S., Mukundan, G., Kraut, M.A., Pomper, M.G. & van Zijl, P.C., 2002. Diffusion tensor MR imaging of the brain and white matter tractography. *AJR Am J Roentgenol,* 178**,** 3-16.

Meyer, A., 1907. The connections of the occipital lobes and the present status of the cerebral visual affections. *Trans Assoc Am Physicians,* 22**,** 7-16.

Miglior, S., Brigatti, L., Velati, P., Balestreri, C., Rossetti, L., Bujtar, E. & Orzalesi, N., 1994. Relationship between morphometric optic disc parameters, sex and axial length. *Curr Eye Res,* 13**,** 119-24.

Miller, N.R., Walsh, F.B. & Hoyt, W.F., 2005. *Walsh and Hoyt's clinical neuro-ophthalmology* Philadelphia, PA, USA: Lippincott Williams & Wilkins.

Moody, D.M., Bell, M.A. & Challa, V.R., 1990. Features of the cerebral vascular pattern that predict vulnerability to perfusion or oxygenation deficiency: an anatomic study. *American Journal of Neuroradiology,* 11**,** 431-9.

Moore, K.L., Agur, A.M.R. & Dalley, A.F., 2011. *Essential clinical anatomy* Baltimore, MD, USA: Lippincott Williams & Wilkins.

Mori, K., Shimada, J., Kurisaka, M., Sato, K. & Watanabe, K., 1995. Classification of hydrocephalus and outcome of treatment. *Brain and Development,* 17**,** 338-348.

Morishima, A. & Aranoff, G.S., 1986. Syndrome of septo-optic-pituitary dysplasia: The clinical spectrum. *Brain and Development,* 8**,** 233-239.

Mosher, J.C., Lewis, P.S. & Leahy, R.M., 1992. Multiple dipole modeling and localization from spatio-temporal MEG data. *IEEE Trans Biomed Eng,* 39**,** 541-57.

Mukherjee, P., Chung, S.W., Berman, J.I., Hess, C.P. & Henry, R.G., 2008. Diffusion tensor MR imaging and fiber tractography: technical considerations. *AJNR Am J Neuroradiol,* 29**,** 843-52.

Mullaart, R.A., Daniels, O., Hopman, J.C., de Haan, A.F., Stoelinga, G.B. & Rotteveel, J.J., 1995. Asymmetry of the cerebral blood flow: an ultrasound Doppler study in preterm newborns. *Pediatr Neurol,* 13**,** 319-22.

Mullen, K.T., Thompson, B. & Hess, R.F., 2010. Responses of the human visual cortex and LGN to achromatic and chromatic temporal modulations: an fMRI study. *J Vis,* 10**,** 13.

National Eye Institute, 2015. Encyclopedia of children's health.

Neil, J.J., Shiran, S.I., McKinstry, R.C., Schefft, G.L., Snyder, A.Z., Almli, C.R., Akbudak, E., Aronovitz, J.A., Miller, J.P., Lee, B.C. & Conturo, T.E., 1998. Normal brain in human newborns: apparent diffusion coefficient and diffusion anisotropy measured by using diffusion tensor MR imaging. *Radiology,* 209**,** 57-66.

Neubauer, F.B., Sederberg, A. & MacLean, J.N., 2014. Local changes in neocortical circuit dynamics coincide with the spread of seizures to thalamus in a model of epilepsy. *Front Neural Circuits,* 8**,** 101.

Newman, N.M., 1992. *Neuro-ophthalmology: a practical text* Norwalk, Conn., USA: Appleton & Lange.

Ngugi, A.K., Bottomley, C., Kleinschmidt, I., Sander, J.W. & Newton, C.R., 2010. Estimation of the burden of active and life-time epilepsy: A meta-analytic approach. *Epilepsia,* 51**,** 883-890.

Ngugi, A.K., Kariuki, S.M., Bottomley, C., Kleinschmidt, I., Sander, J.W. & Newton, C.R., 2011. Incidence of epilepsy: a systematic review and meta-analysis. *Neurology,* 77**,** 1005-12.

NHS, 2013. *Hydrocephalus* [online]. National Health Service. Available from: http://www.nhs.uk/conditions/Hydrocephalus/Pages/Introduction.aspx [Accessed 5 Jun 2015].

NHS, 2014. *Febrile seizures* [online]. National Health Service. Available from: http://www.nhs.uk/Conditions/Febrile-convulsions/Pages/Introduction.aspx [Accessed 8 Sep 2014].

NIH Blueprint, 2015. *The Human Connectome Project* [online]. http://www.humanconnectome.org [Accessed 19 Jul 2015].

Nijboer, C.H., Heijnen, C.J., Degos, V., Willemen, H.L., Gressens, P. & Kavelaars, A., 2013. Astrocyte GRK2 as a novel regulator of glutamate transport and brain damage. *Neurobiol Dis,* 54**,** 206-15.

Nijboer, C.H., Kavelaars, A., Vroon, A., Groenendaal, F., van Bel, F. & Heijnen, C.J., 2008. Low endogenous G-protein-coupled receptor kinase 2 sensitizes the immature

brain to hypoxia-ischemia-induced gray and white matter damage. *J Neurosci,* 28**,** 3324-32.

Nilsson, D., Starck, G., Ljungberg, M., Ribbelin, S., Jonsson, L., Malmgren, K. & Rydenhag, B., 2007. Intersubject variability in the anterior extent of the optic radiation assessed by tractography. *Epilepsy Res,* 77**,** 11-6.

Nilsson, M., van Westen, D., Stahlberg, F., Sundgren, P.C. & Latt, J., 2013. The role of tissue microstructure and water exchange in biophysical modelling of diffusion in white matter. *MAGMA,* 26**,** 345-70.

Nishi, T., Yukawa, E., Taoka, T. & Ogata, N., 2013. Unilateral Optic Nerve Hypoplasia with Contralateral Optic Pathway Hypoplasia: A Case Report. *Neuro-Ophthalmology,* 37**,** 116-119.

Northrup, H. & Krueger, D.A., 2013. Tuberous sclerosis complex diagnostic criteria update: recommendations of the 2012 Iinternational Tuberous Sclerosis Complex Consensus Conference. *Pediatr Neurol,* 49**,** 243-54.

Nuwer, M.R., Comi, G., Emerson, R., Fuglsang-Frederiksen, A., Guérit, J.-M., Hinrichs, H., Ikeda, A., Jose C. Luccas, F. & Rappelsburger, P., 1998. IFCN standards for digital recording of clinical EEG. *Electroencephalography and Clinical Neurophysiology,* 106**,** 259-261.

O'Callaghan, F.J., Shiell, A.W., Osborne, J.P. & Martyn, C.N., 1998. Prevalence of tuberous sclerosis estimated by capture-recapture analysis. *Lancet,* 351**,** 1490.

O'Neill, B.R., Pruthi, S., Bains, H., Robison, R., Weir, K., Ojemann, J., Ellenbogen, R., Avellino, A. & Browd, S.R., 2013. Rapid Sequence Magnetic Resonance Imaging in the Assessment of Children with Hydrocephalus. *World Neurosurgery,* 80**,** 307-312.

Odom, J.V., Bach, M., Brigell, M., Holder, G., McCulloch, D., Tormene, A. & Vaegan, 2010. ISCEV standard for clinical visual evoked potentials (2009 update). *Documenta Ophthalmologica,* 120**,** 111-119.

Orešković, D. & Klarica, M., 2011. Development of hydrocephalus and classical hypothesis of cerebrospinal fluid hydrodynamics: Facts and illusions. *Progress in Neurobiology,* 94**,** 238-258.

Pantoni, L. & Garcia, J.H., 1997. Pathogenesis of Leukoaraiosis: A Review. *Stroke,* 28**,** 652-659.

Parfenova, H., Leffler, C.W., Tcheranova, D., Basuroy, S. & Zimmermann, A., 2010. Epileptic seizures increase circulating endothelial cells in peripheral blood as early indicators of cerebral vascular damage. *American Journal of Physiology - Heart and Circulatory Physiology,* 298**,** H1687-H1698.

Parker, G.J., Haroon, H.A. & Wheeler-Kingshott, C.A., 2003. A framework for a streamline-based probabilistic index of connectivity (PICo) using a structural interpretation of MRI diffusion measurements. *J Magn Reson Imaging,* 18**,** 242-54.

Patel, L., McNally, R.J., Harrison, E., Lloyd, I.C. & Clayton, P.E., 2006. Geographical distribution of optic nerve hypoplasia and septo-optic dysplasia in Northwest England. *J Pediatr,* 148**,** 85-8.

Peltier, J., Travers, N., Destrieux, C. & Velut, S., 2006. Optic radiations: a microsurgical anatomical study. *Journal of Neurosurgery,* 105**,** 294-300.

Pfeifer, R.A., 1920. *Myelogenetisch-anatomische Untersuchungen über das kortikale: Ende der Hörleitung* Leipzig: B.G. Teubner.

Pierpaoli, C. & Basser, P.J., 1996. Toward a quantitative assessment of diffusion anisotropy. *Magn Reson Med,* 36**,** 893-906.

Pierpaoli, C., Jezzard, P., Basser, P.J., Barnett, A. & Di Chiro, G., 1996. Diffusion tensor MR imaging of the human brain. *Radiology,* 201**,** 637-648.

Poliak, S.L., 1957. *The vertebrate visual system* Chicago, USA: Chicago University Press.

Powell, H.W., Parker, G.J., Alexander, D.C., Symms, M.R., Boulby, P.A., Wheeler-Kingshott, C.A., Barker, G.J., Koepp, M.J. & Duncan, J.S., 2005. MR tractography predicts visual field defects following temporal lobe resection. *Neurology,* 65**,** 596-9.

Probst, M., 1906. Uber die zentralen Sinnerbahnen und die Sinnerzentren des menschlichen Gehirnes. *Sitzungs math natl Klakad Wissench Wien,* 115**,** 103.

Pujari, V., Jimbo, H., Dange, N., Shah, A., Singh, S. & Goel, A., 2008. Fiber dissection of the visual pathways: Analysis of the relationship of optic radiations to lateral ventricle: A cadaveric study. 56**,** 133-137.

Purves, D., Augustine, G.J., Fitzpatrick, D., Katz, L.C., LaMantia, A.-S., McNamara, J.O. & Williams, S.M., 2001. *Neuroscience,* Second ed.

Ramon y Cajal, S., 1898. Estructura del quiasma óptico y teoría general de los entrecruzamientos de las vías nerviosas. *Rev. Trim. Micrográfica,* 3**,** 15-65.

Rasmussen, A.T., 1943. The extent of recurrent geniculo-calcarine fibers (loop of Archambault and Meyer) as demonstrated by gross brain dissection. *The Anatomical Record,* 85**,** 277-284.

Ricciardi, E., Tozzi, L., Leo, A. & Pietrini, P., 2014. Modality dependent cross-modal functional reorganization following congenital visual deprivation within occipital areas: a meta-analysis of tactile and auditory studies. *Multisens Res,* 27**,** 247-62.

Riddle, A., Luo, N.L., Manese, M., Beardsley, D.J., Green, L., Rorvik, D.A., Kelly, K.A., Barlow, C.H., Kelly, J.J., Hohimer, A.R. & Back, S.A., 2006. Spatial heterogeneity in oligodendrocyte lineage maturation and not cerebral blood flow predicts fetal ovine periventricular white matter injury. *J Neurosci,* 26**,** 3045-55.

Riordan-Eva, P. & Cunningham Jr, E.T., 2011. *Vaughan & Asbury's General Ophthalmology*: McGraw-Hill Medical.

Roebroeck, A., Galuske, R., Formisano, E., Chiry, O., Bratzke, H., Ronen, I., Kim, D.-s. & Goebel, R., 2008. High-resolution diffusion tensor imaging and tractography of the human optic chiasm at 9.4 T. *NeuroImage,* 39**,** 157-168.

Rosychuk, R.J., Witol, A., Wilson, B. & Stobart, K., 2012. Central nervous system (CNS) tumor trends in children in a western Canadian province: a population-based 22-year retrospective study. *J Neurol,* 259**,** 1131-6.

Rowbotham, G.F. & Little, E., 1965. Circulations of the cerebral hemispheres. *Br J Surg,* 52**,** 8-21.

Rubino, P.A., Rhoton, A.L., Jr., Tong, X. & Oliveira, E., 2005. Three-dimensional relationships of the optic radiation. *Neurosurgery,* 57**,** 219-27; discussion 219-27.

Salmela, M.B., Cauley, K.A., Nickerson, J.P., Koski, C.J. & Filippi, C.G., 2010. Magnetic resonance diffusion tensor imaging (MRDTI) and tractography in children with septo-optic dysplasia. *Pediatric Radiology,* 40**,** 708-713.

Sander, J.W., 2003. The epidemiology of epilepsy revisited. *Curr Opin Neurol,* 16**,** 165-70.

Sanes, D.H., Reh, T.A. & Harris, W.A., 2012. *Development of the nervous system* Amsterdam, The Netherlands: Elsevier/Academic Press.

Satterthwaite, T.D., Shinohara, R.T., Wolf, D.H., Hopson, R.D., Elliott, M.A., Vandekar, S.N., Ruparel, K., Calkins, M.E., Roalf, D.R., Gennatas, E.D., Jackson, C., Erus, G., Prabhakaran, K., Davatzikos, C., Detre, J.A., Hakonarson, H., Gur, R.C. & Gur, R.E., 2014. Impact of puberty on the evolution of cerebral perfusion during adolescence. *Proc Natl Acad Sci U S A,* 111**,** 8643-8.

Scanlon, C., Mueller, S.G., Cheong, I., Hartig, M., Weiner, M.W. & Laxer, K.D., 2013. Grey and white matter abnormalities in temporal lobe epilepsy with and without mesial temporal sclerosis. *J Neurol,* 260**,** 2320-9.

Scherjon, S.A., Oosting, H., Kok, J.H. & Zondervan, H.A., 1994. Effect of fetal brainsparing on the early neonatal cerebral circulation. *Arch Dis Child Fetal Neonatal Ed,* 71**,** F11-5.

Schoth, F. & Krings, T., 2004. Diffusion- tensor imaging in septo-optic dysplasia. *Neuroradiology,* 46**,** 759-763.

Segura, I., De Smet, F., Hohensinner, P.J., Ruiz de Almodovar, C. & Carmeliet, P., 2009. The neurovascular link in health and disease: an update. *Trends Mol Med,* 15**,** 439-51.

Sereno, M.I., Dale, A.M., Reppas, J.B., Kwong, K.K., Belliveau, J.W., Brady, T.J., Rosen, B.R. & Tootell, R.B., 1995. Borders of multiple visual areas in humans revealed by functional magnetic resonance imaging. *Science,* 268**,** 889-93.

Shanker, G., Amur, S.G. & Pieringer, R.A., 1985. Investigations on myelinogenesis in vitro: a study of the critical period at which thyroid hormone exerts its maximum regulatory effect on the developmental expression of two myelin associated markers in cultured brain cells from embryonic mice. *Neurochem Res,* 10**,** 617-25.

Sherman, S.M. & Guillery, R.W., 2002. The role of the thalamus in the flow of information to the cortex. *Philosophical Transactions of the Royal Society B: Biological Sciences,* 357**,** 1695-1708.

Shinnar, S., Bello, J.A., Chan, S., Hesdorffer, D.C., Lewis, D.V., MacFall, J., Pellock, J.M., Nordli, D.R., Frank, L.M., Moshe, S.L., Gomes, W., Shinnar, R.C. & Sun, S., 2012. MRI abnormalities following febrile status epilepticus in children: The FEBSTAT study. *Neurology,* 79**,** 871-877.

Shinnar, S., Hesdorffer, D.C., Nordli, D.R., Jr., Pellock, J.M., O'Dell, C., Lewis, D.V., Frank, L.M., Moshe, S.L., Epstein, L.G., Marmarou, A. & Bagiella, E., 2008. Phenomenology of prolonged febrile seizures: results of the FEBSTAT study. *Neurology,* 71**,** 170-6.

Sie, L.T.L., Rombouts, S.A., Valk, I.J., Hart, A.A., Scheltens, P. & van der Knaap, M.S., 2001. Functional MRI of visual cortex in sedated 18 month-old infants with or without periventricular leukomalacia. *Dev Med Child Neurol,* 43**,** 486-90.

Simmonds, D.J., Hallquist, M.N., Asato, M. & Luna, B., 2014. Developmental stages and sex differences of white matter and behavioral development through adolescence: A longitudinal diffusion tensor imaging (DTI) study. *NeuroImage,* 92**,** 356-368.

Sivaganesan, A., Krishnamurthy, R., Sahni, D. & Viswanathan, C., 2012. Neuroimaging of ventriculoperitoneal shunt complications in children. *Pediatric Radiology,* 42**,** 1029-1046.

Smith-Bindman, R., Lipson, J., Marcus, R., Kim, K.P., Mahesh, M., Gould, R., Berrington de González, A. & Miglioretti, D.L., 2009. Radiation dose associated with

common computed tomography examinations and the associated lifetime attributable risk of cancer. *Archives of Internal Medicine,* 169**,** 2078-2086.

Smith, C.G. & Richardson, W.F., 1966. The course and distribution of the arteries supplying the visual (striate) cortex. *Am J Ophthalmol,* 61**,** 1391-6.

Smith, S.M., Jenkinson, M., Johansen-Berg, H., Rueckert, D., Nichols, T.E., Mackay, C.E., Watkins, K.E., Ciccarelli, O., Cader, M.Z., Matthews, P.M. & Behrens, T.E.J., 2006. Tract-based spatial statistics: Voxelwise analysis of multi-subject diffusion data. *NeuroImage,* 31**,** 1487-1505.

Sowka, J., Vollmer, L. & Reynolds, S., 2008. Superior segmental optic nerve hypoplasia: The topless disc syndrome. *Optometry - Journal of the American Optometric Association,* 79**,** 576-580.

Stanley, O.H., Fleming, P.J. & Morgan, M.H., 1991. Development of visual evoked potentials following intrauterine growth retardation. *Early Human Development,* 27**,** 79-91.

Stanley, O.H., Fleming, P.J., Morgan, M.H. & Stampalija, A., 1986. Visual function in the newborn. *The Lancet,* 328**,** 47-48.

Stejskal, E.O. & Tanner, J.E., 1965. Spin Diffusion Measurements: Spin Echoes in the Presence of a Time‐Dependent Field Gradient. *The Journal of Chemical Physics,* 42**,** 288-292.

Taki, Y., Kinomura, S., Sato, K., Goto, R., Kawashima, R. & Fukuda, H., 2011a. A longitudinal study of gray matter volume decline with age and modifying factors. *Neurobiology of Aging,* 32**,** 907-915.

Taki, Y., Thyreau, B., Kinomura, S., Sato, K., Goto, R., Kawashima, R. & Fukuda, H., 2011b. Correlations among Brain Gray Matter Volumes, Age, Gender, and Hemisphere in Healthy Individuals. *PLoS ONE,* 6**,** e22734-e22734.

Tau, G.Z. & Peterson, B.S., 2010. Normal development of brain circuits. *Neuropsychopharmacology,* 35**,** 147-68.

Teller, D.Y., 1997. First glances: the vision of infants. the Friedenwald lecture. *Invest Ophthalmol Vis Sci,* 38**,** 2183-203.

Terra, V.C., de Paola, L. & Silvado, C.E., 2014. Are children affected by epileptic neuropsychiatric comorbidities? *Epilepsy & Behavior*, 38**,** 8-12.

Thompson, B., Aaen-Stockdale, C., Koski, L. & Hess, R.F., 2009. A double dissociation between striate and extrastriate visual cortex for pattern motion perception revealed using rTMS. *Hum Brain Mapp,* 30**,** 3115-26.

Toosy, A.T., Ciccarelli, O., Parker, G.J.M., Wheeler-Kingshott, C.A.M., Miller, D.H. & Thompson, A.J., 2004. Characterizing function–structure relationships in the human visual system with functional MRI and diffusion tensor imaging. *NeuroImage,* 21**,** 1452-1463.

Traquair, H.M., 1922. The course of the geniculocalcarine visual path in relation to the temporal lobe. *Br J Ophthalmol,* 6**,** 251-261.

Trinka, E., Unterrainer, J., Haberlandt, E., Luef, G., Unterberger, I., Niedermüller, U., Haffner, B. & Bauer, G., 2002. Childhood febrile convulsions—which factors determine the subsequent epilepsy syndrome? A retrospective study. *Epilepsy Research,* 50**,** 283-292.

Tsuneishi, S., 2002. Evaluation of the developing human visual system using flash-visual evoked potential. *No To Hattatsu,* 34**,** 141-146.

Tuch, D.S., Reese, T.G., Wiegell, M.R. & Wedeen, V.J., 2003. Diffusion MRI of complex neural architecture. *Neuron,* 40**,** 885-95.

Tucker, S.M., Enzenauer, R.W., Levin, A.V., Morin, J.D. & Hellmann, J., 1992. Corneal diameter, axial length, and intraocular pressure in premature infants. *Ophthalmology*, 99**,** 1296-300.

Vaegan, T.D., 1979. Critical period for deprivation amblyopia in children. *Trans Ophthalmol Soc UK,* 99**,** 432-9.

van Baarsen, K., Porro, G. & Wittebol Post, D., 2009. Epilepsy surgery provides new insights in retinotopic organization of optic radiations. A systematic review. *Current opinion in ophthalmology,* 20**,** 490-494.

van Buren, J.M. & Baldwin, M., 1958. The architecture of the optic radiation in the temporal lobe of man. *Brain,* 81**,** 15-40.

Van Den Bergh, R. & Van Der Eecken, H., 1968. Anatomy and Embryology of Cerebral Circulation. *In* W. Luyendijk (ed.) *Progress in Brain Research.* Elsevier, 1-25.

Van Essen, D.C., Newsome, W.T. & Maunsell, J.H., 1984. The visual field representation in striate cortex of the macaque monkey: asymmetries, anisotropies, and individual variability. *Vision Res,* 24**,** 429-48.

Vanni, S., Henriksson, L. & James, A.C., 2005. Multifocal fMRI mapping of visual cortical areas. *NeuroImage,* 27**,** 95-105.

Vanni, S., Warnking, J., Dojat, M., Delon-Martin, C., Bullier, J. & Segebarth, C., 2004. Sequence of pattern onset responses in the human visual areas: an fMRI constrained VEP source analysis. *NeuroImage,* 21**,** 801-817.

Vestergaard, M., Pedersen, M.G., Østergaard, J.R., Pedersen, C.B., Olsen, J. & Christensen, J., 2008. Death in children with febrile seizures: a population-based cohort study. *The Lancet,* 372**,** 457-463.

Walker HK, H.W., Hurst JW, 1990. *Clinical Methods: The History, Physical, and Laboratory Examinations* Boston: Elsevier.

Wandell, B.A., Dumoulin, S.O. & Brewer, A.A., 2007. Visual field maps in human cortex. *Neuron,* 56**,** 366-83.

Watson, C., Kirkcaldie, M. & Paxinos, G., 2010. *The brain : an introduction to functional neuroanatomy* Amsterdam, The Netherlands: Elsevier.

Webb, E.A., O'Reilly, M.A., Clayden, J.D., Seunarine, K.K., Dale, N., Salt, A., Clark, C.A. & Dattani, M.T., 2013. Reduced Ventral Cingulum Integrity and Increased

Behavioral Problems in Children with Isolated Optic Nerve Hypoplasia and Mild to Moderate or No Visual Impairment. *PLoS ONE,* 8**,** e59048.

Wichmann, W. & Muller-Forell, W., 2004. Anatomy of the visual system. *Eur J Radiol,* 49**,** 8-30.

Wiener, E., Schad, L.R., Baudendistel, K.T., Essig, M., Müller, E. & Lorenz, W.J., 1996. Functional MR imaging of visual and motor cortex stimulation at high temporal resolution using a flash technique on a standard 1.5 tesla scanner. *Magnetic Resonance Imaging,* 14**,** 477-483.

Winston, G.P., Mancini, L., Stretton, J., Ashmore, J., Symms, M.R., Duncan, J.S. & Yousry, T.A., 2011. Diffusion tensor imaging tractography of the optic radiation for epilepsy surgical planning: A comparison of two methods. *Epilepsy Research,* 97**,** 124-132.

Woldorff, M.G., Fox, P.T., Matzke, M., Lancaster, J.L., Veeraswamy, S., Zamarripa, F., Seabolt, M., Glass, T., Gao, J.H., Martin, C.C. & Jerabek, P., 1997. Retinotopic organization of early visual spatial attention effects as revealed by PET and ERPs. *Hum Brain Mapp,* 5**,** 280-6.

Wong, A.M. & Sharpe, J.A., 1999. Representation of the visual field in the human occipital cortex: a magnetic resonance imaging and perimetric correlation. *Arch Ophthalmol,* 117**,** 208-17.

Woods, D.L., Kwee, I., Clayworth, C.C., Kramer, J.H. & Nakada, T., 1987. Sensory and cognitive evoked potentials in a case of congenital hydrocephalus. *Electroencephalography and Clinical Neurophysiology/Evoked Potentials Section,* 68**,** 202-208.

Xie, S., Gong, G.L., Xiao, J.X., Ye, J.T., Liu, H.H., Gan, X.L., Jiang, Z.T. & Jiang, X.X., 2007. Underdevelopment of optic radiation in children with amblyopia: a tractography study. *Am J Ophthalmol,* 143**,** 642-6.

Yamada, S.M., Kitagawa, R. & Teramoto, A., 2013. Relationship of the location of the ventricular catheter tip and function of the ventriculoperitoneal shunt. *J Clin Neurosci,* 20**,** 99-101.

Yamamoto, A., Miki, Y., Urayama, S., Fushimi, Y., Okada, T., Hanakawa, T., Fukuyama, H. & Togashi, K., 2007. Diffusion tensor fiber tractography of the optic radiation: analysis with 6-, 12-, 40-, and 81-directional motion-probing gradients, a preliminary study. *AJNR Am J Neuroradiol,* 28**,** 92-6.

Yamamoto, T., Yamada, K., Nishimura, T. & Kinoshita, S., 2005. Tractography to Depict Three Layers of Visual Field Trajectories to the Calcarine Gyri. *American Journal of Ophthalmology,* 140**,** 781-785.e1.

Yanoff, M., Duker, J.S. & Augsburger, J.J., 2009. *Ophthalmology* Edinburgh, UK: Mosby Elsevier.

Yasargil, M.G., Ture, U. & Yasargil, D.C., 2004. Impact of temporal lobe surgery. *J Neurosurg,* 101**,** 725-38.

Yogarajah, M., Duncan, J.S. & Koepp, M.J., 2009a. IMAGING | Structure and Function: Imaging Connectivity Using Tractography. *In* A.S. Editor-in-Chief: philip (ed.) *Encyclopedia of Basic Epilepsy Research.* Oxford: Academic Press, 1586-1592.

Yogarajah, M., Focke, N.K., Bonelli, S., Cercignani, M., Acheson, J., Parker, G.J., Alexander, D.C., McEvoy, A.W., Symms, M.R., Koepp, M.J. & Duncan, J.S., 2009b. Defining Meyer's loop-temporal lobe resections, visual field deficits and diffusion tensor tractography. *Brain,* 132**,** 1656-68.

Yoong, M., Seunarine, K., Martinos, M., Chin, R.F., Clark, C.A. & Scott, R.C., 2013. Prolonged febrile seizures cause reversible reductions in white matter integrity. *NeuroImage: Clinical,* 3**,** 515-521.

Yu, B., Guo, Q., Fan, G. & Liu, N., 2011. Assessment of cortical visual impairment in infants with periventricular leukomalacia: a pilot event-related fMRI study. *Korean J Radiol,* 12**,** 463-72.

APPENDIX A: PATIENT CONSENT FORMS

MRI Tractography Consent Form

The following consent form was approved by the Research and Development Office at Great Ormond Street Hospital 08/H0703/130.

INTRODUCTION/PURPOSE

A joint study is being carried out by investigators from the Radiology and Physics Unit, (Dr Chris Clark and Dr Say Ayala-Soriano) and the Departments of Neurosurgery (Mr. William Harkness) and Ophthalmology &Electrophysiology (Dr Alki Liasis) at Great Ormond Street Hospital for Children funded by the Ulverscroft Vision Research Group to determine the relationship between structural measures of the visual pathway and functional measures of this pathway determined by electrophysiology. For this portion of the study, the investigators wish to obtain information from magnetic resonance imaging (MRI) on variation in brain anatomy, and that is why your child has been asked to volunteer.

PROCEDURES

If I agree to participate in this portion of the study, an MRI tractography exam will be performed. You will first be asked a number of questions concerning your child's health, possible presence of metal implants and to confirm absence of claustrophobia. Your child will be weighed, have his/her sitting height and standing height measured. She or he will be asked to lie down on a narrow bed which will then be moved into a tunnel that is 6 feet by 2.5 feet. She or he will lie there quietly for about fifteen minutes during which time he/she will be asked to wear ear phones or ear plugs to reduce noise from the MRI scanner. This noise is normal during the operation of the MRI scanner.

If your child is not having sedation or general anaesthetic he or she may be able to watch a video or listen to a CD so please bring along any favorites.

You are welcome to stay with your child during the scan, but if you are in the first three months of pregnancy, you should let us know before the scan. Communication with the doctors and radiographer outside will be possible at all times by a microphone and loudspeaker. If your child wishes to be removed from the scanner at any time, this will be done

immediately. She or he may be asked to volunteer for a second exam if a surgical or other interventional procedure is performed as part of your child's treatment.

RISKS AND DISCOMFORTS

There are no risks associated with MRI scans. They are painless and generally quick with no lasting effects. The scanner does not touch your child during the scan, only your child is required to lie on a bed inside the scanner.

MRI scans are not suitable for people with any metal inside them (pacemakers, surgical clips or metallic implants) because the scanner emits a strong magnetic field.

Confidentiality: Your child records will be kept as confidential as is possible under law. No individual identities will be used in any reports or publications resulting from this study. In the very unlikely situation your child is injured as a result of participating in these procedures, treatment will be available. The costs of such treatment may be covered by the NHS.

BENEFITS

This study might provide an explanation of the link between structural and physiological abnormalities of the visual pathway. If an abnormal condition is described as a cause of the under development or impairment of the visual pathway those tests may well be used as a follow up. If surgery is required the studies might help in minimizing the risk of postoperative complications related to surgery of brain tissue.

QUESTIONS

If you have any complaints about the way in which this research study has been, or is being conducted, please, in the first instance, discuss them with the researcher. If the problems are not resolved, or you wish to comment in any other way, please contact the Chairman of the Research Ethics Committee, by post via the Research and Development Office, the Institute of Child Health, 30 Guilford Street, London WC1N 1EH, or if urgent by telephone on 020 7242 9789 ex 2620 and the Committee administration will put you in contact with him.

RIGHTS

I have talked with one of the researchers about this study and have had my questions answered satisfactorily.
My participation in research is voluntary. I have the right to decline to participate or to withdraw at any time. I have been given a copy of this consent form. I understand that if I do not wish my child to take part in this study that is entirely my right and will in no way prejudice any future care my child may require.

Subject's Name (Please Print)	Person Obtaining Consent (Please Print)
Subject's Signature	Signature
Date	Date

UCL Institute of Child Health

WHO ARE WE?

We are doctors from Great Ormond Street Hospital in London. We would like to learn more about the brains of children who cannot see well.



WHAT IS THE STUDY ABOUT?

We believe that some children might not be able to see because their eyes do not pass the pictures to their brains properly. We think that children who have tumours or epilepsy are more likely to have this problem. We want to know why so we can help those children who cannot see.



WHAT DO YOU HAVE TO DO?

We would like you to do two things for us!

First, all we ask is that you sit and watch TV or read while we take some pictures of your brain using our clever machine. You won't be able to feel anything, but it will make lots of really good pictures of your brain.

The second thing will only take 30 minutes. One of our doctors will test your vision to make sure that your eyes are okay. She will attach some wires to your head to record what your brain is doing (it won't hurt at all) and then she will show you some pictures.

It is your choice whether you want to take part and help our research, and other children. You can ask Mum and Dad for more information about our work, if you want to.

UCL Institute of Child Health

WHERE DO WE DO OUR WORK?

Our laboratory is at Great Ormond Street Hospital, in the Radiology (X-Ray) and Ophthalmology (Eye) Departments. Your Mum and Dad will be with you all the times during the two tests.

WHY IS IT IMPORTANT THAT YOU TAKE PART?

It is really important that you help us. You can help us to find out why some children cannot see, and we will then try to find a cure for them.

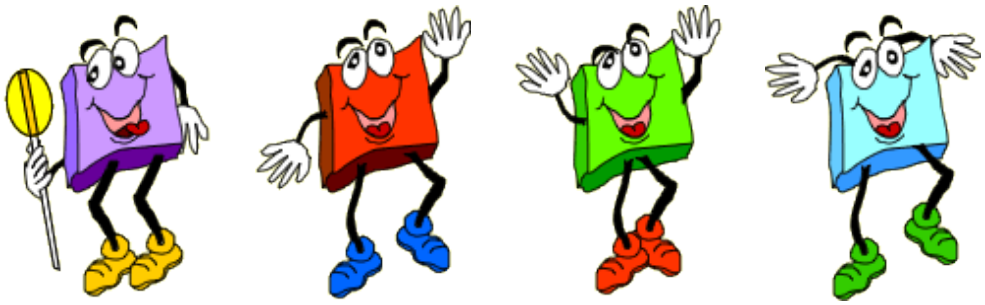

UCL Institute of Child Health

WILL YOU TELL ANYONE WHAT I SAY?

We might write down what you can see and say but we will not let other people see what we have written or recorded. No one except the doctors will know your name or where you live.

HOW CAN YOU TAKE PART?

If you want to help us, you will need to tell us that you agree by signing this form or by asking your Mum to write your name for you. We will need to ask your parents or carer to check that they are happy for you to take part; there is another form for them to fill in.

CAN YOU CHANGE YOUR MIND IF YOU DECIDE TO TAKE PART?

Yes, you can. You can change your mind at any time, even during the scan or eye test. You just have to tell us. We will not mind.

UCL Institute of Child Health

WHAT HAPPENS AFTERWARDS?

We will give you a present to take home: a CD with many pictures of your brain on it!

I am happy to take part in the study:

YES  NO 

My name is: